Quelques études de gravitation observationnelle et expérimentale

Marie-Christine Angonin

UNIVERSITE
PIERRE & MARIE CURIE
E.R.G.A. / *L.E.R.M.A.*- **boîte courrier 142**
4, place Jussieu
F-75252 Paris CEDEX 05

l'Observatoire de Paris

LERMA

Equipe de **R**elativité, **G**ravitation et **A**strophysique

Laboratoire d'**E**tude du **R**ayonnement et de la **M**atière en **A**strophysique (UMR 8112)

DOSSIER D'HABILITATION A DIRIGER DES RECHERCHES

Présenté par

Marie-Christine ANGONIN

Soutenue le 13 décembre 2004 devant le jury composé de :

M. Pierre ENCRENAZ	Président
M. Eric GOURGOULHON	Rapporteur
M. Serge REYNAUD	Rapporteur
M. Jean SURDEJ	Rapporteur
M. Christian BORDE	Examinateur
M. Philippe TOURRENC	Examinateur
M. Philippe TUCKEY	Examinateur

SOMMAIRE

CURRICULUM VITAE

Nom : ANGONIN
Prénom : Marie-Christine
Date et lieu de naissance : 25 octobre 1967 à Paris 17ème
Situation de famille : mariée, 4 enfants, nés en 1993, 1995, 1996, 1999

Etudes :
1985 : Baccalauréat C, mention AB
1987 : Entrée à l'Ecole Normale Supérieure de Paris, concours B, 22ème
1988 : Licence de Physique, mention AB, Paris VI
1989 : Maîtrise de Physique, mention B, Paris VII
DEA d'Astrophysique et Techniques Spatiales, mention TB, Paris VII
1990 : Magistère Interuniversitaire de Physique, mention B, Paris VII
1991 : Agrégation Externe de Physique, option Physique, 43ème (titularisation en sept. 1992)
1993 : Thèse d'Astrophysique et Techniques Spatiales, Paris VII

Statut :
1991 : Agrégé-préparateur à l'Ecole Normale Supérieure
1996 : Maître de conférences à Paris VI (titularisation en sept. 1997)
Congés de maternité en 1993 (3 mois), 1995 (3 mois), 1997 (6 mois) et 1999 (6 mois).

Tâches d'intérêt collectif :

1990-94 :	Membre de la Commission Jeunes Chercheurs de l'Observatoire de Paris
1991-93 :	Membre (collège étudiant) élu au Conseil d'Administration de l'Observatoire de Paris
1997-99 :	Membre du bureau du CLAS de l'Observatoire de Paris.
1999-2001 :	Membre suppléant du Conseil de Service DEUG SCVT Paris VI.
1999-2003 :	Membre nommé au Conseil National des Universités section 34.
1998-2003 :	Membre suppléant, puis titulaire de la CSE section 34/37 ParisVI.
2001-2003 :	Membre nommé de la CSE de l'Observatoire de Paris.
2001-2003 :	Membre élu au Conseil de l'U.F.R. 924 de Paris VI.
2001- :	Membre élu du Conseil de Laboratoire du LERMA.
2002- :	Membre élu du Conseil Scientifique de l'Observatoire de Paris. Membre élu du Conseil d'Administration de l'Observatoire de Paris.
2002-2004 :	Membre nommé du comité de mise en place du Master de Paris VI, Coresponsable de la mention Sciences de l'Univers, Environnement et Ecologie.
2004- :	Coresponsable de la spécialité Astronomie et Astrophysique de la mention SDUEE Membre de la commission d'attribution des Primes d'Encadrement Doctoral et de Recherche.

Information scientifique et technique et vulgarisation :
Encadrement de visites publiques, portes ouvertes et des expositions de l'Observatoire de Meudon et de Paris chaque année.
Interventions dans des classes primaires et collèges.
Emission de radio sur France Culture diffusée le 5 mars 1993 (émission de Jean-Heidman) :
Les télescopes à lentilles gravitationnelles
Emission de télévision diffusée sur France 2 le 15 août 1993 (CQFD) : *Images*
Communication invitée à la session sur les carrières des jeunes chercheurs aux journées de la SFSA à Besançon en 1994.
Conférences invitées lors de réunions d'astronomes amateurs (2001 et 2003):
Galaxies
L'influence des progrès technologiques sur l'astronomie
Conseillère pour des articles dans « Ciel et espace » et « Sciences et vie junior ».
Publication dans l'« Astronomie » en 2001 avec A.-C. Levasseur-Regourd et N. Baumard :
La vie sur Europe est-elle possible ?

ENSEIGNEMENT

En tant qu'agrégé-préparateur à l'Ecole Normale Supérieure (1991-96, 192h par an) :
Magistère Interuniversitaire de Physique :
TD d'électromagnétisme et TP de Physique en première année (licence et maîtrise ; 91-92)
Tutorat d'élèves (91-92)

Préparation à l'Agrégation Externe de Physique :
TD d'électromagnétisme (92-95)
TD de relativité (93-94)
TP de Physique, correction de montages, responsable du renouvellement des polys (91-96)
Responsable de l'enseignement de physique pour l'option chimie (95-96)

En tant que maître de conférences de l'Université Paris VI (depuis 1996):
1er cycle*:*
TPs de physique 1ère année DEUG SCVT (96-97)
TDs de physique-maths 1ère année DEUG SCVT (97-99)
TDs de biophysique 1ère année DEUG SCVT (97-00)
Module méthodologique "Exobiologie et origine de la vie" : mise en place de l'enseignement, responsabilité et animation 1ère année DEUG SCVT (99-02)
Cours optionnel d'astrophysique 1ère année DEUG (99-00)
Participation aux examens des étudiants cumulatifs niveau DEUG (00-01)

2ème cycle:
TDs de physique atomique Licence de Physique (97-98)
TDs de mécanique quantique Licence de Physique (97-98)
TDs de mécanique quantique Maîtrise de Physique Appliquée (98-04)
TDs de physique atomique Maîtrise de Physique Appliquée (98-04)

- *Polycopiés :* Angonin M-C, Tourrenc Ph, 2002, Maîtrise de Physique Appliquée :
  Tome 1 : Mécanique quantique
  Tome 2 : Physique atomique

3ème cycle:

Cours de physique et évolution des galaxies DEA à l'Ecole Doctorale d'Ile de France (96-04)

- *Polycopié :* Angonin M-C, 2000, polycopié d'enseignement de DEA :
  Physique et évolution des galaxies

Jury de soutenance de stage de DEA (96-04)

Parrainage de la thèse de Laurent Chemin sous la direction de Véronique Cayatte (99-02) :
Cinématique et dynamique de galaxies spirales.

Tutorat pédagogique du monitorat de Frédéric Meynadier (01-04).

Préparation à l'Agrégation externe de Physique : TPs, TDs d'électromagnétisme, correcteur de montages et de leçons, représentante de Paris VI (01-04).

Divers :

Interrogatrice pour les TPs du concours d'entrée de l'ENS Ulm (91-95)

Professeur correcteur auxiliaire au CNED (94-99)

Concepteur de sujet et correcteur pour le concours d'entrée de Polytechnique (95-97)

Participation au jury du concours d'entrée de l'ENS Ulm : concepteur de sujet d'écrit et correcteur depuis 1998; examinateur à l'oral depuis 2000

Encadrement des TPs d'informatique lors de l'école des Houches sur ISO (août 98)

ENCADREMENT DE STAGES ET THESE

Stages :

Mars-juin 2001 :	Frédéric Meynadier, DEA, Paris VI *Spectrographie bidimensionnelle de 3C305*
Avril-juin 2002 :	Sébastien Hess et Ulysse Marboeuf, Licence, Paris VI *Programmes sous Maple de calculs usuels en relativité générale*
Juin-sept. 2002 :	Fabien Daniel, Perrine Deshayes et Benjamin Sebag, maîtrise, Paris VI *Etude multi-longueurs d'onde de M31*
Juin 2003 :	Claire Chevalier et Olivier Tiret, Licence, Paris VI *Recherche d'effets de lentille gravitationnelle pour des ondes gravitationnelles dans la direction de l'amas de Virgo*
Mars-Juin 2004 :	Franck Genet, DEA, Paris VII *Anomalie du mouvement des sondes lointaines* *Cavités à ondes de matière*

Thèse :

2001-03 :	Co-encadrement de la thèse de Monica Varvella *Gravitational waves in extended gravity: theory and detection*
2004- :	Encadrement de la thèse de Pacôme Delva : *Etudes des applications gravitationnelles des cavités à ondes de matière*

Membre des jurys de thèse de Monica Varvella, Sante Carloni, Fabio Dell'Arno, Antonio Capolupo à l'Université de Salerne (Italie).

RECHERCHE

Remarques : Un changement important de thématiques a eu lieu en 2001, modifiant notablement les activités de recherche. D'autre part, j'ai publié sous trois noms différents : Angonin, Angonin-Willaime et Willaime.

• *Recherches en astrophysique extragalactique observationnelle, essentiellement centrée autour de l'étude des phénomènes de lentille gravitationnelle (1989-2001) :*

Missions d'observation :

Remarques : Les observations avec SILFID, TIGRE, MOS et ISIS étaient systématiquement couplées avec d'autres programmes d'observations pour lesquels j'étais astronome-assistant.

Juillet 1988 : Observatoire de Bordeaux, P.O.M.2 :
Stage de maîtrise : observation en CO de nuages moléculaires galactiques.

Mars 1989 : T2M, Pic du Midi, photométrie :
TPs de DEA : mise au point d'une camera CDD

Juin 1989 : Observatoire de Haute Provence, Télescope de 193 cm, SILFID mode Méduse :
Stage de DEA : dynamique de galaxies d'amas proches.

Janv. 1990 : Observatoire de Calar-Alto (Espagne), Télescope de 152 cm, photomètre :
Test d'un photomètre et d'une caméra de pointage

Avril 1990 : Télescope Canada-France-Hawaï, TIGRE :
Spectrographie bidimensionnelle de mirages gravitationnels

Déc. 1990 : Télescope Canada-France-Hawaï, SILFID mode Argus :
Spectrographie bidimensionnelle de mirages gravitationnels

Mai 1991 : Télescope Canada-France-Hawaï, MARLIN, spectrographie multi-fentes.
Dynamique des galaxies de l'amas déflecteur de Q0957+561.

Déc. 1991 : Télescope Canada-France-Hawaï, SILFID mode Argus :
Spectrographie bidimensionnelle de mirages gravitationnels

Janv. 1992 : European Southern Observatory, New Technology Telescope, EMMI et SUSI.
Observations photométriques et spectroscopiques de mirages gravitationnels, Recherche systématique d'arcs géants.

Mars 1992 : Télescope Canada-France-Hawaï, SILFID mode Argus
Spectrographie bidimensionnelle de mirages gravitationnels

Juin 1993 : Télescope Canada-France-Hawaï, MOS, mode Argus :
Spectrographie bidimensionnelle de mirages gravitationnels

Janv. 1994 : Télescope Canada-France-Hawaï, ISIS, mode Argus IR
Spectrographie bidimensionnelle de mirages gravitationnels en infrarouge proche

Avril 1998 : IRAM, 30m, Pico Veleta (en complément d'observations obtenues au Plateau de Bure)
Observations en CO (dont espacements courts) du système en interaction Arp 299

Publications :

Thèse *:*

Thèse d'Astrophysique et Techniques Spatiales, sous la direction de Christian Vanderriest, *Etude des grandes amplifications gravitationnelles et des effets de microlensing sur les sources lointaines.*, Université Paris VII, commencée en septembre 1989, soutenue le 07 septembre 1993 à l'Observatoire de Meudon, devant le Jury composé de: P. Léna (président), B. Fort (rapporteur), S. Refsdal (rapporteur), G. Courtès, F. Hammer, J. Surdej, C. Vanderriest.

Publications dans des revues à comité de lecture :

- Angonin M-C, Vanderriest C, Remy M, Surdej J, 1990, Astronomy and Astrophysics, **233**, L5 : *First spectroscopic evidence of microlensing on a BAL quasar? The case of H 1413+117*

- Hammer F, Angonin MC, Le Fèvre O, Meylan G, Smette A, Surdej J, 1991, Astronomy and Astrophysics, **250**, L5 : *MG 1131+0456: discovery of the optical Einstein ring with the NTT*

- Hammer F, Le Fèvre O, Angonin M-C, 1993, Nature, **362**, 324 : *A young source of optical emission from distant radio galaxies*

- Angonin-Willaime M-C, Vanderriest C, Hammer F, Magain P, 1994, Astronomy and Astrophysics, **281**, 388 : *Further observational evidence that MG J0414+0534 is a gravitational mirage*

+ *Erratum* : 1994, Astronomy and Astrophysics, **292**, 722

- Le Fèvre O, Hammer F, Angonin M-C, Gioia I, Luppino G, 1994, Astrophysical Journal, **422**, L5 : *Imaging of 16 distant EMSS clusters with z≥0.2 and $L_{X,44}$≥4: new arcs and first consequences*

- Angonin-Willaime M-C, Soucail G, Vanderriest C, 1994, Astronomy and Astrophysics, **291**, 411 : *Gravitational lensing on Q0957+561: A study of the cluster at z=0.355*

- Hammer F, Rigaut F, Angonin-Willaime M-C, 1995, Astronomy and Astrophysics, **298**, 737 : *Imaging and spectroscopy of B 1422+231 at C.F.H.T.: identification of the mirage and of the lensing galaxy at z= 0.647*

- Angonin-Willaime M-C, Vanderriest C, Courbin F, Burud I, Magain P, Rigaut F, 1999, Astronomy and Astrophysics, **347**, 434 : *About the origin of extinction in the gravitational lens system MG J0414+0534*.

- Casoli F, Willaime M-C, Viallefond F, Gerin M, 1999, Astronomy and Astrophysics, **346**, 663 : *Molecular gas in the system of merging galaxies ARP 299.*

- Willaime M-C, Casoli F., Gerin M., 2001, Astrophysics and Space Science Journal, 276/2-4 , 931 : *Molecular gas in the merging system Arp 299*.

- Willaime M-C, Lequeux J., Hanus M., 2001, Astrophysics and Space Science Journal, 276/2-4, 383 : *ISOCAM observations of the centre of M31*

Communications invitées, revues :

- Vanderriest C, Angonin M-C, 1992, dans "Gravitational lenses" colloque de Hambourg de septembre 1991, Lectures Notes in Physics, **406**, 97 : *Bidimensional spectrography of multiple quasars*

- Angonin-Willaime M-C, Hammer F et Rigaut F, 1993, proceedings du colloque de Liège: Gravitational lenses, 85 : *Ground-based optical observation of gravitational lenses*

- Hammer F, Angonin-Willaime M-C, Le Fèvre O, Wu X-P, Luppino G et Gioia I, 1993, proceedings du colloque de Liège: Gravitational lenses, 609 : *Statistics of gravitational lensing by clusters of galaxies: luminous arcs*

Communications publiées :

- Angonin M-C, Vanderriest C, Surdej J, 1990, dans "Gravitational lensing" colloque de Toulouse de septembre 1989, Lectures Notes in Physics, **360**, 124 : *Bidimensional spectrography of the 'Clover Leaf' H1413+117 at sub-arcsec spatial resolution*

- Angonin M-C, 1992, Journées scientifiques de la S.F.S.A. de novembre 1990, Journal des Astronomes Français, **41,** février, 10 : *Modélisation des arcs géants dans Abell 963: une estimation de la masse des déflecteurs*

- Angonin M-C, Hammer F, Le Fèvre O, 1992, dans "Gravitational lenses" colloque de Hambourg de septembre 1991, Lectures Notes in Physics, **406**, 312 : *New results on Abell 963 and MG 1131+0456*

- Angonin M-C, Soucail G, 1992, dans "Gravitational lenses" colloque de Hambourg de septembre 1991, Lectures Notes in Physics, **406**, 362 : *Spectrography in 0957+561 field*
- Angonin M-C, 1992, proceedings du "Second DAEC Workshop on Large Scale Structures of the Universe.", édités par Mamon et Gerbal (Observatoire de Paris), 90 : *Numerical model of the giant arcs in Abell 963: An estimation of the deflector mass*
- Surdej J, Angonin M-C *et al*., 1992, proceedings du "Second DAEC Workshop on Large Scale Structures of the Universe.", édités par Mamon et Gerbal (Observatoire de Paris), 97 : *ESO Key Programme 'Gravitational Lensing: Quasars and Radio Galaxies: A Status Report*
- Hammer F, Lefèvre O et Angonin M-C, 1993, proceedings du "8th IAP meeting, Paris 1992: First light in the Universe, 139 : *On the (stellar) nature of distant radiogalaxies*
- Angonin M-C, 1994, Journal des Astronomes Français, **45,** décembre, 51 : *Etude des grandes amplifications gravitationnelles et des effets de microlensing sur les sources distantes*
- Angonin M-C, Vanderriest C, 1995, Colloque IAU n° 149 sur la spectroscopie 3D en astrophysique à Marseille, Astronomical Society of the Pacific Conference Series, **71**, 225 : *Integral field spectroscopy of gravitational mirages*
- Surdej J, Vanderriest C, Angonin-Willaime M-C, Claeskens J-F, Felenbok P, 1995, Science with the VLT, Proceedings of the ESO Workshop, Garching, Germany, 28 June - 1 July 1994, Edited by J Walsh and I Danziger. Berlin: Springer-Verlag,, 383 : *Integral Field Spectroscopy of Selected Extragalactic Objects with FUEGOS*
- Vanderriest C, Angonin-Willaime M-C, Rigaut F, 1996, proceedings du colloque UAI n°173 sur les lentilles gravitationnelles, Melbourne, 353 : *Mapping the extinction pattern in dusty lenses: optical and IR imaging of MG J0414+0534*
- Angonin-Willaime M-C, Casoli F, Gerin M., Rouan D., 1996, proceedings of the 11th l'IAP meeting: "The interplay between star formation, ISM and galaxy evolution" éditions Frontières, 493 : *H_2 maps in the infrared of Arp 299 and Arp 220*
- Willaime M-C, Lequeux J., Melchior A-L, Hanus M., 2001, ESA-SP 460, 519 : *ISOCAM observations of M31*.

Divers :
- Angonin M-C, Vanderriest C et Surdej J, 1990, Bulletin d'information du Télescope Canada-France-Hawaï, **22,** 14 : *Spectrographie bidimensionnelle de 2 mirages gravitationnels avec SILFID*
- Angonin M-C, Gioia I, Hammer F, Le Fèvre O, Luppino G, 1993, Bulletin d'information du Télescope Canada-France-Hawaï, **28,** 23 : *Imaging survey of 34 galaxy clusters from the EMSS sample*
- Angonin-Willaime M-C, Casoli F, Gerin M, Rouan D, 1996, Bulletin d'information du Télescope Canada-France-Hawaï **34**, 8 : *Morphologie de l'hydrogène chaud dans des galaxies en fusion*
- Angonin-Willaime M-C, Vanderriest C, Surdej J, 1993, V.L.T. instrumentation plan, FUEGOS a multifibre area spectrograph, Scientific report : *Gravitational lensing on quasars and related objects*

Séminaires, communications non-publiées et participation à des écoles:

- Astrophysical predoctoral summer school on "Late stages in stellar evolution" à Ponte de Lima (Portugal), septembre 1989.
- Poster au colloque "High redshift galaxies", Oxford, juillet 1990 : *Numerical model of Abell 963: an estimation of the deflectors mass*
- séminaire au DAEC ,1992 : *Mirages gravitationnels: un bilan observationnel.*
- séminaire à la journée intergroupe de cosmologie sur la "Masse dynamique des galaxies et des amas" à l'IAP, 1993 : *Distribution de masse dans les amas par les lentilles gravitationnelles*
- séminaire à l'atelier sur l'infrarouge à l'observatoire de Meudon ,1993 : *Objets MG*
- communication aux journées de la SFSA à Besançon, 1994: *Arcs gravitationnels dans les amas lumineux en X: contraintes sur la distribution de masse*
- séminaire au DEMIRM, 1996 : *Observations infrarouge de systèmes de galaxies en fusion.*
- Présentation orale sur les molécules primordiales à une réunion sur FIRST à Leiden, 1997.
- Présentation sur Arp 299 aux journées de collaboration Franco-Japonaises, DEMIRM, 1997
- Monitorat TPs d'informatique et participation à l'école d'été des Houches sur ISO, 1998.

• *Recherches en relativité générale et gravitation expérimentale (depuis 2001) :*

Organisation de rencontres :

Organisation de la journée sur la Gravitation de Paris VI, le 5 décembre 2002.
Organisation des journées du GdR Gravitation Expérimentale en octobre 2003.

Publications :

Publications dans des revues à comité de lecture :

- Angonin-Willaime M-C, Ovido X, Tourrenc Ph, 2004, General Relativity and Gravitation, vol. **36**, Issue 2, 411 : *Gravitational perturbations on local experiments in a satellite : The dragging of inertial frame in the HYPER project*
- Arnaud-Varvella M, Angonin M-C, Tourrenc Ph, 2004, General Relativity and Gravitation, vol. **36**, Issue 5, 983 : *Increase of the number of signal due to gravitational lensing of gravitational waves*
- Tourrenc Ph, Angonin M-C, Ovido X, 2004, General Relativity and Gravitation, vol. **36**, Issue 10, 2237: *Tidal gravitational effects in a satellite*
- Tourrenc Ph, Angonin M-C, Wolf P, 2004, soumis : *The forgotten process : the emission stimulated by matter waves.*

Communications invitées, revues :

- Présentation orale aux journées du GdR GREX à Grasse,2001 : *Hyper et les gradients* (avec Ph Tourrenc)
- Présentation aux journées du GdR GREX à Pise, 2002 : *Temporal dependences in HYPER* (avec Ph Tourrenc)
- Présentation au symposium sur HYPER à Paris, novembre 2002 : *Hyper : local gravito-inertial fields* (avec Ph. Tourrenc et X. Ovido)
- Présentation aux journées du GdR GREX à l'IAP, 2003 : *Les effets de lentilles gravitationnelles peuvent-ils faciliter la détection des ondes gravitationnelles ?* (avec M. Varvella)

Communications publiées :

- Arnaud-Varvella M, Angonin-Willaime M-C, Tourrenc Ph, Proceedings of the meeting "Gravitational lensing: a unique tool for cosmology", Jan. 5-11, 2003, Aussois, Savoie, France, eds D. Valls-Gabaud and J. P. Kneib : *Gravitational lensing of gravitational waves (application to gravitational waves detectors)*
- Arnaud-Varvella M, Angonin-Willaime M-C, Tourrenc Ph, Proceedings of XXXVIII^{èmes} Rencontres de Moriond « Gravitational Waves and Experimental Gravity », Mar. 22-29, 2003, Les Arcs : *Gravitational lensing of gravitational waves applied to gravitational waves detectors*

Communications non-publiées :

- Présentation à journée sur la gravitation à l'Université Paris VI en décembre 2002 : *Propriétés théoriques des expériences relativistes.*
- Présentation au forum sur les astroparticules et la physique fondamentale à l'Observatoire de Paris-Meudon en janvier 2004 : *Gravitation, relativité et tests expérimentaux*.

PRESENTATION GENERALE DES TRAVAUX.

PARCOURS PERSONNEL

Cette partie consiste en une présentation générale des travaux de recherche auxquels j'ai participé. Ces travaux peuvent être divisés en deux périodes. La première période couvre les années 1989 à 2001 et correspond à des recherches orientées vers l'étude observationnelle d'objets astrophysiques extragalactiques, principalement des lentilles gravitationnelles. La deuxième période démarre en 2001 et est associée à une recherche plus théorique dans le domaine de la relativité générale et la gravitation expérimentale. Cette dichotomie n'existe qu'au travers des moyens d'étude utilisés (observations / théorie) ; en effet, les thématiques des deux périodes sont proches, dans la mesure où les lentilles gravitationnelles ont longtemps été un domaine moteur de la gravitation expérimentale. L'objet de cette introduction est donc de montrer mon parcours personnel au travers de ces thématiques.

Avant d'être recrutée Maître de Conférences de l'Université Pierre et Marie Curie, j'ai fait ma thèse dans le Département d'Astrophysique Extragalactique et de Cosmologie (DAEC) sous la direction de Christian Vanderriest et en collaboration avec François Hammer. Cette thèse portait sur l'étude des effets de lentilles gravitationnelles sur les sources distances, ainsi que sur l'étude des diverses applications de tels phénomènes sur la physique des objets mis en jeu. Ces travaux furent essentiellement fondés sur des observations astrophysiques. Pendant cette période, j'ai effectué plusieurs missions d'observation sur différents instruments, dont certains étaient des prototypes : photométrie, spectrométrie à une fente, multi-fentes, bidimensionnelle, en optique et en infrarouge proche. A la suite de cela, j'ai procédé au dépouillement des données (ce qui nécessitait souvent des innovations). Enfin, je participais à l'interprétation des résultats (notamment sous la forme de modélisation numérique). Cela nécessitait alors la prise en compte des effets de relativité dans un formalisme post-Newtonien. J'ai été recrutée en cours de thèse comme agrégé-préparateur à l'Ecole Normale Supérieure de Paris (professeur agrégé détaché dans le supérieur, équivalent temps plein d'enseignement d'un Maître de Conférences), statut qui m'empêchait de faire un séjour post-doctoral à l'étranger. Après ma soutenance de thèse en 1993, je suis donc restée dans ce laboratoire en poursuivant ces travaux jusqu'en septembre 1995.

Du fait de son lien administratif avec l'Ecole Normale Supérieure (qui était alors mon employeur), le Département pour l'Etude du Milieu Interstellaire en Radioastronomie Millimétrique (DEMIRM), actuellement Laboratoire pour l'Etude du Rayonnement et de la Matière en Astrophysique (LERMA), m'a proposé de venir le rejoindre en septembre 1995 tout en me demandant d'orienter mes recherches vers des thématiques plus proches de celles du DEMIRM. J'ai continué ainsi mes travaux sur les lentilles gravitationnelles en me servant du phénomène pour étudier la composition du milieu interstellaire des objets concernés. Parallèlement à cela, j'ai utilisé mes connaissances en dépouillement de données observationnelles multi-longueurs d'onde pour collaborer avec Fabienne Casoli, Maryvonne Gérin, François Viallefond, Anne-Laure Melchior et James Lequeux sur des recherches concernant le milieu interstellaire de galaxies proches en infrarouge proche et lointain et en millimétrique .

De cette façon, une campagne de cartographie à haute résolution spatiale (lobe de 0.8") de Arp 299 en millimétrique avec les télescopes de l'IRAM a été menée en collaboration avec F. Casoli, F. Viallefond et M. Gerin. Elle a mis en évidence les mouvements du gaz moléculaire sous forme de filaments et de régions plus denses entre les noyaux des deux galaxies en interaction. Nous avons obtenus des résultats similaires sur des observations en infrarouge proche des raies d'hydrogène moléculaire ainsi que d'hydrogène ionisé de ce système, observations effectuées au CFHT. Le même type d'observations effectuées sur des systèmes de galaxies en interaction plus avancée a montré que le gaz moléculaire était alors tombé au centre du système (Casoli, Willaime, Viallefond et Gerin, 1999 ; Willaime, Casoli et Gerin, 2001). De même, j'ai effectué le dépouillement des observations ISOCAM de J. Lequeux et collaborateurs sur le centre de la galaxie d'Andromède, M31. Ces données mettent en évidence une structure spirale pour la poussière. Cette structure se retrouve dans les données dans le filtre H_α et dans les cartes d'extinction optique (Willaime, Lequeux et Hanus, 2001 ; Willaime, Lequeux, Melchior et Hanus, 2001).

Dès 1998, j'ai commencé à envisager d'encadrer des étudiants pour ce type de recherche (tutorat sur le dépouillement des données ISO à l'école des Houches). Cela s'est concrêtisé en 2001 lorsque, notamment, j'ai co-encadré, avec Anne-Laure Melchior, les stages de trois étudiants de Maîtrise de Physique, Fabien Daniel, Perrine Deshayes et Benjamin Sebag sur les données concernant M31. L'objet du stage était de refaire les calibrations des données ISOCAM avec les derniers logiciels du moment et de les superposer aux cartes d'extinction en optique. Pour obtenir les cartes, les étudiants durent faire l'astrométrie précise d'images optiques à l'aide des dernières mesures de la MAMA à l'Observatoire de Paris et modéliser le bulbe de M31 afin d'en retirer la luminosité. Au final, ils ont mis en évidence une corrélation spatiale très forte entre les nuages en absorption et l'émission des poussières.

Parallèlement à cela, j'ai eu l'occasion de collaborer avec Philippe Tourrenc pour l'enseignement à partir de 1997, peu après mon recrutement en tant que Maître de Conférences. Ses travaux théoriques sur la gravitation expérimentale faisaient échos aux travaux liés à la relativité que j'avais abandonnés en arrivant au DEMIRM. Aussi, lors de l'insertion de son équipe (de l'ancien Laboratoire de Gravitation et Cosmologie Relativiste) au DEMIRM/LERMA en 2001, j'ai naturellement effectué une reconversion thématique pour me mettre à des recherches plus théoriques. Dès 2002, j'ai encadré des étudiants sur des travaux liés à la relativité générale et la gravitation expérimentale.

Je présente, dans la suite, l'ensemble des travaux observationnels sur les lentilles gravitationnelles de façon globale. Je montre ensuite comment ces travaux se sont articulés vers une orientation plus théorique de mon travail. Enfin, je développe plus en détail les travaux en lien avec la physique fondamentale et plus précisément la gravitation relativiste, thématique que je désire développer à l'avenir. Par ce biais, je souhaite montrer que, exception faite de quelques observations purement astrophysiques mentionnées à divers points de ce manuscrit, l'ensemble de ces travaux portent sur des applications d'effets relativistes dans différentes expériences, à l'échelle du laboratoire aussi bien qu'à l'échelle cosmologique.

LES LENTILLES GRAVITATIONNELLES

L'étude observationnelle de mirages gravitationnels de quasar est un outil dont chaque facette apporte des informations sur l'univers lointain, informations difficiles à obtenir par un autre biais. Lorsque l'on observe différentes images d'un même quasar, non seulement on a accès aux caractéristiques de la source à des temps différents (la lumière met des temps différents à parcourir les trajectoires correspondant aux images), mais, en outre, on sonde une portion non négligeable de l'univers grâce aux différentes trajectoires des photons émis par le quasar. Lorsque j'ai commencé à travailler dans ce domaine, le premier mirage gravitationnel était connu depuis 10 ans[1]. Une poignée de candidats mirages avait été mise en évidence et beaucoup restaient à découvrir. Le travail qu'il y avait à faire était alors un travail de défrichage par les observations : découvrir de nouveaux mirages, confirmer les candidats retenus, déterminer leurs caractéristiques et en déduire les paramètres qu'elles contraignent, vérifier que tout ce qui avait été prédit théoriquement sur le phénomène était bien accessible par les observations. A cela, s'ajoutait la mise au point par Christian Vanderriest d'un spectrographe bidimensionnel à fibres, SILFID, instrument tout à fait adapté à l'étude des mirages gravitationnels de quasars puisque la source est assez brillante et peu étendue pour faire les spectres simultanés de chaque image et, éventuellement de la lentille (Vanderriest et Angonin, 1992). Bien qu'ayant utilisé toutes les configurations d'observation à ma disposition, j'ai donc orienté mon étude observationnelle des mirages gravitationnels vers l'emploi de cet instrument que l'on pouvait alors qualifier d'avant-garde. Je vais faire ainsi, dans une petite parenthèse, une présentation de cet instrument. A la suite de cela, je décrirai mes travaux sur les mirages de quasars.

Utilisation et développement de la spectrographie bidimensionnelle

Parallèlement à l'évolution des techniques d'observation vers des résolutions spatiales toujours meilleures, est apparu le besoin de conserver cette information spatiale en spectrographie. Le passage d'une fente classique d'un spectrographe à un système bidimensionnel peut se faire grâce à une trame de micro-lentilles (comme dans le spectrographe TIGRE) ou par l'intermédiaire d'un anamorphoseur d'images constitué de fibres optiques.

Cette dernière technique a été choisie pour élaborer le spectrographe SILFID. Cet instrument, conçu en 1980 par Christian Vanderriest, a été utilisé au télescope Canada-France-Hawaï (C.F.H.T.) de 1986 à 1992 , puis a été installé définitivement sur un télescope indien. SILFID comporte en fait plusieurs modes de fonctionnement possibles: imagerie directe, spectrographe multi-objets et spectrographe bidimensionnel. Dans ce dernier mode (système à fibres "Argus"), près de 400 spectres peuvent être enregistrés simultanément.

J'ai consacré une partie de mon temps à développer et rationaliser les procédures de dépouillements de données en spectrographie bidimensionnelle. J'ai pu bénéficier ainsi pleinement de cette technique d'observations en plein développement. Notamment, j'ai participé à l'introduction du système Argus dans le MOS du CFHT (collaboration avec l'équipe de P. Felenbok au DAEC) et à son homologue en infrarouge proche sur ce même télescope, ISIS. Par ailleurs, j'ai participé activement à la discussion concernant la conception d'un mode Argus pour le spectrographe FUEGOS qui, pendant un temps, a été

[1] Walsh, Carswell et Weyman, Nature, 1979, **279**, 381.

destiné au VLT et mis au point à l'Observatoire de Paris-Meudon (Angonin-Willaime, Vanderriest et Surdej, 1993, Scientific Report ; Surdej et al., 1995), en cela il a été un précurseur du spectrographe GIRAFFE effectivement utilisé actuellement au VLT. Les techniques de spectrographie bidimensionnelle sont maintenant présentes sur la plupart des grands télescopes mondiaux.

Cet instrument et ceux qui l'ont suivi ont donc constitué une configuration favorable pour l'étude des mirages gravitationnels, mais leur caractère expérimental a constitué une charge de travail supplémentaire pour son utilisation et son accompagnement. J'ai assisté plusieurs astronomes lors de leurs observations propres (les missions d'observation au CFHT correspondaient toujours à plusieurs programmes) avec ces instruments, ainsi que lors du dépouillement des données obtenues.

De même, j'ai participé activement à une collaboration Franco-Espagnole pour la mise au point et le démarrage du spectrographe Albireo (analogue au mode ARGUS de SILFID) sur un télescope de la Sierra Nevada (Collaborateurs : Christian Vanderriest, Georges Herpe, Pascal Teyssandier, Ascension del Olmo Orizco, Justo Sanchez del Rio). Dans le cadre d'un programme d'observations systématiques de galaxies en interaction (autre sujet privilégié de la spectrographie bidimensionnelle), j'ai encadré la formation nécessaire au dépouillement de données. Ce travail s'est poursuivi par l'encadrement du stage de DEA (Ecole Doctorale d'Astrophysique d'Ile de France) de Frédéric Meynadier sur la spectrographie bidimensionnelle de la galaxie 3C305. Je lui ai demandé de faire, dans un premier temps, le dépouillement des données d'Albireo sur ce vestige d'interaction de galaxies. Les particularités d'Albireo ont nécessité de mettre au point de nouveaux programmes, ce qu'il a effectué tout au long du stage en les adaptant pour qu'ils soient d'usage général. Ces données confirment que 3C305 est le résultat d'une coalescence et mettent en évidence des zones de formation stellaire récente dans les zones externes de la galaxie. L'article est en préparation (la rédaction a été suspendue quelques temps suite à la disparition de Christian Vanderriest).

Je reviens, à présent, sur les résultats obtenus, avec SILFID comme d'autres instruments, sur les mirages gravitationnels.

Etude observationnelle des mirages gravitationnels de quasars

Dans le cadre de l'étude observationnelle des mirages, j'ai participé à une coopération internationale sur l'étude des mirages grâce à un programme-clé de l'European Southern Observatory de 1989 à 1993 (responsable scientifique: Jean Surdej), je me suis ainsi initiée à différentes techniques observationnelles (techniques de spectrographies bidimensionnelles et multi-objet, photométrie dans le visible et l'infrarouge). La coopération s'est poursuivie par un réseau de la C.E.E. dans le cadre de Capital humain et mobilité qui a été accepté sur le thème "Gravitational optics and cosmology" réunissant des équipes de Liège, Durham, Barcelone, Toulouse, Paris (Centre d'Analyse d'Image), Hambourg, Oslo et mon équipe (coordinateur: Pierre Magain).

Les observations, que j'ai effectuées, dépouillées et interprétées, ont permis de confirmer l'existence de certains mirages, de donner les caractéristiques des lentilles et de préciser la nature des sources.

• Avec l'instrument SILFID au CFHT, j'ai obtenu le spectre des quatre images de H1413+117 -mirage quadruple surnommé le « trèfle à quatre feuilles »- (Angonin et al., 1990). Ces spectres ont confirmé la nature de mirage gravitationnel de ce quasar, considéré

maintenant comme un archétype du phénomène. Des raies en absorption dans les spectres de certaines images suggèrent deux redshifts possibles pour la ou les lentilles ainsi que la localisation spatiale de celles-ci. La valeur assez élevée de ces redshift explique pourquoi les galaxies associées n'ont pas encore été détectées en photométrie directe à ce jour.

• Avec le spectrographe EMMI (New Technology Telescope, ESO), j'ai effectué la première mesure du décalage spectral de la galaxie déflectrice du mirage quadruple PG1115+080 (Angonin-Willaime, Hammer et Rigaut, 1993). Cette mesure, alors assez bruitée, a été confirmée par la suite[2].

• Avec SILFID au CFHT et différents instruments sur les télescopes de l'ESO, j'ai pu identifier la galaxie déflectrice du mirage quadruple MG J0414+0534 et donner une première estimation de son redshift par une mesure photométrique. Simultanément, j'ai obtenu les spectres de deux images, confirmant, d'une part, qu'il s'agissait bien d'un mirage gravitationnel et, d'autre part, donnant des indications sur la nature de la source et l'extinction qu'elle subit (Angonin-Willaime, Vanderriest, Hammer et Magain, 1994). Quelques années plus tard, en combinant des données photométriques en optique et en infrarouge proche du Hubble Space Telescope et du CFHT, j'ai publié une discussion sur la nature du très fort rougissement détecté sur les spectres du quasar (Angonin-Willaime et al., 1999). J'ai notamment mis en évidence par ces observations que le rougissement est dû, au moins en partie, à la galaxie déflectrice.

• Des données photométriques du CFHT ont permis, à mes collaborateurs, l'identification et une estimation du redshift de la galaxie déflectrice, appartenant probablement à un amas, de B 1422+231 -mirage quadruple de configuration très compacte dont la source était alors une des plus lointaines-. J'ai alors pu élaborer une discussion sur la modélisation du phénomène et donc une estimation par modélisation de la distribution de masse de la lentille (Hammer, Rigaut, Angonin-Willaime et Vanderriest, 1995).

• A l'aide d'observations photométriques et spectroscopiques effectuées sur le NTT à l'ESO, j'ai étudié le système 2016+112 ce qui m'a permis notamment de préciser la nature active (« liner ») de la source (Angonin-Willaime, Hammer et Rigaut, 1993).

Détermination de la constante de Hubble

Un des problèmes sur lesquels je me suis penchée plus particulièrement concerne la détermination de la constante de Hubble par les mirages de quasar. Les quasars étant des sources variables en luminosité sur des périodes assez courtes (de l'ordre de quelques mois), il est possible de mesurer par suivi photométrique le décalage temporel qui existe entre les différentes images. Ce décalage est dû à la différence de trajets optiques et de structure d'espace-temps que traversent les rayons lumineux de chaque image. Il est directement relié à la distance « vraie » de la source. Si la distribution de masse du déflecteur est alors connue, il est possible d'en déduire l'angle de déviation des rayons lumineux, c'est-à-dire la géométrie exacte du système source-lentille-observateur. L'ensemble de ces informations réunies permet une estimation directe de la constante de Hubble H_0 dans l'univers lointain.

Un tel décalage temporel a pu être déterminé dès 1989 par Christian Vanderriest pour le mirage 0957+561, surnommé historiquement le « Quasar Double ». Cette mesure était alors une première. Il manquait donc la détermination de la distribution de masse de la lentille. Dans ce cas précis, la lentille est complexe puisque composée de deux amas de galaxies peu riches. De plus, la galaxie centrale de l'amas le plus proche intervient de façon notable dans le processus de mirage. Avec Geneviève Soucail de l'Observatoire de Toulouse, j'ai effectué

[2] Kundic et al., ApJ, 1997, **487**, 42; Tonry, AJ, 1998, **115**, 1.

des mesures de dispersion de vitesses dans les galaxies du champ du « Quasar Double » afin de contraindre sa distribution de masse. La conclusion de cette étude est que la complexité de la lentille rend difficile l'estimation de contrainte pour la détermination de H_0 (Angonin-Willaime, Soucail et Vanderriest, 1994). Cette étude semble cependant donner favoriser une valeur particulièrement basse de cette constante (H_0 entre 60 et 62 $km.s^{-1}.Mpc^{-1}$). Les mesures effectuées sur d'autres mirages gravitationnels depuis ont confirmé cette tendance[3] vers des valeurs faibles de H_0 (autour de 70 $km.s^{-1}.Mpc^{-1}$), ce qui n'est pas en contradiction avec la plupart des mesures effectuées par d'autres techniques[4].

J'ai donc sélectionné, à ce moment-là, de nouvelles cibles pour cette étude parmi les mirages déjà connus sur des critères concernant la lentille, puis la source, avant d'en faire le suivi photométrique (phase la plus coûteuse du point de vue observationnel pour la mesure de H_0) (Angonin-Willaime, Hammer et Rigaut, 1993).

Observations de scintillations gravitationnelles et conséquences

Un autre phénomène, sur lequel je me suis penchée, est celui de la scintillation gravitationnelle ou microlensing sur les quasars. Lorsqu'une étoile passe dans la ligne de visée d'un quasar, elle induit un effet de "loupe" gravitationnelle qui permet d'atteindre la structure à petite échelle du quasar (structure du noyau et des régions l'entourant) par amplification différentielle des rayonnements caractéristiques de ces régions. L'observation du mirage quadruple H1413+117 en spectroscopie m'a permis de mettre en évidence de tels effets sur la source (Angonin, Vanderriest, Remy, Surdej, 1990). Ces observations ont une incidence sur la nature de la source, car ce mirage porte sur un quasar B.A.L. (possédant des Broad Absorption Lines[5]), catégorie encore mal connue. Cette étude a permis de poser des contraintes sur la taille des nuages de la région d'absorption large, par rapport à la taille caractéristique de l'effet de microlensing. Ces contraintes ont depuis été confirmées et l'idée de se servir des effets de microlensing pour en déduire les tailles des composantes de certains quasars fait depuis son chemin dans la littérature[6].

Avec Christian Vanderriest, j'ai aussi détecté des effets de scintillation sur le mirage quadruple PG1115+080 en faisant un suivi photométrique de cet objet de 1984 à 1992. Le phénomène s'est produit sur les deux composantes rapprochées de 0,5" sans que la spectrographie bidimensionnelle du système n'ait détecté de variation dans l'allure du spectre des composantes (Angonin-Willaime, Hammer et Rigaut, 1993). Ce phénomène est à prendre en compte lors du suivi photométrique de l'objet pour déterminer son décalage temporel.[7]

[3] Voir, par exemple : Schechter et al., ApJ, 1997, **475**, L85 ; Biggs et al., MNRAS, 1999, **304**, 349 ; Burud et al., ApJ, 2000, **544**, 117 ; et la revue de Kochanek et Schechter effectuée sur ce sujet en 2004 au Carnegie Observatories Centennial Symposia (Cambridge University Press).

[4] Par exemple : *Avec les Céphéïdes et les SNIa* : Altavilla et al., MNRAS, 2004, **349**-4, 1344 ; *Avec l'effet Sunyaev-Zel'dovich* : Reese, 2004, Carnegie Observatories Centennial Symposia (Cambridge University Press) ; *Avec les données WMAP* : Tegmark et al., 2004, PhRevD, **69**-10, 103501 ; Avec la relation de Tully-Fisher (galaxies spirales) et le plan fondamental (galaxies elliptiques) : Russell, 2002, ApJ**, 565**, 681.

[5] Le trou noir central et son disque, émetteurs de rayonnement continu, sont masqués par des nuages absorbants, proches, chauds et en rotation rapide autour du trou noir, d'où une large dispersion de vitesses.

[6] Voir à ce sujet, Lewis et Belle, MNRAS, 1998, **297**, 69 ; Lewis et Ibata, MNRAS, 2004, **348**, 562.

[7] Voir, par exemple, la discussion de Barkana, ApJ, 1997, **489**, 21.

Les arcs gravitationnels

Parallèlement à l'étude des mirages sur les quasars, je me suis aussi intéressée aux effets de grandes amplifications gravitationnelles sur les galaxies : les arcs géants. Les arcs géants et anneaux d'Einstein sont la conséquence de la distorsion d'un objet étendu (galaxie en optique, structures radio) par un déflecteur (amas de galaxies en optique). Ces phénomènes sont intéressants par les paramètres accessibles au travers de leur modélisation ; en effet, ces arcs géants correspondent aux configurations d'amplification maximale (les caustiques), ce qui permet de limiter au maximum les inconnues du système. Le but en est de définir précisément la distribution de matière dans le déflecteur. Cela nous amène directement au problème de la matière noire dont on fait, dans ce cas, une mesure "directe", c'est-à-dire non affectée par les effets de projections (contrairement aux mesures dynamiques), ni par des hypothèses sous-jacentes liées aux modèles (masse noire déduite des études de gaz X).

En reprenant un code numérique modélisant les effets de lentille gravitationnelle à partir de distributions de masses, j'ai développé le cas des lentilles à symétrie ellipsoïdale. J'ai pu ainsi étudier deux cas : les arcs dans l'amas d'Abell 963 et l'anneau MG J1131+0456 (Hammer, Angonin et al., 1991; Angonin, Hammer et Le Fèvre, 1992). L'étude observationnelle de cet anneau m'a amenée, dans un même temps, à identifier sa contrepartie optique et à obtenir un spectre de sa galaxie déflectrice. Ces études au cas par cas ont permis de mettre en évidence la présence au cœur des amas d'une composante de masse noire prédominante, non-liée aux galaxies et distribuée sur des échelles plus grandes que celle des galaxies.
Il parut alors nécessaire de généraliser ces résultats dans le but d'acquérir une fonction de masse des amas de galaxies. Dans ce but, un programme d'observations optiques au CFHT et au NTT/ESO d'un échantillon complet d'amas sélectionnés par leur forte luminosité X (collaboration entre l'Université d'Hawaï et Meudon: Hammer, Le Fèvre, Luppino, Gioia, Wu) nous a permis de faire des statistiques sur les effets de lentille de tels amas et de mettre en évidence les conséquences sur les distributions de masse de ces amas. Des résultats sur un échantillon de 40 amas montrent que la matière noire des amas riches doit être distribuée de manière très compacte au centre des amas (rayons de cœur de 50 à 100 kpc), condition remettant en cause le caractère relaxé et virialisé (hypothèse alors souvent utilisée) des cœurs des amas riches (Le Fèvre, Hammer, Angonin, Luppino et Gioia, 1994). Les observations ultérieures[8] de la distribution du gaz X de ces amas a donné des résultats tout à fait similaire, ce qui tend à prouver que, même dans les cas où les amas sont encore en train d'évoluer (par exemple s'il y a plusieurs composantes en coalescence), les effets de la masse noire sont les mêmes quelles que soit la méthode choisie pour les observer.

Bilan

La philosophie de l'étude des effets de lentilles gravitationnelles a évolué au cours des dix dernières années. Mon travail s'inscrivait dans le cadre d'un travail de précurseur : certains astronomes doutaient encore de l'existence des mirages gravitationnels lorsque j'ai débuté et affirmaient avec assurance que cela n'avait, de toutes façons, aucun intérêt[9]. Le but avoué de ces recherches était de vérifier la validité des prédictions théoriques formulées bien des années auparavant. Les progrès instrumentaux permettaient tout juste d'accéder aux premières observables alors nécessaires. En plus de la mesure de constantes cosmologiques

[8] Par exemple : Durret et al., A&A, 1994, **287**, 733.
[9] Pas de citation ici…mais je peux donner des noms !

ou de la distribution de la masse noire, les observations obtenues étaient alors des tests indirects de la gravitation et de la physique sous-jacente sur des échelles astrophysiques.

En une petite décennie, les moyens d'observations ont élargi la gamme de longueurs d'onde accessibles et ont acquis plusieurs ordres de grandeur en sensibilité et résolution spatiale faisant exploser le nombre de mirages gravitationnels et arcs géants connus, permettant la mesure du décalage temporel d'environ une dizaine de mirages ainsi que d'accéder à des effets de lentille gravitationnelle plus ténus tels que l'étude du cisaillement (shear). Il est remarquable de voir le grand nombre de publications qui ont trait à ce sujet ainsi que la fréquence des colloques et ateliers dans ce domaine, notamment le « workshop » qui aura lieu en décembre prochain à Santander en Espagne intitulé : « 25 years after the Discovery : Some current topics on lensed QSOs ». L'évolution rapide des instruments de mesure a transformé petit à petit des observations ponctuelles en une course au plus grand nombre de lentilles observées aboutissant à des sondages systématiques d'effets statistiques ou des catalogues complets de mirages.

L'effet positif de cela est que les effets de lentille gravitationnelle semblent complètement assimilés dans tout sondage du ciel profond quelle qu'en soit la longueur d'onde. On ne parle plus de galaxie lointaine sans en faire mention. La présence de masse noire même à grand redshift dans des proportions identiques à celle mesurée par d'autres méthodes est un fait acquis. La mesure de la constante de Hubble par cette technique a obtenu un statut à part entière, au même niveau que les techniques plus usuelles.

Cependant, le fait d'accéder à une étude plus globale et statistique du phénomène devrait permettre de poser de nouvelles interrogations et de rechercher de nouvelles façons d'utiliser cet outil pour le moins unique. Un retour des observations vers la physique fondamentale théorique devrait pouvoir s'établir. Les observations des lentilles gravitationnelles devraient constituer, dans un avenir proche, un moyen de tester les grands principes[10], de contraindre la distribution de masse noire à l'échelle stellaire[11] ou encore de tester les théories de gravitation[12]. Ces questions semblent encore loin des préoccupations observationnelles actuelles. Je ne m'attarderai donc pas plus longuement dessus. Elles constituent simplement des exemples de sujets potentiellement à développer. En ce qui me concerne, je me suis intéressée à un autre problème : celui de l'utilisation du phénomène de lentilles gravitationnelles dans le cadre d'observations faites avec des ondes gravitationnelles, technique observationnelle qui devrait poindre dans les années à venir.

---

[10] Dans le phénomène de lentille gravitationnelle, la détermination de la distribution de la masse (noire ou non) est faite à partir de la déviation des photons. Les résultats obtenus par différentes modélisations et observations semblent converger sur le fait que la distribution est identique à celle obtenue à partir d'effets gravitationnels sur les baryons (mesures de dispersion de vitesses de galaxies, mesures à partir de l'équilibre hydrostatique du gaz X). A-t-on atteint suffisamment de contraintes pour pouvoir tester certains principes d'équivalence ?

[11] Les mesures de lentilles gravitationnelles ont jusqu'à présent confirmé l'existence de la masse noire aux échelles des galaxies et des amas de galaxies. A l'heure où l'effet Pioneer pose la question de la distribution de masse noire à l'échelle du système solaire et où les théories stellaires ne nécessitent pas de masse noire à l'échelle des étoiles, est-ce que les mesures de microlensing peuvent contraindre la distribution de masse noire dans des systèmes stellaires ?

[12] Les mesures de la constante de Hubble par une dizaine de mirages gravitationnels semblent privilégier systématiquement des valeurs faibles de cette constante, résultat qui ne correspond pas aux valeurs obtenues dans l'univers local. Quelle est l'origine de cet effet ? Est-ce un effet cosmologique (variation de la constante) ? Un effet de biais observationnel, ainsi que le suggèrent Alcock et Anderson (ApJ, 1985, **291**, L29) en faisant remarquer que la configuration des objets d'avant-plan est particulière pour les mirages gravitationnels, ou bien un effet plus fondamental à chercher dans les théories de gravitation ?

ARTICLES SUR LES LENTILLES GRAVITATIONNELLES.

(par ordre chronologique)

- Angonin M-C, Vanderriest C, Remy M, Surdej J, 1990, Astronomy and Astrophysics, **233**, L5 : *First spectroscopic evidence of microlensing on a BAL quasar? The case of H 1413+117*

- Hammer F, Angonin MC, Le Fèvre O, Meylan G, Smette A, Surdej J, 1991, Astronomy and Astrophysics, **250**, L5 : *MG 1131+0456: discovery of the optical Einstein ring with the NTT*

- Vanderriest C, Angonin M-C, 1992, dans "Gravitational lenses" colloque de Hambourg de septembre 1991, Lectures Notes in Physics, **406**, 97 : *Bidimensional spectrography of multiple quasars*

- Angonin-Willaime M-C, Hammer F et Rigaut F, 1993, proceedings du colloque de Liège: Gravitational lenses, 85 : *Ground-based optical observation of gravitational lenses*

- Angonin-Willaime M-C, Vanderriest C, Hammer F, Magain P, 1994, Astronomy and Astrophysics, **281**, 388 : *Further observational evidence that MG J0414+0534 is a gravitational mirage*

+ *Erratum* : 1994, Astronomy and Astrophysics, **292**, 722

- Le Fèvre O, Hammer F, Angonin M-C, Gioia I, Luppino G, 1994, Astrophysical Journal, **422**, L5 : *Imaging of 16 distant EMSS clusters with $z \geq 0.2$ and $L_{X,44} \geq 4$: new arcs and first consequences*

- Angonin-Willaime M-C, Soucail G, Vanderriest C, 1994, Astronomy and Astrophysics, **291**, 411 : *Gravitational lensing on Q0957+561: A study of the cluster at z=0.355*

- Hammer F, Rigaut F, Angonin-Willaime M-C, 1995, Astronomy and Astrophysics, **298**, 737 : *Imaging and spectroscopy of B 1422+231 at C.F.H.T.: identification of the mirage and of the lensing galaxy at z= 0.647*

- Angonin-Willaime M-C, Vanderriest C, Courbin F, Burud I, Magain P, Rigaut F, 1999, Astronomy and Astrophysics, **347**, 434 : *About the origin of extinction in the gravitational lens system MG J0414+0534*.

First spectroscopic evidence of microlensing on a BAL quasar? The case of H 1413+117
Angonin M-C, Vanderriest C, Remy M, Surdej J, 1990, Astronomy and Astrophysics, 233, L5

Astron. Astrophys. 233, L5–L8 (1990)

Letter to the Editor

ASTRONOMY AND ASTROPHYSICS

First spectroscopic evidence of microlensing on a BAL quasar? The case of H 1413+117 ⋆

M.-C. Angonin [1], M. Remy [2], J. Surdej [2], and C. Vanderriest [1]

[1] Observatoire de Paris-Meudon (DAEC) et U.R.A. 173 du CNRS, 5 place Janssen, F-92195 Meudon Cedex, France
[2] Institut d'Astrophysique, Université de Liège, Avenue de Cointe, 5, B-4200 Ougrée-Liège, Belgium

Received April 12, accepted April 24, 1990

Abstract:

We have obtained, under optimal seeing conditions ($\simeq$ 0.6" FWHM), new data for the quadruply lensed quasar *H* 1413 + 117 using the bidimensional spectrograph SILFID at the C.F.H. telescope. The spectra recorded for each of the four individual images turn out to be quite similar, except for the narrow absorption line systems (probably related to the lenses) seen in images A and B and for marked differences in the spectrum of image D. When compared to the 3 other images, the spectrum of D shows smaller values for the emission lines/continuum ratio and a larger equivalent width for absorption features located in the blueshifted P Cygni profile.

We discuss briefly the possible explanations of these observations in terms of micro-lensing and/or intrinsic variability of the source.

Key-words:
Quasars (*H* 1413 + 117), gravitation, observational methods, spectroscopy.

1. Introduction:

The BAL quasar *H* 1413 + 117 has been resolved at optical wavelengths in 4 images having comparable brightness and forming a tight, nearly square, configuration (hence the nickname "clover leaf "). The great similarity existing between the spectra of the 2 most separated images (B, C) and the global spectrum strongly suggested that it is a new case of gravitational lensing (Magain et al., 1988) . However, the compactness of the "clover leaf" has precluded to obtain until now uncontaminated spectra of the 4 images.

We tried to resolve this problem with the help of the bidimensional spectrograph SILFID (Vanderriest et al., 1987; Vanderriest and Lemonnier, 1988) at the Cassegrain focus of the Canada-France-Hawaii telescope. The aim of this letter is to present and discuss the data obtained under optimal seeing conditions with this instrumentation.

Send offprint requests to: M.-C. Angonin
(*) Based on observations made at the Canada-France-Hawaii telescope (Hawaii).

2. Observations:

With SILFID, transforming the 2 spatial dimensions of the focal image of the telescope into a single one (the slit of the spectrograph) is achieved by means of a short fibre optics device: in the focal plane, about 400 fibres are closely packed into an hexagonal array and, at the other end of the device, they are just set in line to form a pseudo "slit". Following the dispersion, we may apply the exactly inverse geometrical transformation in order to reconstruct crude pictures of the object at any chosen wavelength.

Our spectra were obtained on 7 March 1989 during a period of strong wind, but very good seeing. Just in front of the fibre device, a small lens extended the focal length of the telescope so that each 100μm diameter fibre subtended 0.33 arcsec on the sky. The scale is 60μm per fibre on the detector (a Ford CCD with $(512)^2$ pixels of 20μm).

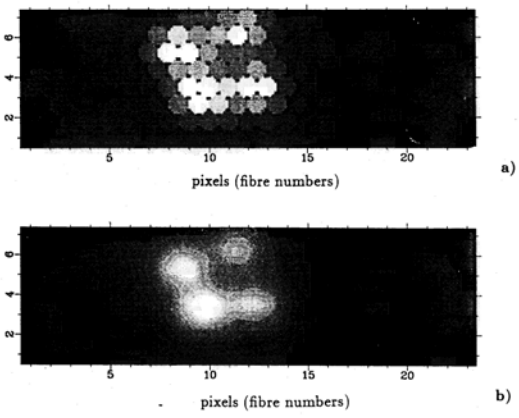

Figure 1:
The field of *H* 1413 + 117 reconstructed from bidimensional spectroscopic data (30 min. exposure at 235 Å/mm).
-a) Direct reconstruction in the wavelength range 4800 - 6600 Å showing the fibre array.
-b) The same picture smoothed with a gaussian filter (FWHM $\simeq$ 0.15").

Fig. 1*a* displays a reconstructed picture in the wavelength range $\simeq 4800-6600$ Å and shows how the fibres were lightened by the object in the focal plane of the telescope. As the size of the CCD did not allow to cover the whole slit length, only about 1/3 of the initial hexagonal field could be reconstructed (160 useful fibres). We see that, even at 0.33" per fibre, the spatial sampling is still too coarse. On the smoothed picture (fig. 1*b*), the average size of the images is about 0.6" (FWHM), corresponding to an initial seeing of the order of 0.5".

Analysing the reconstructed picture, we could select those fibres whose data can be safely added for obtaining the spectra of each of the 4 images A, B, C and D with a minimum of contamination (<10%). This led to disregard many fibres fed with "mixed" light from 2 or more images. The possibility of such an *a posteriori* choice provides the best S/N ratio for a given seeing. Fig. 2 displays the spectra obtained in this way from the sum of two 30 min. exposures at 235 Å/mm. The spectrophotometric standard Feige 67 (Massey et al., 1988), observed in the same conditions with SILFID, provided the flux calibration. Multiplying by a V filter response, one find a global magnitude for the system of 4 images: $V = 17.10 \pm 0.05$.

3. Results:

First of all, we see that the overall shapes of the spectra extracted for each single image are very similar to each other, strengthening the gravitational lensing interpretation for the clover-leaf. The narrow absorption lines, already recognized by Magain et al. (1988) as belonging to two systems at redshifts 1.438 and 1.661, are seen with different intensities in the 4 spectra. Within the limit of accuracy fixed by the data noise, they are absent in image C and hardly significant in D. If we interpret these absorptions as arising in two lensing galaxies, our present data may help in locating these with respect to the 4 images. But direct imaging of the lenses would certainly be more secure.

In hope of detecting the deflectors, we tried to take advantage of the deep C IV absorption trough that reduces the intensity of the quasar almost to zero near 5400 Å. We have thus reconstructed an image within a 32 Å bandwidth around this wavelength but could set only an upper limit to the flux of the deflector corresponding to $V \geq 23.5$. This is not a very stringent constraint since at $z \simeq 1.5$, the deflectors could be 1 or 2 magnitudes fainter than this limit, their masses being of the order of $10^{11} M_{\odot}$ (Magain et al., 1988; Kayser et al., 1989).

Another major spectral difference between the four images may be noticed after inspection of Fig. 2. Indeed, with respect to images A, B and C, the continuum of D is found to be marginally bluer and its ratio to the emission line fluxes is greater. Moreover, specific absorption features in the BAL line profiles appear to be significantly stronger in image D than in the three other images (see the arrows in Fig. 2). One of these features corresponds certainly to the C IV absorption component located at about -8500 km/s from the center of the emission line and reported to be possibly variable, in the integrated spectrum of $H\,1413+117$ over a 4-year period, by Turnshek et al. (1988). This absorption feature is also seen at the same relative velocity in the Si IV and Al III 1857 Å P Cygni profiles.

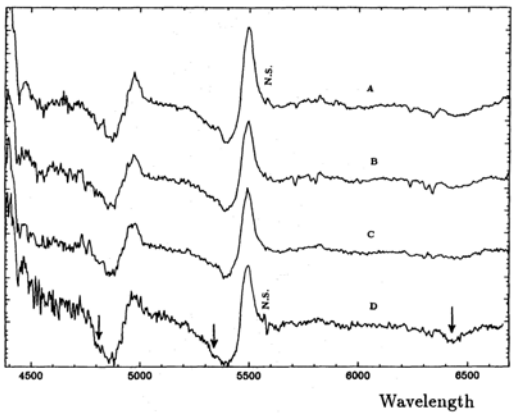

Figure 2:
Spectra of the 4 images extracted from the low dispersion data (sum of two 30 min. exposures, 235 Å/mm, resolution $\simeq$ 12 Å). The vertical scale has been shifted for clarity between each spectrum. N.S. stands for poor Night Sky line subtraction. Note the differences in the structure of the BAL troughs for image D (arrows).

4. Discussion:

There are at least two obvious ways to account for these observed spectral differences.

-a) If real, the difference in the slope of the continuum of D suggests a possible intrinsic variation of the source. The spectral difference observed in the BAL trough between images D and A, B, C could also be explained this way. The equivalent widths of similar features (Al III 1857 Å and high velocity components due to Si IV and C IV) have also been found to be variable in another BAL quasar, UM 232 (Barlow et al.,1989), in apparent correlation with the ionizing flux of the central source. In such a scenario, the characteristics observed for D should be exactly reproduced in the spectra of the other images, with shifts in time characterizing the geometry and mass distribution of the lensing system. For $H\,1413+117$, these time delays are expected to be of the order of a few days or weeks, but their exact values and even their signs are very much model dependent (see Kayser et al., 1989).

The flux of image D seems to be indeed variable. Kayser et al. (1990) have reported a fading of D, with respect to the other images, of $\simeq$ 0.15 mag between their observations and those of Magain et al. (1988), recorded 6 weeks earlier. Prior to the bidimensional spectroscopy described above, we also took a 5 min. direct R CCD frame of $H\,1413+117$ on the night of 7 march 1989. This CCD frame is essentially of good quality and it was straightforward to fit, in the least squares sense, the observed images of the clover leaf system using a four-component Moffat star profile. Fortunately, we could make use of a nearby and well exposed star image in order to determine the three unknown parameters of the single Moffat PSF. Furthermore, the finite size of the pixels was taken into account in the present fitting procedure (Remy and Magain, in preparation).

Table 1: Photometric data:
Intensity ratios of the B, C and D images relative to A. The 08/03/1988 and 07/03/1989 data have been obtained in the R band; the values taken on 27/04/1988 refer to the average of 3 colours B, R and I.

image :	08/03/1988 (*Magain et al.*)	27/04/1988 (*Kayser et al.*)	07/03/1989 (*this work*)
B	0.87	0.87	0.88 ± 0.02
C	0.76	0.77	0.78 ± 0.02
D	0.69	0.60	0.66 ± 0.02

The derived flux ratios for images B, C and D with respect to A are reported in Table 1 and may be compared with previous determinations. The flux level observed for D on 7 march 1989 appears to lie between the two previous measurements by Magain et al. (1988) and Kayser et al. (1990).

In any case, these observed variations seem to be too small for inducing appreciable changes in the ionization level of the BAL clouds.

-b) As already suggested by Kayser et al. (1990) on the sole basis of photometric variations, it is more likely that micro-lensing effects do exist in image D. We suggest that they could be responsible for the observed departures from the spectra of the other images. Knowing that micro-lensing effects are highly dependent on the source's size (see e.g. Kayser et al., 1986), we understand easily that if a star or group of stars, located in one of the lensing galaxies, come in front of the QSO's nucleus, it will lead to a significant magnification of the quasi-stellar continuum without (almost) affecting the broad spectral emission lines formed in the much larger BEL region. This now "classical" effect (see e.g. Rees, 1981) is suspected to be at work in several gravitational lenses and provides a straightforward explanation for the different equivalent widths of similar BELs observed in the spectra of the four lensed images of $H\,1413+117$ (cf. Fig. 2). The same explanation holds for the BALs: if the continuum source is being "resolved" by the microlens and if the BAL region is highly inhomogeneous on such scales, the star will then preferentially magnify one of the BAL components that happens to occult only a part of the continuum core.

Let R_e be the angular critical radius of the microlens. This represents also the typical length of the microlensing magnification gradient. An observable differential effect will take place if two conditions are fulfilled:

-(1) $\quad d_{cont} \not\ll R_e$

-(2) $\quad d_{abs} < d_{cont}$

where d_{cont} is the diameter of the continuum source and d_{abs} the equivalent diameter of the part heavily absorbed by the BAL clouds at the considered wavelength.

For a star of 1 $M_\odot$ in the lensing galaxy (supposed to be at $z \simeq 1.5$), R_e is found to be about 3.10^{-2} pc at the distance of the source. According to the different models, the order of magnitude of d_{cont} is only roughly estimated, from a few 10^{-3} pc to about 1 pc (see for instance Drew and Giddings, 1982), so that inequality (1) is more or less fulfilled; on the other hand, the diameter of the absorbing clouds is not believed to be much larger than d_{cont}, making easy to also fulfill (2) in a random projection of such clouds over the continuum core.

A good way of testing the likelihood of the differential absorption mechanism due to microlensing is to investigate whether the spectrum of image D may be reproduced by a straightforward combination of both a macro-lensing and micro-lensing contributions. In order to check this, we built a "synthetic" spectrum $F_S(\lambda)$ (with S equal to the sum A+B+C cleared of the narrow absorption lines) and, neglecting completely microlensing for the emission lines, we can represent the spectrum $F_D(\lambda)$ of D by:

$$F_D(\lambda) = k\, F_S(\lambda) + k'\, I_c(\lambda)\ R(\lambda)\ e^{-\tau'(\lambda)} \qquad (3)$$

where k (resp. k') is a constant representing an effective amplification of image D due to macro-lensing (resp. micro-lensing), $I_c(\lambda)$ is the underlying QSO continuum observed in spectrum S, $R(\lambda)$ is a wavelength dependent factor correcting for the possibly different shape of the continuum spectrum emitted by the region of the QSO which is magnified by the micro-lens and $\tau'(\lambda)$ is the opacity of this particular region as a function of wavelength. Similarly, we assume that the spectrum of S may be described by the following expression:

$$F_S(\lambda) = I_c(\lambda)\, e^{-\tau(\lambda)} + E(\lambda) \qquad (4)$$

where $\tau(\lambda)$ stands for the opacity, at wavelength λ, of the expanding envelope projected against the whole QSO core along the line-of-sight and where $E(\lambda)$ is the profile of the emission line component. Fitting the spectra of D and S by means of Eqs. (3) and (4) leads to the following best parameter estimates: k = 0.15, k' = 0.07 and $R(\lambda)$ is found to be an almost linear function of λ such that R(5500) = 1 and R(4500) = 2.1. Such values correspond to a moderate differential magnification: with respect to the macro-lensing contribution, it is as if micro-lensing brightens the QSO continuum of D by $\simeq 0.4$ mag. The resulting attenuation factor $e^{-\tau'(\lambda)}$ derived from this spectral decomposition is illustrated in Fig. 3. For comparison, we have also plotted in this figure the profile $F_S(\lambda)/I_c(\lambda)$. Referring to the absorption line profiles in Fig. 3, we see that at least three discrete absorption components located at about $-3\,870$ (C IV and Si IV), $-7\,750$ (C IV, Si IV and Al III) and $-12\,330$ km/s (just C IV) from the center of their corresponding emission line have been enhanced by micro-lensing effects in the spectrum of image D. More details about these observations and the spectral decomposition will be published elsewhere.

So, the hypothesis of differential microlensing is a viable interpretation of the observed spectral differences between the faintest and the three other lensed images of $H\,1413+117$. However, a definite proof is yet to be found. In broad band photometry, image D should display a light curve characteristic of micro-lensing events. We may also predict that the continuum of image D shoud be differently (probably more) polarized than that of the other three images. An even better proof would be to detect spectral variability in the BAL troughs, reflecting the star(s) motion in front of the BAL clouds. It is quite possible that Turnshek et al. (1988) have witnessed such an event between 1981 and 1985, even if centering of the 4 images (not yet resolved at that time) in the spectrograph slit can also be partly incriminated. We may of course predict that the enhancement of the blue component(s) should not last during the whole

transit of the lensing star(s); at some phase, it should be replaced by a weakening.

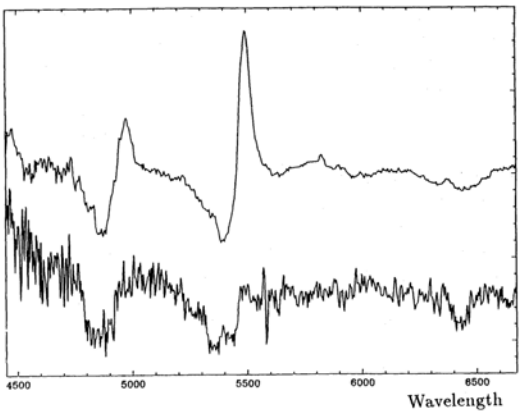

Figure 3:
Because of micro-lensing effects, the attenuation factor $e^{-\tau'(\lambda)}$, calculated by means of Eqs. (3) and (4), accounts for the additional absorption components seen in the P Cygni profiles of image D. It is represented here as a function of λ. We have also illustrated in this figure the profile $F_S(\lambda)/I_e$ whose blue wing gives a good representation of the attenuation factor $e^{-\tau(\lambda)}$ (cf. Eq(4)).

5. Conclusions:

Our bidimensional spectroscopic data strengthen the interpretation of $H\,1413+117$ as a gravitational mirage. The differences observed in the spectrum of image D are either due to intrinsic variations of the source, or to a differential microlensing effect operating on the BAL clouds. We personally favour this second interpretation. In this context, it is therefore quite possible that the spectroscopic variations reported in the integrated image of $H\,1413+117$ by Turnshek et al. (1988) are not intrinsic to the BAL quasar but caused by a mirage effect. Spectroscopic monitoring of the 4 images will help in discriminating between these various possible scenarios.

Detailed modeling of this gravitational lens system was of course beyond the scope of the present letter; it would even be premature to do so considering the paucity of the relevant data (cf. the still unknown precise location(s) and type of the lenses, etc.). We just wished to present here new high angular resolution spectroscopic observations of the clover leaf and to attract the attention of potential observers on the interest and importance of getting further bidimensional spectroscopy of this object, with comparable or better spectral and spatial resolutions.

$H\,1413+117$ has an unprecedented status, being at the same time a BAL quasar and a gravitational mirage. While it is believed that gravitational mirages of "normal" QSOs could help to improve our knowledge on their structure, we bet that the clover leaf will turn out to be a unique tool in order to better understand the BAL phenomenon itself.

References:

- Barlow T., Junkkarinen V., Burbidge M., 1989, Astrophys. J., **347**, 674.
- Drew J., Giddings J., 1982, Mon. Not. Roy. Astron. Soc., **201**, 27.
- Kayser R., Refsdal S., Stabell R., 1986, Astron. Astrophys., **166**, 36.
- Kayser R., Surdej J., Condon J.J., Hazard C., Kellermann K.I., Magain P., Remy M., Smette A., 1990, Astrophys. J., in press.
- Magain P., Surdej J., Swings J.P., Borgeest U., Kayser R., Kühr H., Refsdal S. & Remy M., 1988, Nature, **334**, 325.
- Massey P., Strobel K., Barnes J., Anderson E., 1988, Astrophys. J., **328**,315.
- Rees M., 1981, ESO conf. *"Scientific importance of high angular resolution at Infrared and Optical wavelengths "*, M.H. Ulrich, K. Kjär eds., p.423.
- Turnshek D., Foltz C., Grillmair C., Weymann R., 1988, Astrophys. J., **325**, 651.
- Vanderriest C., Haddad B., Lemonnier J.P., 1987, Annales Phys. Fr., Suppl. **5**, vol. 12, 207.
- Vanderriest C., Lemonnier J.P., 1988, "Instrumentation in Astronomy", proc. IXth Santa Cruz workshop, 304.

MG 1131+0456: discovery of the optical Einstein ring with the NTT

Hammer F, Angonin MC, Le Fèvre O, Meylan G, Smette A, Surdej J, 1991, Astronomy and Astrophysics, 250, L5

Astron. Astrophys. 250, L5–L8 (1991)

ASTRONOMY AND ASTROPHYSICS

Letter to the Editor

MG1131+0456: discovery of the optical Einstein ring with the NTT

F. Hammer[1], O. Le Fèvre[1,2], M.C. Angonin[1], G. Meylan[3], A. Smette[4], and J. Surdej[5,]**

[1] DAEC, Observatoire de Paris-Meudon, F-92195 Meudon Cedex, France
[2] Canada-France-Hawaii Telescope Corporation, P.O. Box 1597, Kamuela, HI 96743, USA
[3] Space Telescope Science Institute, 3700 San Martin Dr., Baltimore, MD 21218-301, USA
[4] European Southern Observatory, Karl-Schwarzschild-Strasse 2, W-8046 Garching bei München, Federal Republic of Germany
[5] Institut d'Astrophysique, Université de Liège, Avenue de Cointe, 5, B-4200 Cointe-Ougree, Belgium

Received June 13, accepted July 23, 1991

Abstract Deep optical imaging and spectroscopy have been obtained for the well known radio Einstein ring MG1131+0456 with the ESO/NTT. The direct CCD frames show a red emission excess at the exact location of the radio ring. Subsequent subtraction of the lensing galaxy, assumed to be an elliptical galaxy, results in the detection of an optical ring which is strikingly similar to the radio ring. Gravitational lensing models, including source reconstruction, predicts that the source is likely a radio-galaxy for which both the optical and extended radio emissions are sufficiently distorted by the foreground lensing galaxy as to produce a nearly complete ring. Our spectroscopy and broad band photometry suggest that the lensing galaxy has a spectral energy distribution typical of a non evolved elliptical, tentatively at z=0.85. The radio-galaxy associated with the radio-ring is likely to be an elliptical at larger redshift, tentatively z=1.13.

Keywords: cosmology — gravitational lenses — galaxies: general — MG1131+0456

1. Introduction

Since the discovery of the first gravitational mirage for the QSO 0957+561 by Walsh et al (1979), observers have identified a large variety of lensing phenomena. The most striking examples are the splitting of QSOs into four images (e.g. Huchra et al, 1985; Magain et al, 1988), the gravitational distortion of faint distant galaxies into giant arcs by foreground rich clusters (Lynds and Petrosian, 1986; Soucail et al, 1987) and the nearly perfect Einstein rings detected at radio wavelengths (Hewitt et al, 1988; Langston et al, 1989). Obviously the unusual morphologies observed for the above images were at the basis of their identifications as gravitational lensing events. They probably correspond to the top and visible tail of the lensing phenomena —strong lensing events — and it is very likely that a larger number of (still) unknown lensing events remain to be discovered.

Radio ring observations fit well with this idea. They are likely caused by the close alignment between a distant extended radio source and a foreground and massive lensing galaxy. They illustrate well the early prediction by Zwicky (1937) that massive galaxies constitute efficient lenses. However, such phenomenon would be nearly impossible to detect at optical wavelengths because the Einstein ring (radius smaller than 1" if the lensing galaxy mass is about $10^{12}M_{\odot}$ and lies at z= 0.5) should be blended with the lensing galaxy image (Hammer, 1987). At radio wavelengths, beautiful rings are produced by radio quiet lensing galaxies. Two such rings were discovered by means of a systematic survey of more than 6000 sources carried out with the VLA (Bennett et al., 1986). As stated by Kochanek (1991), the low rate of success is probably due to observational limits. Indeed, radio sources are expected to be affected by lensing because of the steep slope of the radio luminosity function, especially at its brightest end. The reality of such effects was demonstrated statistically from observations of a sample of high redshift galaxies from the 3CR catalog for which an excess of foreground massive galaxies and clusters has been found (Hammer and Le Fèvre, 1990).

We present in this letter new optical observations of the field around the radio ring MG 1131+0456, obtained with the ESO/NTT in the course of the "gravitational lensing" ESO key program.

2. Observations

2.1 Detection of the optical counterpart of MG1131+0456

The deflecting galaxy was readily identified by Hewitt et al. (1990) and by Gladisher et al. (1990, preprint), and we set to obtain better S/N in order to detect the optical counterpart of the source. Images of the field around MG1131+0456, in B, V, R, and Gunn *i*, were taken in February and May 1990 with the ESO/NTT and the imaging spectrograph EFOSC2 with a 1024^2 pixels Thomson CCD providing a plate scale of 0.164 arcsec/pixel. Exposures of 20 min in B, 20 min in V, 75 min in R and 55 min in Gunn *i* were taken under photometric conditions and with an image quality between 0.7 and 1.0 arcsec FWHM, as measured on the individual frames. Only an upper limit to the B magnitude of the optical counterpart of MG11331+0456 could be derived, due to the faintness of the source and because of the poor CCD sensitivity in the blue spectral range. However, the source was clearly detected in V, R and Gunn *i*: Figures 1 a to c show the final processed (and co-added when applicable) CCD frames as well as the sum of the R and *i* images. We measured the following magnitudes, as derived from observations of standard stars in the E3 and E5 fields (Graham, 1982), B>25, V=22.66±0.25, R=22.14±0.07, *i*=20.67±0.08.

It is clearly obvious, particularly from the R and *i* images, that the optical image of MG1131+0456 is quite extended and different from what is expected for the surface brightness of normal galaxies. Of special interest is the surface brightness excess observed at a distance 1.0<r<2.1 arcsec from the central peak, corresponding to the expected location of the radio ring. Figure 2 shows a radial plot of the pixel intensities observed in the sum of the R and Gunn *i* images; the emission excess is apparent at a distance between 1.0 and 2.1 arcsec from the peak emission at flux levels of μ_{R+i}=24.1 mag/arcsec^2 (S/N>5). One can also note that this flux excess increases from V to *i*.

* Based on observations obtained at the European Southern Observatory, La Silla, Chile in the framework of the "gravitational lensing" key program.
** Also, Chercheur Qualifié au Fond National de la Recherche Scientifique (Belgium)

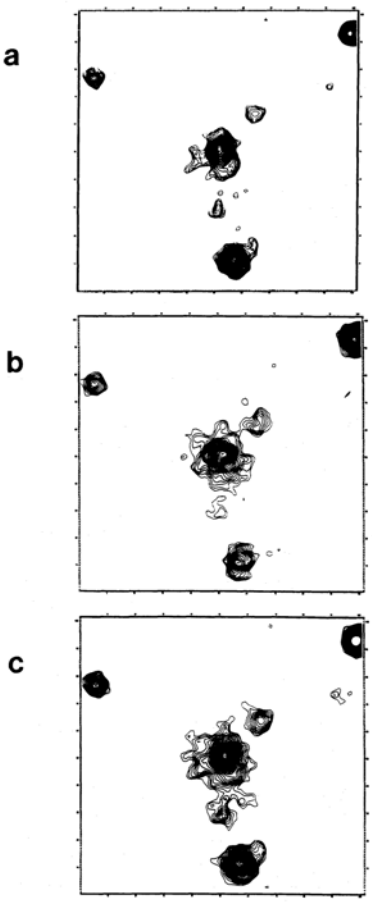

Figure 1 MG1131+0456 ESO/NTT direct imagery: *(a)* Sum of the R images, 75 min total integration, FWHM=0.80"; *(b)* Sum of the *i* images, 55 min. total integration, FWHM=0.95"; *(c)* Sum of the R and *i* images

To better show the spatial location of this luminosity excess, we built a galaxy model image with a $r^{1/4}$ luminosity profile that we later subtracted from the data. We set the peak intensity the same as the central peak intensity of the MG1131+0456 optical counterpart, and we built a set of galaxy models with axis ratios between 0.5 and 1.0 and position angles between 0 and 90° (every 15°), each with effective radii between 0.25 and 1 arcsec (2.5 to 10 kpc if the deflector is at z~0.85, see below). We then subtracted it from our R+*i* image. The best fit to the data was produced for $0.4<r_{eff}<0.6$ arcsec with an axis ratio of 0.8 and a position angle of 36° NW. One must note that by increasing r_{eff}, it was not possible to subtract satisfactorily both the central emission and the emission excess between 1 and 2.1 arcseconds from the peak, and that the model fit to the data was degraded both for the inner 1 arcsec radius and for radii larger than 2.1 arcsec. The result of subtracting a galaxy model with r_{eff}=0.5 arcsec, with a magnitude *i*=21.4, which provides the best fit to the data, is shown in Figure 3, and the corresponding luminosity profile is plotted in Figure 2. Hubble profiles were also used to built model galaxies: they provided slightly worse fit to the data (Figure 2). The residual emission has the shape of a ring, with a S/N of 3 to 10, and an integrated magnitude *i*=21.5. It shows a morphology and location very similar to the radio ring: in particular the North-West gap in the optical emission matches very closely the gap observed in the radio emission (see Figures 1 and 2 in Hewitt et al., 1988). This indicates that the source is an extended object, probably a radio-galaxy. Note that the model parameters for the deflecting galaxy have been checked for consistency against the parameters derived from the gravitational lensing modelling: they are very close to what was used in the model of Kochanek et al. (1989) as well as to our model parameters (see section 3).

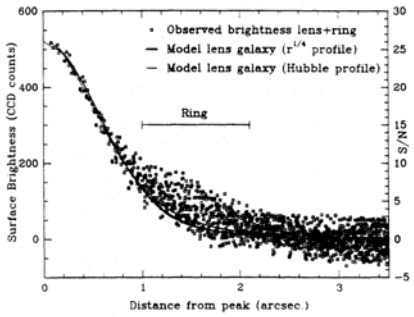

Figure 2 Radial plot of the pixel's intensities in the R+*i* image, centered on the peak intensity. Note the presence of a light excess for radii between 1 and 2.1 arcsec. The best elliptical galaxy model shown as the heavy solid line was built with a $r^{1/4}$ luminosity profile with r_{eff}=0.5", the light line is the best galaxy model built with a Hubble profile; both of them convolved with the PSF

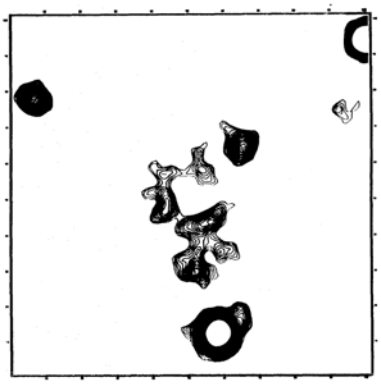

Figure 3 Result of the subtraction of an elliptical galaxy model with a $r^{1/4}$ luminosity profile with r_{eff}=0.5", an axis ratio of 0.8 at a P.A. of 36° NW. The residual image has the shape of a ring; note the gap to the NW, corresponding to the gap observed in the radio ring. The lowest isophote has a S/N=3, and the S/N is increasing by 0.3 between successive isophotes

2.2 Spectroscopy

Low resolution spectroscopy was obtained in February 1990. A red grism provided a spectral coverage between 5000Å and 9300 Å, and a slit of 1.1 arcsec (indicated on figure 1.b) produced an

instrumental resolution of ~50 Å. Integrations of twice 40 min and 30 min were obtained under photometric conditions with an image quality of 0.9" FWHM, the location of the object on the CCD being shifted by ~10 arcsec between successive exposure. Spectra were processed in a standard way using the NOAO/longslit package within the NOAO/IRAF data reduction facilities, and were registered and then co-added to produce the final spectrum displayed in figure 4.

The spectrum of the optical emission associated with MG 1131+0456 is probably due to the blend of both the lens and source spectra: it is featureless, no emission lines are present between 5000 Å and 9300 Å, but it shows a very red continuum consistent with our photometric results. We tentatively note the presence of two breaks in the red part of the continuum at 7400 Å and at 8550 Å. Although their significance are low (S/N ~ 2–2.5), they are not simple artifacts due to the sky-substraction. The recorded spectrum is similar to the spectra of bright ellipticals in distant clusters (z= 0.70– 0.92, Oke, 1984) as well as to the spectrum of the lensing galaxy (z = 1.01) responsible for the multiple images of the QSO 2016+112 (Schneider et al, 1986). The photometric data from B to I suggest changes of the continuum slope between the V and R filters, and even more between the R and I filters and therefore supports the spectroscopic data. The V image is compact, and shows no or little extra emission at the location of the radio ring. It also shares the same peak location as in the other colors. Taken altogether, these properties suggest that the lens spectrum may be responsible for the break at 7400 Å and could be an elliptical galaxy at z= 0.85. This hypothesis is highly consistent with the lensing scenario since: (i) the lens should be a massive galaxy in order to distort gravitationally the background radio source (see next section); (ii) our best substraction is provided for a r_{eff}=5kpc elliptical lens with R= 22.6, which would correspond at z=0.85 to M_B= —21.7 (k-corrected, H_0= 50 km/s/Mpc); (iii) ellipticity and P.A. of the V image are consistent with what Kochanek et al (1989) needed in order to reproduce the north-west gap in the radio ring at 15 GHz.

The absence of emission lines excludes that the MG 1131+0456 source is a radio-galaxy similar to the distant and powerful radio-galaxies as found in the 3CR catalogue. Moreover, the excess of emission associated with the optical ring is much more significant in the I filter than in the R filter. Therefore the background radio-galaxy is likely a radio loud elliptical which might be at z=1.13 if one associates the 8550 Å break with the 4000 Å break at rest. Such a redshift for the source is very speculative and need confirmation from further observations.

3. Reconstruction of the optical and radio sources: lensing model

The gravitational lensing model used here is described by Hammer and Rigaut (1989). The lensing galaxy is assumed to follow a $r^{1/4}$ surface density profile and to be located at z=0.85. Homoeidal symmetry (Schramm, 1989) allows our model to account for the ellipticity of the lensing mass distribution without any a priori assumptions on the associated potential (Angonin et al, in preparation). The first step is to estimate the lensing parameters from the modelling of the radio ring: for simplicity we have assumed a core plus jet morphology for the source (assumed to be at z=1.13). Other combinations of lens and source redshifts would simply change the characteristic lensing mass by a scaling factor. Figure 5 shows the result of the model which best fits the radio ring at 5 GHz (Hewitt et al, 1988). However, similarly to the Kochanek et al. (1989) results, either the modeled ring is too round or the splitting of the radio core is not well reproduced. This

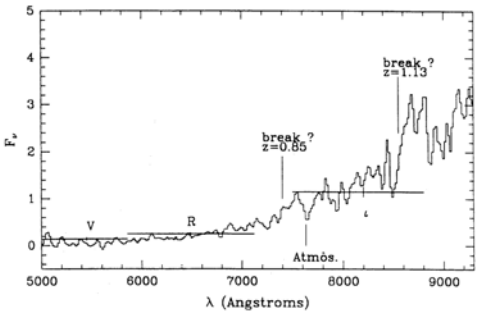

Figure 4 ESO/NTT spectrum recorded for the optical counterpart of MG1131+0456. The total integration time was 110 min. The horizontal bars represent the relative flux levels as derived from our photometric data

may arise because of the presence of another lens such as a cluster around the lensing galaxy, but not centered on it. No evidence for such a cluster had been found from our deep R and *i* exposures, although these bandpasses are not well suited to identify a z~0.8 cluster. The following step was to use this model to fit the optical ring and then reconstruct the optical source. We have improved our numerical model by adding a procedure of source image reconstruction similar to the one described by Kochanek et al. (1989). Image pixels and their intensity have been picked up from the sum of our R and *i* CCD images; only pixels with a S/N>3 have been used. Figure 6 shows the reconstructed image of the optical source, using the same set of parameters as in Figure 5. The optical source morphology appears to be consistent with that of an elliptical galaxy (r_{eff}= 0.5") at large z. Our image analysis lead to a reliable estimation for the optical ring magnitude, *i*= 21.5±0.3, and, although more difficult to estimate R=23.3±0.7. Our modelling provides a magnification factor of about 5–8 and the unlensed radio galaxy would be seen as a *i*= 23.5– 24 galaxy, at least 3 magnitudes fainter than the powerful 3CR radio-galaxies at z > 1. Indeed, the residual radio source is at least ten times less powerful than high-redshift 3CR radio sources: its radio-flux is lower than 40 mJy at 5 Ghz and lower than 8 mJy at 15Ghz after correction for the magnification factor. Another interesting consequence of our modelling is the possibility of deriving the accurate location of the reconstructed optical source relative to the radio source. Indeed, as was pointed out by Kochanek et al. (1989), the location of the lens center is well constrained by the model of the radio ring within an accuracy of about ±0".2. On the other hand, we find that the optical ring is well reproduced by setting the lens center at the peak of the optical emission, which is known down to an accuracy of ±0".1. Gravitational lensing of both the radio and optical galaxy leads to an astrometry for the reconstructed source down to an accuracy of less than ±0".3 with respect to the radio coordinate frame (see Figure 6).

4. Conclusions

New optical observations of the radio ring MG 1131+0456 have been presented. Both observing and modelling could have helped us to disentangle the source properties (the radio galaxy) from the lensing mass properties (the foreground elliptical and maybe a cluster). However, we have found that radio rings are not a very powerful mean to investigate the lensing mass distribution. Numerical simulations based on varying the lensing parameters in a four dimensional space (mass, effective radius, ellipticity and a single parameter for the virtual source location) left open

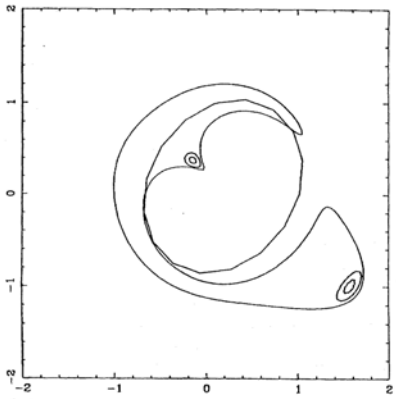

Figure 5 Lensing model reconstruction of the radio ring at 5 GHz. The source was assumed to have a core + jet morphology. Parameters used here are: M=2.5x10$^{12}M\odot$ for r_{eff}=0"5 and an axis ratio of 0.8 for P.A.=30°NW. Our simulations show that the P.A. is well constrained within 20° in order to reproduce the NW gap of emission, while the axis ratio should be between 0.4 to 0.8. However, by using several combinations of (M, r_{eff}), we did not find any strong constraint on the mass distribution as the mass inside the ring is 1.3x10$^{12}M\odot$

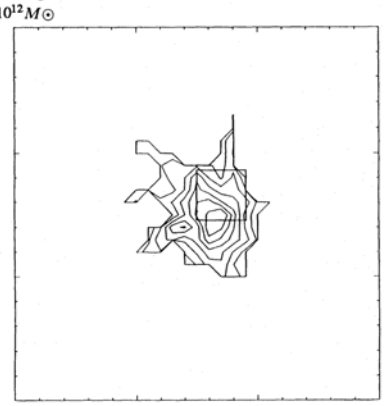

Figure 6 Lensing model reconstruction of the optical ring from the R+*i* images. Same set of parameters as in Figure 5. The square box indicates the location of the radio core as inferred from the accurate astrometry provided by the lensing configuration (see text)

a very large set of possibilities, especially for the lensing mass distribution. Indeed the ring thickness is too large and prevents one against the possibility to set the location of critical lines, contrary to the case of the giant thin and luminous arcs in rich clusters (Hammer and Rigaut, 1989).

However, observations of radio rings might help us to catch a population of radio-galaxies which would be far beyond the scope of the largest telescopes without the help of the gravitational lensing magnification factor. Our excellent seeing images have led to the detection of the optical source associated with the radio ring MG 1131+0456 with a ring-like morphology. Properties of the radio and optical source can be investigated after correcting for the magnification factor, for which there is an uncertainty by a factor 2 in our modelling. The radio source is found to be at least 15 times less powerful than the high-redshift 3CR radio-sources and the optical counterpart appears to be at least 3 magnitudes fainter than 3CR galaxies of comparable redshift. Indeed the MG 1131+0456 optical counterpart does not show any sign of strong emission line activity which would be expected if the rough correlation between emission line activity and radio power (Spinrad, 1986) was extended down to mJy levels. The source of M1131+0456 could be a moderately luminous elliptical (L∼L*), without any sign of strong star formation, while the radio emission dominates the whole energy spectrum. The way this object has been discovered indicates that it belongs to a relatively abundant population of sources with properties very different from the uncommon and very powerful radio-galaxies at high redshifts selected in the 3CR (9Jy at 178 MHz) or 1Jy samples (at 408 MHz, Allington-Smith, 1982). It would be interesting by several aspects to carry on K band observations of this system at high spatial resolution.

Analysis of our data combined with the lensing model show that the lensing galaxy of the MG 1131+0456 system is very likely a massive elliptical, tentatively at z=0.85. This might be another example of a massive galaxy at relatively high redshift which does not show any evidence for strong evolution (or star formation activity) and which can be compared with the lensing galaxy of the gravitational mirage QSO 2016+112 (Schneider et al, 1986). Deeper spectroscopic measurements are needed to confirm the redshifts of the source and lens.

Acknowledgments

The research of Jean Surdej in Liège is partially supported by contract ARC90/94–140 "Action de recherche concertée de la communauté Francaise" (Belgium).

References

Allington-Smith, J.R., 1982, MNRAS, 199, 611
Bennett, C. L., Lawrence, C. R., Burke, B. F., Hewitt, J. N., Mahoney, J., 1986, Astrophys. J. Suppl. Ser., 61, 1
Graham, J.A., 1982, P.A.S.P., 94, 244
Hammer, F., 1987, in 3rd IAP Astrophys. Meeting on High Redshift Objects, Ed. Bergeron et al, Frontieres, P. 467
Hammer, F., Le Fèvre, O., 1990, Astrophys. J. 357, 38
Hammer, F., Rigaut, F., 1989, Astron. Astrophys., 226, 45
Hewitt, J. N., Turner, E. L., Schneider, D. P., Burke, B. F., Langston, G. I., Lawrence, C. R., 1988, Nature, 333, 537
Huchra, J. P., Goreinstein, M., Kent, S., 1985, Astron. J., 90, 691
Kochanek, C. S., Blandford, R. S., Lawrence, C. R., Narayan, R., 1989, M. N. R. A.S., 238, 43
Kochanek, 1991, preprint
Langston, G. I., Schneider, D. P., Conner, S., Carilli, C. L., Lehar, L., Burke, B. F., Turner, E. L., Gunn, J. E., Hewitt, J. N., 1989, Astron. J., 97, 1283
Lynds, R., Petrosian, V., 1986, Bull. Am. Astron. Soc. 18, 1014
Magain, P., Surdej, J., Swings, J. P., Borgeest, U., Kayser, R., Kuhr, H., Refsdal, S., McCarthy, P.J., Kapahi, V.K., van Breugel, W., Subrahmanya, C.R., Astron. J., 100, 1014
Remy, M., 1988, Nature, 334, 325
Oke, J. B., 1984, in "Clusters and Groups of Galaxies", Eds Mardirossian et al, Reidel Publishing Company, P. 99
Schneider, D. P., Gunn, J. E., Turner, E. L., Lawrence, C., Hewitt, J. N., Schmidt, M., Burke, B. F., 1986, Astron. J., 91, 991
Soucail, G., Mellier, Y., Fort, B., Picat, J. P., 1987, Astron. Astrophys., 172, L14
Spinrad, H., 1986, P. A. S. P., 98, 269
Walsh, D., Carswell, R., Weymann, R., 1979, Nature, 279, 381
Zwicky, F., 1937, Phys. Rev., 51, 290

Bidimensional spectrography of multiple quasars

Vanderriest C, Angonin M-C, 1992, dans "Gravitational lenses" colloque de Hambourg de septembre 1991, Lectures Notes in Physics, **406**, 97

Bidimensional Spectrography of Multiple Quasars

C. Vanderriest and M.-C. Angonin

DAEC, Observatoire de Paris-Meudon,
5 place Janssen, 92195 Meudon cedex (FRANCE)

Abstract: Bidimensional spectrography is an efficient technique for extracting informations in the tiny crowded fields of gravitationally lensed quasars. It could allow to obtain simultaneously the spectra of all the images of the source (spectrophotometry, microlensing effects...) as well as that of the main lensing galaxy (redshift, velocity dispersion...).

While *Multi-object spectrographs* are now very common equipments of large telescopes, *integral field spectrographs* are still surprisingly scarce.

Our fibre optics instrument SILFID associated to the CFH telescope allowed to obtain interesting results on the fields of 0957+561 and H 1413+117. As an *a contrario* example, we show the limitation of data recently obtained on 2016+112 with a classical slit spectrograph. In conclusion, we briefly summarize the interest of bidimensional spectrography for a few other gravitational mirages.

1 Recent evolution of spectrographic techniques:

1a) How to make 3 = 2 ?

If we compare the techniques that were in use 25 years ago for the *photometry* of faint objects with the present state of the art, the improvement looks impressive. In those times, painstaking photometric measurements of 22^{th} or 23^{th} mag objects took several hours, even with large telescopes (remember, for instance, the works of A. Sandage on remote galaxies). The detector was an essentially zero-dimension photoelectric photometer that allowed to measure only 1 object at a time. Now, CCDs seem to be nearly perfect bidimensional photometers. On a single frame, hundreds of very faint objects can be measured and 27^{th} or 28^{th} magnitudes can be reached by averaging several exposures.

A similar evolution is under way for spectrography, but it is not yet completed.

One difficulty with spectrography is that the flux is a function of 3 variables (α, δ and λ) while the detector still has only 2 dimensions. So, if

we want to keep 2 spatial variables, either we use the time as a third auxiliary dimension (scanning Perot-Fabry interferometer or simple succession of long slit spectra) or we must find a way to "pack" 3 dimensions in the surface of the detector. Let us briefly summarize the possible solutions for this geometrical change.

1b) For multi-object spectroscopy:

• *Multi-slit spectrographs:*
Several slitlets can be used instead of a single long slit. This solution has the best efficiency for very faint and nearly point-like objects (very good transmission, accurate sky subtraction). It can be used on moderately extended fields (1'-10') like those of galaxy clusters at intermediate redshifts (see for instance the results on the field of 0957+561: Garrett et al.; Angonin and Soucail, these proceedings). However, the wavelength range is not identical for all the recorded objects and several masks could be necessary for the complete study of a cluster. For these reasons, it can be considered as a kind of spectrographic technique with a dimension certainly larger than 1 but less than 2.
⇒ The number of such spectrographs in operation is growing (see for instance the MOS instrument, near completion at CFHT).
• *Multi-fibre spectrographs:*
For larger fields (up to 1 degree or so), optical fibres allow to collect light from anywhere in the focal plane. The fibres can be plugged manually in a focal "aperture plate" or be moved by robot arms. By reordering the field elements into a pseudo-slit, they give the same wavelength range for all the objects and make the best possible use of the detector's area.
⇒ Such spectrographs are now very numerous and are mostly used as "redshift machines" for the study of large structures.

1c) For area ("integral field") spectroscopy:

Two more or less similar approaches exist for obtaining in a single exposure independent spectra of all the spatial elements in an extended object (which could be the definition of bidimensional or "integral field" spectroscopy).
• *Multi-pupil integral field spectrographs:*
In this configuration, the (enlarged) focal image is "split" by an array of micro-lenses into an array of micro-pupils that could be taken as entrance slits of the spectrograph (see fig.1). If the micro-lenses have a square section, this gives a full coverage of the observed field but, like with the multi-slit solution, the wavelength range is not the same for all the field elements; in order to avoid overlapping of the spectra, it may be necessary, also, to limit the free spectral range with a pass-band filter. On the other hand, each pupil is a uniform light source, which ensures an optimum accuracy in wavelength measurement (unlike with slits).

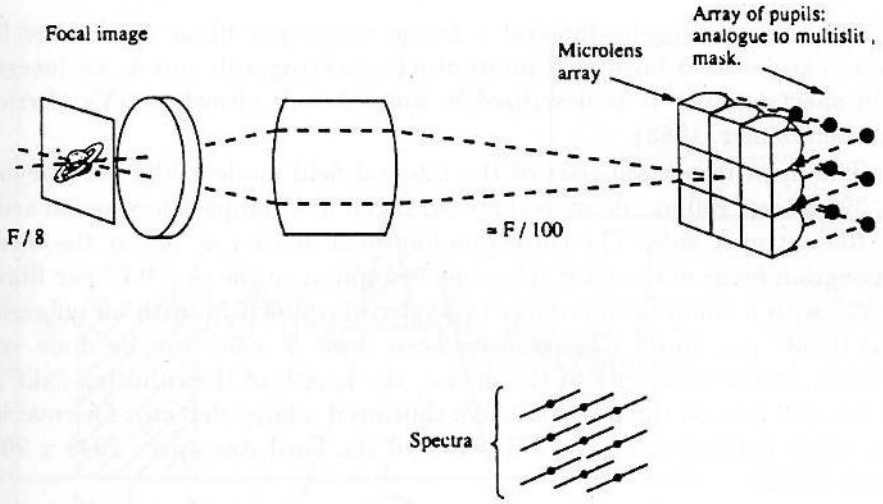

Fig. 1. Principle of multi-pupil integral field spectroscopy (after Courtès et al.)

⇒ The spectrograph TIGER was build on these principles by astronomers of the Lyon and Marseille Observatories (Courtès et al., 1988).

• *Multi-fibre integral field spectrographs:*
Using a fibre bundle as an "image slicer" that will transform a bidimensional image into a pseudo-slit is by no means a new idea. It was already suggested by Kapany in 1958. Now, the progress in fibre technology makes it easy to realize such devices but, quite surprisingly, only a very few attempts have been done.
⇒ At Kitt Peak, the "Dense-pack" device (Barden and Wade, 1988) comprises only 49 fibres, not really "densely" packed; at La Palma, the Hexaflex system (Rasilla et al., 1990) has 61 fibres in a compact hexagonal array. The most efficient instrument of this kind is still SILFID, used routinely since 1985, which provides almost 400 independent spectra.

• *Combining lens array and fibres:*
Maybe, the best possible bidimensional spectrograph could be obtained by combining the 100% image coverage of square lens array and the geometrical transformation of fibres. Following a suggestion by G. Courtès, such a system was built by Afanasiev and colleagues for the soviet 6 m telescope (Afanasiev et al., 1990). It allows to obtain 225 independent spectra.

2 SILFID: a fibre optics Integral Field Spectrograph:

SILFID (Spectrographe Intégral à Linéarisation par fibres de l'Image Directe) can be used both as a multi-object spectrograph and as an integral field spectrograph. It is described in more details elsewhere (Vanderriest and Lemonnier, 1988).

The most important part of the integral field mode is the fibre device. Its 397 fibres (100 μm diameter) are arranged in a compact hexagonal array on the entrance side. The corresponding field of view is 16" at the direct Cassegrain focus of the CFH telescope (sampling on the sky: 0.7" per fibre), or 32" with a small focal reducer (1.4" per fibre), or 7.5" with an enlarging lens (0.33" per fibre). Changing between these 3 scales can be done very quickly. At the other end of the device, the length of the resulting "slit" is 53 mm (32 mm on the detector). We thus need a large detector for covering the whole field of view (at CFH, we used the Ford Aerospace 2048 x 2048 pixels CCD).

The reduction of the bidimensional spectrographic data is now largely automatized. Wavelength calibration, XY calibration, flat field correction and flux calibration are made directly on the bidimensional frame. Then, spectra of the individual fibres are automatically extracted and it is possible to reconstruct different maps of the field: fluxes in preselected wavelength bands and preselected emission or absorption lines, redshifts and FWHM of these lines. The lines are automatically processed if their amplitudes are above a chosen threshold; in the present version of the software, the parameters for the maps are obtained from a gaussian fitting (fig. 2).

Such maps allow to recognize the physical structures of the field and to add optimally, within their limits, the data from individual fibres. These limits are chosen *a posteriori* and adapted to the seeing at the moment of the observation, which ensures a minimal contamination. The resolution of the resulting spectra is constant, depending only on the dispersion of the spectrograph and on the size of the fibres ("slicer" effect). Also, the effects of differential atmospheric refraction can be taken into account and the spectrophotometric accuracy is optimally preserved.

3 Bidimensional spectrography of gravitational mirages:

For the measurement of the lensing galaxies (redshifts and velocity dispersion), the above qualities are precious. They are also useful for investigating the spectroscopic effects of microlensing: differential amplification of the continuum with respect to the broad emission lines (Rees, 1981), slight modifications of the line profiles (Nemiroff, 1988).

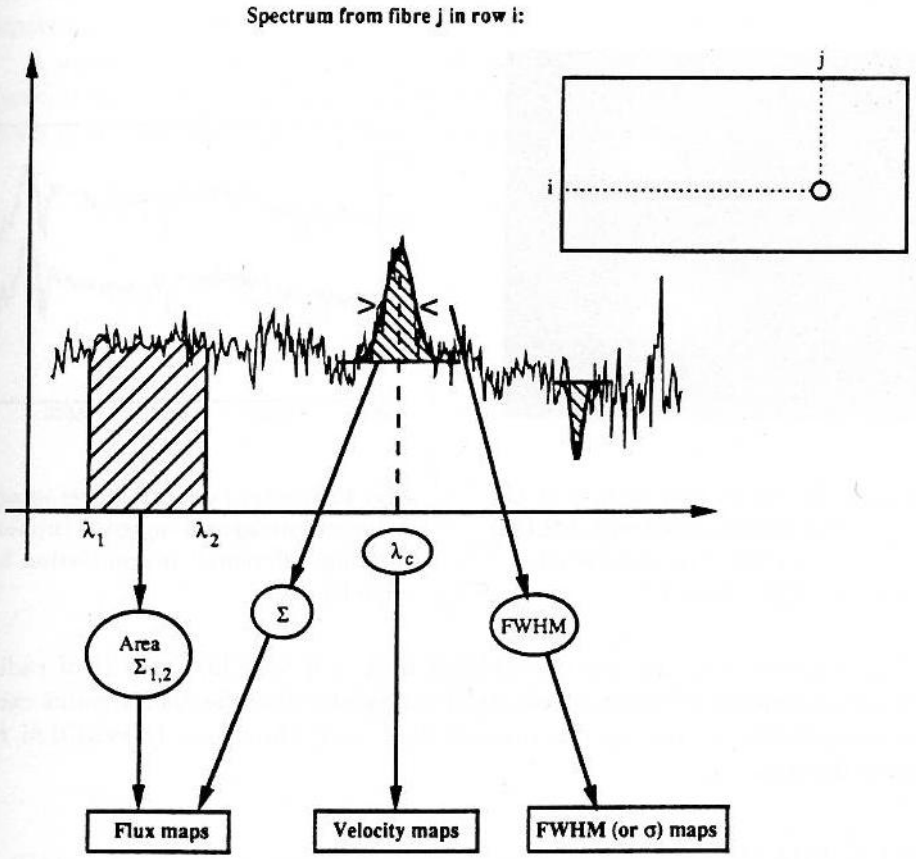

Fig. 2. Principle of map reconstitution from SILFID spectra

3a) The case of 0957+561:

The first gravitational mirage is still the most intensively studied one, in the scope of a possible direct determination of H_o. The issues of measuring Δt and modeling the lens cluster are addressed elsewhere in these proceedings. Another important point is the measurement of the velocity dispersion σ_v in the main deflecting galaxy G_1. A first measurement was done recently (Rhee, 1991) but bidimensional spectroscopy could bring better data if the integration time is sufficient. At the same time, high S/N spectra of images A and B could be obtained for studying the differential microlensing effects.

A few exposures with a 2K x 2K CCD have been obtained in 1990 and more are expected soon at the CFH telescope. Figure 3 shows the total field covered (with a 0.7" per fibre sampling); the core of galaxy G_1 is visible on this reconstructed picture. On figure 4, note the smaller equivalent width of the Mg II emission line for image B. This is compatible with an intrinsic

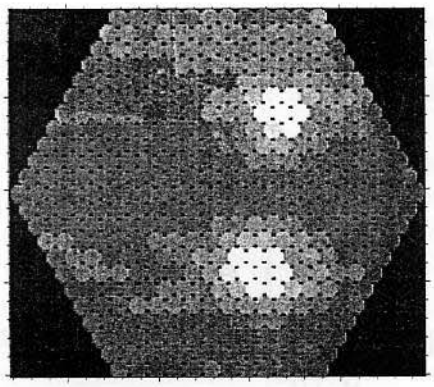

Fig. 3. Reconstructed picture of the 0957+561 field observed with SILFID (December 1990) The wavelength range is 4000 - 7000 Å

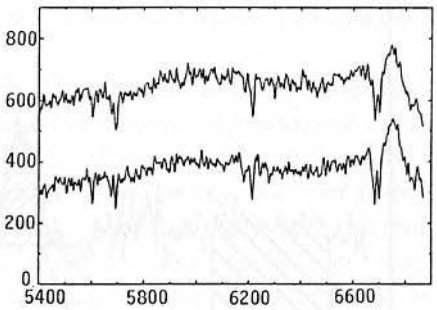

Fig. 4. Spectra integrated over image A (lower curve) and image B (upper) showing differential magnification by microlensing

amplification ratio (by the macro-lens) B/A $\simeq$ 0.75. The analysis of radio brightness ratios (Conner et al., 1991) suggests that the VLBI radio core is comparable in size to the optical BLR and, thus, poorly sensitive to microlensing.

3b) H 1413+117

This system is very interesting because it is the only known case of gravitational mirage acting on a BAL quasar. From bidimensional spectrographic data obtained in 1989, the differential amplification effects expected for microlensing have been clearly recognized on one of the 4 images (see Angonin et al., 1990). With respect to the other 3 images, the continuum seems to be more amplified than the emission lines and some BAL components are selectively enhanced; the bluer shape of the continuum that was observed could also result from differential magnification on an accretion disk with temperature gradient (Wambsganss, these proceedings).

If the interpretation is correct, we forecast that these effects will change with time. With a ray-tracing software, we made a crude simulation of a microlensing event: a 1 $M_\odot$ star of the deflecting galaxy (z $\simeq$ 1.5) is launched with a transverse velocity of 300 km/s in front of H1413+117 (z = 2.54). The structure of the source is approximated by a uniform disk with 1.2 10^{-6}" diameter for the continuum and a 1.2 10^{-6}" x 0.3 10^{-6}" ellipse for the (supposed perfectly absorbing) BAL cloud. This leads to measurable variations of the BAL strength within a few years (fig. 5; see also contribution of Hutsemekers et al.). In the real case, the behaviour of

the other components of the source (emission lines, continuum) will help to constrain the model and to estimate directly the size of the BAL clouds.

A second epoch observation in bidimensional spectroscopy would be very useful if the seeing is excellent. Then, if the results are promising, one could think of a short spectroscopic monitoring with the Space telescope.

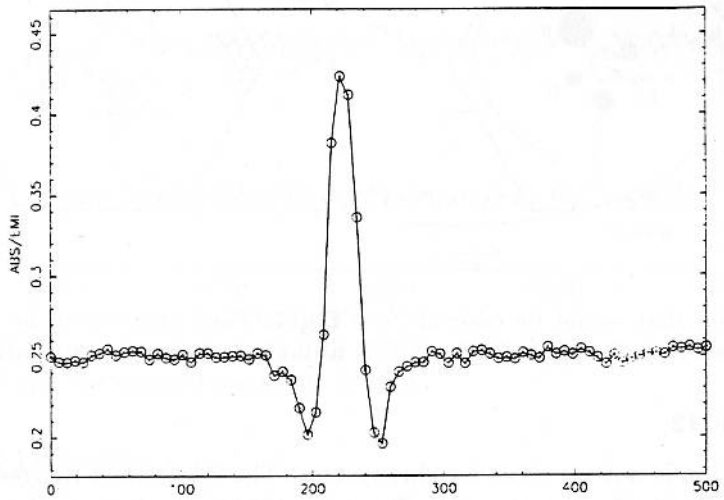

Fig. 5. Variation of the relative BAL strength for a simulated microlensing event on H 1413+117

4 Other cases that could benefit of the technique:

Comparing to classical slit spectrography, the gain introduced by bidimensional spectrography is mostly noticeable for crowded fields. Among others, one can think of the following multi-component systems:

4a) 2237+0305

Microlensing is likely on at least one of the 4 images (Irwin et al., 1989 and these proceedings) but the spectroscopic effects have not yet been properly investigated. Also, the possible fifth image E (Racine, 1991) as well as the narrow emission feature discovered by De Robertis (these proceedings) could be best detected and characterized by bidimensional spectrography. A deep integration on the field with a spatial sampling of 0.33" could help to investigate these points. At the same time, the velocity field of the inner parts of the galaxy could be mapped. Figure 6 summarizes the proposed observation.

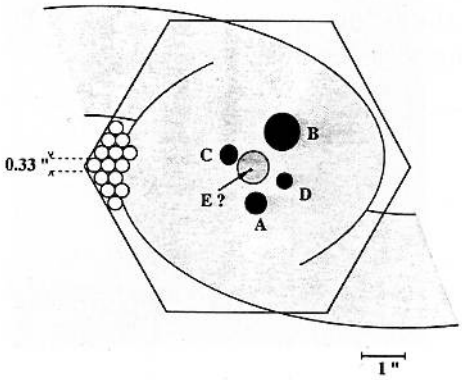

Fig. 6. Field that would be covered at 0.33" resolution for 2237+0305

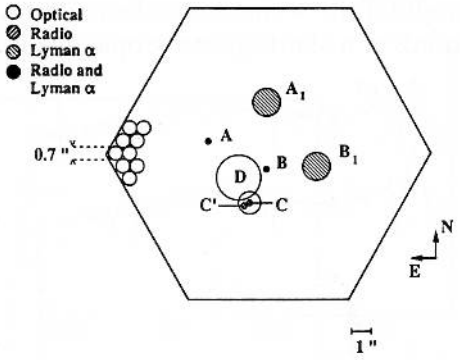

Fig. 7. Field that would be covered at 0.7" resolution for 2016+112

4b) 2016+112

The situation is not yet clear for this system. The 2 brightest images A and B have similar radio structures (Heflin et al., 1991) as well as similar optical spectra; they are certainly 2 images of the same source. A third compact component is detected also in radio and Ly α imaging (but it is found at slightly different positions for these two wavelength ranges), superimposed to a galaxy (C). Until now, no good spectrum was obtained in this part of the field.

There are also another galaxy (D), at a redshift $\simeq$ 1.01, and two extended Ly α clouds (or 2 images of a single cloud ?) at the redshift of A and B (Schneider et al., 1987). The current balance between observational constraints and model parameters does not yet lead to an unique representation. For Narasimha and Chitre, it is an example of "double lensing", with galaxies C and D equally involved, but new data (Langston et al., 1991) suggest that D is largely dominant. Clearly, deep bidimensional spectrography would help to solve the puzzle (fig. 7).

One interest of 2016+112 is that the main source (corresponding to images A and B) is quite unusual. It is not a *bona fide* quasar; in fact, its spectrum closely resembles the one of 53W002, recently discussed by Windhorst et al. (1991). The source could be a starburst galaxy or a mixed starburst/AGN, observed at a very high redshift thanks to the magnification by the lens(es). Observations with EMMI associated to the NTT (fig. 8) show that the intrinsic width of the emission lines is of the order of 400 km/s. The limited spatial resolution (slit width: 1.5") and sensitivity does not allow to resolve the source.

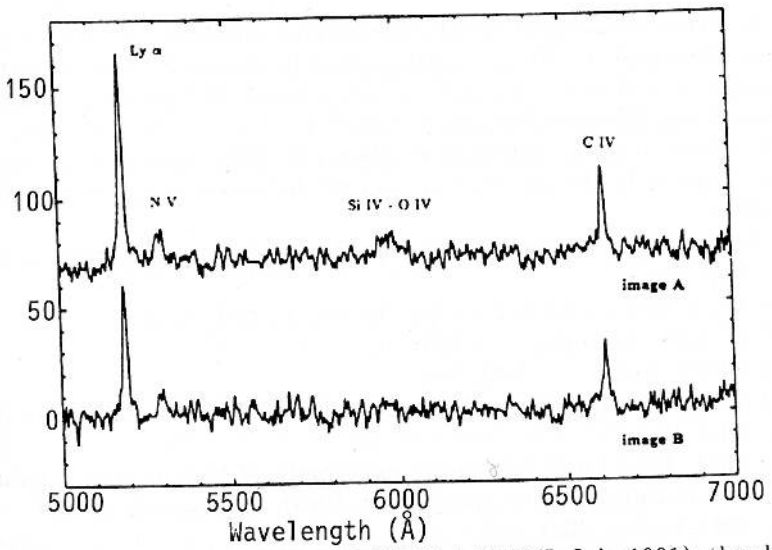

Fig. 8. Spectra of 2016+112 A and B (NTT + EMMI, July 1991); the slit width was 1.5" and the spectral resolution $\simeq$ 12 Å.

4c) PG 1115+080

Again, for this system, there are photometric evidences of microlensing on the close double A_1-A_2 (Vanderriest et al., 1986). The redshift of the lensing galaxy detected by Christian et al. (1987) is not well determined. Photometry is compatible with $z \simeq 0.3$ - 0.4 but a (quite noisy) unpublished spectrum rather suggests $z \simeq 0.25$.

5 Conclusion:

Bidimensional spectrography is a rewarding technique for almost each and every field of astronomy. But it would be especially useful for extracting key informations in the tiny crowded fields of several gravitational mirages. Considering that, in the present state of the art, it is quite easy to manufacture efficient fibre devices that transform a 2-D field into a pseudo-slit, we hope that they will be widespread equipments of the new large telescopes.

References

Afanasiev V., Vlasiuk V., Dodonov S., Silchenko O.: 1990, *Academ. Nauk. USSR*, preprint 54.

Angonin M.-C., Remy M., Surdej J., Vanderriest C.: 1990, Astron. Astrophys., **233**, L.4.

Barden S., Wade R.: 1988, *Astron. Soc. Pac. Conf. Ser.* , **3**, 113.

Christian C., Crabtree D., Waddell P.: 1987, Astrophys. J., **312**, 45.

Conner S., Lehar J., Burke B.: 1991, Astrophys. J., in press.
Courtès G., Georgelin Y., Bacon R., Monnet G., Boulesteix J.: 1988, in *Instrumentation for ground-based optical telescopes*, proceed. IXth Santa Cruz workshop, Robinson ed., Springer publish., p. 266.
Heflin M., Gorenstein M., Lawrence C., Burke B.: 1991, Astrophys. J., **378**, 519.
Irwin M., Webster R., Hewett P., Corrigan R., Jedrzejewski R.: 1989, Astron. J., **98**, 1989.
Kapany N.: 1958, in *Concepts of classical optics*, J. Strong ed., Freeman publish. (San Francisco).
Langston G., Fisher J., Aspin C.: 1991, Astron. J., **102**, 1253
Nemiroff R.: 1988, Astrophys. J., **335**, 593.
Racine R.: 1991, Astron. J., **102**, 454.
Rasilla J.-L., Arribas E., Mediavilla E., Sebastian J.-L.: 1990, *Astrophys. Sp. Sc.*, **171**, 301.
Rees M.: 1981, ESO Conf. "*Scientific importance of high angular resolution at Infrared and Optical wavelengths*", M.H. Ulrich, K. Kjär eds., p.423.
Rhee G.: 1991, Nature, **350**, 211.
Vanderriest C. et al.: 1986, Astron. Astrophys., **158**, L.5.
Vanderriest C., Lemonnier J.P.: 1988, in *Instrumentation for ground-based optical telescopes*, proceed. IXth Santa Cruz workshop, Robinson ed., Springer publish., p. 304.
Windhorst et al.: 1991, Astrophys. J., **380**, 362.

Ground-based optical observation of gravitational lenses

Angonin-Willaime M-C, Hammer F et Rigaut F, 1993, proceedings du colloque de Liège: Gravitational lenses, 85

Ground-based optical observations of gravitational lenses.

M.-C. Angonin-Willaime [1], F. Hammer [2] and F. Rigaut [2]

[1]D.A.E.C., Observatoire de Meudon, France
[2]C.F.H.T. Corporation, Hawaii, U.S.A.

Abstract: Following the reviews by Jean Surdej on this subject, this paper presents the last results concerning the optical observations of gravitational mirages by ground-based telescopes. The last two years were marked by discoveries of new candidates. We briefly discuss the characteristics of these new cases as well as new data on already-known ones in relation to the "classical" uses (astrophysical and cosmological). This includes determination of the Hubble constant, study of foreground objects using absorption lines, importance of microlensing and possibilities of discovering new categories of distant objects due to gravitational magnification.

1 Introduction

The present review on optical ground-based observations of gravitational lensing describes the latest results on this subject since the Hambourg Conference two years ago. We have left the pleasure of a precise count of the number of papers concerning this field during these two years to the master of gravitational lens bibliography: Jean Surdej. Anyway his impressive list of references demonstrates directly the importance of gravitational lensing in astronomy... It is now well-known that anyone interested in this field can find usually something to read in each issue of *A&A MNRAS* or *Ap J*. The explosion of the subject since the discovery of the first gravitational mirage (0957+561, Walsh *et al.*, 1979) can be explained by the fact that gravitational lens observations are not only aesthetic views of our universe but also real astrophysical and cosmological tools. A gravitational lens event is a means to study all the components that constitute the phenomenon: source, lens, propagation space (... and sometimes observers).
To determine the distribution of mass inside the lens, a minimum of constraints are needed and can be provided only in the cases of gravitational lensing on extended sources. Individual studies of giant arcs and arclets have already shown their powerful possibilities in revealing characteristics of the mass distributions in clusters of galaxies (see Soucail, these proceedings). A statistical study of arc distributions in X-ray clusters has been recently developed theoretically and observationally and is beginning to produce spectacular results on mass profile constraints (see Hammer, these proceedings). The subject is fully described in this book, we will not continue it.

What kind of information can we extract from gravitational mirages on small (pointlike) sources? The most certain way to conclude that we are observing a gravitational lens event on pointlike source is the presence of a gravitational mirage. From a statistical point of view, the existence and the frequency of such mirages in the universe give limits on the fraction of matter in form of compact bodies. The ESO key-programme on "Gravitational Lensing" presents in these proceedings the results of its quasar survey on this subject. If we look at each candidate one by one, a gravitational mirage means multiple images of a single source amplified, following different ray paths and separated by time delays. A lens thus provides the possibility of studying faint populations of the distant universe unreachable without magnification, comparing the absorption lines in the spectra of each image, constraining the size of foreground objects (Lyman α clouds) and measuring the age of the universe. Furthermore, small sources are excellent for microlensing events which act as a magnifying glass on the small scale structure of the source. The existence of microlensing has been confirmed, but its frequency and amplitude are not well defined observationally. We will present here all these aspects of gravitational lensing with an up-to-date status of the candidates for the ground-based optical observations.

2 New candidates

2.1 Introduction

The two past years were particularly fruitful concerning the discovery of new gravitational mirage candidates. The strategy is more or less well defined: systematic search in a quasar catalog, snapshot survey, study of pairs of pointlike blue objects with or without variability criteria, ... In fact, all these techniques present a common characteristic: to find new candidates you must search first for multiple images of a given source. Then you search for a lens. The philosophy is totally different when the problem is to find new gravitational lens images of extended sources. For example, in the cases of giant arcs or arclets, the suspected lenses (clusters of galaxies) are surveyed in which deep imaging should provide gravitational lens structures.

Anyway, the question is still the same: what are the characteristics that make a difference between a physical pair (or cluster?) of quasars and a gravitational mirage? Especially when, as it often occurs, the lens is not observed? The similarity of two spectra is a subjective notion dependent on obvious observational biases. The controversy around 2345+007 (see preceding reviews of Surdej for references and summary) is the best example of what can be inferred about an ambiguous candidate... The discovery of chromatic microlensing effects on the images complicates the situation. A quantification of these effects in realistic cases should be very useful to discriminate between subjective points of view. Except for the quadruple quasars, it is very difficult to conclude in favour of the gravitational lens hypothesis without the discovery of the gravitational lens! But some clues can help to support the hypothesis: symmetry in VLBI structure (when observable) of each images, same absorption lines of foreground objects...

.2 Individual cases

1009-0252: Another indication of gravitational lensing can be extracted from the vicinity of mirage. In the case of 1009-0252 (see the contribution of J. Surdej in these proceedings), the double quasar ($\theta = 1.55$", $z = 2.74$) is very close (4.6") to another quasar at $z = 1.62$. Such association between moderately bright quasars is highly unlikely unless we consider that gravitational lensing acts to bias this observation. Comparison of each quasar's spectrum nor-

malized in the emission lines clearly shows a chromatic difference in the continuum. This does not mean necessarily that the lensing hypothesis should be abandoned, because contamination by the lens and microlensing effects are theoretically able to infer such chromaticity. It would be desirable, however, to support these explanations by observations (monitoring) and models. Further observations of this system, especially with the aim of discovering the deflecting body, are thus really needed.

• *HE 1101-184:* This double quasar discovered by Reimers *et al.* (these proceedings) is at redshift z = 2.303. The two components are separated by 3.0". The spectra of the two images have been used to determine the size of the Lyman α forest clouds (see Smette *et al.*, these proceedings). As in the preceding case, spectrometry shows a chromatic difference between the normalized continua. Such a discrepancy is difficult to explain in terms of microlensing but this hypothesis cannot yet be ruled out. Further investigation of the possibilities of microlensing and an observational confirmation of the mirage hypothesis are necessary.

• *1208+101:* The mirage is composed of a very close (0.45") double quasar at z = 3.80. The discovery was made simultaneously by the ESO key-programme on gravitational lensing (Magain *et al.*, 1992) and the HST survey (Maoz *et al.*, 1992). The difficulty in resolving this mirage makes it a priority target for adaptative optics and spatial observation.

• *BRI0952-01:* The existence of this new candidate is mentioned by only one paper (McMahon *et al.*, 1992). It is the highest redshift double quasar (4.5) with a sub-arcsecond separation (0.9"). It is quite satisfying to see that with the evolution of the observing techniques the discovery of sub-arcsecond mirages begins to reconcile the lack of small separation in observed lensing statistics compared to theoretical predictions.

• *B1422+231:* This quadruple quasar was discovered in 1992 by Patnaik *et al.*. The source is at redshift z = 3.62. The four images are well resolved in radio (angular separation $\leq$ 1.3"). Infrared imaging (K band) has been obtained by Lawrence *et al.* (1992) showing the same structure and brightness ratio. Remy *et al.* (these proceedings) present optical V, R and I images of the four images. Three weeks before this colloquium, Hammer and Rigaut observed this source with the CFHT (Hammer *et al.*, 1993). Images in I and V under seeing FWHM = 0.65" were deconvolved using the maximum entropy method. In both V and I images, intensity ratios and positions are consistent with radio measurements except for A/B which is 0.83$\pm$0.08 (against 0.98 in radio). The lensing galaxy is detected after subtraction of gaussian (stellar) profiles on the rough image (Fig. 1). Medium and low resolution spectroscopy in two different slit orientations confirm the redshift of the source. Fig. 2 presents medium resolution spectra of the A and C components (FWHM = 4Å, pixel size = 1.5Å). The Slit was 0.5" width in seeing of 0.9". The spectra are identical except that A presents a red excess relative to C. The subtraction of these two spectra gives residuals with a red continuum plus a (possible) emission line. Fig.3 shows the same subtraction but for the low resolution spectroscopy. The 2" slit was centered at the lens position. The spectrum is polluted by the QSO light from all the components which explains the difficulty in making a correct subtraction of the QSO emission lines. An [OIII] emission line plus CaII K, H and MgII absorption line are identified and match well with the preceding emission line ([OII]): the redshift of the lensing galaxy is z = 0.64. Moreover, in the QSO spectra, one can notice strong absorption lines of MgII and MgI at z = 0.64 (absorption of the QSO light). With its compactness and configuration, this mirage constitutes a good target for bidimensional spectrography. One should confirm the position of

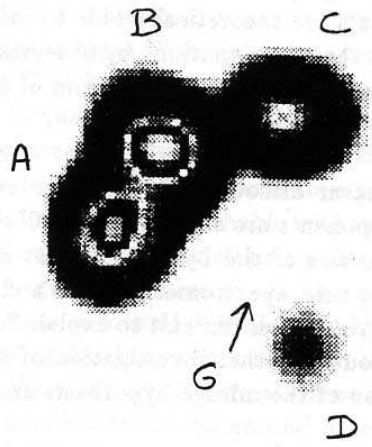

'igure 1: I Image of the mirage B1422+231 after MEM deconvolution. The position of the :nsing galaxy is given by the arrow.

ıe lensing galaxy and explain the difference in brightness ratios between optical and radio. .s it seems to be an excellent candidate for H_0 determination, a monitoring in radio (and in ɔtical if one can resolve the images) should be very interesting.

What about the sources?

ravitational mirage sources constitute a fair sample of distant universe populations. Magnifi- :tion allows us to observe objects at high redshift (up to 4.5) which would not been detectable herwise. The gravitational lensing phenomenon is rare enough to make us consider that the urces represent the abundant populations at such redshift. For the point-like sources, the ɔst usual case is multiple images of a quasar. But few candidates show unexpected spectral ɔperties.

2016+112: MG 2016+112 was discovered by Lawrence *et al.* (1984) by a systematic VLA :vey. The mirage is composed of three images A, B and C' at z = 3.27. The existence of two flecting galaxies C and D has been demonstrated. Galaxy D is at z=1.01 and observations in band by Lawrence *et al.* suggest that the redshift of C should be higher than 2. We should ntion also the presence of two diffuse narrow line emission regions located near images A l B (Schneider *et al.*, 1986). NTT EMMI (ESO) spectra of images A and B of this source ve been obtained by Vanderriest in July 1991. These spectra (Fig. 4) show identical line ofiles (for example, the blue part of the Lyman alpha line). The lines are marginally resolved: rinsic FWHM = 400 km/s, and the N V doublet is well seen. The small width of the lines l the faintness of the continuum suggest that the source is not a quasar but a Seyfert II cleus, a starburst or something between starburst and AGN. In addition to the already ob- ved lines it should be interesting to elaborate IR spectra of this source in aim to precise its ure and evolution. The presence of two deflecting galaxies implies that this candidate is not ly usable as Hubble constant indicator.

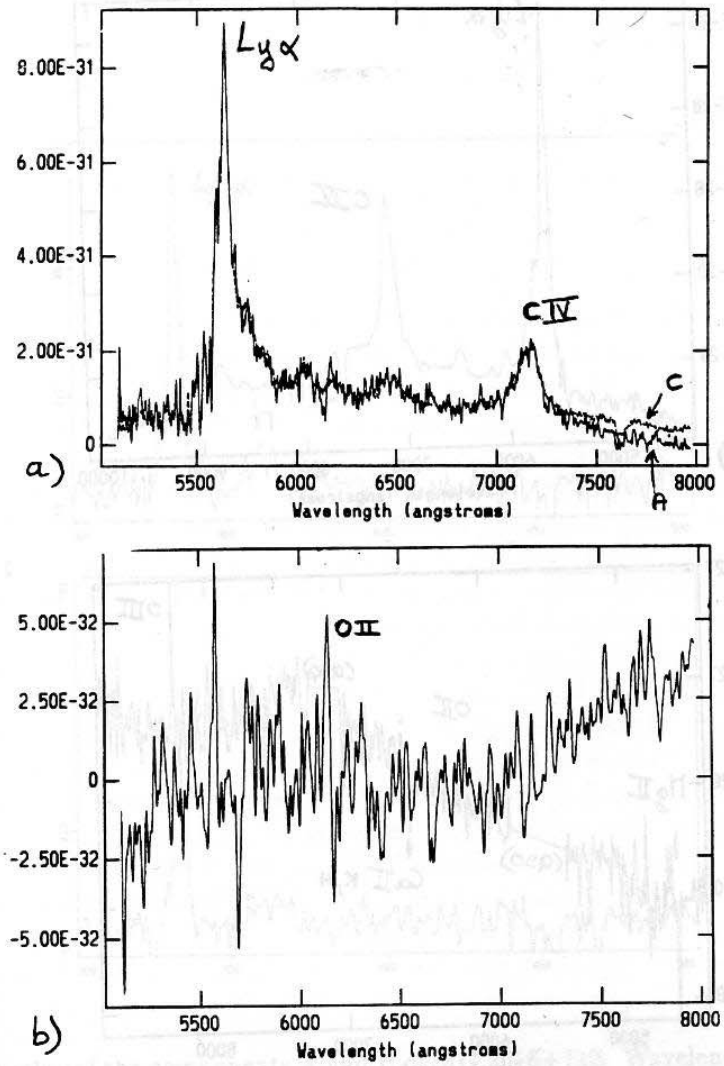

Figure 2: (a) Medium resolution spectra of components A and C. (b) Residuals of the subtraction of the two spectra.

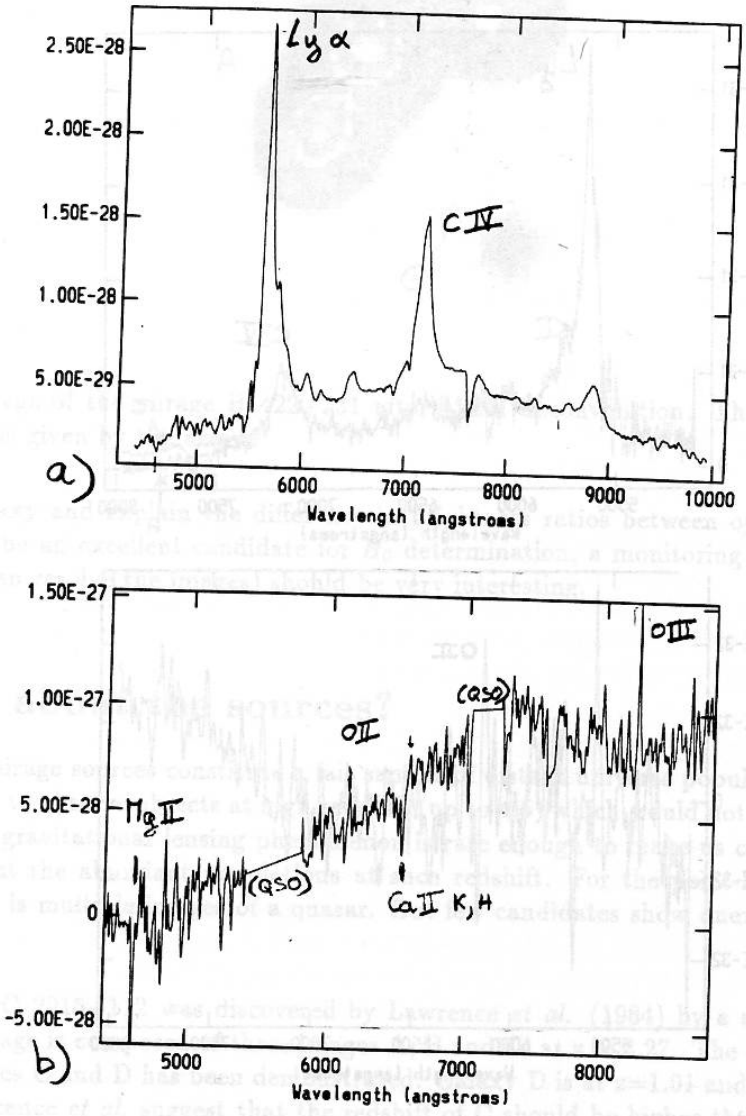

Figure 3: (a) Low resolution spectrum of the quasar. (b) Residuals of the subtraction of the same components.

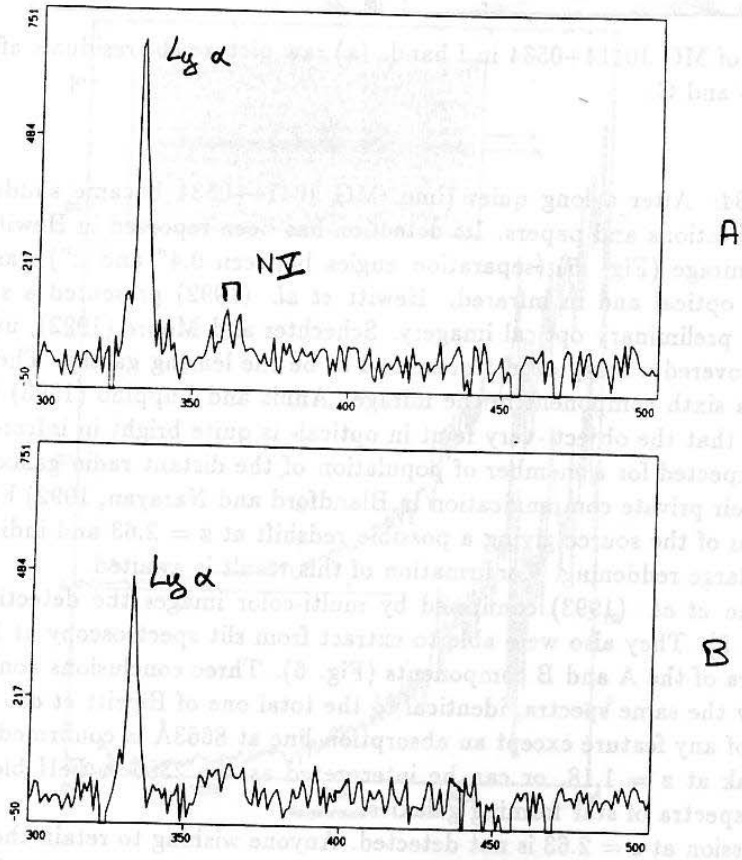

Figure 4: Spectra of the components A and B of MG 2016+112. Wavelength axis is in arbitrary units.

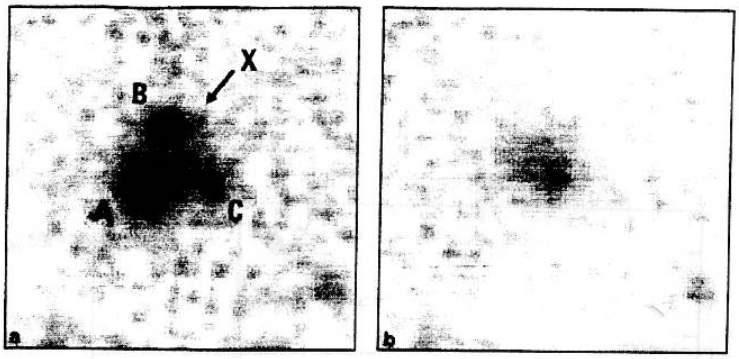

Figure 5: Picture of MG J0414+0534 in I band. (a) raw picture (b) residuals after subtraction of the image A, B and C.

• *MG J0414+0534:* After a long quiet time, MG J0414+0534 became suddenly the target of numerous observations and papers. Its detection has been reported in Hewitt *et al.* (1988). This quadruple mirage (Fig. 5) (separation angles between 0.4" and 2") was first observed in radio, then in optical and in infrared. Hewitt *et al.* (1992) presented a spectrum of the whole object and preliminary optical imagery. Schechter and Moore (1992), using further optical studies, discovered a fuzzy object presumed to be the lensing galaxy. They reported also the existence of a sixth component in the mirage. Annis and Luppino (1993) have shown, by K-band imaging, that the object -very faint in optical- is quite bright in infrared and presents characteristics expected for a member of population of the distant radio galaxies. Elston and Lawrence (see their private communication in Blandford and Narayan, 1992) have obtained an infrared spectrum of the source giving a possible redshift at $z = 2.63$ and indicating that it is a quasar with a large reddening. Confirmation of this result is awaited.
Angonin-Willaime *et al.* (1993) confirmed by multi-color images the detection of Schechter and Moore (Fig. 5). They also were able to extract from slit spectroscopy at NTT (ESO) the individual spectra of the A and B components (Fig. 6). Three conclusions come consequently:
1) A and B show the same spectra, identical to the total one of Hewitt *et al.*.
2) The absence of any feature except an absorption line at 8663Å is confirmed. It corresponds to a 4000Å break at $z = 1.18$, or can be interpreted as the 2380 Å FeII blend at $z = 2.63$ observed in the spectra of star forming galaxies.
3) Lyman α emission at $z = 2.63$ is not detected. Anyone wishing to retain the hypothesis of a quasar at this redshift has to consider a very large reddening of the source itself. The nature of this source is thus not very clear. It can be compared to the source of two other gravitational lens sources: MG J1131+0456 and 0218+357 the spectra of which bear some resemblance to that of this mirage.
The optical faintness of the source and lens does not favour the use of this gravitational lens as a Hubble constant indicator (the time delays are measurable in radio, but the redshift and the velocity dispersion of the lens will be very difficult to obtain). The study of this object in order to discover its nature (infrared spectra) should be very useful to determine the characteristics of what may be a population of red faint radiosources in the deep universe.

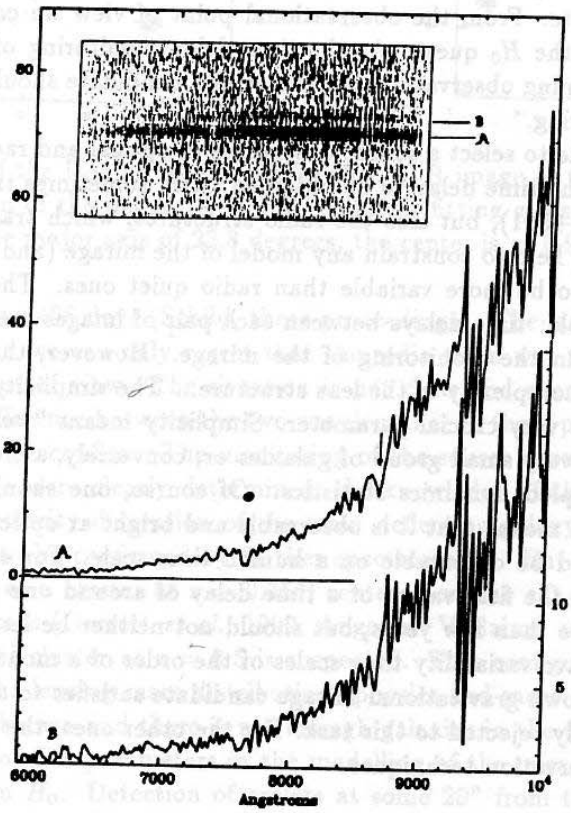

Figure 6: Spectra of images A and B. The fluxes are in units of $10^{-21} W m^{-2} \AA^{-1}$ (left scale for A, right scale for B). Inserted is the bidimensional representation of the data, after removal of the night sky emission.

4 Cosmological parameters

4.1 Recipe: how to find H_0

The idea was first suggested by Refsdal (1964, 1966). As the light rays of each image follow different paths through the propagation space, the components of a gravitational mirage are images of the source at different epochs. The time delays between the images are indicative of the distances and thus of the scale of the universe: H_0. To link these two quantities, the astrophysicist has to determine one parameter: the lensing mass. The possibility to determine H_0 depends directly on the possibility to measure the time delays and the lensing mass of the chosen mirage candidate. From the observational point of view we can define the profile of the ideal candidate for the H_0 quest. As the time delay monitoring of a candidate is the most telescope time consuming observation, the choice of a candidate should be made on other criteria before any monitoring.

First, it would be preferable to select a source observable in optical and radio. This allows two independant measures of the time delay to be obtained (with sometimes trouble in reconciling them, see the case of 0957+561), but also the radio structures, which transform the compact source in an extended one, help to constrain any model of the mirage (and its lens). Moreover, radio loud quasars seem to be more variable than radio quiet ones. The number of images should be a large as possible: time delays between each pair of images are independant values simultaneously reachable in the monitoring of the mirage. However, the number of mirage images increases with the complexity of the lens structure... The simplicity of the lensing mass distribution seems to be a very crucial parameter. Simplicity means "well-known" structures such as a single galaxy, a very small group of galaxies or, conversely, a cluster of galaxies rich enough to allow well-sampled dynamics statistics. Of course, one should not forget that a complete study of the lens means that it is observable and bright at optical wavelengths.

Finally, time delays should be observable on a human time scale. For example, at least ten years were needed to give the first values of a time delay of around one and half year... The time delay cannot be more than few years, but should not neither be less than a few months because mirage sources have variability time scales of the order of a month.

Up to now, no already-known gravitational mirage candidate satisfies to all these criteria. But few of them can be directly rejected to this task. For the other ones, the situation can change with the evolution of observation techniques.

4.2 Status of the candidates

• *0957+561:* For historical reasons, this mirage is by far the best known gravitational lens system. 0957+561 is the first gravitational mirage discovered in 1979 by Walsh *et al.* It is composed of a double quasar at $z = 1.41$ with an angular separation of 6.1". The main deflecting galaxy (Fig. 7) was detected very early by Young *et al.* (1980); it is a cD galaxy at $z = 0.356$ (Rhee, private communication). This double quasar has been observed in all the wavelengths accessible for gravitational lens observers mostly with the aim to confirm the lensing hypothesis. Recent X-ray images obtained with the High Resolution Imager of the Einstein satellite (Jones *et al.*, 1992) show the existence of an arc of radiation between the two images. From the radio observations with the VLA and VLBI, Conner *et al.* (1991) have derived an amplification ratio (B/A) of 0.697 ± 0.003 considering the core + jet structure and a value of 0.75 ± 0.03 compatible with optical amplification ratios for the core alone. More than ten years of the source monitoring in radio and optics provide two values for the time delay between the two images. The radio data gives a value of 536 days (Lehár *et al.*, 1992)

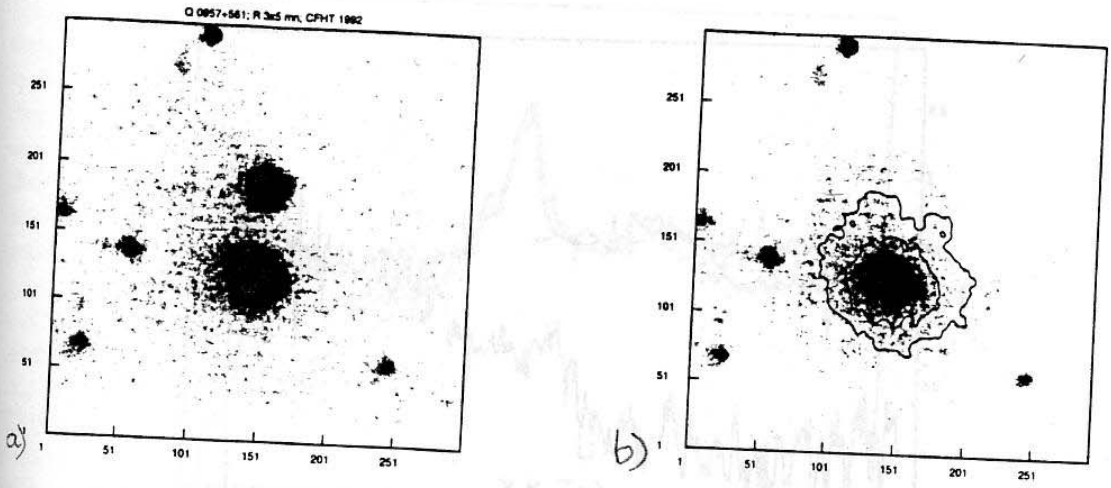

Figure 7: Images of the Double Quasar 0957+561: a) R image of the field, b) the lens after a gaussian subtraction of the images A and B (elliptical fitting gives an ellipticity of 0.76 and a position angle of the major axis of 22.8 degrees, the center is at 0.91" from B image).

whereas optics favour 406 days (Schild, these proceedings). The last light curves of Schild are quite convincing and we can only regret that the radio team was not present at this meeting to discuss their point of view. The situation is not clear and even if a value is accepted, we must explain the difference between the two wavelengths. In these proceedings, Schild develops an idea that should be confirm. The monitoring of the source should then continue... Even if the time delay value were clearly determined, the knowledge of the mass distribution is still rather poor. The velocity dispersion of the main deflecting galaxy is estimated at 303 $\pm$ 50 km/s (Rhee, 1991; to be confirmed by further spectroscopy). But this galaxy is not alone in the field: it is part of a cluster at $z = 0.355$, centered on the cD galaxy and with a velocity dispersion of 715 km/s (Garrett *et al.*, 1992; Angonin- Willaime *et al.*, 1993). Moreover, the existence of a second cluster at $z = 0.5$ is suspected. This configuration is certainly not the best to determine the lensing mass distribution: physics and mass distribution of such a poor cluster is largely unknown and there is not enough galaxies in the field to put real constraints on it. The number of free parameters in the modelling of the mirage is probably too large to put serious limits on H_0. Detection of arclets at some 20" from the mirage by Bernstein *et al.* (1993) could give more constraints on the deflector models. These authors have presented the results of various models and gave an upper limit for H_0 of 87. While this mirage is not the ideal candidate to determine the Hubble constant, further observations (for example deep imaging or spectrography of faint field galaxies) could help to understand the lens morphology but would certainly not give more information for H_0.

• *PG1115+080:* Discovered by Weyman *et al.* (1980), this quadruple quasar is chronologically the second gravitational mirage. The lensing galaxy was detected independantly by Christian *et al.* (1987) and Shaklan and Hege (1986). The field is quite empty around the mirage, with only three galaxies at $z = 0.304$ present (Henry and Heasley, 1986). Except for the fact that the QSO is radio quiet, this mirage is a good candidate for time delay monitoring. Angonin-Willaime and Hammer did spectroscopy in good seeing conditions (FWHM = 0.8") of the deflecting galaxy in January 1992 with EMMI at the NTT (ESO) (Fig. 8). Cross-correlation with an elliptical galaxy spectrum gives a redshift of 0.295 $\pm$ 0.005. This galaxy is bright (R = 19.8) allowing observations in order to determine its mass distribution. The time delay be-

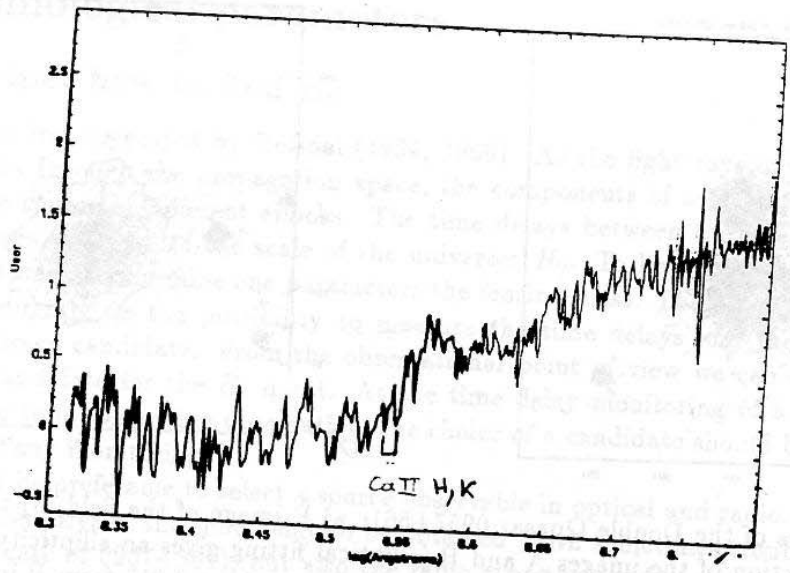

Figure 8: Spectrum of the deflecting galaxy G5 of PG 1115+080.

tween the two components of the double image A should be in order of days. A variation in the ratio of the two intensities can be interpreted as microlensing effects (see next section). From March 1984 to March 1992, four CCD frames of this mirage and four spectra of image A have been taken. Whereas no spectroscopic microlensing signature has been found by comparing the four spectra (Fig. 9) , the intensity ratio A1/A2 varied from 1.05 (Vanderriest *et al.*, 1986) to around 1.6 (Angonin-Willaime, Vanderriest and Hammer, in preparation). The last value is compatible with the HST observations (Kristian *et al.*, 1993) and those of Schechter (these proceedings)(Fig. 10).

• *UM 673:* This mirage is a very good candidate for H_0 determination: a bright well-separated double quasar with a single deflecting galaxy (Surdej *et al.*, 1987). The expected time delay is around 7 weeks. Unfortunately, the monitoring of this mirage in the last years shows a flat light curve (Daulie *et al.*, these proceedings). UM 673 is also the best example of determine the size of the Lyman α clouds from absorption lines (Smette *et al.*, these proceedings).

5 Microlensing

5.1 Generalities

Microlensing is a term used to describe the effects of a stellar or sub-stellar mass passing in front of the source image (Chang and Refsdal, 1979). If the source size is small compared to the critical radius of the star, the magnification can be significant. The source light curve presents, theoretically , symmetric achromatic magnification signatures. The source size is a crucial parameter in this phenomenon: any sub-structure of the small size source is differen-

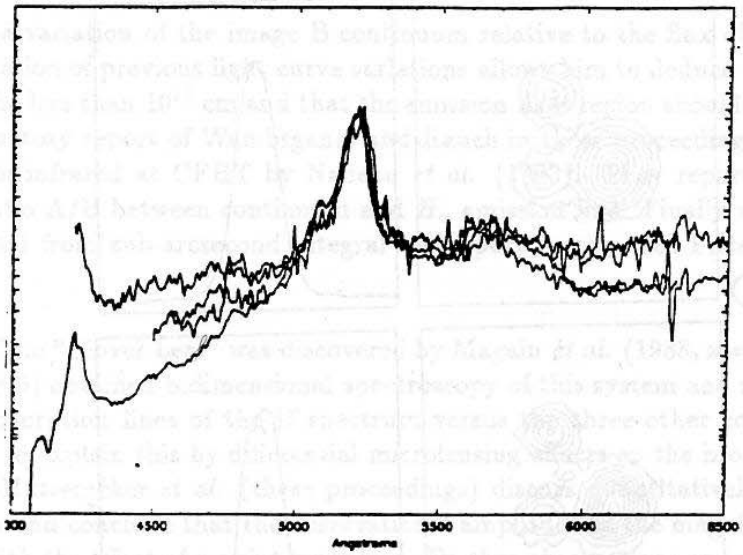

Figure 9: Comparison between 4 spectra (February and December 1986, march 1987 and March 1992) of global A component of PG 1115+080. The emission line is CIII] and the spectra are normilized in the continua.

tially magnified and, consequently, spectral characteristics are modified. The simplest way to confirm the existence of microlensing existence is to use gravitational mirage. A single variation of a component not observed in the other ones (modulo time delays) is very likely the result of microlensing effect. Moreover the lensing galaxy of macro-imaged quasars should have a large optical depth. However, some statistical studies can be interpreted as microlensing signatures: Borgeest and Schramm (1992, 1993) have detected more variability in the light curves of quasars in the close vicinity of galaxies than for those in empty fields. Furthermore, spectroscopic and photometric signatures of microlensing have been detected in a large fraction of the already-known gravitational mirage candidates: 0957+561 (Vanderriest, 1990; Schild, 1991), 2237+0305, H1413+117, PG 1115+080 (see after), 1009-0252, HE 1101-184, ... Microlensing is consequently a common phenomenon.

5.2 A magnifying glass to examine the small scales

Microlensing can be regarded as a magnifying glass to examine the small scales structures of the source for two reasons. The first is based on the fact that a well-sampled light curve can give information on the source size by deconvolution. The second uses the differential magnifications of the source substructures to compare their sizes. The two examples presented here do not describe very new observational results but illustrate these assumptions by reporting the last interpretations of the observations.

• *2237+0305:* By its "Einstein cross" configuration (separation angles between 1.4" and 1.8") and the proximity of its lens (a spiral galaxy at 0.04), this quadruple quasar (z = 1.69) is the typical mirage that can display microlensing effects. Indeed, its time delay is very short (a few days) so that any variation of the image intensities ratio should be explain by microlensing. Discovered by Huchra (1985), it became very soon the monitoring target of several teams (Corrigan *et al.*, 1991; ESO Key-Programme; ...). The components showed light variations, in particular, the A/B brightness ratio varied from 1.3 to 0.8 in less than one year. Racine

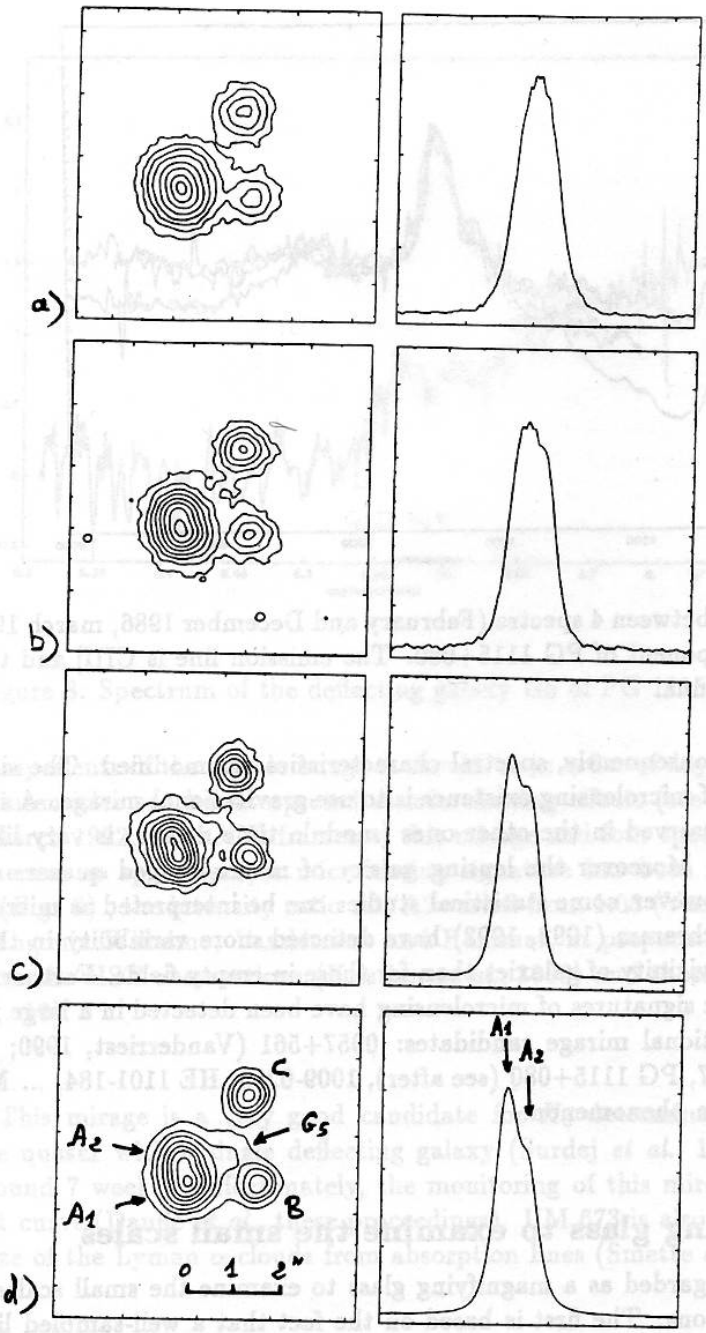

Figure 10: Pictures of PG 1115+080: variations of A1/A2. (a) March 1984 - electronographic camera - B filter - seeing 0.75"- A1/A2 = 1.05 (Vanderriest *et al.*) (b) March 1985 - electronographic camera - V filter - seeing 0.62"- A1/A2 = 1.35 (Vanderriest *et al.*) (c) May 1987 - Photon counting camera (pupil segmentation) - RG695 filter (R+I) - seeing 0.45"- A1/A2 = 1.4 (Arnaud *et al.*, private communication) (d) March 1992 - CCD SILFID imaging mode - I filter - seeing 0.54"- A1/A2 = 1.6 (Angonin-Willaime *et al.*, in preparation)

(1992) showed a variation of the image B continuum relative to the flux of the CIII] emission lines. Interpretation of previous light curve variations allows him to deduce that the continuum region have to be less than 10^{15} cm and that the emission lines region should be ten times larger (see the introductory report of Wambsganss and Rauch in these proceedings). 2237+0305 was also observed in infrared at CFHT by Nadeau *et al.* (1993). They reported an inversion of the intensity ratio A/B between continuum and H_α emission line. Finally microlensing effects was also deduced from sub-arcsecond integral field spectroscopy (see Fitte and Adam, these proceedings).

• *H1413+117:* The "Clover Leaf" was discovered by Magain *et al.* (1988, $z = 2.55$) at ESO. Angonin *et al.* (1990) obtained bidimensional spectroscopy of this system and showed a difference in the broad absorption lines of the D spectrum versus the three other components spectra. They proposed to explain this by differential microlensing effects on the broad absorption lines region clouds. Hutseméker *et al.* (these proceedings) discuss quantitatively the modelling of such a situation and conclude that the observational amplitude of the magnification can hardly be reconciled with the effect of a point mass lens. Further observations are needed to conclude. The first results of the photometric monitoring by the ESO Key-Programme were presented at this colloquium (see Arnould).

5.3 A search for small mass stars

A way of searching for compact objects in the universe with masses in the range of 10^{-5} to $100 M_\odot$ is based upon the detection of microlensing effects on pointlike sources (quasar, star). To make the detection a certainty, the ideal method can be found with instantaneous parallax observations from a large baseline (around 100 AU for a quasar), but there is as yet no such satellite available... With drastic criteria on the achromaticity, symmetry and aperiodicity of the source lightcurve, it is also possible to observe microlensing events on compact sources. Following this assumption some observational surveys in the direction of the Magellanic clouds and the Galaxy center have been launched by different teams (Alcock *et al.*, 1991; Paczynski, 1992; Griest *et al.*, 1991; see also contributions in these proceedings). First candidates detections have been announced this Autumn...

6 Conclusions

All these new optical results on gravitational lenses demonstrate the importance of the optical observation for this subject. From the nearly complete study of the "first" gravitational mirage it is possible to conclude that gravitational mirages can really provide a direct measurement of distance to remote objects and thus H_0. The problems occur with the fact that the candidate has not a structure as simple as we would like it. This means that the next candidate(s) should be very well known BEFORE beginning any monitoring. Nevertheless the quest for H_0 using gravitational mirages is still worth continuing because the telescope time cost is negligable in comparison to the other H_0 determination methods (no need for statistics) and because this is an unique direct measurement in the distant universe.

The tricky point in this study concerns the lens mass determination. Until now, this mass was measured with the dynamical properties of the lens using the virial theorem. This method is questionable because it is not a measure of the lensing mass, but it is the only method available. A suggestion to solve this problem is to select candidates for which the lens is massive enough to induce distortion of background galaxies. This means searching for arclets in the field of

already known mirages (as it has been done for 0957+561) or, conversely, searching for multiple QSOs behind rich clusters. It is not clear whether this suggestion is really an improvement in the mass determination because the lensing mass that takes place in the multiple QSO event is not strictly the same that the one for giant arcs, but it is certainly a way to verify model hypothesis.

H_0 determination is not the only point that recent observations have developed. Other gravitational lens effects have increased their scientific importance: gravitational arcs in probing the mass distribution (dark matter), microlensing in scanning the source structure and in detecting brown dwarfs. Unfortunately, all these projects are very consuming of telescope time (monitoring, surveys, spectrography of very faint objects, ...). It was the justification of the existence of a ESO key-programme which is just finishing and from which some results are described in many paper of these proceedings. It is thus not totally absurd to think of a dedicated telescope (2m?) for such tasks (see Schramm's suggestion...). Another benefit will be to use image stabilization techniques (active or adaptative optics, ...) in order to get the best seeing from the ground, either in direct imaging or integral field spectroscopy. At last, the correction of the HST and the appearance of 10m class telescopes will represent a great improvement in the observational field of gravitational lensing. Such effects should be perceptible within the next two years...

Acknowledgements

M.-C. Angonin-Willaime wishes to thank C. Vanderriest and M. Crawford for corrections of this text and helpful conversations.

References

Alcock, C., Axelrod, T., Parks, H.S.: 1991, *BAAS*, **21**, 1149
Angonin, M.C., Remy, M., Surdej, J., Vanderriest, C.: 1990, *A&A*, **233**, L5
Angonin-Willaime, M.C., Soucail, G., Vanderriest, C.: 1993, *A&A*, submitted
Angonin-Willaime, M.C., Vanderriest, C., Hammer, F., Magain, P.: 1993, *A&A*, in press
Annis, J., Luppino, G.: 1993, *Ap J*, **407**, L69
Bernstein, G.M., Tyson, J.A., Kochanek, C.S.: 1993, *A J*, **105**, 816
Blandford, R., Narayan, R.: 1992, *ARAA*, **30**, 311
Borgeest U., Schramm J.: 1992, *Lect Notes in Phys*, **406**, 164
Borgeest U., Schramm, J.: 1993, preprint
Chang, K., Refsdal, S.: 1979, *Nature*, **282**, 561
Christian, C.A., Crabtree, D., Waddell, P.: 1987, *Ap J*, **312**, 45
Conner, S., Lehár, J., Burke, B.F.: 1992, *Ap J*, **387**, L61
Corrigan, R., *et al.*: 1991, *A J*, **102**, 34
Griest, K., *et al.*: 1991, *Ap J*, **372**, L79
Hammer, F., Rigaut, F., Angonin-Willaime, M.C.: 1993, *A&A*, submitted
Henry, J.P., Heasley J.N.: 1986, *Nature*, **321**, 139
Hewitt, J., Burke, B., Turner, E., Schneider, D., Lawrence, C., Langston, G., Brody, J.: 1988, *Lect Notes in Phys*, **330**, 147
Hewitt, J., Turner, E., Lawrence, C., Schneider, D., Brody, J.: 1992, *A J*, **104**, 968

Huchra, J., Gorenstein, M., Kent, S., Shapiro, I., Smith, G., Horine, E., Perley, R.: 1985, *A J*, **90**, 691
Jones, C., Stern, C., Falco, E., Forman, W., David, L., Shapiro I.: 1993, preprint
Kayser, R., Surdej, J., Condon, J.J., Kellerman, K.I., Magain, P., Remy, M., Smette, A.: 1990, *Ap J*, **364**, 15
Kristian, J., *et al.*: 1993, *A J*, **106**, 1330
Lawrence, C.R., Neugerbauer, G., Weir, N., Matthews, K., Patnaik, A.R.: 1992, *MNRAS*, **259**, 5
Lawrence, C.R., Schneider, D.P., Schmidt, M., Bennett, C.L., Hewitt, J.N., Burke, B.F., Turner, E.L., Gunn, J.E.: 1984, *Science*, **223**, 46
Lehár, S., Hewitt, J.N., Roberts, D. H., Burke, B.F.: 1992, *Ap J*, **384**, 453
McMahon, R., Irwin, M., Hazard, C.: 1992, *Gemini* **36**, 1
Magain, P., Surdej, J., Swings, J.P., Borgeest, U., Kayser, R., Kühr, H., Refsdal, S., Remy, M.: 1988, *Nature*, **334**, 327
Magain P., Surdej, J., Vanderriest C., Pirenne, B., Hutsmeker, D.: 1992, *A&A*, **253**, L3.
Maoz *et al.*: 1992, *Ap J*, **386**, L1.
Nadeau, D., Doyon, R., Rowlands, N.: 1993, *CFHT Bulletin*, **28**, 19
Paczynski, B.: 1992, *Lect Notes in Phys*, **406**, 163
Patnaik, A.R., Browne, I.W.A., Walsh, D., Chaffee F.H., Foltz C.B.: 1992, *MNRAS*, **259**, 1
Racine, R.: 1992, *Ap J*, **395**, L65
Refsdal, S.: 1964, *MNRAS*, **128**, 295
Refsdal, S.: 1964, *MNRAS*, **128**, 307
Refsdal, S.: 1966, *MNRAS*, **132**, 101
Refsdal, S.: 1966, *MNRAS*, **134**, 315
Rhee, G.: 1991, *Nature*, **350**, 211
Schechter, P., Moore, C.: 1993, *A J*, **105**, 1
Schild, R.E., Smith, R.C.: 1991, *A J*, **101**, 813
Schneider, D.P., Gunn, J.E., Turner, E.L., Lawrence, C.R., Hewitt, L.W., Schmidt, M., Burke, B.F.: 1986, *A J*, **91**, 991
Shaklan, S.B., Hege, E.K.: 1986, *Ap J*, **303**, 605
Surdej, J., Magain, P., Swings, J.P., Borgeest, U., Couvoisier, T.J.L., Kayser, R., Kellerman, K.I., Kühr, H., Refsdal, S.: 1987, *Nature*, **329**, 695
Surdej, J., Magain, P., Swings, J.P., Couvoisier, T.J.L., Kayser, R., Kellerman, K.I., Kühr, H., Refsdal, S.: 1988, *A&A*, **198**, 49
Vanderriest, C.: 1990, *Lect Notes in Phys*, **360**, 210
Vanderriest, C., Wlérick, G., Lelièvre, G., Schneider, J., Sol, H., Horville, D., Renard, L., Servan, B.: 1986, *A&A*, **158**, L5
Walsh, D., Carswell, R.F., Weymann, R.J.: 1979, *Nature*, **279**, 381
Weymann, R.J., Latham, D., Angel, J.R.P., Green, R.F., Liebert, J.W., Turnshek, D.A., Turnshek, D.E., Tyson, J.A.: 1980, *Nature*, **285**, 641
Young, P., Gunn, J.E., Kristian, J., Oke, J.B., Westphal, J.A.: 1980, *Ap J*, **241**, 507

Further observational evidence that MG J0414+0534 is a gravitational mirage

Angonin-Willaime M-C, Vanderriest C, Hammer F, Magain P, 1994, Astronomy and Astrophysics, **281**, 388

+ *Erratum* : 1994, Astronomy and Astrophysics, **292**, 722

Astron. Astrophys. 281, 388–394 (1994)

ASTRONOMY AND ASTROPHYSICS

Further observational evidence that MG J0414+0534 is a gravitational mirage*

M.-C. Angonin-Willaime[1], C. Vanderriest[1], F. Hammer[1], and P. Magain[2]

[1] DAEC, Observatoire de Paris-Meudon, 5 Place Janssen, F-92195 Meudon Cedex, France
[2] Institut d'Astrophysique, Université de Liège, 5 avenue de Cointe, B-4000 Liège, Belgium

Received May 10, accepted July 26, 1993

Abstract. Deep imaging of MG J0414+0534 with R and I filters reveals a faint, fuzzy and red object at the exact location expected for a lensing galaxy in the gravitational mirage hypothesis. Furthermore, the (extremely red and almost featureless) spectra of the 2 brightest components are very similar.

These are strong indications that the system results from multiple gravitational imaging of a single source, but the nature of this source is not yet clear. It could be the nucleus of a low metallicity galaxy at a high redshift or a new type of object.

Significant differences are observed between the flux ratios of the images at radio and optical wavelengths. The most likely explanation for this effect is a differential amplification of the image pair A_1-A_2 because of the large magnification gradient near a caustic.

Key words: gravitational lensing – radio sources – MG J0414+0534

1. Introduction

Among the various effects of gravitational lensing, the gravitational mirage phenomenon (i.e.: multiple imaging of a distant source) is a rare but especially interesting occurence. Seeing a single object through different pathways may have several astrophysical applications. Of the very few cases discovered until now, almost each one is singular and MG J0414+0534 (although is has been omitted until now, we add the prefix J because the coordinates are expressed for equinox 2000) is a candidate with puzzling characteristics.

The peculiar morphology of this source was recognized during a search for gravitational mirages candidates in the MIT-Green Bank Survey (Bennett et al. 1986). High resolution VLA maps showed 4 unresolved images with similar radio indices between 5 and 15 GHz, in a configuration closely ressembling that of the radio-quiet PG 1115+080 (Hewitt et al. 1988a). At optical wavelengths, faint images are seen at the locations of the radio components, with approximately the same intensity ratios. This constitutes a good evidence for a gravitational lensing system, without being a definite proof; in particular, no lensing body was detected until recently (Schechter & Moore, 1993; hereafter SM) and the nature of the source is still unknown (Hewitt et al. 1992; herafter HTLSB).

The new observational results on MG J0414+0534 presented in this article throw some light on these two issues and reinforce the gravitational lens interpretation.

Send offprint requests to: M.C. Angonin

* Based on observations collected with the Canada-France-Hawaii Telescope at Mauna Kea (Hawaii, USA) and with the NTT of the European Southern Observatory (Chile)

2. Observations

The observations were made at ESO (in the framework of a Key-Programme on gravitational lensing) and at CFHT. A set of CCD pictures has been obtained in good seeing conditions and with a fair sampling; the spectroscopy of the 2 brightest components was also attempted with the spectrograph EMMI on the NTT. The best data, which we will analyse here, are listed in Table 1.

2.1. Imagery

The data from CFHT were obtained with the imaging mode of the spectrograph SILFID (Vanderriest & Lemonnier 1988). In this configuration, the transmission of the optics is around 0.7 - 0.8 for the considered wavelength range. The same is true for the data obtained with EFOSC2 on the NTT.

2.1.1. Analysis of the optical structure; detection of the lensing galaxy

On all the individual frames in I band and on the best frames in R, a fuzzy component is already visible, very near the expected position for a lensing galaxy (see for instance the model in HTLSB).

We generated a composite picture in I by summation of the CFHT and the NTT exposures, after reduction to a common

Table 1. Journal of observations

Date (y-m-d)	telescope + instrument	filter or grism	exposure time (mn)	seeing or slit width ($''$)	sampling ($''$/pixel)
91-12-07	CFHT + SILFID	V	20	$1.0''$	$0.21''$
91-12-08	CFHT + SILFID	V	2×15	$0.85''$	$0.21''$
91-12-09	CFHT + SILFID	V	30	$0.9''$	$0.21''$
90-08-24	NTT + EFOSC2	R	30	$0.65''$	$0.15''$
91-12-07	CFHT + SILFID	R	2×15	$0.8''$	$0.21''$
91-12-08	CFHT + SILFID	R	15	$0.85''$	$0.21''$
92-09-21	2.2m ESO + CCD	R	2×30	$0.85''$	$0.18''$
92-09-25	NTT + SUSI	R	20	$0.75''$	$0.13''$
92-03-01	CFHT + SILFID	I	2×10	$0.6''$	$0.18''$
92-09-25	NTT + SUSI	I	15	$0.7''$	$0.13''$
92-01-11	NTT + EMMI	G1	45	$2''$	$0.46''$
92-01-12	NTT + EMMI	G4	45+30	$2''$	$0.46''$
92-09-26	NTT + EMMI	G4	2×40	$1''$	$0.46''$

sampling of $0.13''$ by a spline interpolation. The final picture, slightly smoothed (gaussian filter with FWHM = 1 pixel) has a resolution around $0.73''$ and shows very conspicuously the fuzzy component (Fig. 1a) suspected on individual frames. The images B and C are not resolved, while the elongation of image A can be reproduced by a model of 2 point sources (A_1 and A_2) with an intensity ratio $\simeq$ 2-3 and separated by around $0.45''$. This configuration is in good agreement with the radio maps from the VLA (Katz & Hewitt 1993), except for the A_1/A_2 ratio . In order to measure the extended ("galaxy") component, we thus have to subtract 4 point sources with proper locations and amplitudes.

We firstly used an automatic decomposition algorithm with synthetic bidimensional PSF, especially written for the processing of such complex images (Magain et al. 1993). It works extremely well when the PSF is invariant in the field, which is not strictly realized in this case. The best fit corresponds to A/B = 3.2 and B/C $\simeq$ 2.0 and gives very small residuals in the outer parts of the complex image, thus confirming that the source is not resolved. As there is no real overlap between A (taken globally), B and C, we could also attempt a direct decomposition by interactive gaussian fitting in X and Y. This method gives also a good result, with A/B = 3.2 and B/C $\simeq$ 3.0. The profile of the left-over "galaxy" looks even smoother in the region of image C (Fig. 1b). In fact, the decomposition depends on the assumed profile of this galaxy. The difference for the amplitude of the faintest image between the 2 methods is thus not too surprising. A closer examination of the raw data suggests that the real value for B/C is somewhere between the above values; we adopt B/C = 2.5 $\pm$ 0.5. The galaxy G is definitely extended, with FWHM $\simeq 1.5''$.

A combination of our best R pictures (Fig. 2a), giving a final resolution of $0.87''$, shows also clearly the galaxy G and was processed in the same way as the I picture, producing the residual displayed on fig 2b. The relative importances of the different components is very similar to those of the I picture.

On the composite V picture (Fig. 3a), MG J0414+0534 is hardly detectable. The position of the most conspicuous feature indicates that it results from a mixing of G and A; the isophotes of G (average of R and I data) are superimposed on Fig. 3b for comparison. The image B is just emerging from the noise, while C is below the detection threshold.

2.1.2. Photometry

The flux calibration of the different frames relies on observations of a few standard stars from Landolt (1983) or a sequence in NGC 2264 (Christian et al. 1985). The agreement between these independent calibrations is very good, indicating a zero point error probably less than 0.05 mag. The resulting magnitudes are listed in Table 2 for the source images and the galaxy G, as well as for a few reference stars and 3 typical galaxies in the field (identification in Fig. 3). The flux ratios of the images are given in Table 3 and compared to other measurements; their relative positions are in Table 4. The measured flux of galaxy G is in good agreement with SM in I filter; for the R filter, it is much larger (by 2 magnitudes) than the upper limit given by HTLSB. The most likely explanation of this discrepancy is that galaxy G is not well resolved in their data because of the poorer seeing and S/N. As a consequence, the flux of the faintest image (C), which is also the closest to G, was largely overestimated.

The colour indices of the different objects in the field can be obtained from Table 2. The putative deflecting galaxy is very red (redder than galaxies g_1 to g_3) but not as much as the radio source itself. We notice the similar colours of the 3 images, near 1.8 in (R-I) and no contradiction of our data with the hypothesis of similar colours in (V-R).

Finally, we added together the composite I and R pictures, in order to reach a deep detection level on red objects. On this frame (fig 4) we notice the presence of some very faint galaxies in the field (the R magnitude of the faintest objects detected is around 26.5) without obvious clustering around the mirage.

Table 2. Photometric data

Object :	V	R	I	(R-I)
M	22.67 ± 0.08	21.09 ± 0.04	19.23 ± 0.04	1.95 ± 0.1
2	22.59 ± 0.08	21.41 ± 0.04	20.21 ± 0.05	1.2 ± 0.1
3	22.61 ± 0.08	21.98 ± 0.05	21.09 ± 0.06	0.9 ± 0.1
4	23.80 ± 0.15	23.04 ± 0.07	21.92 ± 0.08	1.1 ± 0.1
5	> 25	24.03 ± 0.10	22.07 ± 0.10	1.95 ± 0.15
6	24.7 ± 0.4	23.70 ± 0.10	22.09 ± 0.10	1.6 ± 0.15
g_1	24.3 ± 0.3	23.8 ± 0.15	22.9 ± 0.15	0.9 ± 0.2
g_2	23.6 ± 0.2	23.0 ± 0.10	22.2 ± 0.12	0.8 ± 0.15
g_3	23.0 ± 0.15	22.4 ± 0.08	21.55 ± 0.10	0.85 ± 0.15
G	24.4 ± 0.5	22.4 ± 0.15	20.85 ± 0.10	1.55 ± 0.2
A	24.7 ± 0.5	22.15 ± 0.08	20.33 ± 0.06	1.8 ± 0.1
B	25.5 ?	23.35 ± 0.12	21.61 ± 0.10	1.7 ± 0.2
C	> 25.5	24.6 ± 0.2	22.6 ± 0.2	2.0 ± 0.3
"X"	> 25.5	26.3 ± 0.5	24.7 ± 0.5	1.6 ± 0.7

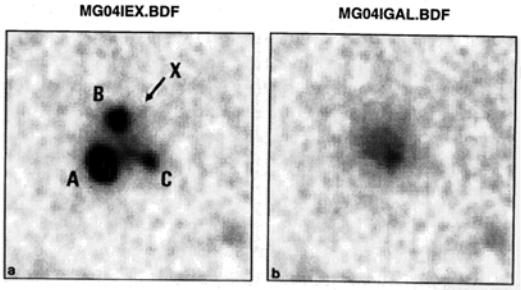

Fig. 1a and b. Composite picture of MG J0414+0534 in I band (see text). The field is 10″ on a side. Galaxy g_1 is on the lower right corner. **a** raw picture **b** residuals after subtraction of the images A, B and C

A very faint component is seen near the position of the "object X" detected by SM. On both the R and I composite pictures, it is close to the 3 σ magnitude limit, but still measurable. The (R-I) colour index is too poorly determined to be really useful. It is compatible with X being another image of the source, but a more likely interpretation is that it is a distant galactic star unrelated to the lens system.

The R data, independently reduced for the 3 epochs of observation (August 90, December 91 and September 92), do not show clear evidence for a variability of the source: the total amplitude found for image A, $\Delta R = 0.20 \pm 0.12$, could not be considered significant. Moreover, the global flux (A+B+C+G) is comparable to the previous measurements (HTLSB) in 1987 and 1989. Let us also notice that we should be cautious when comparing different observations of this objet: because of the steepness of its spectrum, the photometry is very sensitive to the exact shape of the instrumental passband, which includes filter, CCD response curve and atmospheric extinction. For instance, this explains the notable difference between our photometric data in I band and the I' data from SM.

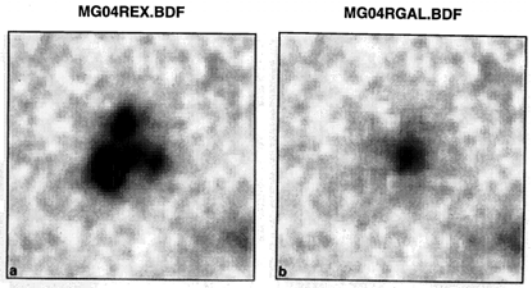

Fig. 2. Composite picture of MG J0414+0534 in R band (same processing than for Fig. 1)

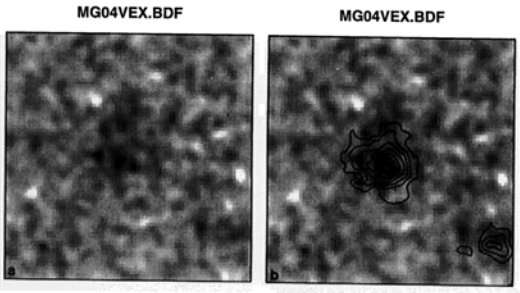

Fig. 3a and b. Composite picture of MG J0414+0534 in V band. **a** raw picture **b** Superimposed to the same picture, an isophotal plot of the galaxy, from the average of the I and R data

2.2. *Spectroscopy*

For the observations with EMMI, the slit was positioned along the A-B direction. The seeing was around 0.8″ in all cases, allowing a good separation of the 2 spectra (Fig. 5, insert). In January 1992, the 2″ slit width gave resolutions around 20 Å and 45 Å, respectively, for the 2 used grims. For the September data, the slit width was 1.0″, giving a resolution of 10 Å. The spectrophotometric standard was H 600 (Massey et al. 1988; Massey & Gronwall 1990).

Figure 5 shows the sum of all the exposures with grism G4, reduced to the lowest resolution and slightly smoothed (final resolution 30 Å). The 2 spectra have a very similar shape, with a constant flux ratio (around 3) in the whole wavelength range. As already known for the sum A+B, the continuum is very red and without obvious feature, except for a deep absorption line near 8663 Å (HTLSB). This line, seen on both spectra, does not seem to be an artefact from night sky subtraction. A sky emission band from O_2 is close to the measured wavelength and quite strong, but not as strong as the surrounding OH(6,2) and (7,3) emission complexes. Beyond 9250 Å, the spectrum is plagued by atmospheric absorption and poor Signal/Noise; nothing reliable could be measured.

The 8663 Å absorption is the only secure feature. We observe also a slight raising of the continuum redwards of this

Table 3. Flux ratios

Ratio:	radio 1987 (HTLSB)	I 1987 (HTLSB)	I 1991 (SM)	I 1992 (this work)
A/B	5.0 ± 0.2	2.9 ± 0.1	3.2 ± 0.2	3.2 ± 0.2
A/C	14 ± 1	(4.3 ± 0.2)	7.3 ± 0.5	8 ± 1
B/C	2.8 ± 0.2	(1.5)	2.3 ± 0.3	2.5 ± 0.5

Table 4. Relative astrometry (origin on B)

	radio (HTLSB)		optical (this work)	
	$\Delta\alpha$ ($''$)	$\Delta\delta$ ($''$)	$\Delta\alpha$ ($''$)	$\Delta\delta$ ($''$)
A	+0.66 ± .01	− 1.72 ± .01	+0.61 ± .03	− 1.77 ± .03
C	−1.34 ± .01	− 1.64 ± .01	−1.39 ± .04	− 1.56 ± .04
G	−0.38 ± .01	− 1.24 ± .01	−0.45 ± .06	− 1.27 ± .04
	(calculated position for G)			

line, already noticed in HTLSB but attributed to residuals of sky subtraction. The feature could be real, since we can trace it between 8670 and 8760 Å, a region almost free of sky emission on the best resolution data. A priori, this would suggest an identification with the 4000 Å break, the 8663 Å absorption being then identified with Ca H + Hϵ, which gives the tentative redshift $Z_S = 1.18$.

Another value $Z_S = 2.63$ has been mentioned for this object (for instance in a review paper by Blandford & Narayan 1992) but the data are not yet published. This value is neither strongly supported nor excluded by our spectra: nothing is detected at the expected position of Ly α from the data with the grism G1, which cover the interval 4000-10200 Å. It would imply a very large reddening in the source itself. The 8663 Å absorption feature could be interpreted as the 2380 FeII blend observed in the spectra of star-forming galaxies (Kinney et al. 1993); it could also be a feature related to the lensing galaxy or a foreground object. So, in the following, we will consider that the redshift of the source is *at least* 1.18; the conclusions about the lensing are essentially the same for a higher value.

3. Discussion

3.1. The nature of the source

The extremely red colour of MG J0414+0534 could result, in part, from strong absorption by dust and reddening. In this area, the instellar absorption is negligible (Burstein & Heiles 1982), corresponding to E(B-V) < 0.2. A reddening by the lens galaxy G is unlikely: in order to explain the observed colours, such a reddening should be exactly the same for image A and B (and, with a lesser precision, C) while these images are seen through different parts of G. This would mean a surprisingly uniform absorption on a scale of 10 kpc. Thus, if a large reddening is involved, it is more likely intrinsic to the source.

We do not understand exactly the nature of this source, but could find similarities with two other lensed objects which have also a very red spectrum and a strong radio flux. The "Einstein ring" MG J1131+0456 (Hewitt et al. 1988b; Hammer et al. 1991) is bright in infrared and is described as an "unusually red radiogalaxy" (Annis 1992). The ring 0218+357 (O'Deal et al. 1992; Patnaik et al. 1993) is very red too and its optical spectrum, with an almost vanishing 4000 Å break, bears some ressemblance with the one of MG J0414+0534.

Indeed, MG J0414+0534 and MG J1131+0456 are among the reddest extragalactic objects, with R-K indices larger than 6. The latter one can be classified as a radiogalaxy because of its optical extension (Hammer et al. 1991), while the compactness of MG J0414+0534 (size smaller than 5 kpc for $Z_S > 1$ and $H_o = 50$) makes it more similar to the infrared objects that Walsh et al. (1985) classified as QSOs. It could be, also, the bright nucleus of a faint radiogalaxy. Anyway, despite their large radio fluxes, MG J0414+0534 and MG J1131+0456 are not classical radiogalaxies; neither could they be assimilated to classical BL Lac. objects. Taking into account the magnification by lensing (cf. Hammer et al. 1991), their infrared luminosities are comparable to the ones of 3C galaxies (Annis & Luppino 1993), but they are about 3 magnitudes fainter in visible light (UV at rest) and radio. Another striking difference is the absence of any emission line activity linked with starbust or active nucleus. We thus guess that, aside from the classical powerful radiogalaxies, a new and relatively abundant population of fainter radiogalaxies should exist at high redshifts, with a quite different stellar content. The knowledge of the properties of such objects and their evolution could be important for understanding the galaxy formation process.

3.2. The nature of the lens

We do not know the redhift Z_G of the lens galaxy, but its apparent magnitude and size (1.5″ FWHM) suggest a value around 0.7-0.8 and the colour indices agree with an elliptical in this range.

The $(M/L)_V$ ratio for Z_G=0.7 and Z_S=1.2 is of the order of 50 if we assume, for the sake of simplicity, a mass distribution corresponding to a singular isothermal sphere or a point mass and the K_V correction of a normal elliptical galaxy. This rough estimate only suggests that the contribution to the lensing by a cluster and/or a dark matter component is not dominant.

For a realistic model, the most needed data now seem to be the reshifts of the source and of the lensing galaxy G. Measuring also the redshifts of the less feeble galaxies in the field (at least, g_2 and g_3) would help to probe the existence of an associated cluster.

3.3. MG J0414+0534 as a gravitational mirage

Even if we do not know precisely the nature of the source and its distance, there is no doubt that it is a remote extragalactic object. The similarity between the two images spectra, the component configuration and especially the detection of a fuzzy object at the "right" place are cumulative evidences for a scenario of gravitational lensing by a medium distance galaxy.

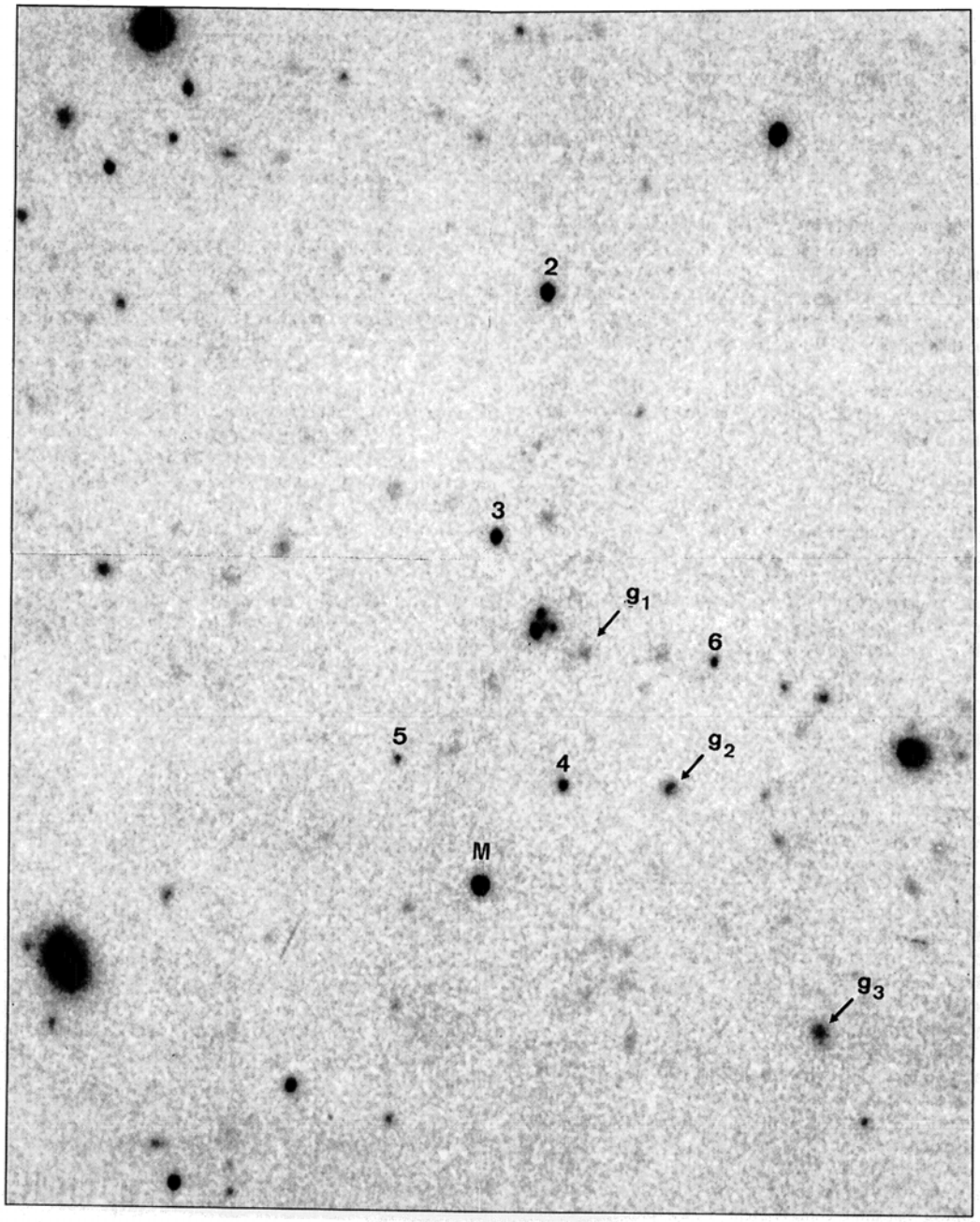

Fig. 4. Sum of all the I and R exposures, with identification of the photometric sequence (field $\simeq 1'45'' \times 2'\ 10''$). Note that most of the faint galaxies are elongated and that g_2 and g_3 show resolved structures

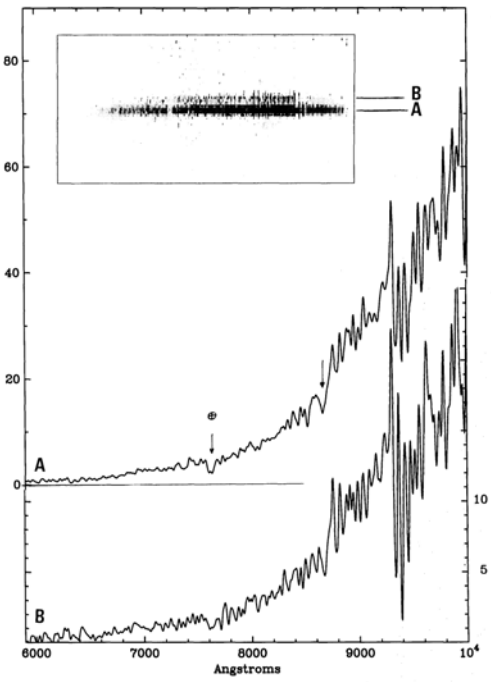

Fig. 5. Spectra of images A and B from the data with grism 4. The fluxes are in units of 10^{-21} W m^{-2} Å^{-1} (left scale for A, right scale for B). The strongest telluric absorptions are identified. Inserted is a bidimensional representation of the coadded data, after removal of cosmetic defects and of the night sky emission

But the flux ratios of the images (Table 3) do not seem to support, at first sight, such a conclusion. The radio data presented in HTLSB correspond to very similar flux ratios at both frequencies of 5 GHz and 15 GHz: 5.0±0.2 for A/B and 14±1 for A/C (thus B/C = 2.8±0.2). On the other hand, our optical data from 1991-92 give A/B = 3.2±0.2, A/C=8±1 (i.e. B/C = 2.5±0.5) in I and A/B=3.0±0.3, A/C=9.5±1.5 (i.e. B/C=3.2±0.5) in R. Our new photometric decomposition is in better agreement with the radio data than the one published in HTLSB; however there remains a significant discrepancy for the A/B ratio, which is rather well measured. This does not mean that the lensing hypothesis must be rejected. Firstly, within the precision of measurements, the radio and optical B/C ratios are identical and everything would be "in order" if the A component were dimmed by a factor 1.6 between the two domains of wavelengths. We can think of several explanations:

(1) *Extinction by galaxy G*: On the high resolution VLA maps published by Katz & Hewitt (1993) the flux ratio A1/A2 is measured at 1.15 ± 0.05 while we estimate it near 0.3 ± 0.1 from the best I pictures. Most of the optical/radio discrepancy is then due to component A1. If obscuration by a cloud in the lensing galaxy is the explanation, it amounts to about 1.5 magnitude in I, which means more than 2 magnitudes in R. We should thus have in this colour A1/A2 = 0.18 and A/B = 2.9. Clearly, this explanation could not be ruled out by the present data. More precise photometry on A1/A2 is needed. However, as G seems to be an elliptical galaxy, such an heavy obscuration seems unlikely.

(2) *Intrinsic variability of the source and time delay effect*: This explanation is also unlikely. There is no well defined variability (cf. Sect. 2.1.2). There is also a significant discrepancy between the radio and optical data obtained almost simultaneously in 1987 by HTLSB. Although their flux measurements of component C are questionable because of the presence of G, the A/B ratio seems secure.

(3) *Variability of image A by microlensing*: Again, there is no direct evidence for a variability with the required amplitude of $\simeq 0.5$ magnitude.

(4) *Differential magnification by microlensing*: This is a well known effect if the positions and/or sizes of the optical and radio sources are slightly different on a scale comparable to the Einstein radius of the microlens. This can also produce a differential magnification between emission lines and optical continuum of a quasar, an effect observed in Q0957+561 (Vanderriest 1990; Schild & Smith 1991) and H1413+117 (Angonin et al. 1990).

(5) *Magnification gradient near a caustic*: There is no real need for a microlensing event. What is needed is a magnification gradient on angular scales comparable to the characteristic size of the source. In the most likely gravitational lensing models of MG J0414+0534, the source would be at a distance $< 0.1''$ from the tangential (inner) caustic and thus already in a region of large magnification gradient.

This effect is invoked in the case of 0957+561 for explaining the different flux ratios observed at radio and optical wavelengths (Conner et al. 1992). It is certainly present here if the source is resolved in radio on a scale of a few $10^{-2}''$ (HTLSB). The radio flux is large enough for VLBI observ ations, which makes it possible to check this interpretation. If a resolved structure is found, like for 0957+561 (Gorenstein et al. 1988) and 2016+112 (Heflin et al. 1991), the magnification variations could be mapped quite precisely.

4. Conclusions and suggestions

We think that MG J0414+0534 is another example of gravitationally lensed source with unusual characteristics: strong radio emission, extremely red and almost featureless optical spectrum. To some degree, it shares these properties with the "Einstein rings" MG J1131+0456 and 0218+357. It is extremely unlikely that such unusual sources have been lensed by chance if they were rare. The best hypothesis is that they belong to a new category of quite common objects which were not previously noticed (maybe because they are abundant only at high redshifts and optically faint when not magnified by the gravitation). In this case, numerous unlensed representants should be found in

the MG catalogue, for instance. It would be interesting to undertake a small photometric and spectroscopic survey among the MG sources that are not (or hardly) resolved with the VLA and have no optical counterpart at the limit of the POSS.

More generally, an interesting property of gravitational mirages is to reveal populations that would stay otherwise unnoticed. As it occurs at random, the magnification lessens the observational biases, while multiple imaging is an efficient "flag" for drawing attention to the imaged source. Without magnification, MG J0414+0534 would be fainter than R = 24 and nobody would have taken the trouble to make a spectrum.

Aside from the still unknown nature of its source, this gravitational mirage could be an interesting candidate for astrophysical applications like the measurement of H_o. Even more for this system than for PG 1115+080 (because of the supplementary advantage of being a radio-source), the observations could constraint strongly the models. MG J0414+0534 is the brightest gravitational mirage in radio and shows a simple structure at the resolution of the VLA, unlike H 1413+117 for instance (Kayser et al. 1990). A VLBI study of the 4 images could thus be very informative. Because of the optical faintness of the source, its seems also easier to determine the time delays between the images from radio observations. The lens does not seem to be as complex as the one of 0957+561, but it is not possible to exclude that faint galaxies associated to G are involved in the lensing. Deeper imaging is needed to check this point.

Then, remains the problem of measuring the redshifts of the source and of the lens. The tentative redshift for the source could be confirmed with better S/N optical spectra, which is essentially a matter of integration time with large telescopes. Near IR spectra could also be useful for the determination of Z_S and would give at the same time the shape of the continuum beyond 1 μm. For measuring the redshift of the lens Z_G, bidimensional spectroscopy techniques (e.g. Vanderriest & Angonin 1992) seem required, associated with very powerful light collectors, like the 8-10 m telescopes that will be soon available.

References:

Angonin M.-C., Remy M., Surdej J., Vanderriest C. 1990: A&A, 233, L.5.

Annis J. 1992: ApJ., 391, L.17.

Annis J., Luppino G. 1993: ApJ., 407, L.69.

Bennet C., Lawrence C., Burke B., Hewitt J., Mahoney J. 1986: ApJS., 61, 1.

Blandford R., Narayan R. 1992: ARAA, 30, 311.

Burstein D., Heiles C. 1982: AJ., 87, 1165.

Christian C., Adams M., Barnes J., Butcher H., Hayes D., Mould J., Siegel M. 1985: P.A.S.P., 97, 363.

Conner S., Lehar J., Burke B. 1992: ApJ. Lett., 387, L. 61.

Gorenstein M., Cohen N., Shapiro I., Rogers A., Bonometti R., Falco E., Bartel N., Marcaide J. 1988: ApJ., 334, 42.

Hammer F., LeFèvre O., Angonin M.-C., Meylan G., Smette A., Surdej J., 1991: A&A, 250, L.5.

Heflin M., Gorenstein M., Lawrence C., Burke B. 1991: ApJ., 378, 519.

Hewitt J., Burke B.,Turner E., Schneider D., Lawrence C., Langston G., Brody J. 1988a, in: *"Gravitational lenses"*, Lecture Notes in Physics, 330, p. 147.

Hewitt J., Turner E., Schneider D., Burke B., Langston G., Lawrence C., 1988b: Nature, 333, 537.

Hewitt J., Turner E., Lawrence C., Schneider D., Brody J. 1992: A.J., 104, 968. (HTLSB)

Katz C., Hewitt J. 1993: ApJ., 409, L.9.

Kayser R., Surdej J., Condon J., Kellermann K., Magain P., Remy M., Smette A. 1990: ApJ, 364, 15.

Kinney A., Bohlin R., Calzetti D., Panagia N., Wyse R. 1993: ApJS, 86, 5.

Landolt A. 1983: A.J., 88, 439.

Lawrence C., Bennett C., Hewitt J., Langston G., Klotz S., Burke B., Turner K. 1986: ApJS, 61, 105.

Magain et al. 1993: preprint

Massey P., Gronwall C. 1990: ApJ., 358, 344.

Massey P., Strobel K., Barnes J., Anderson E. 1988: ApJ., 328, 315.

O'Dea C., Baum S., Stanghellini C., Dey A., van Breugel W., Deusta S., Smith E. 1992: A.J., 104, 1320.

Patnaik A., Browne I., King L., Muxlow T., Walsh D., Wilkinson P. 1993: MNRAS, 261, 435.

Schechter P., Moore C. 1993, A.J., 105, 1. (SM)

Schild R., Smith C. 1991: A.J., 101, 813.

Vanderriest C. 1990, in: *"Gravitational lensing"*, Lecture Notes in Physics 360, 210.

Vanderriest C., Lemonnier J.-P. 1988, in: *"Instrumentation for ground based optical Astronomy"* (Robinson ed.), p.304.

Vanderriest C., Angonin M.-C. 1992, in: *"Gravitational lenses"*, Lecture Notes in Physics, 406, 97.

Walsh D., Lebofsky M., Rieke G., Shone D., Elston R. 1985: MNRAS, 212, 631.

Astron. Astrophys. 292, 722 (1994)

ASTRONOMY
AND
ASTROPHYSICS

Erratum

Further observational evidence that MG J0414+0534 is a gravitational mirage

M.-C. Angonin-Willaime[1], C. Vanderriest[1], F. Hammer[1], and P. Magain[2]

[1] DAEC, Observatoire de Paris-Meudon, 5 Place Janssen, F-92195 Meudon Cedex, France
[2] Institut d'Astrophysique, Université de Liège, 5 avenue de Cointe, B-4000 Liége, Belgium

Astron. Astrophys. **281**, 388–394 (1994)

In Sect. 3.3, the identifications of components A1 and A2 for the optical data were inadvertently inverted. This does not change substantially the discussion; just read A1 for A2 and vice versa. In particular, the ratio A2/A1 = 0.3 cannot be made compatible with the radio value without one or several of the mechanisms we suggested.

We appologize for the error and thank Dr S. Mao for bringing it to our attention.

Imaging of 16 distant EMSS clusters with $z \geq 0.2$ and $L_{X,44} \geq 4$: new arcs and first consequences

Le Fèvre O, Hammer F, Angonin M-C, Gioia I, Luppino G, 1994, Astrophysical Journal, **422**, L5

THE ASTROPHYSICAL JOURNAL, 422:L5–L8, 1994 February 10

IMAGING OF 16 DISTANT EMSS CLUSTERS WITH $z \geq 0.2$ AND $L_{X,44} \geq 4$: NEW ARCS AND FIRST CONSEQUENCES[1]

O. LE FÈVRE,[2,3] F. HAMMER,[2,3] M. C. ANGONIN,[3] I. M. GIOIA,[4,5,6] AND G. A. LUPPINO[4]

Received 1993 September 13; accepted 1993 November 15

ABSTRACT

Medium-deep V, R, and I observations of a subsample of 16 clusters of galaxies in the EMSS sample defined from the *Einstein* satellite data are presented. Three new cases of clusters with giant luminous arcs (length/width > 10, $V < 22$) have been discovered together with six new arcs ($4 < l/w < 10$, $V < 22$), and we propose that these arcs are new examples of gravitational lensing of background galaxies by the rich clusters. Combined with giant luminous arcs already observed in the EMSS sample, there is a total of six giant luminous arcs observed in the sample of 16 clusters. This high rate of success in finding arcs added to their axis ratio distribution is consistent with very small core radii (< 100 kpc) for the dark matter distribution in rich clusters, and rules out models in which dark matter follows the X-ray gas.

Subject headings: dark matter — galaxies: clustering galaxies: clusters of — gravitation — gravitational lensing

1. INTRODUCTION

The giant luminous arcs, lensed images of background galaxies observed in clusters of galaxies, represent a unique mean to get direct information on the deflecting cluster mass distribution. They provide an independent mass estimation which can be compared to other estimations, for example, from dynamical analysis and X-ray data. Furthermore, while these methods have to assume nontrivial conditions for the cluster the axis ratio, and locations for giant arcs in rich distant clusters have been found to be critically dependent on the cluster mass density profile (Hammer 1991; Wu & Hammer 1993). For instance, one giant luminous arc is expected for every three or four rich distant clusters observed ($L_X > 5 \times 10^{44}$ ergs s^{-1} and $z > 0.15$) if the cluster density profiles follow a $r^{1/4}$ law, while this should be 10 times lower if cluster mass profiles follow the X-ray hot gas profile.

close to the detection limit or in cD galaxy halos. When available, images obtained with different filters were similarly explored. When an arclike object was found, we tried to confirm the detection from a different bandpass image.

Three new giant luminous arcs (defined as having a length to width ratio larger than 10 and $V \lesssim 22$) and more than eight other new arcs either fainter than $V = 22$ or with $4 \leq l/w \leq 10$ have been found in our images. New arc candidates are identified in Table 1. We give here a description of the new arc candidates:

MS 0451.5+0250.— This object has a complex X-ray structure and may be a composite source. The field is rich with galaxies in a very irregular distribution. The candidate arc is near a bright elliptical galaxy to the NE of the densest region of galaxies.

MS 1006.0+1202.—Three new gravitational arcs are observed in this field (Fig. 1 [Pls. L1–L4]). They all show a linear structure, that is, no curvature is observed. The orientation of the arcs major axis may be an indication of some irregularity in the cluster potential.

MS 1008.1−1224.—A thin arc is seen to the north and a bright arc to the east (Fig. 1). A large radial arc is possibly observed and looks resolved.

MS 1455.0+2232.—An arclike structure is observed 19″.4 from the giant cD galaxy (Fig. 1). It breaks into two peaks in R that might represent source structures or two images association.

MS 1910.5+6736.—A straight structure is observed 67″ from the central galaxy and is 6″.1 in length (Fig. 1). It can be classified as a giant luminous arc ($l/w > 10$) since it is not resolved in width (see Table 1). Another straight object is observed in R 48″ from the central galaxy, but the V image shows a very definite central core that indicates that this is probably an edge-on spiral galaxy.

3.2. *Completeness of the Sample*

All the 16 clusters discussed in the present sample have been observed by us or by others (MS 0302.7+1658: Mathez et al. 1992; MS 1621.5+2640 and MS 2053.7−0449: Luppino & Gioia 1992; MS 2137.3−2353, Fort et al. 1993, see Table 1) among the EMSS clusters in the Gioia et al. (1990a) sample, which was used to investigate the X-ray luminosity function and its evolution (Gioia et al. 1990b). This forms a complete sample of rich distant clusters of galaxies with $L_X > 4 \times 10^{44}$ ergs s^{-1} and $z > 0.2$.

The field of view (minimum 3′ × 3′) ensures that we have indeed detected all of the giant arcs associated with one cluster (see also Table 1). All our images have a surface-brightness limit, $\mu_V > 25.3$, $\mu_I > 25.2$ mag arcsec^{-2} (1 σ), which ensures that we are able to detect securely any gravitational images ("arcs") having $V \lesssim 22.5$ or $I \lesssim 21.5$. One could wonder about the possible bias which favors the detection of thin arcs that present a better contrast than thicker and well-resolved arcs. $I < 21.5$ (or $V < 22.5$) arcs should be detected above the 1 σ level for sizes (length × width) lower than 20 arcsec^2 (14 arcsec^2 in V). There is no indication that extremely large arcs (with extremely low surface brightness) are present in our sample, although this will be checked when deeper images are available.

3.3. *Arc Sample and the Arc Identification Criteria*

To define a sample of relatively bright gravitational images, one should carefully account for the contamination by foreground galaxies, and especially of the cluster galaxies. Indeed some of these images present no curvature, which could be either due to the flatness of the lensing cluster potential or, more likely, to the presence of a secondary deflector near the line of sight. These images could be difficult to distinguish from (unlensed) edge-on spiral galaxies.

Moreover, we have to consider possible arclike structures belonging to the cluster or background/foreground objects: cooling flows, projected spiral galaxies, and galaxies interactions. One such occurrence was found by us in the cluster Cl 0018−20 where the spectroscopy of the supposed arc (Giraud, Triay and Infante, 1991) indicated it is likely to belong to the "lensing" cluster and might be the result of two interacting galaxies. Infrared observations would help to eliminate the undesirable cases ($I-K$, $V-I$ color-color diagram; see Rigler et al. 1992). Since these observations are not yet available, we can estimate the rate of projected spiral galaxies in our fields in the following way. Since the clusters we are studying are very rich, we can use well-known rich clusters to get an estimate of the fraction of spiral galaxies in the core: Mac Laren, Ellis, & Couch (1988) and Mellier et al. (1988) have found nearly 50% of spiral galaxies in Abell 370 and in other rich Abell clusters. Only Sa, Sb, Sc, or Sd galaxies have a disk contribution providing axis ratio larger than 4, and MacLaren et al. (1988) have found 25% of such galaxies. In each field we have around 60 galaxies ($I < 22$), and we therefore expect 15 to be spirals. For the sake of simplicity, if we suppose that these galaxies are only composed of a thin disk and that the angles of the planes of the spirals disks from the line of sight are homogeneously spread in all directions, 0.5% will have an axis ratio larger than 10 and 1% larger than 4. In the current sample of 16 clusters, we then expect that 2.4 spiral galaxies will present an axis ratio larger than 4 and only 0.5 with an axis ratio of more than 10. Contamination by field spiral galaxies is expected to be about 0.5 galaxies from galaxy counts up to $I = 22$ (Lilly, Cowie, & Gardner 1991).

In order to check for the possible contribution from elongated objects other than gravitational arcs, we searched for all objects with a ratio = major axis/minor axis larger than 4 in an area 3′ × 3′ on all the cluster fields. We found a total number of 13 objects verifying this criterion, which is by far more than what can be expected from the random projection of cluster/field galaxies (>7 σ excess). Two of them are likely to be edge-on spiral galaxies, easily recognizable from their high surface brightness, the presence of a well-defined nucleus, and the absence of any curvature. This number of unlensed galaxies with a (projected) axis ratio larger than four is then in good agreement with what one can expect from a rich cluster and superposed field galaxies (two against three), although infrared colors will be required to identify the nature of a possible ambiguous case. The 11 other elongated images are likely to be gravitational images of background galaxies either because their widths are not spatially resolved, or because they present a well-defined curvature.

4. DISCUSSION AND CONCLUSION

The sample of 11 gravitationally imaged galaxies should then be representative of the lensing properties of our complete sample of highly X-ray luminous clusters. Six of them are not spatially resolved in width (intrinsic width <0″.6) which suggests a compact mass distribution for the lensing clusters (Hammer 1991). Out of the 11 arcs, six are reaching the criterion defined by Wu & Hammer (1993) for giant luminous

1994ApJ...422L...5L

TABLE 1

LIST OF EMSS CLUSTERS AND ARCS IDENTIFIED IN THE PRESENT SAMPLE

Cluster	z $L_{X,44}$	1 σ Isophote of Current Observations (mag arcsec^{-2})	Magnitudes of the Arcs	Morphology: Length l/w d (center)	Notes
MS 0015.9+1609	0.54 14.32	$\mu_R = 24.75$ $\mu_V = 26.4$	...	...	...
MS 0302.7+1658	0.424 4.99	...	$B = 23.83$ $R = 22.35$ $I = 21.71$	10″ 11.1	Mathez et al. 1992 ...
MS 0353.6−3642	0.32 5.23	$\mu_V = 26.2$	...		...
MS 0451+0250	0.202 9.96	$\mu_R = 26.55$	$R = 23.32$	5 5.5 25	New arcs
MS 0735.6+7421	0.216 6.10	$\mu_V = 26.2$ $\mu_I = 26.2$	...	...	...
MS 1006+1202	0.221 4.80	$\mu_V = 26.2$ $\mu_I = 26.2$	Arc 1: $V = 22.18$ $I = 20.47$ Arc 2: $V = 21.92$ $I = 21.47$ Arc 3: $V = 20.05$ $I = 20.91$ Arc 4: $V = 22.34$ $I = 21.49$	Arc 1: 5.8 6.0 31 Arc 2: 5.9 10.5 26 Arc 3: 3.7 3.1 17.5 Arc 4: 4.9 7.0 62	New arcs
MS 1008−1224	0.301 4.48	$\mu_V = 26.20$ $\mu_I = 26.2$	Arc 1: $V = 21.53$ $I = 19.72$ Arc 2: $V = 22.28$	Arc 1: 4.5 10 47 Arc 2: 4.0 6.5 51	New arcs
MS 1224+2007	0.327 4.59	...	...	...	...
MS 1333.3+1725	0.460 5.39	$\mu_I = 25.2$	...	...	...
MS 1358.4+6245	0.328 10.65	$\mu_V = 25.71$ $\mu_I = 25.16$	...	...	...
MS 1455+2232	0.259 15.98	$\mu_R = 25.81$ $\mu_V = 26.24$	$V = 23.24$ $R = 22.91$	8.7 6.7 19.4	New arc
MS 1512+3647	0.372 4.8	$\mu_R = 25.81$ $\mu_V = 26.24$	...	...	...
MS 1621.5+2640	0.426 4.52	$\mu_I = 25.00$ $\mu_R = 26.36$ $\mu_V = 26.70$	$V = 21.16$ $R = 21.08$	9.8 19.6	Luppino & Gioia 1992
MS 1910.5+6736	0.246 4.38	$\mu_R = 25.16$ $\mu_V = 25.38$	$V = 22.29$ $R = 20.63$	6.1 10.5 67	New arc
MS 2053.7−0449	0.583 5.76	$\mu_R = 25.55$	$R = 21.91$	10.5 17.5 15.8	Luppino & Gioia 1992
MS 2137.3−2328	0.313 15.58	...	$B = 22.04$ $V = 22.00$ $R = 21.55$ $I = 21.22$	14.2 17.8 15.5 ...	Fort et al. 1993

arcs ($l/w > 10$ and $B < 22.5$ or $R < 21.5$). This rate, of six giant luminous arcs among 16 highly luminous X-ray clusters, is expected by lensing statistics if clusters have compact density profile, such as $r^{1/4}$ law. However, this is by far much larger than the rate predicted by the lensing model if the dark matter is following the X-ray gas with a typical core radius of 250 kpc ($H_0 = 50$), in which case one would expect less than one giant luminous arc in this sample of 16 clusters (see Wu & Hammer 1993, Table 3). Moreover, all the observed arcs but one have an axis ratio larger than 10. This is again highly suggestive that the dark matter in rich clusters has a smaller core radius than the X-ray gas, since with $r_c = 250$ kpc, less than one-third of the arcs would have an axis ratio larger than 10.

In this *Letter*, we have presented the preliminary results from a survey of a sample of X-ray luminous clusters from the EMSS sample (Gioia et al. 1990a), aimed at searching for gravitational images of background galaxies. These clusters characterize the high end of the X-ray cluster luminosity function, and because of the high rate in finding luminous arcs in this sample, one can reasonably assume that clusters with gravitational arcs adequately represent the X-ray luminous clusters. We have added three new cases of giant luminous arcs ($l/w < 10$, $V < 22$) to the ~ 20 already known, as well as six other arcs ($4 < l/w$, and/or $V > 22$), and therefore the success rate of finding arcs in this sample is extremely high (11 arcs in 16 clusters). This, combined with the distribution of the arcs axis ratio is highly incompatible with a distribution of dark matter following the X-ray gas. A more detailed discussion can be found in Hammer et al. (1993) who test the validity of several models for the cluster density profile by comparing the predicted values to the observed one. Observations of the complete sample of 42 EMSS clusters [$L_X(0.3\text{–}3.5\ \text{keV}) > 2 \times 10^{44}$ ergs s^{-1} ($H_0 = 50$) and $z > 0.15$] are being finalized and are expected to provide unprecedented constraints on the dynamics of rich clusters of galaxies and their evolution (Luppino et al., in preparation).

This work has received a partial financial support from NASA grant NAG 5-1880 and from NSF grant AST 91-19216. The CCD development at IFA has been supported by NST AST 90-20680.

REFERENCES

Christian, C., Africano, J., Adams, M., Barnes, J., Butcher, H., Mould, V., & Siegel, M. 1985, PASP, 97, 383
Fort, B., Le Fèvre, O., Hammer, F., & Cailloux, M. 1992, ApJ, 399, L125
Gioia, I. M., Maccacaro, T., Schild, R. E., Wolter, A., Stocke, J. T., Morris, S. L., & Henry, J. P. 1990a, ApJS, 72, 567
Gioia, I. M., Henry, J. P., Maccacaro, T., Morris, S. L., Stocke, J. T., & Wolter, A. 1990b, ApJ, 356, L35
Giraud, E., Triay, R., & Infante, L. 1991, 2d DAEC Meeting on the Distribution of the Matter in the Universe, ed. G. Mamon & D. Gerbal, 94
Hammer, F. 1991, ApJ, 383, 66
Hammer, F., Angonin, M. C., Annis, J., Gioia, I., Le Fèvre, O., Luppino, G., & Wu, X. P. 1993, Proc. Liege Conf., Gravitational Lensing, ed. J. Surdej et al. in press
Lilly, S. J., Cowie, L. L., & Gardner, J. P. 1991, ApJ, 369, 79
Luppino, G. A., & Gioia, I. M. 1992, A&A, 265, L9
MacLaren, I., Ellis, R. S., & Couch, W. J. 1988, MNRAS, 230, 249
Mathez, G., Fort, B., Mellier, Y., Picat, J. P., & Soucail, G. 1992, A&A, 256, 343
Mellier, Y., Soucail, G., Fort, B., & Mathez, G. 1988, A&A, 199, 13
Pello, R., & Soucail, G. 1993, 8th IAP Meeting, Paris, First Light in the Universe, ed. B. Rocca-Volmerange, in press
Rigler, M. A., Lilly, S. J., Stockton, A. N., Hammer, F., & Le Fèvre, O. 1992, ApJ, 385, 61
Stocke, J. T., Morris, S. L., Gioia, I. M., Maccacaro, T., Schild, R., Wolter, A., Fleming, T. A., & Henry, J. P. 1991, ApJS, 76, 813
Tyson, J. A., Valdes, F., & Wrenk, R. A. 1990, ApJ, 349, L1
Wu, X. P., & Hammer, F. 1993, MNRAS, 262, 187

1994ApJ...422L...5L

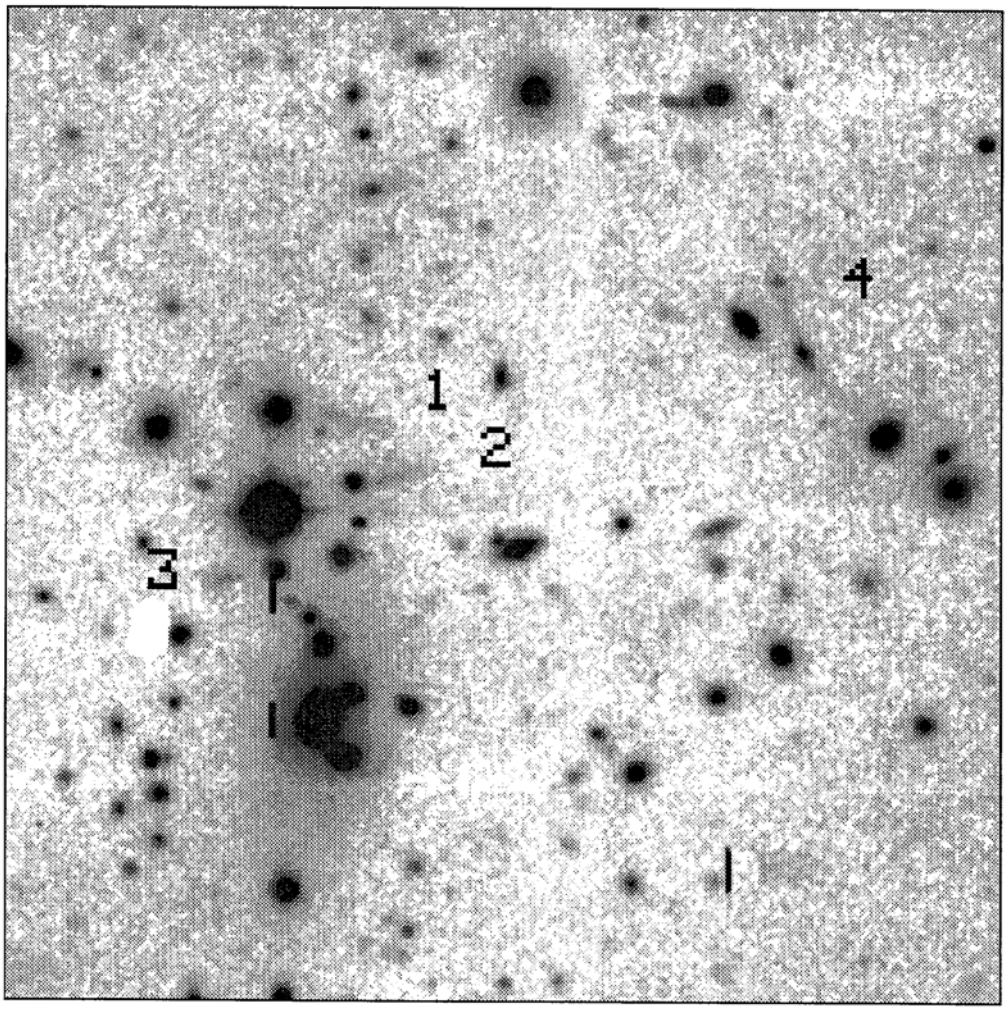

FIG. 1a

FIG. 1.—(*a*) Cluster MS 1006+1202. Sum of 20 minute integration in *V* and 20 minute integration in *I*, seeing 0.″9 FWHM, CFHT/SIS. North is up, east to the left; the image is 100″ on a side. (*b*) Cluster MS 1008−1224. 20 minute integration in *I*, seeing 1″ FWHM, CFHT/SIS. North is up, east to the left; the image is 100″ on a side. (*c*) Cluster MS 1455+2232. 10 minute integration in *V*, seeing 1.″1 FWHM, CFHT/MOS. North is up, east to the left; the image is 100″ on a side. (*d*) Cluster MS 1910.5+6736, 15 minute integration in *R*, seeing 0.″95 FWHM, CFHT/SIS. North is at the bottom, east to the right; the image is 100″ on a side.

LE FÈVRE et al. (see 422, L6)

PLATE L2

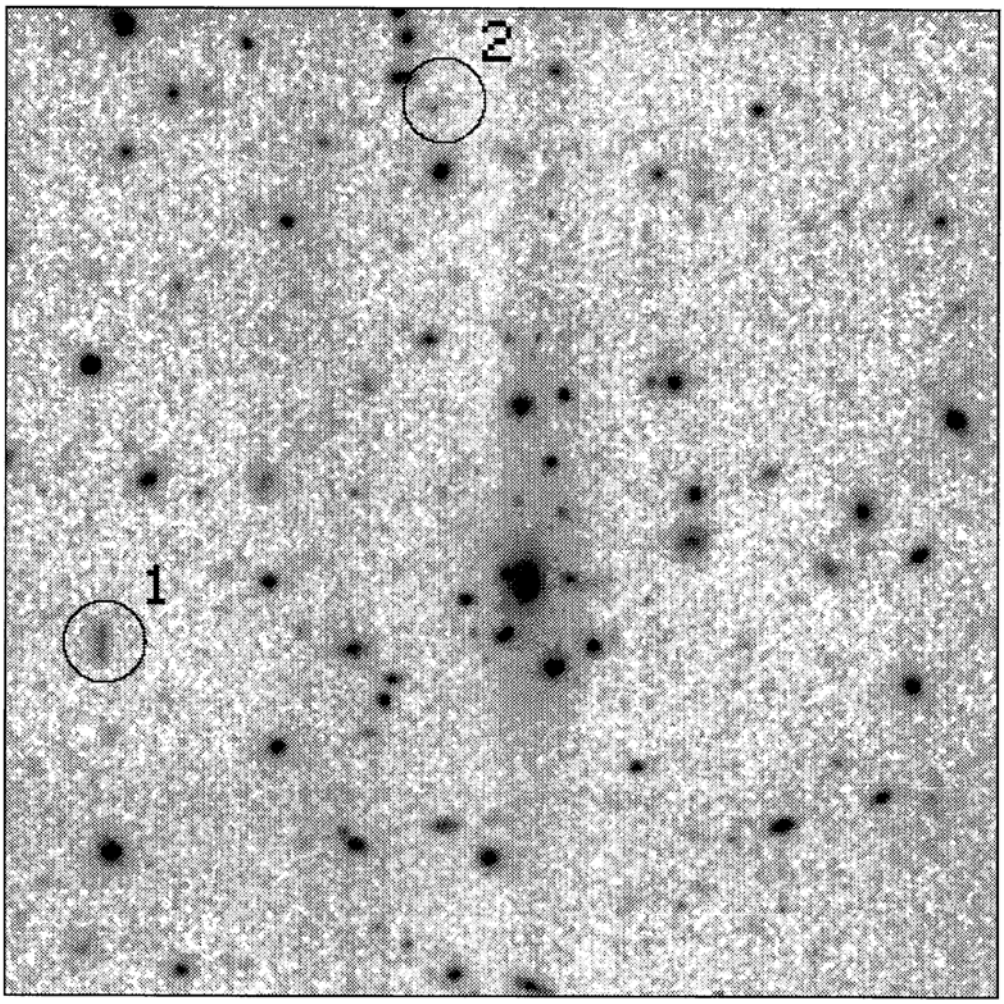

FIG. 1*b*

LE FÉVRE et al. (see 422, L6)

1994ApJ...422L...5L

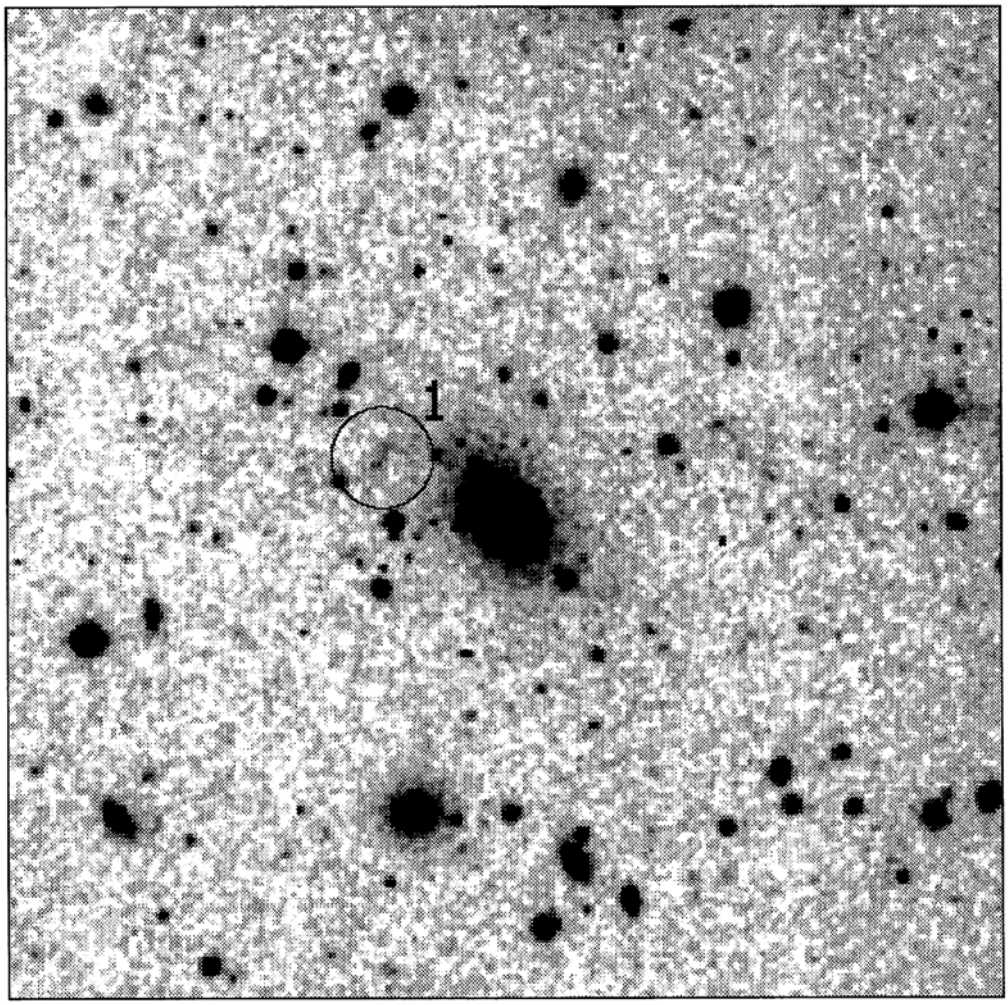

FIG. 1c

LE FÈVRE et al. (see 422, L6)

PLATE L4

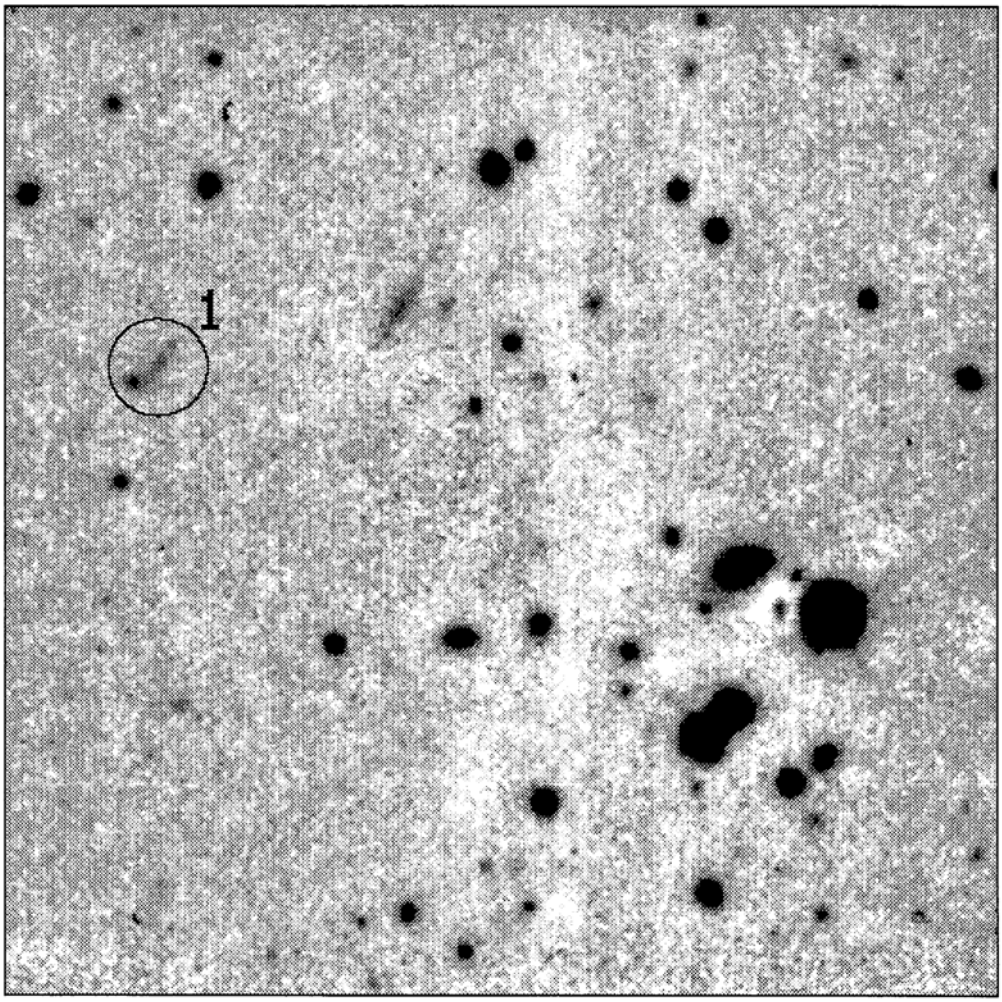

FIG. 1*d*

LE FÈVRE et al. (see 422, L6)

Gravitational lensing on Q0957+561: A study of the cluster at z=0.355

Angonin-Willaime M-C, Soucail G, Vanderriest C, 1994, Astronomy and Astrophysics, **291**, 411

Astron. Astrophys. 291, 411–419 (1994)

ASTRONOMY AND ASTROPHYSICS

Gravitational lensing of Q 0957+561: a study of the cluster at z=0.355

M.-C. Angonin-Willaime[1], G. Soucail[2], and C. Vanderriest[1,3]

[1] Observatoire de Paris-Meudon (DAEC and URA 173), 5 Place Jules Jansen, F-92195 Meudon Principal Cedex, France
[2] Observatoire Midi-Pyrénées (Laboratoire d'Astrophysique de Toulouse and URA 285), 14 Avenue Edouard Belin, F-31400 Toulouse, France
[3] CFH Telescope Corp., p.o. box 1597 Kamuela, 96743 Hawaii, USA

Received 8 February 1994 / Accepted 13 June 1994

Abstract. Redshift measurements for 38 objects as well as VRI photometric data for ∼200 objects have been obtained in the field of the multiply imaged QSO 0957+561.

The data analysis leads to the identification of a cluster at $< z > = 0.355$ surrounding the central lens galaxy G1, with a velocity dispersion 715 ± 130 km/s. This cluster is identified as a poor to medium-rich cluster, dominated by a giant elliptical galaxy (G1), and with a large fraction of late type galaxies. Another group or cluster, located at about 2′ from G1 and centered on G5, is identified at a redshift of 0.5, in accordance with previous results. The high degree of contamination along the line-of-sight is also examined.

The consequences of these observational results for the modeling of the lens and the evaluation of the Hubble constant H_0 are briefly discussed.

Key words: gravitational lensing – galaxies: clusters of – quasars: individual: Q 0957+561 – galaxies: distances and redshifts – distance scale

1. Introduction

Essentially for historical reasons, the "double" QSO 0957+561 (z = 1.41) is presently the best studied gravitational lens system. Since its discovery (Walsh et al. 1979), an abundant set of data was collected in all the observable wavelength ranges (radio, IR, optical, UV and X) and the system has been described by several models, although no simple one based on a single galactic deflector is able to give satisfying results.

One of the motivations for such assiduous efforts is that, according to the theoretical predictions of Refsdal (1964, 1966), it is believed that gravitational mirages may provide a method for a direct measurement of the Hubble parameter H_0 over long distances in the Universe. Up to now, Q 0957+561 is the only case with a measured time delay, even if the exact value is not yet firmly established and if a possible discrepancy between the optical data (Vanderriest et al. 1989; Schild 1990) and the radio data (Lehár et al. 1992; Press et al. 1992) is not fully understood (Pelt et al. 1993; Schild 1994).

Anyway, it seems more and more clear that a realistic model of the deflector must consist of at least 2 components: a bright and massive galaxy usually denoted G_1 (Young et al. 1980) whose velocity dispersion has been estimated (Rhee 1991) and a surrounding cluster of galaxies at $z \simeq 0.36$ (Garrett et al. 1992). The existence of an additional group of background galaxies at $z \simeq 0.5$ is also suspected to contribute to the lensing effect. Recently, Bernstein et al. (1993) have detected a possible pair of gravitational arcs near Q 0957+561, in the direction of the background group. Having explored a large range of parameters for the modeling of the lens, they consider that the effect of the second group must be included in the lens to explain the shear around this two putative arclets. The effects on the double QSO are not so clear. But, in order to have access to H_0, we need to know with sufficient accuracy the parameters of the lens, especially the detailed mass distribution around the double QSO. It is known that the confidence on the estimation of H_0 is directly related to the accuracy of the lens parameters (see for instance Kochanek 1991 and references therein).

We present here a spectroscopic and photometric study of the field around Q 0957+561, aimed at improving our knowledge of the cluster components of the lens. The details of the spectrophotometric analysis of the data are given in Sect. 2. In Sect. 3, the improvements brought by these observations are presented: we analyse the cluster content, with a significantly larger number of redshifts for cluster members, as well as a better estimate of the velocity dispersion of the cluster. Moreover, additional photometric information over a large field allows a better determination of the optical center of the lens. Section 4 is devoted to the analysis of the background galaxies detected in the field, and an analysis of the photometric properties of galaxy G1 is given in Sect. 5. We finally propose some conclusions about the future of the measurement of H_0 with gravitational

* Based on observations collected at the Canada-France-Hawai Telescope at Mauna Kea, Hawaii, USA
Send offprint requests to: M.-C. Angonin-Willaime

Table 1. Characteristics of the direct imaging data: filter, date, number of exposures, exposure time and measured seeing

Filter	date	N	exp. (sec)	seeing
V	92-02-28	3	480	1.1″
	92-03-02	2	600	0.65″
R	92-02-28	3	300	0.7″
I	92-02-28	2	300	1.0″

lenses in Sect. 6. Throughout the paper, absolute quantities will be computed with $H_0 = 50$ km/s/Mpc and $q_0 = 0.5$.

2. Observations and data reduction

2.1. Photometric sample

A photometric study of the field was performed with the imaging mode of the spectrograph SILFID (Vanderriest & Lemonnier 1988) at the Cassegrain focus of the 3.6m CFH telescope during a run in February-March 1992. The weather was photometric and the seeing was between 0.65″ and 1.1″. The CCD was the Lick2 2048×2048 with a pixel size of 0.178″, and the filters were the V and R standard filters usually in use with the spectrograph and the standard I filter from CFHT. The field was limited to 1500×1500 pixels (i.e. 4.5′ on a side) because of vignetting in the imaging mode of the spectrograph. Table 1 summarizes the characteristics of the different exposures in each filter.

The calibration stars were S95132, G16350 (Landolt 1983) and a sequence in the field of NGC 2264 (Christian et al. 1988). We used also as a confirmation the photometric sequence established in the field of the quasar itself for monitoring its variations (Vanderriest et al. 1982). From comparison of these different standards, we estimate the accuracy in absolute calibration of the frames to be approximatively 0.05 mag.

Images through each filter were re-centered on the R image, chosen as the reference frame, co-added and finally binned 2×2 (i.e. a pixel size of 0.356 ″) in order to increase the detected signal. We then ran the FOCAS package of the IRAF software on these images (Jarvis & Tyson 1981; Valdes et al. 1982), with a detection level of 4σ above the sky background in each filter. This corresponds to a surface brightness in R of 24.0 mag arcsec^{-2} or equivalently 4×10^{-2} of the sky background. In order to measure the colour indices, we computed isophotal magnitudes within the R limiting isophote for each color. Finally we attempted to separate the stars and the galaxies using the FOCAS classifier. This separation is quite accurate up to a magnitude $R \simeq 22$, but is much less secure at fainter magnitudes. The final sample is complete to $R = 24$, and in the range 17-25 we obtained the photometry of 198 objects with the three magnitudes measured with good accuracy, and acceptable colours indices ($0 < V - R < 2.5, 0 < R - I < 2$).

2.2. The spectroscopic sample

Spectroscopic observations were performed with the MARLIN focal reducer and spectrograph at the Cassegrain Focus of the 3.6m CFH telescope during the nights of May 13-17, 1991. The nights were clear and the seeing was between 0.8″ and 0.9″ throughout the run. The CCD was the SAIC1 1024×1024 with a pixel size of 0.341″and a field of view for the imaging mode of 6′×6′. We used the multiaperture spectroscopic mode with metallic masks cut with the LAMA (Laser Machine) system. The slitlets were about 1.5″×10″, thus allowing a good subtraction of the sky background. We used the grism O300 (7 Å/pixel in the binned mode), with a maximum wavelength range from 4400 Å to 8400 Å. This configuration of the spectrograph gives an intrinsic resolution of 15 Å. However, most of the spectra are truncated by the CCD, depending on the position of the slit in the direction of dispersion and the spectral range common to all the objects is smaller. We used 2 different masks, with respectively 23 and 25 slitlets. For the first mask, 4 exposures were taken with integration times of respectively 2 × 40min, 60min and 75min, giving a total integration time of 3h 35min. The second mask, which was positioned on some fainter objects, was exposed for 3 × 75min and 60min, with a total integration time of 4h 45min. A 5 minutes R-image was used for object identification in order to compare our data with previous work (Fig. 1).

The data reduction for the spectroscopic observations was done with an upgraded version of the semi-automatic software developed in the Toulouse Observatory for multiaperture spectroscopy (Soucail et al. 1987). An automatic procedure provides the wavelength calibration and the extraction of the individual spectra on the CCD image. Then, an optimal sky subtraction is performed for each spectrum, after identification of the object in the slitlet. Finally, the spectra are calibrated in flux with the reference spectrum of BD +26 2606 (Oke & Gunn 1983). For those objects which were selected on both masks, the spectra are co-added, giving a final spectroscopic sample of 38 objects.

The redshifts are obtained by cross-correlating the spectra with synthetic spectra from Guiderdoni & Rocca-Volmerange (1987). It is also generally possible to check these values by direct fitting of individual lines. The uncertainty of measurement is typically around 10 Å, or equivalently 0.001 in redshift, for spectra with aborption lines only. But it can be better for spectra with well defined, high S/N, absorption lines or spectra with emission lines such as [OII] (λ 3727), Hβ or the [OIII] doublet ($\lambda\lambda$ 4959, 5007). In favourable cases, the redshift uncertainty can be lowered to 0.0003. In the following, all the redshifts are given with only 3 digits but a fourth digit has been retained, when significant, for the computations. Only one object failed to be measured and the useful sample finally contains 34 galaxies (excluding stars).

The spectral type of the galaxies is also tentatively determined from a comparison between the observed spectra and a set of synthetic spectra (Guiderdoni & Rocca-Volmerange 1987), corresponding to different histories of star formation and evolution. These templates were synthesized in order to match the

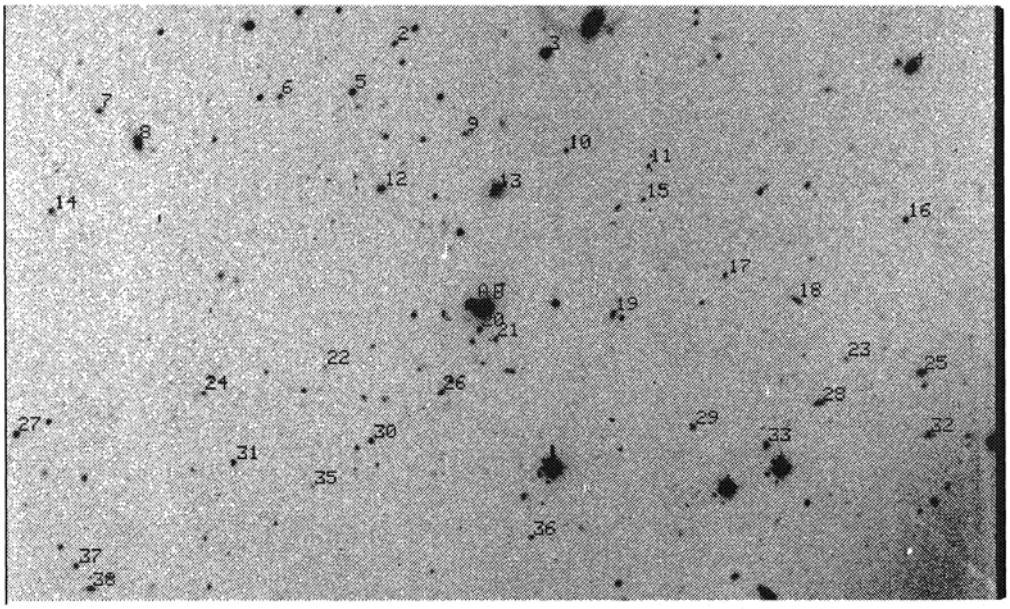

Fig. 1. Identification chart for the 38 objects of the spectroscopic sample discussed in Sect. 2. The two components A and B of Q 0957+561 are also noted. North is up, East is right

integrated spectra of present-day galaxies, so it could seem questionable to use them for objects at redshifts $\sim$ 0.3-0.5 without correction for evolution. But the uncertainty on Hubble type determination is still dominated by the flux calibration, not better than 10% for the best cases, which corresponds roughly to one classification step. It thus seems useless to include other parameters in the spectral type identification. A more refined study would need better spectra (higher S/N ratio, flux calibration reliable to 2 to 5%). A representative sample of the spectra is given in Fig. 2; the data for the full sample can be found elsewhere (Angonin-Willaime 1993).

2.3. Comparison with previous works

A summary of the data collected on the 38 different objects selected in the masks is presented in Table 2. For the galaxies referenced in Young et al. (1981, hereafter YGKOW) their identification number is reported. For simplicity, we adopted the same system of coordinates with an extension of the field of view. Also when available, we inserted for comparison the redshift measured by Garrett et al. (1992). There are 11 objects common to the 2 samples, with a mean difference between the measured redshifts $< z_{ASV} - z_{GWC} >= +0.6\ 10^{-3}$ and a dispersion of $\Delta z = 1.1\ 10^{-3}$. The slight shift between the two sets of measures is not very significant; it could result from a small difference in the wavelength origin and/or systematic decentering of the objects in the slitlets (about 3 Å or 1/2 pixel).

3. The cluster at z=0.355

3.1. Identification from the spectroscopic data

In the above defined sample, we can extract 16 galaxies having a redshift around 0.355, i.e. very near the redshift of G1 itself (z = 0.356, Rhee, private communication).

The existence of a cluster of galaxies containing the main deflecting galaxy G1 of the Double Quasar is thus confirmed, after the first data published by Garrett et al. (1992). Moreover, we can infer that G1 is the central galaxy of the cluster and the brightest one, definitely excluding galaxies like G3 and G5, for instance, as cluster members. This cluster is thus rather poor, with a large contamination by background or foreground objects: 50% of our spectroscopic sample are galaxies which do not belong to the main cluster! In order to increase the statistics of the cluster members, we included in the sample 4 objects observed by Garrett et al. but not by us, leading to a final sample of 21 cluster members (including G1) with available redshifts.

3.2. The cluster structure

From this working sample, we derived the optical barycenter of the cluster, computed with a weighting proportional to the

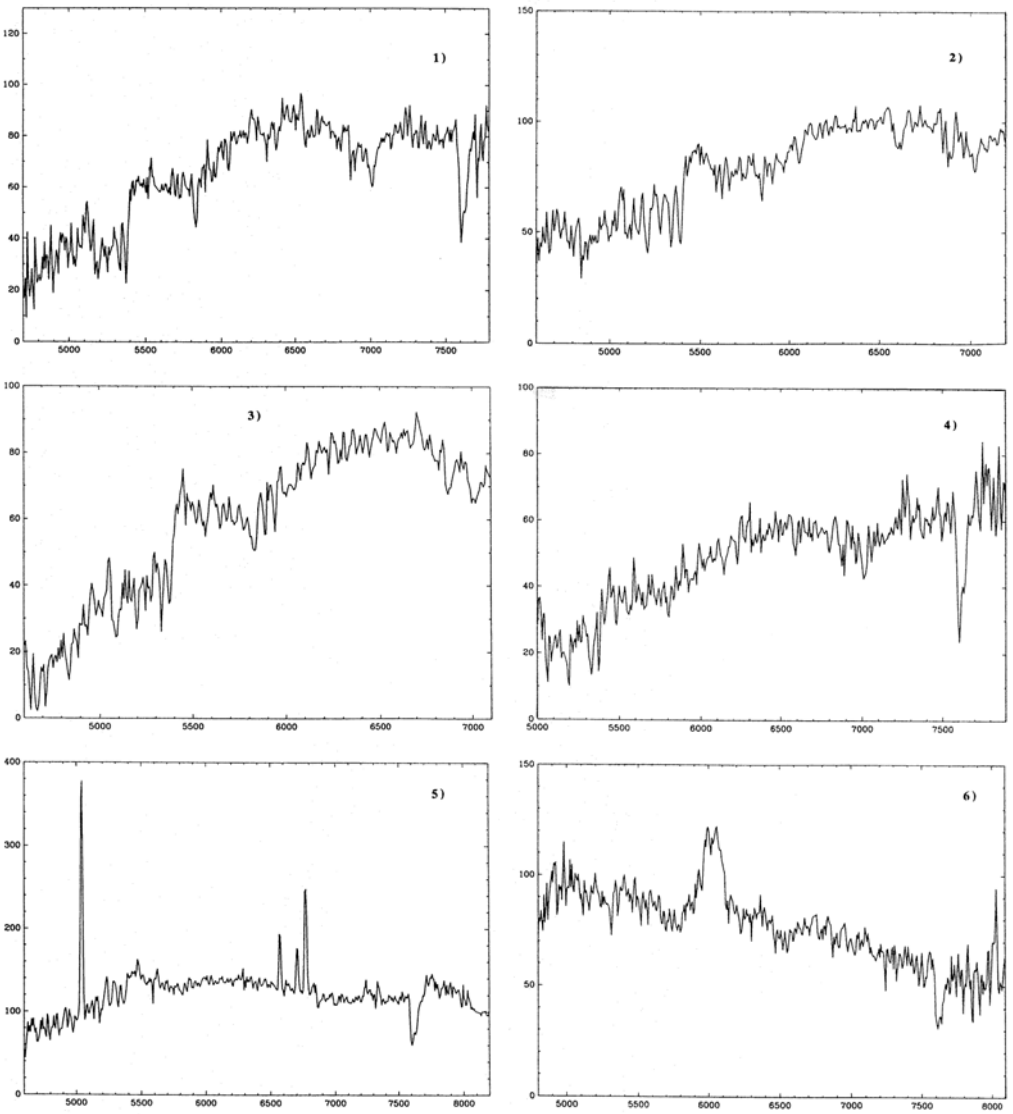

Fig. 2. A few representative spectra of galaxies around Q 0957+561 (galaxies at the cluster redshift and one background quasar, x-axis is in Angströms and y-axis in F_λ): -1) galaxy 20 at $z = 0.355$, an elliptical-type spectrum; -2) galaxy 13=G2 at $z = 0.359$, a typical spiral-type spectrum; -3) galaxy 8 at $z = 0.355$, another spiral-type spectrum; -4) galaxy 21, one with the poorest Signal/Noise in the $z = 0.355$ cluster; -5) galaxy 31 at $z = 0.352$, a Seyfert 2 galaxy ; -6) object 24 at $z = 1.154$, a QSO/Seyfert 1-type object

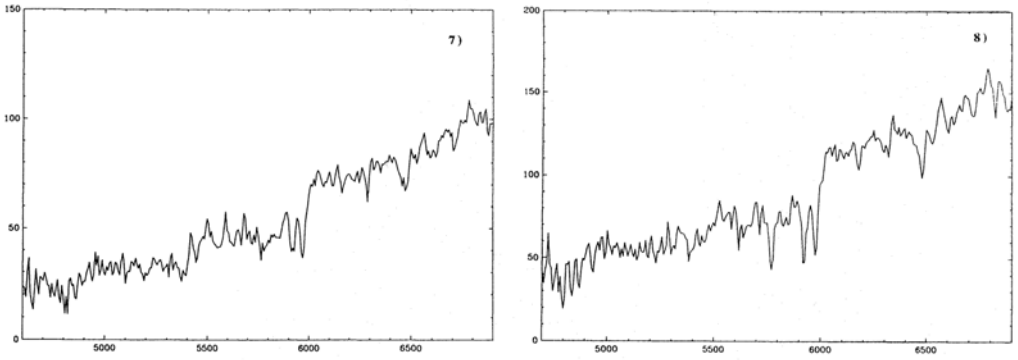

Fig. 2. (continued) A few representative spectra of galaxies around Q 0957+561 (group at z $\simeq$ 0.5): -7) galaxy 5=G5 at z = 0.504; -8) galaxy 6 at z = 0.506

R-luminosity, a value well related to the total luminosity of the galaxies and also to their masses. To do that, we included a magnitude of R = 17.5 for G1, a value close to the one measured by Bernstein et al. (1993) and compatible with our photometric data. If all the galaxies are taken into account, we find a position for the barycenter at (–13.7″,–19.6″) in the reference system centered on image B of the quasar. This position is less close to G1 than the position found by Garrett et al.: (–3.5″,+1.2″). However, as the number of galaxies in our sample is still small, including or not a single member could change notably the values. For instance, if the bright and excentric galaxy 4 (not in the Garrett's sample) is excluded, the barycenter moves to (–0.7″,+7.2″). This shows clearly that the cluster parameters are still poorly determined by the present statistics.

An instrumental effect exists in the spatial distribution of the measured galaxies: with this multi-object spectroscopic technique, the objects are selected for optimal coverage of the CCD area, which does not necessarily match their real distribution. For the field of Q 0957+561, the concentration of galaxies near G1 is not properly sampled because of this technical constraint. Thus, we can expect that the real centre of mass of the cluster at z=0.355 should be closer to G1. Note also that a similar analysis applied to the larger photometric sample is useless because of the high contamination in this field. Anyway, with an extension over 2 h_{50}^{-1} Mpc, this cluster appears as a rather loose structure.

One of the methods used to characterise the richness of a cluster is to compute the value of $N_{0.5}$, i.e. the number of galaxies in a radius of 0.5 Mpc around the center with magnitudes ranging from m_1 to m_3+2 (Bahcall 1980). At a redshift of 0.36, a linear distance of 0.5 h_{50}^{-1} Mpc scales as 1.4′ ($q_0 = 0.5$). For the cluster around Q 0957+561 we find $N_{0.5}$ = 13 from the R-data and $N_{0.5}$ = 14 from the I-data. The data are extracted from the catalogues containing only objects classified as galaxies. This is justified because we do not have any comparison fields, so we cannot correct exactly the counts from the contamination. Using only the objects classified as galaxies allows a correction for the contamination from galactic stars, and is probably correct for the relatively bright objects used in the computation of $N_{0.5}$. The galaxy contamination is not taken into account, except that we excluded galaxy 3 (= G3) as the second brightest cluster member, because of its redshift of 0.24.

The value of $N_{0.5}$ in this cluster is small and is representative of rather poor clusters. On the contrary, the values found for Coma ($N_{0.5}$ = 28) or for the distant cluster A370 (z = 0.374, $N_{0.5}$ = 31, Mellier et al. 1988) are representative of very rich and evolved clusters. The cluster around Q 0957+561 is thus a poor but extended cluster: one should note that both the second and third ranked galaxies are at a distance larger that 0.5 Mpc from the brightest cluster member G1.

3.3. The cluster dynamics

With 21 galaxies in the spectroscopic sample, we compute a mean redshift of z = 0.355 and a velocity dispersion σ_V = 715 ± 130 km/s, which is slightly higher than the value found by Garrett et al. but within the error bars. Such a value is typical of poor to medium-rich clusters. Once again, since the galaxies are spread all over our field, we can hardly claim that the dynamics of the cluster is clearly understood. It is possible that the virial mass does not represent the cluster mass. Anyway, this calculated value is quite sensitive to the limit in velocity assigned for the definition of a cluster member. For instance, galaxy 4, which is at the edge of the spatial distribution is also at the edge of the velocity distribution. Removing it gives a velocity dispersion of 660 km/s. Conversely, galaxy 34, at a redshift of 0.371 has a velocity difference with the mean redshift larger than 3σ and was eliminated in the statistics, but we cannot exclude that it is dynamically related to the cluster.

At this stage, it is worth noticing that the empirical correlation found by Bahcall (1981) between the uncorrected density count and the velocity dispersion: $N_{0.5} = 21(\sigma_V/1000)^{0.8}$ would give σ_V = 600 km/s for $N_{0.5}$ = 14, which makes us confident about the reliability of our measurements. For improving our knowledge of the dynamical state of the cluster, a more com-

Table 2. Summary of the data collected on the spectroscopic sample. In columns 1 and 2 are the identification numbers of the objects, and their coordinates are given in columns 3 and 4 with respect to the position of QSOB. The magnitudes R, V and I are given in columns 5 to 7. Columns 8 to 11 concern the spectroscopic analysis of the spectra, i.e. redshift measurement, comparison with othe works, spectral type and comments on the spectra. For some objects of the spectroscopic sample, the photometric data are missing, as the objects lie outside the photometric field of view. GWC means Garrett et al. 1992.

(1) N°	(2) YGKOW Id.	(3) $\Delta\alpha$ ($''$)	(4) $\Delta\delta$ ($''$)	(5) R	(6) V	(7) I	(8) z	(9) z from GWC	(10) Spectral type	(11) Emission lines (w=weak, s=strong)
1		−100.25	−42.97	17.06	17.28	16.70	0.072		Seyfert	Hβ, [OIII], Hα
2	2	−96.15	29.13	21.02	22.51	20.26	0.504	0.5024	Sa	
3	G3	−90.48	−25.11	19.12	22.51	20.26	0.240	0.2391	Im	
4		−80.00	−155.65	—	—	—	0.349		E	
5	G5	−79.31	45.17	19.86	21.06	19.25	0.505	0.5030	E	
6	20	−78.62	71.39	20.63	21.80	20.04	0.506	0.5052	Sa	
7		−75.98	136.45	21.08	21.45	20.39	0.126		Im	[OIII](w)
8		−64.25	122.95	19.23	19.97	18.86	0.355		Sa	
9	36	−62.32	5.00	22.00	22.67	21.49	0.690		Im	[OII](w)
10	42	−54.93	−31.03	21.40	22.47	20.70	0.356		E	
11	50	−48.52	−60.10	21.71	22.34	21.21	—		⋆	
12	G4	−43.9	36.11	20.01	21.28	19.44	0.357	0.357	E	
13	G2	−41.99	−5.02	19.49	20.31	18.95	0.359	0.3587	Sb	
14		−40.71	154.97	—	—	—	0.299		Sa	
15	59	−36.37	−57.87	22.23	22.78	21.57	0.305		Sc	[OII], Hβ(w), [OIII]
16		−25.30	−151.02	—	—	—	—		?	
17	80	−7.97	−86.07	21.45	21.88	21.09	0.114		Sd	Hβ(w), Hα
18		1.77	−111.17	—	—	—	0.351		Sc?	[OII], Hβ(w)
19	94	4.03	−45.43	20.63	21.43	20.06	0.353	0.353	Sa	
20	97	7.69	2.91	20.69	21.84	19.90	0.355	0.3535	E	
21	100	11.05	−2.55	21.37	22.42	20.75	0.355		E	
22	106	18.37	59.21	22.60	23.39	22.56	0.356		Sd	[OII], Hβ(w), [OIII](w)
23		23.07	−127.78	—	—	—	0.900		QSO	MgII(w), [OII](s)
24	119	26.03	103.51	21.89	23.03	21.64	1.154		QSO	MgII, [OII]
25		29.38	−154.42	—	—	—	0.435		Sc	[OII], Hβ(w), [OIII](w)
26	122	29.47	17.75	20.44	21.54	19.73	0.354	0.353	E	
27		38.01	171.04	—	—	—	—		⋆	
28		38.74	−117.73	—	—	—	0.435		Sc	[OII], Hβ(w)
29	134	45.30	−72.06	21.48	19.27	19.34	0.353	0.3548	E	
30	135	45.55	43.88	20.72	—	19.85	0.606	0.6047	Sb	[OII]
31	144	51.59	93.71	20.85	21.14	20.42	0.352	0.3523	Seyfert	[OII], Hβ, [OIII]
32		51.81	−155.96	—	—	—	0.358		Sc	
33		52.63	−97.96	—	—	—	0.363		Sc?	[OII], Hβ(w)
34		55.16	−178.53	—	—	—	0.371		?	
35	154	61.45	65.82	22.90	23.78	22.36	0.408		Im	[OII], [OIII]
36	167	82.76	−12.25	20.79	22.08	19.64	—		⋆	
37		86.33	151.67	21.45	22.82	21.01	0.456		Im	[OII], Hβ(w), [OIII]
38		94.90	147.13	20.44	—	20.02	0.359		Sc	[OII], Hβ, [OIII]

plete (i.e. significantly fainter) spectroscopic survey would be necessary.

3.4. The cluster content

If we trust the spectral identification in Table 2, we immediately see that more than 50% of the cluster members are spiral-type galaxies or emission lines ones. This high fraction is also a characteristic of poor clusters (Bahcall 1980) and is again consistent with the small value of $N_{0.5}$. In fact, this cluster is typical of a Richness class 0 cluster, dominated by a cD galaxy. We can reinforce our spectral identification by looking at the morphology of the galaxies on the CCD frames. Indeed some of the brightest galaxies of the cluster (for instance G2 or galaxy 8) show clear evidence for a spiral pattern. This also means that the evolutionary effects which could affect the spectral identification are not so important compared to the richness effect of the cluster. We have looked at the images to try to detect some possible signs of interaction around some of the star-forming galaxies, but there is no clear positive signal.

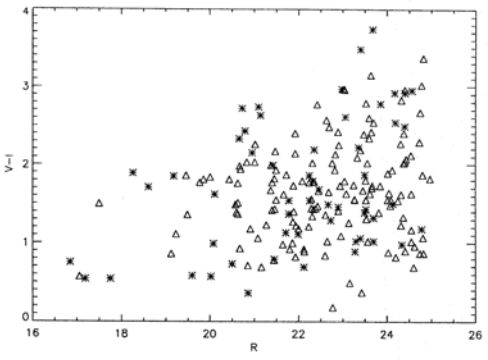

Fig. 3. (V–I) versus R colour diagram of the objects detected in the field of Q 0957+561. The triangles represent objects classified as galaxies, the asterisks are the stars

An example of the colour diagrams of the field can be seen in Fig. 3. The V–I versus R diagram shows a slight concentration of galaxies around V–I = 1.8 but there is no obvious sequence of ellipticals, as in rich clusters. In fact, it would not be possible to deduce the existence of a lensing cluster from this diagram alone, because of the strong contamination of the field. *A fortiori*, it seems hopeless to try to separate photometrically the members of the two clusters with the present data. However, it is interesting to look at the spatial distribution of the galaxies that could be involved in the lensing. To do that we plot both the isodensity and the isoluminosity map of the field, derived from the photometric catalogs with galaxies only (143 objects with $17.5 < R < 24$, Fig. 4). The isoluminosity map is clearly centered on galaxy G1 which is the dominant luminous component. The cluster also appears fairly circular around it, although slightly elongated in the North-South direction, and with no other bright clump. On the contrary, the isodensity map shows that there exists a numerical overdensity centered on galaxy G2, although not as dense as the central one. The background group at $z \simeq 0.5$ is also visible in the map. This map is more or less similar to the one used by Kochanek (1991) when smoothing the Young image, but the different structures are more clearly identified.

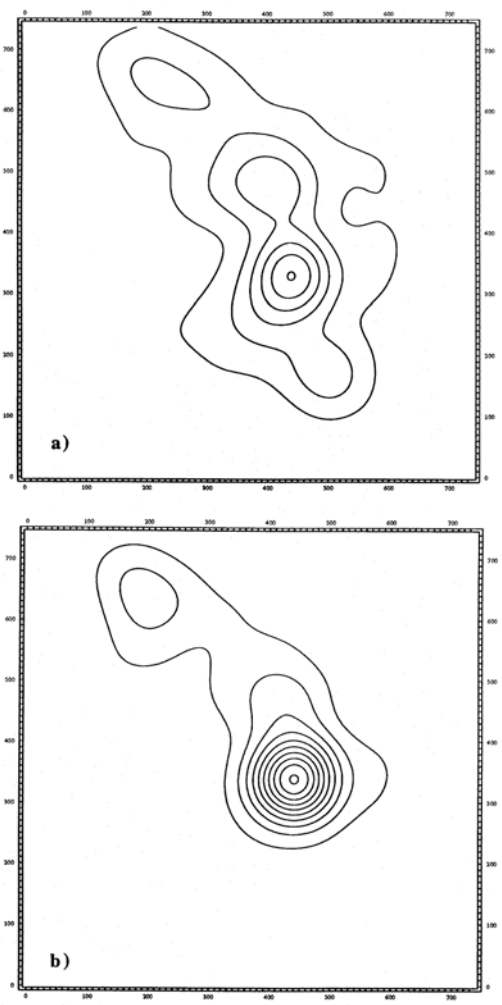

Fig. 4a and b. Isodensity map of the field around Q 0957+561, showing a strong concentration around G1, a smaller one around G2 and a spatial extension at the location of the background group at $z = 0.5$ (**a**). The isoluminosity map (**b**) is strongly concentrated on the brightest galaxy G1 and the two other numerical overdensities nearly completely vanish, because of their much lower mean brightness. North is up, East is right. 1 arcminute corresponds to 170 pixel units on the plot

4. The foreground/background galaxies

4.1. Another group or cluster at $z \simeq 0.50$

In our sample, the cluster at z=0.355 is heavily contaminated by galaxies at various redshifts. Only one other structure shows up clearly, near $z = 0.505$: our independant measurements confirm the values of the redshifts for 3 of the galaxies measured by Garrett et al. in this group. This second structure is still poorly defined although it is detected both from the spectra of 4 members and from the photometric analysis of our catalogs (Fig. 4b). More spectroscopic data are needed for a full understanding of its role in the lensing configuration, although Bernstein et al. (1993) have already stressed its importance in the evaluation of the local shear around the two arclets. In any case, G5 seems to be the dominant galaxy, with an absolute magnitude of –23.60 (including a k-correction from Rocca-Volmerange &

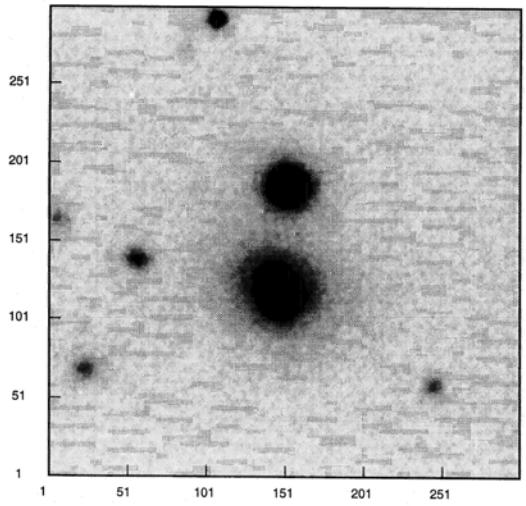

Fig. 5a. Image of Q 0957+561 in R band (3×5 mn). The field is ∼26″ on a side

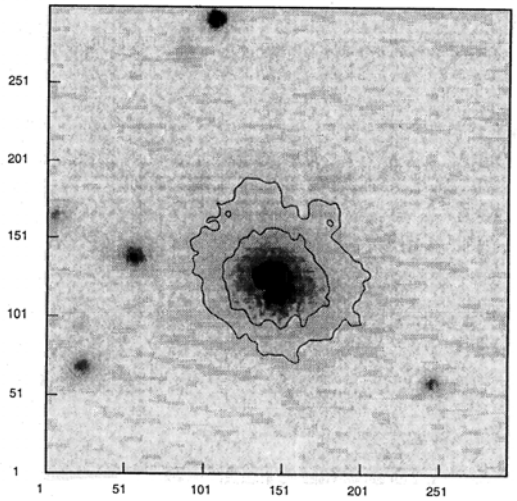

Fig. 5b. Result of the PSF subtraction, isolating the main deflecting galaxy G1. Outer isophotes corresponding to μ_R = 25 and 24 are also displayed, together with the fitting ellipses

Guiderdoni 1988), slightly fainter than G1 (absolute magnitude of –24.80, a value typical of cD or bright Elliptical galaxies).

4.2. Other objects in the field

As already discussed in previous sections, among our spectroscopic sample, 17 galaxies do not belong to the cluster. This extremely large value for the field contamination can be partly explained by the fact that the cluster is not rich and dense. The selection of objects for mask preparation is consequently probably biased especially far from the center. It is interesting to note that most of the contaminating galaxies are spatially located at more that 1′ from the cluster center. They probably do not affect too much the lensing configuration, except the well identified group around G5, although their effects remain unclear. Anyway, the redshift distribution of these galaxies is spread over a large range, from nearby objects at $z \sim 0.1$ to distant ones at $z > 0.6$. A special attention is given to the two very distant emission lines objects, numbered 23 and 24. Both display a broad MgII emission line, characteristic of QSOs and Seyfert 1 galaxies. In particular object 24 also has a very blue underlying continuum, and object 23 a strong and narrow [OII] line. But they can hardly be classified as QSOs because of their faint magnitude and are probably more representative of Seyfert 1 galaxies. Note also that object 24 shows a very faint extension in the CCD image similar to the one detected around object 1, although fainter.

5. The galaxy G1

We also used our direct pictures to check the parameters of the main galaxy G1. On the R picture we try to subtract the quasar images with the PSF subtraction methods already used in the case of MG J0414+0534 (Angonin-Willaime et al. 1994), i.e. an interactive multi-gaussian fitting on each line of the bidimensional image. The result is displayed in Fig. 5. The position of the galaxy center with respect to image B is in right ascension +0.14″±0.03 and declination 0.95″±0.05. Then, when fitting the most external isophotes with ellipses, we find ellipticities in the range 0.3–0.4 and position angles of the major axis of 60–80 degrees. These results are compatible with the ones of Bernstein et al. (1993) and Stockton et al. (1980) considering that ellipticity and position angle could change slightly with the radius. In good agreement with these authors, we find also that the elliptic profile of the galaxy follows a de Vaucouleurs law up to a radius of 5″ but we could not find any evidence for the presence of an additional extended envelope.

The morphology of this galaxy is not clearly determined: the hypothesis of a cD galaxy cannot be totally excluded but a bright elliptical member of cluster is more probable. Anyway, the nature of G1 and its brightness are strong arguments in favour of a cluster centered on it. The photometry gives a R magnitude of 18.3 for a radius of 5″. This value is very near the one published by Young et al. and is not in contradiction with the photometry by Bernstein et al. over larger radii and deeper detection levels.

6. Conclusion: a way towards H_0 ?

The main results of this study are:

1) With the redshift measurement of 38 objects, we confirm the existence of at least 2 mass structures in the field of

0957+561, one cluster of galaxies at z=0.355 and another concentration (group or cluster) of galaxies near z=0.5. The contrast of these 2 structures is low, with a lot of foreground and background galaxies in the field.

2) While very little is known about the group at z=0.5, the cluster at 0.355 is now better defined. It is an extended but poor cluster, containing a large proportion of Spirals and centered on the dominant galaxy G1, which is a cD or a bright Elliptical. The velocity dispersion of this cluster, determined from the redshifts of 21 members, is about 700 km/s.

This situation is not ideal for an accurate determination of the lensing mass distribution, which is needed for the measurement of H_0. Although the main deflecting galaxy is the brightest observed for lensed quasars (excepting, of course, the atypical case of Q2237+0305, which is useless for estimating H_0 because of too short time delays), the measurement of its velocity dispersion is a difficult task. Trying to confirm and improve the value obtained by Rhee (1991) is certainly a priority. The fact that G1 is a member of a loose cluster complicates also the determination of H_0, the physics and mass distribution of such structures being largely unknown. Moreover, its large extension and the presence of a bright galaxy in the periphery suggest that the mass distribution is probably not fitted by a simple virialised cluster model. A solution to this challenge is classically to be found in more spectroscopic data on the cluster galaxies. But there are clearly not enough bright galaxies in the field to put real constraints on them. More than 75% of the galaxies brighter than R = 22 have been already observed in spectroscopy. Only 8–10m class telescopes can go significantly deeper in a reasonable time.

An alternative way to dynamical analysis of the lens by such an extensive spectroscopic survey could be to observe the distortion pattern of background galaxies on very deep exposures of the field (Kneib et al. 1994). Of course, the lensing mass traced by the arc(let)s is extended over a larger scale than the one involved in the double quasar phenomenon. But such a study should confirm the mass center location and would test if the mass profiles used for modeling the real mass distribution are appropriate. The presence of gravitational arcs in the field needs thus to be confirmed by further deep imaging.

From a more theoretical point of view, some doubts have been raised on the feasibility of H_0 determination with Q 0957+561 (Kochanek 1993) because it seems difficult to have more constraints than free parameters for such a complex lens. More specifically, the dark matter distribution of a poor cluster is less constrained than the one of a single galaxy and should certainly be distributed over larger scales. The effect of such matter on the H_0 measurement can be deduced from the degeneracies exposed by Gorenstein et al. (1988): it essentially increases the upper limit of 87 (Bernstein et al. 1993). But more optimistic points of view have been expressed (Falco et al. 1991).

Anyway, Q 0957+561 is the only gravitational mirage for which we have hints on the time delay, a *sine qua non* measurement and the most expensive one in telescope time. Without excluding the use of other candidates, it thus seems worth continuing the observational efforts on Q 0957+561 for the determination of H_0.

References

Angonin-Willaime M.-C., 1993, Thèse Univ. Paris VII.
Angonin-Willaime M.-C., Vanderriest C., Hammer F., Magain P., 1994, A&A 281, 388.
Bahcall N., 1980, ApJ 238, L117.
Bahcall N., 1981, ApJ 247, 787.
Bernstein G., Tyson J., Kochanek C., 1993, AJ 105, 816.
Christian C., Adams M., Barnes J., Butcher H., Hayes D., Mould J., Siegel M., 1985, PASP 97, 363.
Falco E., Gorenstein M., Shapiro I., 1991, ApJ, 372, 364.
Garrett M., Walsh D., Carswell R., 1992, MNRAS 254, 27p.
Gorenstein M., Falco E., Shapiro I., 1988, ApJ, 327, 693.
Guiderdoni B., Rocca-Volmerange B., 1987, A&A 186, 1.
Jarvis J.F., Tyson J.A, 1981, AJ 86, 476.
Kneib J.P., Mathez G., Fort B., Mellier Y., Soucail G., Longaretti .Y., 1994, submitted.
Kochanek C., 1991, ApJ 382, 58.
Landolt U., 1983, AJ 88, 439.
Lehar J., Hewitt J., Roberts D., Burke B., 1992, ApJ 384, 453.
Mellier Y., Soucail G., Fort B., Mathez G., 1988, A&A 199, 13.
Oke J., Gunn J., 1983, ApJ 266, 713.
Pelt J., Hoff W., Kayser R., Refsdal S., Schramm T., 1994, A&A (in press).
Press W., Rybicki G., Hewitt J., 1992, ApJ 385, 416.
Refsdal S., 1966, MNRAS 132, 101.
Rhee G., 1991, Nature 350, 211.
Rocca-Volmerange B., Guiderdoni B., 1988, A&AS 75, 93.
Schild R., 1990, AJ 100, 1771.
Schild R., 1993, Proceedings Liège meeting (in press).
Soucail G., Mellier Y., Fort B., Picat J.P., Cailloux M., 1987, A&A 184, 361.
Stockton A., 1980, ApJ 242, L141.
Valdes, F., 1982, Proc. SPIE 331, 465.
Vanderriest C., Lemonnier J.-P., 1988, in: *"Instrumentation for ground based optical Astronomy"* (Robinson ed.), p.304.
Vanderriest C., Bijaoui A., Félenbok P., Lelièvre G., Schneider J., Wlérick G., 1982, A&A 110, L11.
Vanderriest C., Schneider J., Herpe G., Chevreton M., Moles M., Wlérick G., 1989, A&A 215, 1.
Walsh D., Carswell R., Weymann R., 1979, Nature 279, 381.
Young P., Gunn J., Kristian J., Oke J., Westphal J., 1980, ApJ 241, 507.
Young P., Gunn J., Kristian J., Oke J., Westphal J., 1981, ApJ 244, 736.

This article was processed by the author using Springer-Verlag TEX A&A macro package 1992.

Imaging and spectroscopy of B 1422+231 at C.F.H.T.: identification of the mirage and of the lensing galaxy at z= 0.647

Hammer F, Rigaut F, Angonin-Willaime M-C, 1995, Astronomy and Astrophysics, **298**, 737 :

Astron. Astrophys. 298, 737–742 (1995)

ASTRONOMY AND ASTROPHYSICS

Imaging and spectroscopy of B 1422+231 at C.F.H.T.: identification of the mirage and of the lensing galaxy at z= 0.647⋆

F. Hammer[1,2], F. Rigaut[1], M.-C. Angonin-Willaime[2], and C. Vanderriest[1,2]

[1] C.F.H.T., P.O. Box 1597, Kamuela, HI 9673, USA
[2] DAEC, Observatoire de Paris-Meudon, 5 Place Jules Jansen, F-92195 Meudon Principal Cedex, France

Received 6 July 1994 / Accepted 20 October 1994

Abstract. The optical counterpart of B 1422+231 has been imaged under very good seeing conditions (FWHM=0"65), and well resolved into 4 components found to be at the same location as the radio components. Component relative intensities are also consistent with the radio values although one component (A) appears slightly fainter. Subtraction of the four components has revealed the lensing galaxy (I=21) nearby the faintest component (D). Moderate resolution spectroscopy has shown that two components have the same emission line spectra, which definitively confirms the lensing hypothesis for B 1422+231. The lensing galaxy is revealed by a relatively red continuum and by several emission and absorption lines providing z=0.6471+ 0.001. Its spectrum is likely that of a spiral galaxy where some star formation is still at work. We also did photometry of the two galaxies lying a few arcseconds off the lensing system, which supports the idea that they are at the same redshift as the lensing galaxy. Consequences for modelling this gravitational mirage are exposed.

Key words: gravitational lensing – quasars, individual: B1422+231 – galaxies, distances and redshifts – galaxies, photometry

1. Introduction

B 1422+231 was first observed at the VLA by Patnaik et al. (1992) during a survey of about 1750 flat-spectrum radio sources (from 5 to 8.4 GHz). It was resolved into four unresolved components, and hence proposed as a new gravitational lens candidate, since most of the flat-spectrum radio sources are found to have a simple core plus jet structure. B 1422+231 was also identified with a luminous QSO at z= 3.62, and high resolution imaging in the infrared (Lawrence et al. 1992) and optic (Remy et al. 1993; Yee & Ellingson 1994). provided an additional support of the lensing hypothesis. In this article, we describe optical imagery and spectroscopy of this object and the nearby galaxies which definitively confirm the lensing hypothesis and provide the required information (lens location, magnitude and redshift, image ratio intensities etc...) to model it.

Send offprint requests to: F. Hammer

⋆ Based on observations made at the Canada-France-Hawai Telescope at Mauna Kea, Hawaii, USA

2. Imagery: the lensing galaxy

B 1422+231 was observed on March 22nd, 1993, at 13:25 UT. A 300 second exposure was taken through the I filter and a 600 second exposure through the V filter with the CFHT Faint Object Camera (FOCam) and a RCA CCD. This set-up gives a pixel scale of 0.203 arcsec/pixel. At the time of the observation, the seeing was quite stable with a FWHM of 0.65 arcsec.

The data reduction was done using IRAF and IDL. In addition to the standard bias subtraction and flat–fielding procedures, and to get the best results out of the image enhancement methods described hereafter, we applied a spatial filter that consists in removing the spatial frequencies higher than the cut-off imposed by the turbulence (λ/r_0 rd^{-1}) in the image spectrum. This operation suppresses part of the noise without modifying the actual physical content of the image.

Although the seeing somewhat blurs the individual components of B1422+231, the very large signal to noise ratio allows to apply image restoration algorithms with a high degree of confidence. Figure 1 shows the result of the Lucy–Richardson deconvolution of the quasar image using a nearby star (16″ South, 7″ West) as a PSF. The FWHM of point source components in the restored image is 0.17″. The deconvolution was stopped after a thousand iterations. The 4 radio components are found in this image, with positions matching well the radio positions (cf. Table 1). There is no evidence in this image of a fifth component, but it has to be noticed that the reconstructed image of component D (the faintest one) is slightly shifted with respect to its radio position.

However, it is well known that the photometry of deconvolved images (at least using straightforward methods like the one described above) is questionable. To derive the relative photometry of the individual components, we have used the more

classic method of subtracting PSFs at given locations. Providing that a minimum of a–priori information is supplied, here for instance the number of objects and their approximate locations, this method delivers accurate results. It has also the great advantage of being linear. In the case of B 1422+231, we set the number of objects to 4 and allowed the object positions to slightly vary about the radio positions. The 12 free parameters were therefore the position and the amplitude of each component. The variation domain of these parameters was scanned. Minimization of a chi–square statistic led to the results summarized in Table 1. The positions match very well with the radio positions. The relative amplitudes of components B,C and D also agree with the radio results, but A is definitely fainter. This was already noted by Lawrence et al. from their infrared observations. Figure 2 shows the I band image of B1422+231 (left). The crosses show the position of the ABC and D components as per Table 1. The second image of Fig. 2 shows the same image after subtraction of 4 PSFs at locations and with amplitudes reported in Table 1. This residual image features a large diffuse emission and an intensity peak (approximately 3 times brighter than the diffuse halo). This residual peak –let us call it component E–, if treated as another point source, has an amplitude which is typically of the order of the amplitude of component D. The location and amplitude of component E was found to be quite dependent on the particular set of parameters chosen for components ABCD. However, for the whole range of variation of the parameters, this fifth component was always present and located within the boundary of a rectangle drawn in Fig. 2. For the particular set of position and amplitude given in Table 1, we found a position of component E reported as a diamond in Fig. 2. Let us note at this point that the shift of component D noted in the Lucy restored image, even if it does not contitute a proof, fits well with the presence of a fifth source located close to component D. Given the low amplitude of this component, it was impossible to determine with certainty whether it is a point source or not. Our interpretation is that Component E is in fact the lensing galaxy. This hypothesis is confirmed by the observations of Yee & Ellingson (1994) who have discovered the existence of a fifth object at the same location than Component E. Different models of this mirage (Narashima & Patnaik 1993; Hogg & Blandford 1994) also suggest that the fifth object is at the right place to be the lensing galaxy.

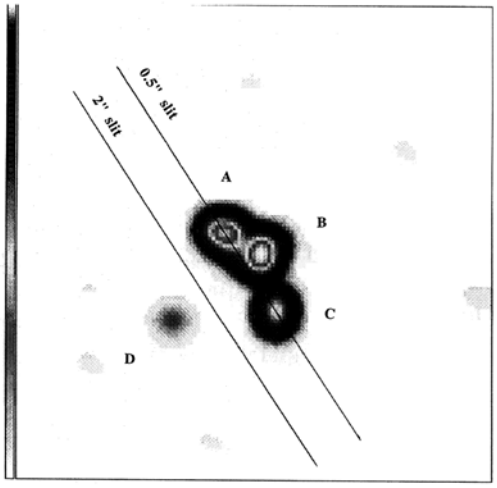

Fig. 1. I Band image of B 1422+231 after deconvolution using the Lucy–Richardson method (1000 iterations). The four components are clearly restored. Slit positions of the spectroscopy are drawn

3. Spectroscopy

Spectroscopy was performed at the C.F.H.T. 3.6m telescope in May 1993, having M.O.S. at the f/8 and the new Loral 3 CCD (2048X2048) which is sensitive from 3800 Å to 10000 Å. Two grism/slit combinations were used, the first one at moderate spectral resolution (FWHM= 2.7 Å), the other at lower spectral resolution (FWHM= 22 Å), and slit positions are drawn in Fig. 1. Data have been processed using a script (multiextract) written by Le Fèvre (1994) and based upon tasks in the NOAO/IRAF data reduction package (bias subtraction, flat field from the fit of corresponding quartz lamp spectrum, sky spectrum subtraction from the fit of the sky spectra on both sides of the objects by spline function, wavelength calibration relative to helium and argon lamps). Spectra have been flux- calibrated using the standard star LDS749B for the moderate spectral resolution and BD+25 for the lower spectral resolution. The moderate resolution spectrum has been corrected for distortion (1 pixel or 1.7 Å) by building and then applying a distortion map with the procedure task geomap of the iraf software. A 0"5 slit was used in the first exposure, combined with the O600 grism, and set in order to include components A, C and partly B (P.A.= -56°). Seeing was 0"8-0"9 during the 15mn exposure, and a direct image through the slit was used to define the three apertures (0"5 wide) corresponding to each component. Angular separation between A and C is 1"3 which means that the contamination of the C aperture by the A light due to the point spread function is marginal. Superposition of the 2 aperture spectra (Fig. 3) strikingly shows that they originate from a common source, i.e. A and C are gravitationally lensed images of the same QSO. The B aperture spectrum also presents the same emission lines (position, shape and relative intensities) as both A and C. Compared to C, the A and B spectra present a slight excess in the red part of their continua (beyond 7000 Å). Weighted to have the same intensity in the Lyα emission line, the C spectrum has been subtracted from the A spectrum (Fig. 4a), and the absence of residuals in emission lines (Lyα, NV, CII, SiIV, CIV, HeI) implies that A and C have identical emission line features (position, shape and relative intensities) down to an accuracy of 0.2 Å(or 10 km/s at the redshift of the QSO) after a gaussian fit of the lines.

A second spectroscopic exposure of 40 min was dedicated to detecting the lensing galaxy, and a relatively wide slit (2")

Table 1. Relative position and photometry of the ABCD components of B 1422+231. "Radio" refers to data derived by Patnaik et al. (1992). "I (PSF subtraction)" refers to the classic method of PSF subtraction at given locations (see text for details). For this method, the error on the relative positions is 0.01 arcsec (based on the results of the chi-square analysis) and the error on the relative amplitude is 4% (idem) except on the D component for which it reaches 30%. For comparison, the last column reports the relative component amplitudes derived from the Lucy deconvolved image (Fig. 1)

	Radio			I (PSF Subtraction)			I (Lucy)
Component	$\Delta\alpha$	$\Delta\delta$	Ampl.	$\Delta\alpha$	$\Delta\delta$	Ampl.	Ampl.
A	-0″.38	0″.31	0.977	-0″.39	0″.32	0.72	0.78
B	0.00	0.00	1.000	0.00	0.00	1.00	1.00
C	0.33	-0.75	0.520	0.33	-0.75	0.50	0.45
D	-0.95	-0.82	0.020	-0.94	-0.81	0.03	0.04

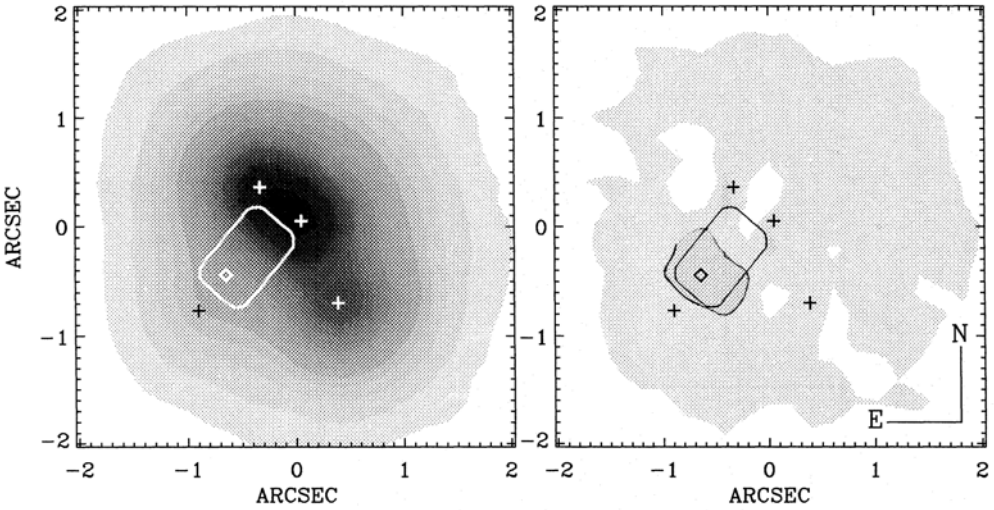

Fig. 2. B 1422+231 in the I band. Left : raw image. The crosses indicate the position determined in this paper. The rectangle shows the possible range of position of component E (underlying galaxy), and the diamond reports the position of E for the particular set of parameters given in Table 1. Right : Residual image after subtraction of the 4 components. The peak corresponding to the galaxy is surrounded by a dark line. For the sake of visibility, the square root of the images is displayed

was centered on the peak detected in imagery (see Fig. 2) and then combined with a low dispersion grism (O300), in order to better detect extended sources and to be able to detect features from 3800 Åto 10000 Å. However the resulting spectrum was mostly due to the QSO features, where the shape and position of the emission lines were the result of a complex convolution of the 4 image intensities with the slit/grism response, the latter depending on the exact location of the image relative to the slit center (a 0".5 offset from the slit center also corresponds to an apparent shift of 6 Åin λ). Hence the subtraction of one aperture spectrum from another in order to remove Lyα emission line, was very noisy at the position of the strongest emission lines (namely Lyα and CIV). Figure 4b shows the result of such a subtraction, which was made using two apertures (0."5 wide) centered from both sides of the peak continuum and separated by 1"3. One emission line and two absorption lines have been found, corresponding to [OIII]λ5007, CaII+HI λ3968 and MgII λ2799 at z= 0.6471. Signal to noise in the [OIII] line is larger than 4 and [OIII]λ4959 and [OII]λ3727 lines are also found but with a smaller S/N. On the other hand, the residual spectrum found after subtraction of the moderate resolution spectra of components A and C shows [OII]λ3727 and a red continuum beyond the expected G band at z= 0.647. Moreover MgII λ2799 and MgI λ5175 band are responsible for two strong absorption lines at the same redshift in the QSO spectrum, explaining why in the subtracted spectrum the MgII λ2799 absorption apparently reaches negative values (the QSO continuum being far more intense than the galaxy one).These lines provide the redshift determination of the lens, with a dispersion z=0.001 or 250 km/s at the lens redshift. From its spectral properties, the lens-

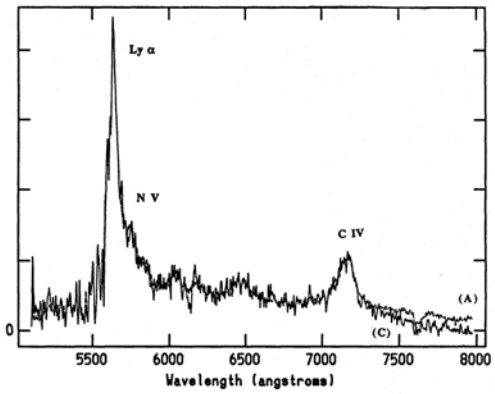

Fig. 3. Spectra of the A and C components with O600 grism and 0.5"slit

ing galaxy of B 1422+231 is likely a late type spiral galaxy in which star formation is still at work. This is a relatively bright galaxy (M_V = -22 for H_0= 50) and so it can be a S0 galaxy with a very elliptical mass distribution in order to explain the four image configuration.

4. Neighbouring galaxies

Hogg & Blandford (1994) suggest that the two bright galaxies G2 and G3 located several arcseconds from the quasar contribute to the lensing phenomenon. It is thus interesting to collect some characteristics of these galaxies. In the V and I pictures (see Table 2), the two galaxies were resolved. One presents a fuzzy extension around it. Using NOAO/IRAF software, the photometry of the field was processed by comparing with the field NGC 4147.

These figures do not exclude the hypothesis that these two galaxies are at the same redshift as the main deflecting galaxy. In that case, with H_0 = 50, the absolute blue magnitude at rest is -22.7 for G2 which has a spiral Sb type, and -23.14 for G3 which has a spiral Sa type (Tresse, private communication, based on Bruzual & Charlot 1993, software). These results correspond to the brightest members of galaxy clusters. The possibility of a group of galaxies or a cluster as lens should be kept in mind. The presence of faint objects in the field corroborates this idea.

5. The lensing hypothesis

Several models of the mirage have been suggested. Narashima and Patnaik explain the four-image configuration with a single lens inside the image circle. In that case the deflecting galaxy presents an extended massive halo with a large ellipticity (around 0.6) which is not very realistic. The Hogg and Blandford model uses the perturbating effect of the two nearby galaxies to describe the lensing phenomenon with a spherical

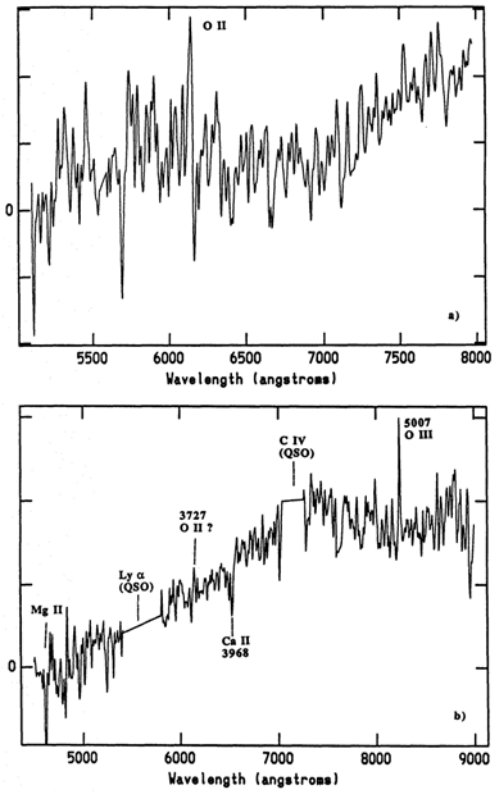

Fig. 4. a Result of the subtraction of A and C spectra obtained with the O600 grism. **b** Result of the same subtraction with spectra obtained with the O300 grism and 2" slit. The spectra are flux-calibrated in F_λ, but since the scales are relative only the zero level has been reported

Table 2. Relative position and photometry of galaxies G2 and G3. Errors are 0.1 mag

	Positions		V	I	V-I
G2	– 9.0	– 5.2	21.8	19.7	2
G3	– 3.6	– 7.3	21.5	19.3	2.2

main deflecting galaxy. This model suggests large values for the mass of the two bright galaxies G2 and G3. Modelling of the 4 images was also done using our software developed at the Meudon Observatory (Hammer & Rigaut 1988; Angonin 1993). The lens mass distribution is assumed to follow a $r^{1/4}$ density profile with spherical or elliptical symmetry while the intensity ratios of the point images are estimated from the following technique: image positions are calculated using a moderate resolution map (grid of 500X500 points in a 11.5"X 11.5" region around the QSO). Image and lens positions are provided by our

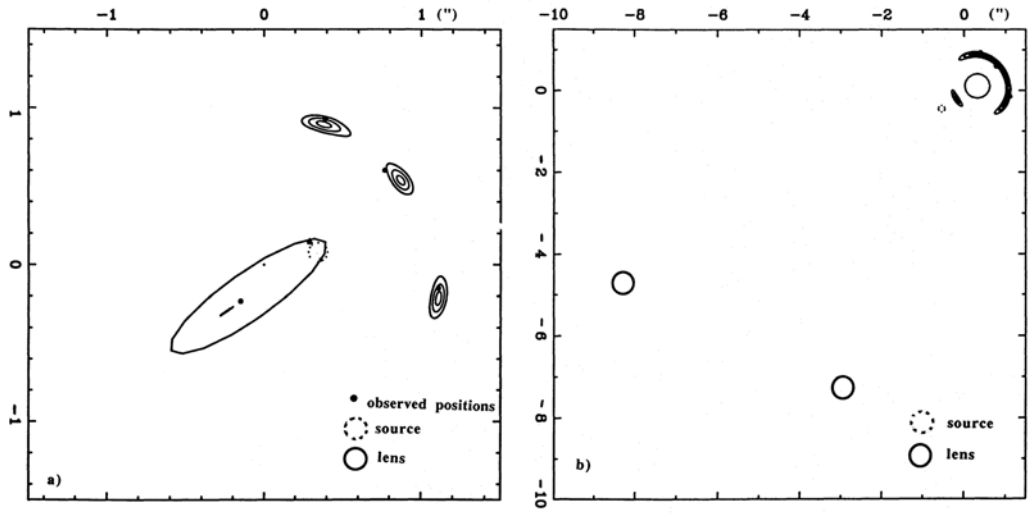

Fig. 5a and b. Two examples of Q1422 models: **a** Configuration with galaxy G1 alone with 8 10^{12} solar masses and an ellipticity of 0.7; **b** Configuration with galaxies G1, G2 and G3, the three masses are respectively 8.7, 41 and 4.7 10^{12} solar masses and are distributed with spherical symmetry

observations (from Table 1) while the image intensity ratios are chosen from the radio measurements (Patnaik et al. 1992) since the latter are unlikely to be contaminated by either microlensing or the presence of extended emission line regions (Lyα or CIV). The different hypotheses for the lensing geometry have been successfully tested (see Fig. 5 for examples): the four image configuration can be explained either by the ellipticity of the main deflecting galaxy or by the perturbating presence of the other two galaxies.

The main deflecting galaxy alone can reproduce the four images but with a great mass (5 10^{11} – 10^{12} solar masses) and a large value of ellipticity (0.6–0.7). With our observations, the obtained mass would correspond to M/L = 70 – 160. Such a high amount of dark matter would have an extreme elliptical distribution.

More likely is the possibility that the two nearby galaxies are contributing to the lensing system either in a cluster at z = 0.65 or not. Having masses similar to the ones computed by Hogg and Blandford, it is compatible with no ellipticity main lens. They mentioned the existence of additional images near G2 and G3. Such an artifact vanishes when the mass distribution of the two galaxies differ from point mass.

The more realistic model of such a mirage should be found in an intermediate model including the role of G2 and G3 and ellpticity in G1 mass distribution. In that case, the parameters are more numerous than the constraints and it is not possible to conclude more with the actual observational results.

6. Discussion and conclusion

In this letter we present the good quality optical images (FWHM = 0.6") of B1422+231 obtained at CFHT. Deconvolution techniques have been applied to them and provided accurate photometry of the four images, despite they lie within 1 arcsecond. Spectroscopy of the system shows that the positions of emission lines agree within 10 km/s from one component to another. This definitely proves that B1422+231 is a gravitational mirage. The redshift of the deflecting galaxy (z=0.647) is also derived. Modelling the configuration cannot provide additional constraint on the mass distribution of the lens. Indeed both a single lens with large ellipticity and a group/cluster of galaxies can produce the lensing geometry. We feel the latter case as more probable, since two additional galaxies near the lensing system have colors and magnitudes supporting they lie at the same redshift as the main lens. This should be easily checked by future spectroscopic investigations. Deep imaging and spectroscopy of neighbouring galaxies would be welcome in order to check the possibility of the presence of a massive cluster around the main deflecting galaxy. This would lead to a better estimation of the predicted time delay (1 month in the three-galaxy configuration) and then to investigate if this system is more suitable for time survey than Q0957 (Angonin et al. 1994).

Last but not least, is the fact that the intensity ratio of the two brightest components differs significantly between optical and radio wavelengths. One of us (C.V.) has done high quality imagery with SIS at CFHT one year after our first observation of the system, which shows no variation of the optical intensity ratio. It is therefore unlikely that microlensing is causing a

differential intensity ratio of the brightest conponents between radio and optical wavelengths. We rather believe that differential macrolensing is due to the differences between geometry and locations of the radio and optics. VLBI observations would almost certainly provide interesting new constraints to that configuration.

Acknowledgements. G. Monnet and J. Glaspey, director of CFHT (discretionary time), O Le Fèvre, help during the data reduction, B. Monart, support during the observations, K. Willaime for his cooperation on the 22nd of march, 1993, F. Hammer and M.-C. Angonin-Willaime acknowledge support from EC HCM Networks CHRX-CT92-0044.

References

Angonin-Willaime, M.C., 1993, PhD thesis.
Angonin-Willaime, M.C., Soucail, G., Vanderriest, C., 1994, to be published in A&A.
Bruzual, A., Charlot, S., 1993, ApJ, 405, march 10.
Hammer, F., Rigaut, F., 1989, A&A, 226, 45.
Hogg, D.W., Blandford, R.D., 1994, MNRAS, 268, 889.
Lawrence, C.R., Neugebauer, G., Weir, N., Matthews, K., Patnaik, A.R., 1992, MNRAS, 259, 5p.
Le Fèvre, O., 1994, in preparation.
Narashima, D., Patnaik, A.R., 1993, Proceedings of the 31st Liège International Astrophysical Colloquium on Gravitational Lenses in the Universe, Edited by J. Surdej et al. 295.
Patnaik, A.R., Browne, I.W.A., Walsh, D., Chaffee, F.H., Foltz, C.B., 1992, MNRAS, 259, 1p.
Remy, M., Surdej, J., Smette, A., Claeskens, J.-F., 1993, A&A, 278, L19.
Yee, H. K. C., Ellingson, E., 1994, AJ, 107, 28.

This article was processed by the author using Springer-Verlag TEX A&A macro package 1992.

About the origin of extinction in the gravitational lens system MG J0414+0534
Angonin-Willaime M-C, Vanderriest C, Courbin F, Burud I, Magain P, Rigaut F, 1999, Astronomy and Astrophysics, **347**, 434.

Astron. Astrophys. 347, 434–441 (1999)

ASTRONOMY AND ASTROPHYSICS

About the origin of extinction in the gravitational lens system MG J0414+0534*

M.-C. Angonin-Willaime[1], C. Vanderriest[2,], F. Courbin[2,3,4], I. Burud[3], P. Magain[3,***], and F. Rigaut[5]**

[1] DEMIRM, Observatoire de Paris-Meudon, France
[2] UMR 8631, CNRS-DAEC, Observatoire de Paris-Meudon, F-92195 Meudon Cedex, France
[3] Institut d'Astrophysique et de Géophysique, Université de Liège, Avenue de Cointe 5, B-4000, Liège, Belgium
[4] Universidad Catolica de Chile, Department of Astronomy and Astrophysics, Casilla 22, Santiago 22, Chile
[5] European Southern Observatory, Karl-Schwarzschild-Strasse 2, D-85748 Garching bei München, Germany

Received 21 January 1999 / Accepted 25 March 1999

Abstract. Photometric measurements of the highly reddened gravitational mirage MG J0414+0534 have been carried out either by PSF subtraction or by applying accurate deconvolution algorithms to optical (R, I) and near-infrared (K) images obtained at CFHT and NOT under sub-arcsecond seeing conditions. It is confirmed that the close pair of images A1-A2 suffers a larger extinction than B and C. While the colours of image A2 obtained from ground-based data seem inconsistent with a simple reddening law, higher resolution images available from HST archives reveal an additional extended component (arc) which introduces significant errors in the photometric decomposition. When the arc component is properly taken into account, the colours of the 4 nucleus images do agree with a classical reddening law, with A2 being by far the most obscured component. Such a differential extinction (maximum difference ΔE(R-I) $\simeq$ 0.6) is likely due to the lensing galaxy. This does not mean that *all* the extinction occurs into the lens. Indeed, the fact that the arc is much less red than the images of the nucleus suggests that an important part of the reddening is intrinsic to the source. Finally, no significant variability is observed within this data set, i.e. between 1994 and 1997, while a discrepancy from earlier data is noticed for (A1 + A2).

Key words: galaxies: ISM – galaxies: quasars: individual: MG J0414+0534 – cosmology: gravitational lensing – infrared: galaxies

1. Introduction

MG J0414+0534 is one of the gravitational lens systems found in the MIT-Green Bank radio survey (Bennett et al., 1986). Its high radio flux allowed a detailed mapping with the Very Large Array (Hewitt et al., 1988, Hewitt et al., 1992, Katz & Hewitt, 1993), revealing a trapeziform configuration (almost identical to that of PG 1115+080) with 4 bright images labelled A1, A2, B and C.

This system is remarkable because, in the optical domain, the counterparts of the radio images are extremely red and faint, and their spectrum is almost featureless. The source appears to be a very obscured quasar; its redshift (z_S = 2.639) could only be obtained from infrared spectra (Lawrence et al. 1995a). The strong and broad H_α emission line, as well as other fainter Balmer and Fe II lines, indicate a classical active nucleus spectrum after correction for the reddening. The most prominent spectral feature in the optical may be identified with an absorption complex of Fe II lines at redshifts close to the emission redshift of the quasar (Lawrence et al. 1995b). The lensing galaxy is easily detected on sub-arcsecond images (Shechter & Moore, 1993, Angonin-Willaime et al., 1994) but its redshift, z_L = 0.958, remained unknown until recently (Tonry and Kochanek 1998).

The exact value of the reddening in MG J0414+0534 depends on its origin, but is high in any case. The H_α/H_β flux-ratio as well as the upper limit for L_α/H_α (Lawrence et al. 1995a) suggest an extinction $A_v \simeq 6$ mag for the brightest QSO pair, assuming it occurs in the lensing galaxy. The fact that the flux ratios between the different QSO images change with wavelength can be interpreted in terms of differential reddening along different line of sight, through the lensing galaxy. Lawrence et al. (1995a) proposed that most of the extinction occurs in the lens, rather than close to the source (galaxy hosting the quasar, associated cluster...). The present paper compares optical and infrared data in order to test this interpretation. The ground-based optical and near-IR data are presented and discussed in Sect. 2. Sect. 3 presents a re-analysis of archival HST data and shows how the presence of a gravitational arc may affect the photometry derived from lower resolution images. Finally, the origin of the measured extinction is discussed in Sect. 4.

Send offprint requests to: M.-C. Angonin-Willaime

* Based on observations collected with the Canada-France-Hawaii Telescope at Mauna Kea (Hawaii, USA), the Nordic Optical Telescope (Canary, Spain) and archive data from the Hubble Space Telescope (NASA/ESA)

** Visiting Astronomer, Canada-France-Hawaii Telescope

*** Also Maître de recherches au FNRS, Belgium

Table 1. Photometry of MG J0414+0534 (ground-based and HST data)

Data set:	1	2	3	4	5	6	7	8
Parameters of the observations:								
Date(UT)	94-08-15	94-08-16	94-09-12	94-09-12	95-09-01	97-12-03	94-11-08	94-11-09
Tel./Instr.	CFHT/SIS	CFHT/RedEye	CFHT/Focam	CFHT/Focam	CFHT/SIS	NOT/Hirac	HST/WFPC2	HST/WFPC2
colour	R	K	R	I	I	I*	R	I
exp.(mn)	2×10	13×2	2×25	3×10	10	8×15	135	175
resol.($''$)	0.68	0.62	0.80	0.81	0.57	0.55	0.12	0.09
pixel ($''$)	0.173	0.201	0.206	0.206	0.173	0.108	0.044	0.044
Photometry of the components:								
A1	23.28 ± 0.04	14.27 ± 0.03	23.29 ± 0.04	20.38 ± 0.03	20.50 ± 0.03	20.76 ± 0.02	23.29 ± 0.03	20.50 ± 0.02
A2	23.45 ± 0.04	14.63 ± 0.03	23.52 ± 0.04	21.22 ± 0.03	21.28 ± 0.03	21.68 ± 0.05	24.79 ± 0.04	21.55 ± 0.03
B	23.41 ± 0.05	15.34 ± 0.04	23.44 ± 0.04	21.20 ± 0.04	21.22 ± 0.04	21.50 ± 0.03	24.11 ± 0.04	21.36 ± 0.03
C	24.43 ± 0.07	16.23 ± 0.06	24.48 ± 0.07	22.08 ± 0.05	22.14 ± 0.06	22.49 ± 0.08	24.82 ± 0.04	22.16 ± 0.03
G	22.9 ± 0.3	18.0 ± 0.15	22.7 ± 0.2	21.00 ± 0.15	20.95 ± 0.10	21.6 ± 0.2**	–	–
A/B	2.09 ± 0.10	4.60 ± 0.15	2.07 ± 0.10	3.11 ± 0.08	2.89 ± 0.08	2.83 ± 0.07	2.65 ± 0.08	3.06 ± 0.07
A1/B	1.12 ± 0.06	2.68 ± 0.10	1.15 ± 0.06	2.13 ± 0.06	1.95 ± 0.08	1.98 ± 0.08	2.12 ± 0.06	2.22 ± 0.06
A2/B	0.97 ± 0.05	1.92 ± 0.10	0.93 ± 0.06	0.98 ± 0.05	0.95 ± 0.05	0.85 ± 0.06	0.53 ± 0.05	0.84 ± 0.05
C/B	0.39 ± 0.05	0.44 ± 0.05	0.38 ± 0.05	0.44 ± 0.04	0.43 ± 0.05	0.41 ± 0.05	0.52 ± 0.04	0.48 ± 0.04
Photometry of surrounding stars:***								
M	21.42 ± 0.04	–	21.39 ± 0.04	19.18 ± 0.03	19.20 ± 0.04	19.19 ± 0.02	–	–
2	21.41 ± 0.03	–	21.41 ± 0.03	20.21 ± 0.03	20.21 ± 0.04	20.21 ± 0.03	–	–
3	21.88 ± 0.05	19.15 ± 0.1	21.83 ± 0.04	21.07 ± 0.03	21.09 ± 0.05	21.01 ± 0.03	21.95 ± 0.05	21.07 ± 0.03
4	23.01 ± 0.07	–	23.12 ± 0.06	21.90 ± 0.05	21.97 ± 0.07	21.87 ± 0.04	23.09 ± 0.05	22.02 ± 0.04
5	24.07 ± 0.10	–	24.13 ± 0.10	22.10 ± 0.06	–	22.16 ± 0.04	24.06 ± 0.10	22.33 ± 0.05
6	23.68 ± 0.10	19.70 ± 0.1	23.76 ± 0.10	22.05 ± 0.06	22.01 ± 0.07	22.03 ± 0.04	–	–

* See discussion about the photometric systems in Sect. 2.2

** Measurement in a $1.8''$ diameter aperture, while it was $\sim 4''$ for the other data.

*** Identification as in Angonin-Willaime et al. (1994). For the visible ground-based data, star 2 was chosen as the main local photometric reference, while it was star 3 for HST data.

2. Ground-based observations

Several high-resolution data sets have been obtained with the Canada-France-Hawaii Telescope (CFHT) and the Nordic Optical Telescope (NOT) between 1994 and 1997, allowing to measure individually the fluxes of the 4 images of the source. Six data sets corresponding to four epochs (Table 1) have been analysed.

2.1. Optical: observations and reduction methods

The data from CFHT have been obtained with SIS (Subarcsecond Imaging Spectrograph), which uses an active guiding mirror for a first order (tip-tilt) correction of the atmospheric turbulence, or with the direct imaging unit FOCAM. The same combination of detector (a CCD from Loral) and filters was used for both instruments. The individual frames were re-centered and co-added for each data set whenever several exposures were available. The typical spatial resolution is $0.6''$with SIS and $0.8''$with FOCAM.

The photometric measurements of the lensed images of the nucleus were performed by direct PSF subtraction: a synthetic PSF is built from the average of several surrounding stars, then properly scaled and subtracted at the positions of the 4 images, A1, A2, B and C. Scaling factors and positions are adjusted by trials and errors, using procedures from the IRAF package. For evaluating the quality of decomposition and the photometric accuracy, the same PSF subtraction method is applied to a few stars belonging to the photometric sequence established in the field (Angonin-Willaime et al., 1994). After a few iterations, the procedure leaves a clear picture of the lensing galaxy (Figs. 1 and 2). The residuals close to the positions of the lensed images are similar to the residuals around field stars, except for some faint excess of flux between A1-A2 and B. This structure, barely emerging from noise, is the mark of the arc component detected more easily with the HST (see Sect. 3).

The data from NOT have been obtained with the HiRAC camera under very good seeing conditions. The excellent spatial stability of the PSF provided by this instrument gave the opportunity to take full advantage of the MCS deconvolution code (Magain et al., 1998). The algorithm decomposes the images into a sum of point sources plus a diffuse background; the final resolution is chosen according to the signal/noise ratio in the object. When applied to one single image, this procedure of "controlled deconvolution" already allows to improve both the resolution and sampling of the data (see Courbin et al.,

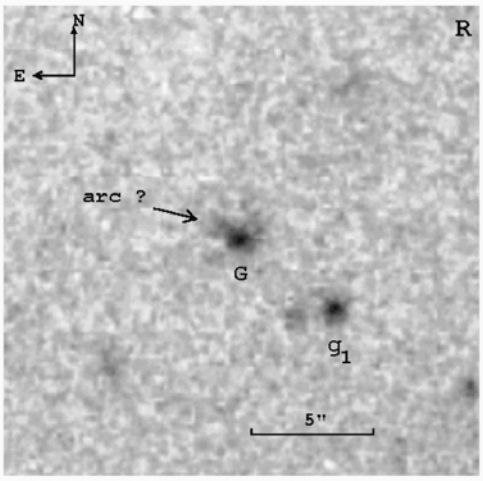

Fig. 1. Processing of the R images from CFHT (sum of data sets 1 and 3). The figure displays the residuals after "optimal" PSF subtraction at the locations of the 4 images of the nucleus. This allows an accurate photometry of the lensing galaxy G. An excess of light is clearly present at the location of the arc detected with HST. The nearby galaxy g_1 was already identified by Angonin-Willaime et al. (1994).

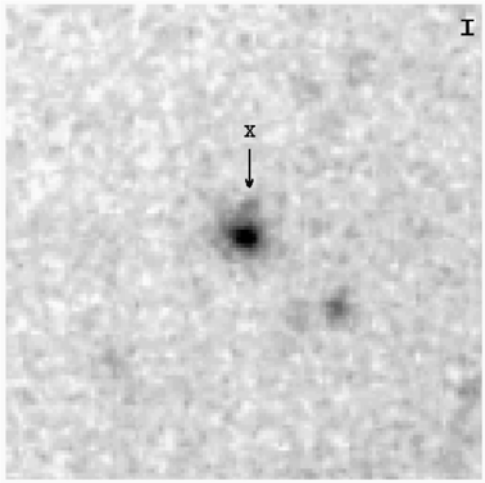

Fig. 2. Same as Fig. 1 for the I-band image obtained at CFHT (sum of data sets 4 and 5; scale and orientation as in Fig. 1). The arc is not clearly seen, while object "X" is easily detected. Note that the lens is very red compared with surrounding galaxies.

1997 for an application to PG 1115+080), but better results are achievable when several dithered frames of the same object are deconvolved simultaneously (Courbin et al., 1998a, Burud et al., 1998). In the present case, 8×15 mn exposures were deconvolved simultaneously, with a final resolution of 0.16″, using a pixel scale of 0.0535″. The programme determines the intensities of the point sources independently for each frame. The standard deviation of the eight intensities therefore provides a reasonable estimate of the 1σ error bar on the photometry. The quality of the deconvolution is checked by inspecting the residual maps obtained for each frame (see Courbin et al., 1998b for more details). The final deconvolved image is displayed in Fig. 3 and should be compared with Fig. 7. The arc between A1-A2 and B is clearly visible; the "object X" from Schechter & Moore (1993) is measurable with I = 24.0 ± 0.2, i.e. in agreement with previous photometry (Angonin-Willaime et al., 1994). First order moment of the light distribution allows one to estimate the position of the lensing galaxy; more detailled analysis also reveals the flattening of the isophotes, as well as some rotation of its major axis with the surface brightness level, suggesting it could be either a giant Spiral or a triaxial Elliptical.

For all our ground-based data, photometric measurements are related to the local reference star 2, which was also independently checked against primary standards. The results for the local sequence are in good agreement with previous values (Angonin-Willaime et al., 1994). The only significant difference may be for the R magnitude of star M, which could indicate slight, but significant, photometric variability. The optical positions found for the QSO components agree very well with the radio positions (Katz et al., 1997), while the intensity ratios do not, confirming the reddening of the source.

2.2. *Comments on the optical photometry*

Table 1 summarizes our photometric measurements. We notice that the magnitudes of the images did not vary significantly over the period of observations for the CFHT data sets (1 and 3 in R, 4 and 5 in I). The magnitudes from NOT are apparently ∼ 0.2–0.3 mag fainter. Similarly, when comparing with data from 1991–92 (Angonin-Willaime et al., 1994), we remark a small brightening of all the QSO images in I (see the concluding section). If real, this would indicate a synchronous variation of *all* the 4 images of the source, which is not unlikely with short time delays. However, it should be kept in mind that the very red spectrum of the source makes its photometry extremely sensitive to the precise shape of the red cut-off of the instrumental passband. This is especially true for the I-band. In fact, when we build the I-band instrumental responses for CFHT and NOT by combining the filter and CCD responses, both show a small departure from the theoretical I system: too red for CFHT and too blue for NOT (for details, see the instrument manuals of these telescopes). We checked, by integrating the source spectrum multiplied by the response curves, that such small discrepancies are quantitatively sufficient for explaining the observed effect. There is no noticeable effect on the surrounding stars of the photometric sequence because, although some of them are quite red, the shapes of their spectra are less "extreme".

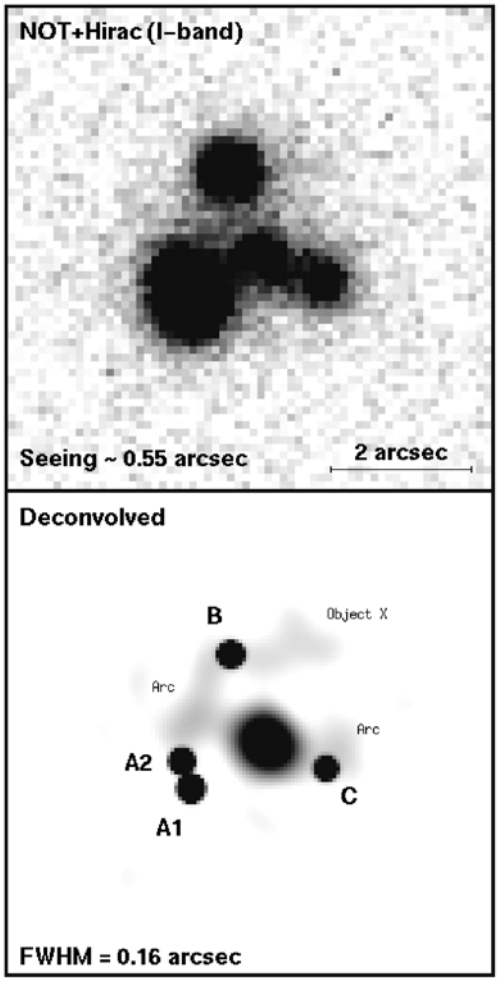

Fig. 3. Processing of the I image obtained at NOT (data set 6); upper panel shows the direct sum of 8 images; lower panel displays the result of running the MCS algorithm simultaneously on the 8 images (see text). One may see clearly the lensing galaxy as well as residual structures, emerging significantly from the background noise, which correspond respectively to the arc (between A1+A2 and B, and close to C), and to object "X". See Fig. 7 for a comparison with HST images.

This discussion shows that one should be extremely cautious with apparent variations of MG J0414+0534 measured with different instruments. Variation of the flux *ratios* would be a better clue to real variations, since the spectra of the 4 gravitational images are similar (except for the differential extinction which, in this case, is a second order effect). No such variation is detected

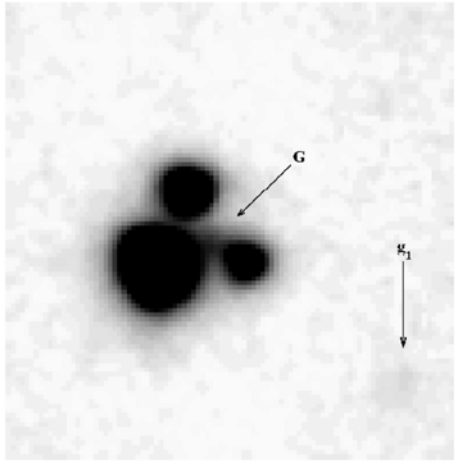

Fig. 4. K-band image obtained at CFHT (data set 2). The lensing galaxy G is clearly seen at $K = 18.0$ and the nearby galaxy g1 at $K \simeq 19.8$.

with our data. Finally, within the error bars, the observations are compatible with a total stability of the source.

2.3. Infrared

Observations in K band with the RedEye infrared camera (Simons et al., 1994) were made one night after optical observations (data sets 1 and 2). This quasi-simultaneity insured that any measured colour difference cannot result from intrinsic variability coupled with time-delay effects. We took 13 successive exposures, each of 120 s duration, shifted by $4''$ along a square pattern. An accurate flat field is obtained by correlation of all the individual frames. After rebinning to $0.1''$/pixel, recentering and coaddition of the frames, the final image has a useful field of view $\sim 40''$. The stars present in this field are much too faint for building an accurate PSF. It was therefore determined iteratively from the object itself. After PSF subtraction, the photometric accuracy on the nucleus images, although somewhat deteriorated by the process, is still comparable to the one in optical. Likewise, the lensing galaxy is measurable with an accuracy comparable to optical. The absolute photometric calibration was carried out by using the standard stars FS26 and FS35 (Casali & Hawarden, 1992). The near-IR photometric results are summarized in Table 1 and astrometry is given in Table 2.

The magnitudes of the 4 components agree, within the error margins, with those measured by McLeod et al. (1998) in 1992–93, but there is an obvious discrepancy of almost 2 magnitudes for the lensing galaxy. Owing to the better signal-to-noise ratio and resolution, the magnitude derived here seems to be more reliable (it is already obvious on Fig. 4 that galaxy G cannot be as bright as claimed by McLeod et al.). The $(R-I)/(I-K)$ colour ratio agrees with that of a giant elliptical at z $\simeq$0.9 with

Table 2. Relative astrometry in K (CFHT data) and in optical (HST data)

	CFHT (K)		HST	
	$\Delta\alpha('')$	$\Delta\delta('')$	$\Delta\alpha('')$	$\Delta\delta('')$
A1	$+0.60 \pm 0.01$	-1.93 ± 0.01	$+0.60 \pm 0.01$	-1.94 ± 0.01
A2	$+0.74 \pm 0.01$	-1.54 ± 0.01	$+0.73 \pm 0.01$	-1.55 ± 0.01
B	0.00	0.00	0.00	0.00
C	-1.35 ± 0.02	-1.65 ± 0.02	-1.345 ± 0.01	-1.64 ± 0.01
G	-0.53 ± 0.05	-1.31 ± 0.04	-0.475 ± 0.01	-1.28 ± 0.01
$\star$ 3	$+4.60 \pm 0.03$	$+9.23 \pm 0.03$	$+4.61 \pm 0.01$	$+9.23 \pm 0.01$
$\star$ 6	$+18.79 \pm 0.03$	-6.01 ± 0.03	–	–

Note: Astrometry based on psf subtraction for the source images and stars; barycenter for the galaxy.

very little reddening (Kodama et al., 1998). Conversely, if we assume that the lensing galaxy is a giant elliptical with small reddening, the observed I magnitude alone suggests a redshift comparable to that measured by Tonry & Kochanek (1998).

3. HST data

WF/PC2 frames of MG J0414+0534 are available from the HST archives. As discussed in Falco et al. (1997), the high resolution allowed to discover a lensed arc, in addition to the 4 point-like images. We retrieved these frames via the CADC network and did our own processing (Figs. 5 to 8). The arc that links images A_1, A_2 and B shows up very clearly in both colours. A fuzzy extension north of image C is also visible, especially in R. As noted by Falco et al., these structures indicate that the source is made of a point-like core (the nucleus of the quasar) and a very asymmetric underlying galaxy or a close companion.

3.1. Photometric measurement of the nucleus images

Measuring the magnitudes of the 4 core images was done by PSF subtraction, in the same way we did for ground-based data. For each image, the intensity of the PSF was adjusted for obtaining the "best" residuals. However, two difficulties arise here: (i) the PSF of the WF/PC2 is undersampled ($\sim$ 2 pixels FWHM) and (ii) it is difficult to evaluate the arc profile underneath the core images. Anyway, our photometric method (Figs. 6 and 8) gives significantly different results than those previously obtained by Falco et al., who just integrated the flux inside an aperture. The chequered pattern of the image residuals at the position of the subtracted PSFs (best visible in the I image of Fig. 8) is an artifact due to the undersampling. This effect probably contributes to increase the error of our photometry, but not to an extent that would make it compatible with the estimate of Falco et al. As can be seen from Figs. 6 and 9, light contamination by the lensed arc is *not negligible at all*, especially around component A2. This casts some doubts on the reliability of the aperture photometry carried out by Falco et al. (1997), at least for component A2.

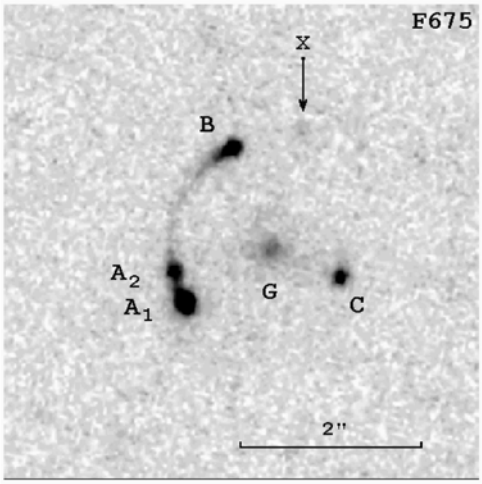

Fig. 5. Close-up on the arc structure from HST images in R.

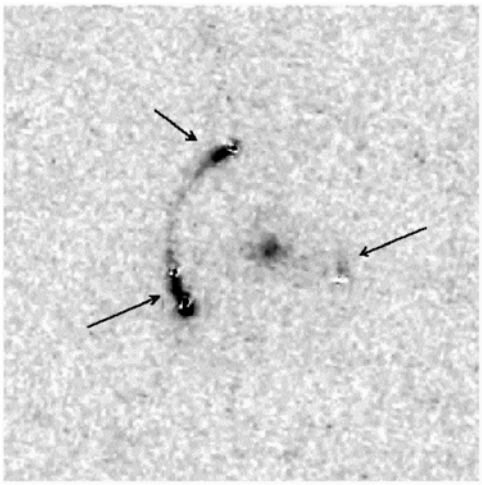

Fig. 6. Same as Fig. 5 after PSF subtraction at the locations of A1, A2, B, C and "X" (contrasts have been slightly stretched with respect to Fig. 5). Note the bright arc portions close to the nucleus images (arrows), especially between A1 and A2.

3.2. Comparison of HST and ground-based photometric measurements: influence of an extended structure

Having processed the images as described above, one may note that the photometric results from HST differ notably from the ground-based results. This cannot be due to difference in the photometric systems. The rattachment to the standard photometric system is done quite accurately by using the formulae given

Table 3. Colour indices of the components of the lensing system

	$(R\text{-}I)_{CFH}$	$(R\text{-}K)_{CFH}$	$(R\text{-}I)_{HST}$	$R_{HST}-K_{CFH}$
A1	2.9 ± 0.05	9.0 ± 0.04	2.8 ± 0.04	9.0 ± 0.04
A2	2.3 ± 0.05	8.8 ± 0.04	3.25 ± 0.05	10.15 ± 0.04
B	2.25 ± 0.06	8.05 ± 0.06	2.75 ± 0.05	8.75 ± 0.05
C	2.4 ± 0.09	8.2 ± 0.08	2.65 ± 0.05	8.6 ± 0.07
G	1.7 ± 0.3	4.9 ± 0.3	–	–
arc	–	–	1.4 ± 0.3	–

by Holtzman et al. (1995), and any remaining effect should be a systematic shift of the magnitude scale. The observed differences are rather due to the presence of the arc, which brightness is maximum near A1-A2 and varies significantly on a scale comparable to the resolution of ground-based data. In such a case, the errors with the direct PSF subtraction method or even the deconvolution method could be important, especially for the relatively faint component A2. Note on Figs. 1–3 that the arc is totally "lost" underneath A1-A2 and the residuals seem nevertheless acceptable. This failure is explained by the very important photon noise from the QSO images spread over the arc, while HST images are naturally exempt of contamination.

We verified this interpretation by smoothing and rebinning the HST data to match the parameters of ground-based data (resolution $\simeq 0.6''$, pixel $\simeq 0.1''$), then applying the same procedure of PSF subtraction as for real ground-based data. The "best" results obtained this way give almost unchanged fluxes, within 0.1 mag, for components A1 and C but over-estimates the flux of B by 0.1 mag in I and 0.3 mag in R, and the over-estimation for A2 reaches 0.4 mag in I and 1.0 mag (!) in R. In other words, standard processing of the (degraded) HST data yields almost exactly the flux values measured from data set 5. This exercise shows quantitatively how the presence of a faint extended structure, hardly detected with $0.6''$ resolution, could induce substantial errors on PSF subtraction results. However, the correction needed to retrieve the "true" photometry depends only on the final resolution and, since the seeing of our ground-based data set is almost constant around $0.6''$- $0.8''$, it would make sense to search for variability by inter-comparison.

4. Extinction

Table 3 gives the final colours of the various components (rounded to the nearest 0.05 mag). As discussed above, the most realistic colours of the nucleus images are those involving HST observations. Then, it becomes obvious that A2 is much more reddened than the other images of the nucleus. The order of increasing reddening is: C, B, A1, A2, with a ΔE(R-I) of 0.6 mag between A2 and C.

4.1. Estimation of the extinction and discussion of its origin

The high extinction in MG J0414+0534 could be due to dust in the foreground lensing galaxy as well as dust in the quasar itself (or, more likely, a combination of both). A first value of the extinction A_V can be inferred from the $R-I$ colour of the nucleus images, through a relation A_V = k.E(R-I) in which k depends on the shape of the extinction curve and on the redshift of the absorber. A typical z=2.6 quasar should have R-I $\simeq$ 0.5 (Irwin et al., 1991; Véron & Hawkins, 1995), thus E(R-I) is close to 2.15 for C and 2.75 for A2. Assuming that this colour excess is due entirely to the lensing galaxy at z$\sim$0.9, we could compute

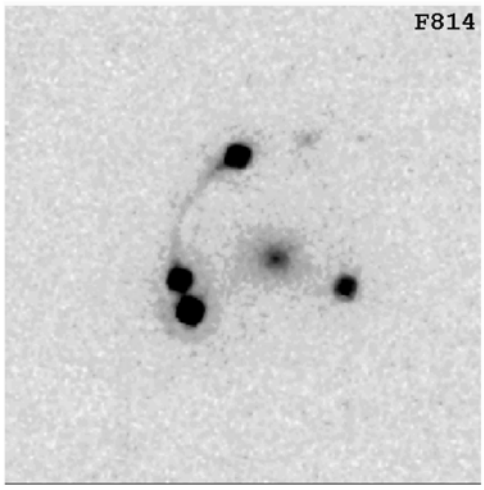

Fig. 7. Close-up on the arc structure from HST images in I.

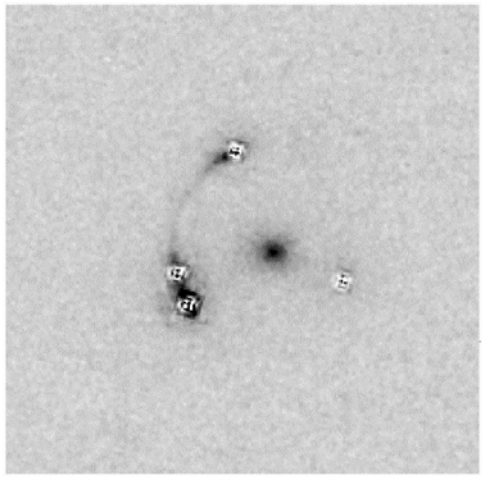

Fig. 8. Same as Fig. 7 after PSF subtraction at the locations of A1, A2, B, C and "X" (contrasts have been slightly stretched with respect to Fig. 7). The arc is visible between A1 and A2 with a relativly high surface brightness.

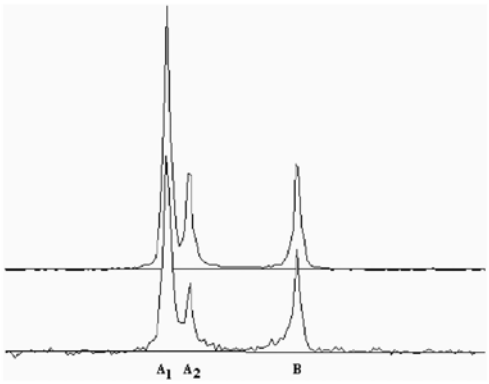

Fig. 9. Flux distribution projected along the arc in I (upper curve) and R (lower curve), showing the important contribution of the arc underneath A2.

A_V provided that the extinction law is well known. An "SMC-like" extinction law, without the 2200 Å "bump" observed in our Galaxy (see e.g. Prévot et al., 1984) is needed to fit the spectrum of the quasar. Then, the best fit is obtained with a flat source spectrum and $A_V \simeq 4$ for image C and 6 for A2 (C. Lawrence, private communication).

Lawrence et al. (1995a) showed also that it is difficult to fit the observed spectrum assuming the dust is at the redshift of the source, even using the "SMC-like" extinction law. This favours extinction by the lens. It is unclear, however, which law should be used for an extinction intrinsic to the quasar. Low metallicity is expected for high-redshift objects, but absorptions associated with quasars (i.e at $z_{abs} \approx z_{em}$) seem to indicate in most cases solar or higher metallicities (Franceschini & Gratton, 1997). Moreover, Lawrence et al. (1995b) had shown that the quasar spectrum displays large equivalent width Fe II lines which support a non-negligible local extinction contribution. An evidence for the contribution of such "in situ" extinction is the colour of the arc (Falco et al., 1997 and this work). If its reddening is similar to that of the less reddened image of the nucleus (C), the real (R-I) colour becomes $\sim$ -1.3, which is bluer than the typical colour of even a starburst galaxy or H II region at z=2.6.

4.2. Consequences

The existence of differential extinction between the images implies that at least a part of the total extinction should be due to inhomogeneities of the lensing galaxy. A lower limit for this contribution is $A_V = 1.9$ in the direction of A2. Finally, the constraints on the relative contributions from, respectively, dust in the vicinity of the source ($A_V(S)$) and in the body of the lensing galaxy ($A_V(G)$) are still rather loose. With the present data, we can only securely assess that:

(i) $0 < A_V(S) < 3.5$ (assuming an SMC-like extinction curve at z=2.6) and

(ii) $0 < A_V(G) < 4.$ (for image C) or $1.9 < A_V(G) < 6.$ (image A2).

Assuming that all the extinction is due to the lens ($A_V(S)$=0), we find a total mass of dust in G of the order of $5.10^8 M_\odot$ with a screen model of radius 1.5″ giving an homogeneous extinction (Aoki et al., 1991). Then, using a gas-to-dust ratio around 100, the mass of gas is $\sim 5.10^{10} M_\odot$, which is hard to reconcile with a giant elliptical. It thus seems likely that a significant part of the extinction occurs in the lensed object itself. Obtaining a spectrum of the arc or, at least, HST images in V band would help to ascertain its extinction. If the true colour is indeed $R - I$ = -1.3, this implies a population of very hot stars, hence strong emission lines are expected. HI 21 cm observations at the redshifts of the FeII clouds could also help to constrain the metallicity and resolve the ambiguity on the extinction law to be used.

5. Conclusion

The analysis of new data and the re-discussion of older ones from HST presented in this study lead to the following main conclusions:

1) Good resolution imaging at visible and IR wavelengths confirms the existence and precises the amplitude of differential extinction between the images of the quasar nucleus.
2) A reanalysis of HST data shows that the arc should be carefully taken into account for a correct photometry of these nucleus images. After doing so, the observed properties of the nucleus images become compatible with a classical extinction by dust.
3) It is not yet possible to make a clear departure between the contributions of the source and of the lensing galaxy to the global extinction. Fitting the observed spectrum with dust at both redshifts would certainly work well, but the quality of present data is not sufficient for putting strong constraints on the fit parameters.
4) The source was not significantly variable during the period 1994–1997.

Concerning the last point, one may note that, compared to earlier observations in 1991–1992 (Angonin-Willaime et al., 1994), a significant ($\sim$ 0.5 magnitude) dimming is observed in R for the close pair (A1+A2) while B and C remain constant. In I, there is no mesurable effect, save for a small global shift of the zero point that is imputable to passband differences (see the discussion in Sect. 2.2). This could be the signature of an intrinsic change in the quasar combined with the different time delays of the images. Another possible explanation is that we were witnessing in 1991–92 the termination of a microlensing event that ended before 1994. However, the difference in behaviour between I and R is not easily explained with such mechanisms.

The simplest explanation for this chromatic effect is that we are in presence of time-dependent absorption of the image(s) by the lens. The time scale seems *a priori* inadequate, but the lensing would help to shrink it. A1-A2 is a very amplified pair

of images (A $\sim$ 20 to 30 in flux) near a caustic. This flux amplification is only a geometrical effect (magnification matrix of the lens), which acts on the vectors of relative proper motion as well as on position vectors. Statistically, the modulus of a randomly oriented proper motion vector should be increased by $\sqrt{A}$, with possibly higher amplifications for favourable orientations. In the specific case of the pair A1-A2 in MG J0414+0534, the beam of light coming from the source may thus scan the lens galaxy with a relative velocity of several thousands, or even tens of thousands of km s^{-1}. The same line of reasoning used for discussing the time scale of microlensing events holds also for the time scale of extinction variations across small clouds. If the clouds have a fine patchy structure, variable extinction may be observed with a time scale compatible with the data.

Acknowledgements. The data have been obtained partly on discretionary time from the direction of CFHT. The authors are grateful for this privilege. FC and IB are supported by contracts ARC 94/99-178 "Action de Recherche Concertée de la Communauté Française" (Belgium), and Pôle d'Attraction Interuniversitaire P4/05 (SSTC, Belgium). Retrieval of HST archive images was done through the service of CADC, which is operated by NRC, Herzberg Institute of Astrophysics and Dominion Astrophysics Laboratory. Finally, thanks are due to the referee for his very useful suggestions.

References

Angonin-Willaime M.-C., Vanderriest C., Hammer F., Magain P., 1994, A&A 281, 388
Annis J., Luppino G., 1993, ApJ 407, L69
Aoki T., Hiromoto N., Takami H., Okamura S., 1991, PASJ 43, 755
Barvainis R., Alloin D., Guilloteau S., Antonucci R., 1998, ApJ 492, L13
Bennett C., Lawrence C., Burke B., Hewitt J., Mahoney J., 1986, ApJS 61, 1
Burud I., Courbin F., Lidman C., et al., 1998, ApJ, submitted
Casali M., Hawarden T., 1992, JCMT-UKIRT Newsletter, 33
Courbin F., Magain P., Keeton C., et al., 1997, A&A 324, L1
Courbin F., Lidman C., Magain P., 1998a, A&A 330, 57
Courbin F., Lidman C., Frye B., et al., 1998b, ApJ, 501, L5
Falco E., Lehar J., Shapiro I., 1997, AJ 113, 540
Franceschini A., Gratton R., 1997, MNRAS 286, 235
Hewitt J., Burke B., Turner E., et al., 1988, In: Gravitational lenses. Lecture Notes in Physics 330, 147
Hewitt J., Turner E., Lawrence C., Schneider, 1992, AJ 104, 968
Holtzman J., Burrows C., Casertano S., et al., 1995, PASP, 110, 2570
Irwin M., McMahon R., Hazard C., 1991, ASP Conf. Ser. 21, 117
Katz C., Hewitt J., 1993, ApJ 408, L9
Katz C., Moore C., Hewitt J., 1997, ApJ 475, 512
Kodama T., Arimoto N., Barger A., Aragón-Salamanca A., 1998, A&A 334, 99
Lawrence C., Elston R., Jannuzi B., Turner E., 1995, AJ 110, 2570
Lawrence C., Cohen J., Oke J., 1995, AJ 110, 2583
Magain P., Courbin F., Sohy S., 1998, ApJ 494, 472
Malhotra S., Rhoads J., Turner E., 1997, MNRAS 288, 138
Moore C., Hewitt J., 1997, ApJ 491, 451
McLeod B., Bernstein G., Rieke M., Weedman D., 1998, AJ 115, 1377
Prévot M., Lequeux J., Maurice E., Prévot L., Rocca-Volmerange B., 1984, A&A 132, 389
Schechter P., Moore C., 1993, AJ 105, 1
Simons D., Clark C., Kerr J., et al., 1994, S.P.I.E. 2198, 185
Tonry J., Kochanek C., 1998, AJ, in press
Véron P., Hawkins M., 1995, A&A 296, 665

QUANTIFICATION DES EFFETS DE LENTILLE GRAVITATIONNELLE SUR LES ONDES GRAVITATIONNELLES

Depuis juillet dernier, l'interféromètre Virgo[13], situé à Cascina en Italie, est opérationnel. Avec ses deux homologues américains LIGO ainsi que les expériences GEO 600 et TAMA 300, ce détecteur peut espérer détecter des événements d'émission d'ondes gravitationnelles jusqu'à l'amas de galaxies de la Vierge (d'où son nom). En l'état actuel des connaissances, les prédictions sur le nombre de détections vont de 1 à 10^3 par an[14]. La question est de savoir s'il est possible que la source subisse un effet de lentille gravitationnelle suffisant pour faciliter sa détection, voire pour permettre de détecter des objets situés à des distances plus grandes que celle de l'amas de la Vierge.

Dans un premier temps, j'ai demandé à deux stagiaires de Licence de Physique, Claire Chevalier et Olivier Tiret, de réunir toutes les informations sur les positions et masses (mesurées ou déduites des luminosités) des galaxies dans la direction de l'amas de la Vierge dont nous disposions dans les bases de données internet. Ils ont recherché ainsi les paires de galaxies proches susceptibles de former une structure de lentille gravitationnelle. Je leur ai fait calculer ensuite l'amplitude de ces effets. Le résultat était pessimiste.

Le reste du travail fut fait en collaboration avec Monica Varvella. Cette étudiante de l'Université de Naples est venue effectuer sa troisième année de thèse dans notre équipe, après deux années passées sur des thématiques plus instrumentales liées à Virgo. J'ai ainsi co-encadré sa thèse avec Philippe Tourrenc.

Dans la littérature, le problème de l'amplification gravitationnelle des ondes gravitationnelles avait été abordé[15], parfois avec des résultats positifs, surtout dans le cas d'effets de diffraction ou de microlensing. Une étude systématique et complète manquait pour conclure sur le sujet. J'ai tout particulièrement orienté à Monica Varvella vers la démarche suivante. Tout d'abord, il était important de présenter un bilan des caractéristiques des ondes gravitationnelles et des ondes électromagnétiques pour s'assurer que les effets d'amplification gravitationnelle ne diffèrent pas. Puis, nous avons estimé à partir des caractéristiques des détecteurs présents et à venir quels effets de diffraction peuvent entrer en jeu dans le phénomène. La conclusion est que l'approximation géométrique est valide, au moins pour les détecteurs terrestres. Les effets de diffraction n'interviennent pas dans le phénomène. Cela élimine une grande partie des possibilités de grandes amplifications décrites dans certains articles sur le sujet.

[13] Pour plus de détail, voir le site web officiel : http://www.virgo.infn.it/ , http://www.ligo.caltech.edu/ , http://www.geo600.uni-hannover.de/ , http://tamago.mtk.noao.ac.jp/

[14] Voir, par exemple, Gourgoulhon, Grandclément et Bonazzola, Int.J.Mod.Phys., 2002, **A17**, 2689.

[15] Voir : Zakharov et Baryshev, Cl.Q.Gr., 2002, **19**, 1361 ; Ruffa, ApJ, 1999, **517**, L31 ; De Paolis, Ingrosso et Nucita, AA, 2001, **366**, 1065

Nous avons ensuite estimé le nombre de signaux supplémentaires apportés par la présence d'une lentille gravitationnelle dans le champ d'observation. Ce calcul a été fait pour une distribution en luminosité homogène et isotrope des sources, ce qui induit une estimation supérieure du nombre d'événements. Il est nécessaire alors de faire un certain nombre d'hypothèses sur la lentille, en particulier sur sa distribution de masse. Plusieurs modélisations ont été explorées ainsi que plusieurs configurations[16] de sources et de lentilles ; les résultats varient beaucoup d'une modélisation à l'autre : plus la lentille est complexe et plus il y a accroissement d'événements. Mais, dans tous les cas, l'accroissement est si faible que la probabilité pour qu'un tel événement se produise peut être considérée comme négligeable. Il est possible de modérer un peu cette conclusion en faisant remarquer que, si un événement de forte amplification gravitationnelle se produit, alors il sera détecté beaucoup plus facilement que les sources normales, ce qui perturbe les statistiques de détection des sources lointaines (Arnaud-Varvella, Angonin et Tourrenc, 2004).

Ce travail constitue une étape vers une nouvelle approche des problèmes astrophysiques liés à la détection des ondes gravitationnelles. En effet, la préoccupation des physiciens impliqués dans la construction des détecteurs d'ondes gravitationnelles concerne aujourd'hui la capacité de ces détecteurs à observer des signaux, bien plus que l'exploitation des observations pour compléter nos connaissances en astrophysique ou contribuer à la solution de problèmes étudiés par ailleurs. Cette attitude, nécessaire aujourd'hui, ne doit cependant pas interdire une approche plus optimiste où serait posée l'hypothèse d'un fonctionnement satisfaisant des détecteurs qui fourniraient des signaux assez nombreux pour constituer un observatoire. Dès lors, les problèmes instrumentaux passeraient au second plan, tandis que les questions d'astrophysique occuperaient l'essentiel du propos. Par exemple, dans ce contexte, il serait intéressant de définir et quantifier précisément les contraintes d'observations de trous noirs par des détecteurs d'ondes gravitationnelles afin de définir des stratégies d'observations à long terme. La recherche des trous noirs dans les galaxies à l'aide des détecteurs d'ondes gravitationnelles peut définir un projet de recherche pour l'avenir.

[16] l'amas de la Vierge comme source et comme lentille, le trou noir central de notre galaxie comme lentille, …

ARTICLE SUR LES EFFETS DE LENTILLES GRAVITATIONNELLES SUR LES ONDES GRAVITATIONNELLES

Increase of the number of signal due to gravitational lensing of gravitational waves

Arnaud-Varvella M, Angonin M-C, Tourrenc Ph, 2004, General Relativity and Gravitation, vol. **36**, Issue 5, 983

Increase of the Number of Detectable Gravitational Waves Signals due to Gravitational Lensing

M. Arnaud Varvella [*], M.C. Angonin [†], Ph. Tourrenc[‡]

23rd July 2004

Abstract

This article deals with the gravitational lensing (GL) of gravitational waves (GW). We compute the increase in the number of detected GW events due to GL. First, we check that geometrical optics is valid for the GW frequency range on which Earth-based detectors are sensitive, and that this is also partially true for what concerns the future space-based interferometer LISA. To infer this result, both the diffraction parameter and a cut-off frequency are computed. Then, the variation in the number of GW signals is estimated in the general case, and applied to some lens models: point mass lens and singular isothermal sphere (SIS profile). An estimation of the magnification factor has also been done for the softened isothermal sphere and for the King profile. The results appear to be strongly model-dependent, but in all cases the increase in the number of detected GW signals is negligible. The use of time delays among images is also investigated.

Keyword(s): gravitational waves; gravitational lensing; interferometric detectors of gravitational waves.

[*]Dipartimento di Fisica E.R. Caianiello, Universitá di Salerno - 84081 Baronissi (Sa), Italy and LERMA/ERGA, Université Paris VI, 4 pl.Jussieu - 75005 Paris, France. e-mail: varvella@sa.infn.it or varvella@ccr.jussieu.fr

[†]LERMA/ERGA, Université Paris VI, 4 pl. Jussieu - 75005 Paris, France. e-mail: mc.willaime@obspm.fr

[‡]LERMA/ERGA, Université Paris VI, 4 pl. Jussieu - 75005 Paris, France. e-mail:pht@ccr.jussieu.fr

1 Introduction

Gravitational waves (GW) have been already predicted by A. Einstein [1] in 1918, but they have not yet been observed directly because of the weakness of the signal. However, their existence has been indirectly established by the long-term study of the binary pulsar 1913+16 [2]. The giant interferometers currently under development [3, 4, 5, 6] appear presently to be the most promising GW detectors. They should reach better sensitivities (and over larger bandwidths) than the network of existing resonant bars [7], which have already been taking data for years.

Yet, detecting GW signals will not be straightforward, at least with the first generation of interferometers [8, 9]. So, any amplification mechanism such as Gravitational Lensing (GL) should be studied accurately to estimate the improvements it could provide.

GL of electromagnetic radiation has been already studied in details (see e.g. Ref. [10]) and the same formalism can also be applied to GW, because gravitational radiations propagating on a gravitational background are affected in the same way than electromagnetic radiations [11].

This topic has been addressed in the literature by many authors with various points of view: cosmological waveguides for GW [12], GW detection using gravitational lenses as detectors [13] and finally, microlensing [14] and macrolensing [15, 16] of gravitational radiation in the high frequency

approximation as well as in the diffraction case [17, 18]. In this article we use the same approach as Ref. [19].

GL produces magnified images of GW which could be detected more easily if their magnifications are high enough, it could be detected more easily. Similarly, the magnification effect allows one to explore a larger volume of the Universe, and thus it increases the number of potentially detectable sources. Yet, we will see in the following that the increase in the number of events is limited for the lens models we study. But it depends significantly on the particular model of deflector considered. So, forthcoming papers should study more realistic and sophisticated models to get a more accurate conclusion.

On the other hand, the successful amplification of one single signal may strongly help a first detection within a not too far future; therefore, studying this problem is important, even if the probability of such a lensing event is small. In addition, it is important to see whether other lensing effects associated to the GW signal amplification (e.g. delays between images) can also be used.

In the sequel, we analyze the GL effect of GW in the frequency domains which Earth and space-based GW detectors are sensitive to. First, a comparison between Electromagnetic Waves (EMW) and GW is reported. Going to GL of GW, the diffraction limit is then estimated: from this computation, it turns out that geometrical optics can be used for Earth-based

detectors and even for LISA, the space-based interferometer project [20], provided that the mass of the deflector is big enough. Then, we compute the increase in the number of GW signals due to GL, and we apply this computation to some lens models. The possibility to use the time delay between two images produced by GL is also investigated. Finally, some conclusions and prospects for future analysis are reported.

2 Electromagnetic and Gravitational Radiation

GW [11, 21] are ripples in the curvature of spacetime, which propagate at the speed of light like EMW. GW are characterized by their wavelength λ_g, much smaller than the radius of curvature of the background spacetime. As shown in Tab. 1, EMW and GW are very different on many aspects. In particular, the latter are almost insensitive to matter, which makes them important probes for astronomy [8, 9]. Moreover, GW detectors are sensitive to the amplitude of the signal – scaling like 1 / distance – while EMW are mostly detected through their power, scaling like the square of the distance. Finally, the two frequency ranges are also very different: below few tens of kHz for GW, above tens of million Hz for EMW.

Yet, as both are waves, we assume that all the formula for the GL of EMW can be used for GW, provided that the geometrical optics approximation is valid. Therefore, we estimate the validity range of this critical

assumption in the following section, by computing the diffraction limit parameter and the diffraction cut-off frequency.

3 Diffraction limit

The characteristic angular scale in the GL by a point mass M_L is the Einstein angle [10], $\theta_E = \left(4GM_L D^{-1}/c^2\right)^{1/2}$ where $D = D_{OL}D_{OS}/D_{LS}$ is the distance parameter. The various parameters, such as D_{OL}, D_{OS}, etc., are shown in Fig. 1 and defined in the corresponding caption.

Lensing effects are expected to be significant only when the source, the lens and the observer are aligned within approximately the angle θ_E. When the angular size of the source is greater than θ_E, the relative influence of the lensing is reduced [22] by dilution. Wave effects in GL of EMW by a point mass M_L depend on the parameter y

$$y \;=\; \frac{4\,\pi\,G}{c^2}\frac{M_L}{\lambda} \;=\; 2\times 10^4\left(\frac{1\;m}{\lambda}\right)\left(\frac{M_L}{M_\odot}\right) \;=\; 6\times 10^{-5}\left(\frac{\nu}{1\;Hz}\right)\left(\frac{M_L}{M_\odot}\right) \tag{1}$$

where λ is the wavelength and ν the frequency of the radiation. Using the parameters of a point mass lens, y can be written as

$$y \;=\; \frac{\pi\;D}{\lambda}\,\theta_E^2 \;=\; \frac{\pi\;\nu\;D}{c}\,\theta_E^2 \tag{2}$$

where all these quantities have been already defined.

In terms of the Schwarzschild radius $R_S = 2GM_L/c^2$:

$$y \;=\; 2\,\pi\,\frac{R_S}{\lambda} \;=\; 2\,\pi\,R_S\,\frac{\nu}{c} \quad . \tag{3}$$

The parameter y measures the number of Fresnel zones [22, 23] contributing to the lensing effect: when $y \sim \infty$ geometrical optics applies, while for $y \sim 1$ severe effects of diffraction occur and more precise solutions of the wave equation are required.

Like in another similar computation [24], we estimate the diffraction limit in the case of GW with this formalism. To distinguish from EMW, the wavelength λ becomes λ_g and the frequency ν, ν_g. In the broad frequency domain of GW [8], GW detection efforts focus on four frequency bands shown in Tab. 2: the extremely low frequency (ELF), the very low frequency (VLF), the low frequency (LF) and the high frequency domain (HF). The probes used to search these GW are the following: the polarization of the Cosmic Microwave Background (CMB) radiation for the first range, the pulsar timing for the second one, the LISA experiment [20] for the third one and finally the Earth-based detectors (interferometers and resonant mass) for the last one.

Fig. 2 shows the diffraction parameter evolution in the full range of frequencies listed in Tab. 2. The calculation has been made for two different values of the lens mass M_L: $10^6\ M_\odot$ (massive black hole case) and

$10^9\ M_\odot$ (galaxy case) respectively. Tab. 3 shows the values of the diffraction parameter y computed with Eq. 1, the corresponding Einstein radius $R_E = D_{OL}\ \theta_E$ depending on the distances, and the Schwarzschild radius R_S for the two lens masses. For cosmic distances (i.e. $d >> 10^8 m$) the relation $R_S \ll R_E$ holds true. Therefore, the formula for a point mass lens is valid [25].

From Fig. 2 we can deduce that $y \gg 1$ in the frequency range sensitive for Earth-based detectors; so, geometrical optics is valid. This can be true also for LISA: in fact, the region where $y > 1$ covers partially the LF range for $M_L = 10^9\ M_\odot$ (galaxy case), but for $M_L = 10^6\ M_\odot$ (black hole case), one is immediately in the diffraction regime.

We need to estimate a limit on the mass to be sure that geometrical optics is valid also in this domain. Solving $y = 1$ for $\nu = 10^{-4}\ Hz$ and $1\ Hz$ gives $M_L \sim M_{max} = 2 \times 10^8\ M_\odot$ and $M_L \sim M_{min} = 2 \times 10^4\ M_\odot$ respectively (see Eq. 1). When $M_L > M_{max}$, geometrical optics is always valid in the LF domain and so in the HF range, while for $M_L < M_{min}$, diffraction cannot be neglected. The Black Hole BH Sgr A* is intermediate (see Tab. 4) and so the lens formalism considered here does not apply in the whole GW LF region. Of course, in the HF domain, the geometrical optics approximation extends to smaller masses.

We also consider another method to compute the diffraction limit in the case of gravitational radiation. If we have a Newtonian gravitational lens,

i.e. a lens whose effects can be described by the weak field approximation, we can evaluate the diffraction limit for the lens, i.e. a cut-off frequency, ω_c, such as geometrical optics is valid at frequencies higher than ω_c, while diffraction effect near a caustic are possible at lower frequencies.

The cut-off frequency is given by [26]

$$\omega_c = \left(\frac{\pi}{10}\frac{GM_L}{c^3}\right)^{-1} = \left(\frac{\pi}{5}\frac{R_S}{c}\right)^{-1} \quad . \tag{4}$$

Fig. 3 shows the decrease of the cut-off frequency ω_c with the mass M_L. For a mass M_L bigger than $10^6\ M_\odot$, the cut-off frequency is lower than $1\ Hz$. Considering Tab. 2, it appears that geometrical optics is relevant for Earth-based detectors because the corresponding relevant frequencies are higher than the cut-off. Therefore, an amplification can be expected under conditions similar to the electromagnetic case. In the LF domain, the relevant frequencies for LISA [20] are lower than the cut-off for $M_L = 10^6\ M_\odot$; therefore diffraction effects are expected in suitable conditions for this value of the mass. However for $M_L > 10^9\ M_\odot$, geometrical optics remains valid for GW potentially detectable in LISA.

In conclusion, in most cases, geometrical optics is valid in particular for Earth-based detectors. For this reason we will consider in the sequel that this is the case.

4 Gravitational lensing contribution

We want to estimate how GL increases the number of detectable GW signals coming from a given direction: if the increase is relevant, GL can be considered as an important tool for GW detection. Calling N_0 the number of detectable signals in the absence of GL, the presence of a gravitational lens increases this number by a quantity ΔN.

First, we estimate the number of GW signals detectable without GL effect. To do this, we consider arbitrary sources of GW with wave amplitude h_0 at a fixed distance r_0 from the source scaled; let $h_s = h_0\ r_0/r_s$ be the amplitude at the distance r_s. We also introduce a threshold, h_{th}, to model the detection process: if $h_s > h_{th}$, the signal is detected whereas one has a false dismissal in the other case. From the GW amplitude scaling law, this threshold can be converted in a distance r_{th}. Knowing the detection threshold h_{th} from GW detectors sensitivity [3, 4, 5, 6, 20], we can write the detection condition $h_s > h_{th}$ as $r_s < r_{th} = (h_0/h_{th})\ r_0$.

Let n be the GW pulse density, that is the number of signals per unit volume and per year. The total number of detectable sources per year up to a distance r_s is $N_0 = 4\pi r_s^3 n/3$, assuming a homogeneous distribution of the source, which is valid at large scale.

Now, we compute the number of GW signals which can be detected in the presence of GL. GW detectors are sensitive to the signal amplitude

rather than to its intensity. The GW amplitude h is proportional to the square root of the energy flux [27]; therefore the lensed amplitude, h_l, on the detector is $h_l = h_s\sqrt{A}$, where A is the magnification factor and h_s the unlensed GW amplitude.

The magnification factor depends on the angle β and on the distance r_s of the source, $A = A(\beta, r_s)$. The function $A(\beta, r_s)$ is model-dependent. The condition for the source to be detected is

$$r_s \; < \; \frac{h_0}{h_{th}} \; r_0 \; \sqrt{A(\beta, r_s)} \; = \; \rho(\beta) \quad . \tag{5}$$

Thus, the number of detectable signals in the presence of GL is

$$N \; = \; n \; \int_0^{\pi} \left(\int_0^{\rho(\beta)} 2\pi r^2 dr \right) \sin\beta \; d\beta \; = \; \frac{2}{3} \; n \; \pi \int_0^{\pi} \rho^3(\beta) \; \sin\beta \; d\beta \quad . \tag{6}$$

Using Eq. 5, we finally find

$$N = \frac{N_0}{2} \int_0^{\pi} \left(\frac{\rho(\beta)}{r_{th}} \right)^3 \sin\beta \; d\beta \quad . \tag{7}$$

The relative increase in the number of signals is

$$\frac{\Delta N}{N_0} = \frac{1}{2} \int_0^{\pi} \left(\left(\frac{\rho(\beta)}{r_{th}} \right)^3 - 1 \right) \sin\beta \; d\beta \quad . \tag{8}$$

Taking into account Eq. 5, Eq. 8 becomes

$$\rho = \frac{h_0}{h_{th}}\, r_0\, \sqrt{A\left(\beta\right)} \Rightarrow \frac{\Delta N}{N_0} = \frac{1}{2}\int_0^{\pi} \left(A\left(\beta\right)^{3/2} - 1\right) \sin\beta\, d\beta \quad . \tag{9}$$

If two images occur, one has to take into account separately $A_+(\beta, r)$ and $A_-(\beta, r)$. In this case, the total number of signals is

$$N = N_+ + N_- = 2N_0 + (\Delta N)_+ + (\Delta N)_- \tag{10}$$

where N_+ and N_- are the contributions of the positive and negative part of the magnification factor, each of them corresponding to an image. Thus, the total relative increase is

$$\frac{(\Delta N)}{N_0} = 1 + \frac{(\Delta N)_+ + (\Delta N)_-}{N_0} \quad . \tag{11}$$

The two relative variations can be computed with Eq. 8.

5 First lens models comparison

Different lens models [10] can be considered to describe the gravitational sources. We start our analysis with the simplest one, the point mass lens (or Schwarzschild lens); we also study the singular isothermal sphere. In both cases, the increase in the number of signals is computed.

5.1 Point Mass (Schwarzschild lens) Model

This model considers a point mass lens M_L: it always gives two images. Notations follow Fig. 1 and the GW source is also punctual. We

consider the case $D_{LS}/D_{OL} \gg 1$, for which the Einstein angle θ_E becomes independent from the source distance:

$$\theta_E \;=\; \sqrt{\frac{4\,G\,M_L}{c^2}\,\frac{D_{LS}}{D_{OL}\,D_{OS}}} \;\approx\; \sqrt{\frac{4\,G\,M_L}{c^2}\,\frac{1}{D_{OL}}} \quad . \tag{12}$$

So, the magnification factor $A(\beta, r)$ depends only on the angle β. In this model, one can prove [10] that the two contributions to the amplification are

$$A_{\pm} \;=\; \frac{u^2+2}{2\,u\sqrt{u^2+4}} \;\pm\; \frac{1}{2} \tag{13}$$

with $u = \beta/\theta_E$.

Looking at Eq. 8 and Eq. 12, the relative increases of the number of signals are

$$\frac{(\Delta N)_{\pm}}{N_0} \;=\; \frac{\theta_E}{2}\,\int_0^{\pi/\theta_E} \left(\left(\frac{u^2+2}{2u\sqrt{u^2+4}} \pm \frac{1}{2} \right)^{3/2} - 1 \right) \sin\,(u\;\theta_E)\;du \quad . \tag{14}$$

5.2 SIS (Singular Isothermal Sphere) Profile

This model uses as lens a sphere of radius R with a mass distribution $M(R)$ confined in this volume [10]. The velocity dispersion σ_v scales with the rotational velocity v_{rot} as $v_{rot} = \sqrt{2}\sigma_v$. This model gives multiple images only if the source lies inside the Einstein ring, i.e. for $\beta < \theta_E$; if the source lies outside the Einstein ring, i.e. for $\beta > \theta_E$, there is only

one image. For this model the positive and negative contribution to the magnification factor are

$$A_+ \;=\; 1+\frac{1}{u} \qquad A_- \;=\; \left|1-\frac{1}{u}\right| \tag{15}$$

where $u = \beta/\theta_E$.

We consider again the case $D_{LS}/D_{OL} \gg 1$. For a given lens distance, the Einstein angle θ_E becomes independent of the distance D_{LS} and is indeed constant

$$\theta_E = \frac{4\pi\sigma_v^2}{c^2}\frac{D_{LS}}{D_{OS}} \sim \frac{4\pi\sigma_v^2}{c^2} \quad . \tag{16}$$

Again, the magnification factor $A(\beta, r)$ depends only on β; from Eq. 8, we obtain

$$\frac{(\Delta N)_\pm}{N_0} = \frac{\theta_E}{2}\int_0^{\beta_\pm/\theta_E}\left(\left|1\pm\frac{1}{u}\right|^{3/2}-1\right)\sin(u\theta_E)\;du \tag{17}$$

where $\beta_+ = \pi$ and $\beta_- = \theta_E$ because $(\Delta N)_-/N_0$ depends only on the sources for which $\beta < \theta_E$.

5.3 Applications to possible lens candidates

It is interesting to estimate the increase of the number of signals computed in Sec. 4 for the two particular models we have considered above using three hypothetical sources whose mass and distance are respectively the mass and the distance of the Virgo cluster, of a typical galaxy at 1 Mpc

and of the black hole BH Sgr A* in the center of the Galaxy.

Tab. 4 shows the relative variation of the number of GW signals for these different examples. It is clear that the contribution due to the GL effect is really negligible. However the results are strongly model-dependent. The dependence on the model is emphasized in Fig. 4 where it is clear that the results from the SIS profile are better than the results from the Schwarzschild lens by several orders of magnitude. From Fig. 4, one can also notice that the more aligned the source with the observer and the lens the higher the magnification factor.

6 Other interesting lens profiles

We now consider two other lens profiles used by several authors to describe the mass distribution of the deflector: the softened isothermal sphere and the generalized King profile.

6.1 The softened isothermal sphere

The softened isothermal sphere [28] is more complex than the SIS profile. The mass distribution includes a characteristic core of radius r_c.

Let us define $\theta_c = r_c/D_{OL}$, the core angular position. Then the magnification factor for this model is

$$A_{\pm} = 1 \pm \frac{D_{LS}}{D_{OS}} \frac{4\,\pi\,\sigma^2}{c^2} \frac{1}{\beta} \frac{\theta}{(\theta_c^2 + \theta^2)^{1/2}} \tag{18}$$

where θ is the image position given in Fig. 1, while σ has the same meaning as σ_v in the SIS profile above. When $\theta_c = 0$ we obtain the SIS profile.

Fig. 5 shows the estimation of the magnification factor for a lens with the softened isothermal sphere profile: the computation has been made for the three different lens candidates already considered for the Schwarzschild lens and the SIS profile. The magnification factor depends on the ratio $x = \theta_c/\theta$. One can remark that the higher the lens mass, the stronger the amplification.

6.2 The generalized King profile

The second model we consider in this section is a generalization of the King profile [29, 30]. The mass distribution family is characterized by a core radius r_c and an exponent α, for which values 1/2 and 0 have been considered.

The magnification factor is

$$A = \left(1 - 2\frac{\Sigma}{\Sigma_0} + \frac{\Sigma^2}{\Sigma_0^2} - \frac{1}{2}\,\frac{\Sigma_0\Sigma}{\Sigma_c^2}\,\frac{(1+2\alpha)^2 x^4}{2+(1-2\alpha)x^2}\right)^{-1} \qquad (19)$$

where Σ is the mass density depending on the distance R; the quantities Σ_0 (the core mass density projected on the lens plan), $I_{1+\alpha}$ and Σ_c (the critical density), are defined below

$$\Sigma_0 = \frac{4}{3}\,I_{1+\alpha}\,\rho_0\,r_c\,, \qquad \Sigma_c = \frac{c^2}{4\,\pi\,G}\,\frac{D_{OL}\,D_{LS}}{D_{OS}}$$

$$I_{1+\alpha} = \int_0^{+\infty} \frac{dx}{(1+x^2)^{1+\alpha}} \quad . \tag{20}$$

Fig. 6 shows the estimation of the magnification factor for a lens with the generalized King profile: the computation has been made considering Virgo-like clusters as lens and for two particular values of the exponent α: 0 and 1/2. As we can see, the best amplification is obtained with $\alpha = 1/2$. The magnification factor depends on the ratio $x = R/r_c$. The relative increases of the number of signals can be computed using Eq. 8. Yet, under reasonable assumptions, the computed increases are very small.

7 Twin signals

Two images of the same lensed source reproduce an identical GW signal. This could be very helpful for a first GW detection for which the signal amplitude does not exceed significantly the noise level. One can distinguish two kinds of twin signals. In the first case, an angular separation between the two images can be achieved: the twin signals correspond to two directions in the sky. On the other hand, when no angular separation is achieved, only a time delay exists between the two images: this is the second case.

Burst sources can be detected by GW detectors in coincidence, for instance between Virgo and the LIGO interferometers. Periodic signals can be detected by a single detector using their periodicity. Rough calcula-

tions show that an angular separation could happen for periodic signals, observed over one year in a single detector, but not for GW pulses in a network of Earth-based detectors. In both cases, the gravitational signal will be the repetition of two identical signals (or more if the lens gives more than two images), coming from the same direction.

Tab. 5 displays some orders of magnitude for the delay between the two signals: the source position angle β is normalized to 60 $''$. Yet, uncertainties on β are so large that one cannot estimate accurately the delay without additional information on the source.

7.1 Detectability

In principle, the analysis of Sec. 4 can be carried out for both Earth-based and Space-based detectors. Tab. 6 shows the values of the foreseen sensitivities (at the frequency of 1 kHz) of Earth-based GW interferometers presently working or under construction; for each of them the arm-length is also given as it is a key parameter for the interferometer final sensitivity. In case of LISA, the threshold for the amplitude is different because the GW frequency range is lower and the expected detectable sources are different: h_{th} has a value 10^{-23} at 10^{-3} Hz for an integration time of 1 year and an isotropic average over source directions.

In order to observe two or more images, the weakest has to be detected, therefore the detectability condition becomes

$$h_s\sqrt{A_-} \gtrsim h_{th} \quad . \tag{21}$$

If the two signals have to be detected by the four interferometers quoted in Tab. 6, one must choose for common threshold h_{th} the value h_m giving the worst sensitivity.

Once more, considering the two lens models presented in Sec. 5, gives disappointing results. For the Schwarzschild lens, in the case $u < 0.5$ (i.e. $\beta < \theta_E/2$) one finds $\sqrt{A_-} > 0.8$ and thus $h_s \gtrsim 1.25\ h_m$. Even if the images could be detected, this result does not change dramatically the order of magnitude of the amplitude for which GW which can be observed. Moreover, the number of such twin signals will be extremely low because the GW corresponding sources must lie in the solid angle $(\theta_E/2)^2$, where $\theta_E \ll 1$.

The result is very similar for the SIS profile. We have outlined that in this case the condition $\beta < \theta_E$ must hold true in order to have two images (see Sec. 5.2). This is a necessary condition for the signal to be amplified. Therefore the corresponding sources must lie in the very small solid angle $(\theta_E)^2$. So, the number of such signals will be dramatically low.

On the other hand, if we want to observe a large part of the sky, we must choose for instance $u \lesssim 1/\theta_E$ (i.e. $\beta_E \lesssim 1$ rad). One calculates $\sqrt{A_-} \lesssim \theta_E^2$ and therefore $h_s \gtrsim h_m/\theta_E^2$. This is a so high amplitude that

there is no chance that such a signal exists.

8 Conclusions

We analyzed GL effects on gravitational radiation. First, we showed that the diffraction is negligible for Earth-based GW detectors (and for LISA in a limited GW frequency range depending on the lens mass) and that geometrical optics is relevant in our analysis. This is true for a point mass lens, but it has to be verified for lenses with a different mass distribution.

We showed it is possible to compute precisely the relative increase of the number of GW signals due to GL for a single deflector. We performed the calculation for two simple lenses, the Schwarzschild lens and the singular isothermal sphere: the variations obtained are negligible for both models. This computation proved also that for similar lenses (with same mass and same distance to the observer) the results are clearly model dependent (see Fig 4). Some other characteristic profiles of the mass distribution have also been considered: the softened isothermal sphere and the generalized King profile for which the magnification factor is directly computed. Lens candidates used for numerical computations are Virgo-like clusters (same mass and distance), galaxies at 1 Mpc and BH-like Sgr A*.

Results obtained suggest the necessity to repeat in the future the same analysis with more realistic and sophistical lens models, for instance the

elliptical ones [31, 32]; moreover, better results could be achieved considering a system of deflectors instead of a single one, averaging on the value of each single amplification.

Time delay could be an useful tool to detect periodical GW sources: yet, a classification of these sources is necessary to make this possibility more realistic.

According to the results obtained in this article, we can affirm that the GL of GW is not statistically interesting and it will not contribute significantly to the new astronomy based on the observation of GW. However, our results came out from the hypothesis that GW interact in the same way of EMW with the matter; this is only a first approach of the problem. The study of exceptional situations remains useful: in fact, the estimation of the GL effect due to the interaction of GW with matter could produce better GW amplifications as GW can pass through the matter and are very few absorbed. This will be the aim of future investigation.

References

[1] A. Einstein, Preussiche Akademie der Wissenschaften, Sitzungsberichte, p. 154-167 (1918).

[2] R. A. Hulse & J. H. Taylor, *Ap. J.* **195** L51-L53 (1975).
T. Damour and J.H. Taylor, *Ap. J.* **366** 501-511 (1991).

[3] http://www.geo600.uni-hannover.de

[4] http://www.ligo.caltech.edu

[5] http://tamago.mtk.nao.ac.jp

[6] http://www.virgo.infn.it

[7] http::/igec.lnl.infn.it

[8] C. Cutler & K. S. Thorne, *An overview of gravitational wave sources* in Proceedings of the GR16 Conference on General Relativity and Gravitation, ed. N. Bishop and S. D. Maharaj (World Scientific), pp. 72-111, (2002).

[9] L. P. Grishchuk, gr-qc/0305051, Invited contribution to be published in the first volume of "Astrophysics Update" (Praxis-Springer, 2003).

[10] P. Schneider, J. Ehlers & E. E. Falco, "*Gravitational Lenses*", eds Springer-Verlag, Berlin (1992).

[11] K. S., Thorne in "The theory of gravitational radiation: an introductory review" in "Gravitational Radiation",ed N.Deruelle and T.Piran (North-Holland,Amsterdam, 1983), pp. 1-57.

[12] G. Bimonte, S. Capozziello, V. Man'ko & G. Marmo, *Phys. Rev.* D **58**, 4009 (1998).

[13] B. Allen *Phys. Rev. Lett.* **63**, 2017 (1989).

[14] F. De Paolis, G. Ingrosso & A. A. Nucita, *Astron. Astrophys.* **366**, 1065 (2001).

[15] Y. Wang, A. Stebbins & E. L. Turner, *Phys. Rev. Lett.* **77**, 2875 (1996).

[16] T. Wickramasinghe & M. Benacquista, "Detection of Gravitational Waves from Gravitationally Lensed Systems", 20th Texas Symposium on relativistic astrophysics, Austin, Texas, 10-15 December 2000, Melville, NY: American Institute of Physics, 2001, xix, 938 p. AIP conference proceedings, Vol. 586. Edited by J. Craig Wheeler and Hugo Martel, (2001).

[17] A. Ruffa, *Ap. J.* **517**, L31 (1999).

[18] R. Takahashi & T. Nakamura astro-ph/0305055, accepted for publication in ApJ.

[19] M. Arnaud Varvella, M. C. Angonin Willaime & Ph. Tourrenc, "Gravitational lensing of gravitational waves applied to gravitational waves detectors" to appear in Proceedings of XXXVIII Rencontres de Moriond 'Gravitational Waves and Experimental Gravity', 22-29 March 2003, Les Arcs (France).

[20] http://lisa.jpl.nasa.gov/; http://sci.esa.int/home/lisa/

[21] K. S. Thorne in "Gravitational radiation" in "Three Hundred Years of Gravitation", eds Hawking, S. W. and Israel, W. (Cambridge,Amsterdam, 1983), pp. 330-457 .

[22] S. Deguchi & W. D. Watson, *Phys. Rev.* **34**, n.6, 1708 (1986).

[23] S. Deguchi & W. D. Watson, *Ap. J.* **307**, 30 (1986).

[24] A. F. Zakharov & Y. V. Baryshev, *Class. Quantum Grav.* **19**, 1361 (2002).

[25] T. Alexander & A. Stenberg, *Ap. J.* **520**, 137 (1999).

[26] R. J. Bontz & M. P. Haugan, Astrophys. Space Sc, **78**, 204 (1981).

[27] S. L. Shapiro & S. A. Teukolsky, "*Black Hole, White Dwarfs and Neutron Stars*", eds. John Wiley & Sons, New York, (1983).

[28] R. Narayan & M. Bartelmann, astro-ph 9606001 (1996) "Gravitational Lensing" Formation of Structure in the Universe. Edited by A. Dekel and J. P. Ostriker. Cambridge University Press, 1999, p.360 .

[29] G. Golse, PhD Thesis "Contraintes cosmologiques déduites des effets de lentille gravitationnelle dans les amas des galaxies", Université de Toulouse III "P. Sabatier" (2002).

[30] I. R. King, *Astron. J.* **71**, 64 (1966).

[31] R. D. Blandford & C. S. Kochanek, *Ap. J.* **321**, 658 (1987).

[32] C. S. Kochanek & R. D. Blandford, *Ap. J.* **321**, 676 (1987).

	Electromagnetic Radiation	Gravitational Radiation
Nature	EM fields through space-time	Geometry of space-time
Source	Incoherent superpositions of particles	Mass-energy coherent motion
Wavelength	Small compared to sources	Comparable to or bigger than sources
Properties	Easily absorbed, scattered, dispersed	Nearly unperturbed by matter
Frequency range	Above 10^7 Hz	$[10^{-18}\,\text{Hz}\,;\leq$ few tens of kHz$]$
Detectable quantity	Power	Amplitude

Table 1: Differences between electromagnetic and gravitational radiation.

Frequency [Hz]	Range	Probes
$10^{-18} \div 10^{-15}$	ELF	CMB radiation
$10^{-9} \div 10^{-7}$	VLF	Pulsar timing
$10^{-4} \div 1$	LF	LISA experiment
$1 \div 10^{4}$	HF	Earth-based detectors

Table 2: Explored GW frequency ranges and corresponding probes.

	M_L $[M_\odot]$	R_E $[m]$	R_S $[m]$	y
black hole	10^6	7×10^4 d	3×10^9	60 ν_g
galaxy	10^9	4×10^4 d	3×10^{12}	6×10^5 ν_g

Table 3: Characteristic values for two examples of lens, with $d = (D_{OL} D_{LS} / D_{OS})^{1/2}$.

Model	Lens	M_L [$M_\odot$]	D_{OL} [Mpc]	θ_E ["]	σ_v [km/s]	$\left(\frac{\Delta N}{N_0}\right)$
Point mass	Virgo-like cluster	10^{14}	15	231		5×10^{-7}
	galaxy-like	10^9	1	2.8		10^{-10}
	BH-like Sgr A*	2.6×10^6	8×10^{-3}	1.6		3×10^{-11}
SIS profile	Virgo-like cluster	10^{14}	15	14.1	700	10^{-4}
	galaxy-like	10^9	1	1.1	200	8×10^{-6}
	BH-like Sgr A*	2.6×10^6	8×10^{-3}	0.6	150	4×10^{-6}

Table 4: Comparison between two lens models: the Schwarzschild lens and the SIS profile.

Model	Lens	Δt $[(\beta/60'')$ years]
Point mass	Virgo-like cluster	1.2×10^5
	galaxy-like	120
	BH-like Sgr A*	0.3
SIS profile	Virgo-like cluster	6×10^3
	galaxy-like	37
	BH-like Sgr A*	0.2

Table 5: Time delay comparison between two lens models: the Schwarzschild lens and the SIS profile.

Interferometer	Arm-Length [m]	Threshold Amplitude h_{th} @ 1 kHz [$\mathrm{Hz}^{-1/2}$]
VIRGO	3000	3×10^{-23}
LIGO	4000	1×10^{-22}
GEO600	600	2×10^{-22}
TAMA300	300	5×10^{-21}

Table 6: Threshold amplitudes for Earth-based interferometers.

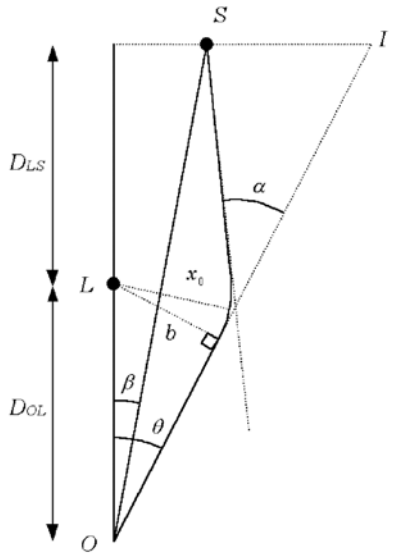

Figure 1: Lensing diagram for a point mass lens L. S is the source at angle β and I its actual image deflected at angle α, D_{LS} is the distance between the lens and the source, D_{OL} the distance between the observer and the lens and D_{OS} the distance between the observer and the source.

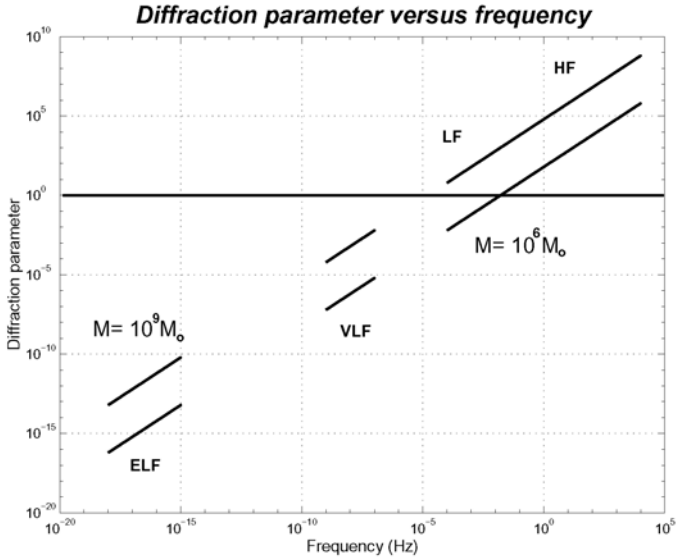

Figure 2: Diffraction parameter versus GW frequency range for two different values of the lens mass M_L: $10^6\ M_\odot$ (black hole case) and $10^9\ M_\odot$ (galaxy case) respectively. In the frequency range sensitive for Earth-based detectors $y \gg 1$, so geometrical optics is valid. In the case of LISA, the region where $y > 1$ covers partially the LF range for the galaxy case, but for the black hole case, one is immediately in the diffraction regime. Note that both scales are logarithmic.

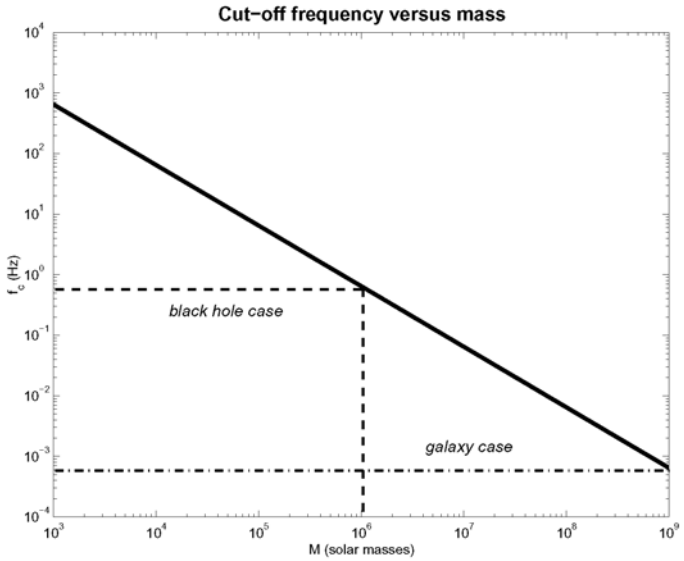

Figure 3: Cut-off frequency ω_c versus lens mass M_L. For a mass $M_L > 10^6\ M_\odot$ (black hole case), the cut-off frequency is lower than $1\ Hz$: geometrical optics is relevant for Earth-based detectors because the corresponding relevant frequencies are higher than the cut-off. In the LF domain, the relevant frequencies for LISA are lower than the cut-off for the black hole case, but for $M_L > 10^9\ M_\odot$ (galaxy case), geometrical optics remains valid for GW potentially detectable in LISA. Note that both scales are logarithmic.

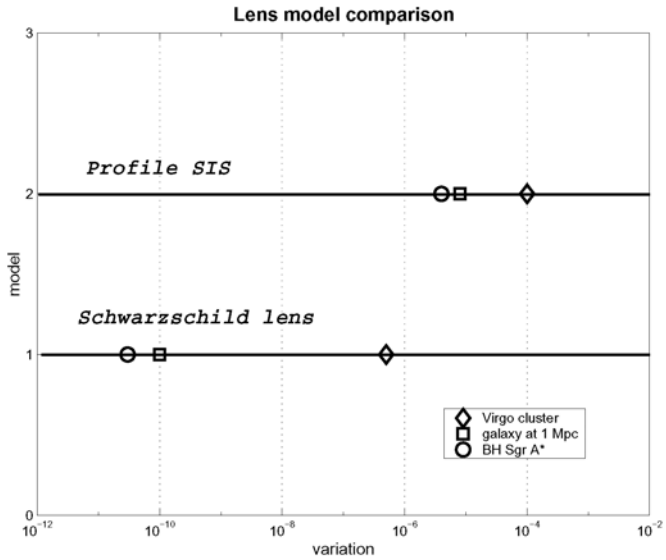

Figure 4: Model dependence evidence for two different lens models: from the bottom, the first one is the Schwarzschild lens and the second one is the SIS one. Each lens model has been considered with the three lens candidates: the Virgo-like cluster, a galaxy-like at 1 Mpc and the Black Hole-like BH Sgr A*. Results from the SIS profile appear to be better than ones from the Schwarzschild lens by several orders of magnitude.

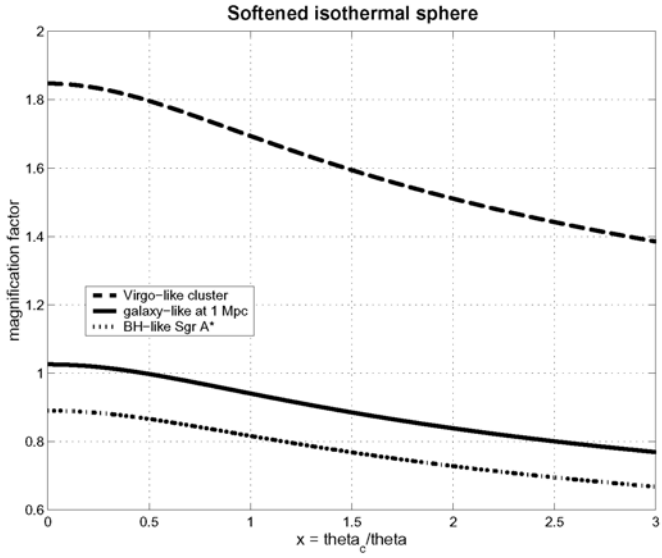

Figure 5: Magnification factor estimation for the softened isothermal sphere profile in the case of three lens candidates: the Virgo-like cluster, a galaxy-like at 1 Mpc and the BH-like Sgr A*. The magnification factor is showed as a function of the ratio x depending on the core radius of the lens mass.

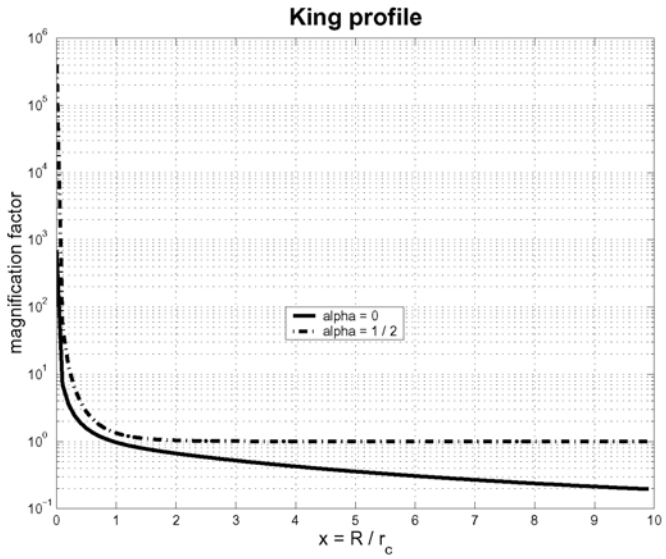

Figure 6: Magnification factor comparison between two models of the generalized King profile obtained with two particular values of the exponent α: 0 and 1/2, choosing the Virgo-like cluster as lens. The magnification factor is showed as a function of the ratio $x = R/r_c$ depending on the core radius of the lens mass. The best amplification is obtained with $\alpha = 1/2$.

LA GRAVITATION EXPERIMENTALE A L'ECHELLE DU LABORATOIRE

Comme je l'ai déjà signalé, les lentilles gravitationnelles, objet des recherches présentées jusqu'ici, constituent un effet relativiste de la gravitation qui vient « perturber » les mesures astrophysiques effectuées sur le ciel profond. Cela peut constituer un avantage dans la mesure où cet effet représente un outil précis pour étudier les objets lointains. De la même façon, je me suis aussi intéressée aux effets relativistes de la gravitation détectables à l'échelle du laboratoire.

La gravitation est, sans doute, l'interaction physique la moins bien connue empiriquement du fait des ordres de grandeurs qui la caractérisent. Mais, depuis une dizaine d'années, les expériences de laboratoire et spatiales atteignent de telles sensibilité et précision que les perturbations de la gravitation relativiste ne peuvent plus être négligées et nécessitent d'être comprises et identifiées pour interpréter les résultats. Réciproquement, il convient d'établir de nouvelles expériences pour améliorer la modélisation des effets des champs de gravitation et d'inertie. L'élaboration de méthodes générales reste encore du domaine de la recherche et, bien que cette recherche soit théorique, il est nécessaire que celle-ci se développe en étroite collaboration avec l'expérimentation.

En développant des travaux sur la gravitation expérimentale, j'ai été amenée à interagir avec les laboratoires français travaillant autour de cette thématique, en particulier, ceux en lien avec l'Université Pierre et Marie Curie : ERGA/LERMA, SYRTE, ESPCI, LKB, LPTENS et GRECO/IAP. Cela se traduit par mon insertion au sein du GdR 2062 du CNRS, Gravitation et Expérience dans l'Espace ou GREX[17]. J'ai notamment organisé les journées du GREX en octobre 2003, journées qui ont réuni à Paris plus de 110 personnes de différentes nationalités (même si les exposés étaient en français pour la plupart). Pour l'Université Pierre et Marie Curie, j'ai aussi organisé une journée de présentation des activités autour de la thématique de la gravitation en décembre 2002. Enfin, je participe au Plan Pluri-Formation GRAVitation, Inertie, Tests Expérimentaux qui réunit les laboratoires cités ci-dessus, PPF demandé en 2003 qui a vocation à devenir fédération d'équipes.

Dans le cadre de ces collaborations, je me suis donc intéressée aux problèmes liés aux lentilles gravitationnelles et à la détection des ondes gravitationnelles , mais aussi, ai travaillé sur les senseurs gravito-inertiels à ondes de matières. En particulier, j'ai participé aux discussions sur la sensibilité du satellite HYPER à l'effet Lense-Thirring et j'ai mené une réflexion sur le comportement des ondes de matière en présence de photons. Je décris, à présent, plus en détail ces travaux.

Détection de l'effet Lense-Thirring par des gyroscopes spatiaux

En parallèle avec la mise au point d'interféromètres à ondes de matière de type Ramsey-Bordé[18], s'est développé un projet d'utilisation de ces gyroscopes ultra-précis dans l'espace. Deux conditions justifient cette idée : d'une part la longueur d'onde de de Broglie des ondes de matière est 10 ordres de grandeur plus faible que la longueur d'onde des lasers, ce qui

[17] Pour plus d'information : http://www.spectro.jussieu.fr/GREX/

[18] Par exemple, à Hannovre, Paris et Orsay : Jentsch et al., 2003, Verhanal DPG (VI) **38**, 167 ; Oberthaler et al., Phys. Rev. A, 1996, **54**, 3165 ; Gustavson et al., CQG, 2000, **17**, 2385 ; Le Coq et al., Phys Rev Lett, 2001, **87**, 170403 ; Snadden et al., Phys Rev Lett, 1998, **81**, 971.

favorise l'utilisation des interféromètres à onde de matière comme gyroscope ; mais, d'autre part, les condensats de Bose-Einstein créés pour ces configurations sont lents (quelques décimètres par seconde) et leur trajectoire est profondément affectée par la gravité terrestre. Une expérience d'interféromètre à atomes froids dans l'espace permet donc d'associer le gain en sensibilité dû à la longueur d'onde au gain dû à l'accroissement de la taille physique de l'interféromètre en microgravité. La sensibilité étant proportionnelle à la surface embrassée par les atomes froids, un interféromètre dans l'espace constituerait ainsi un gyroscope aux performances largement supérieures à ceux de facture plus classique.

Le projet s'appelle HYPER[19] (High Precision Atom Interferometry in Space). En regard de la difficulté technologique que représente ce satellite, il n'est pas envisagé de le réaliser dans un avenir proche, mais il reste cependant un objectif pour les recherches actuelles. Autour de ce projet s'est construite une collaboration européenne (Allemagne, France, Royaume-Uni, Hollande) autour de son « principal investigator » E. M. Rasel. Je participe à la réflexion sur la faisabilité des expériences proposées en physique fondamentale d'un point de vue théorique. Un des objectifs du projet est de mesurer l'effet Lense-Thirring de la Terre, appelé aussi effet gyromagnétique terrestre, à l'aide d'un ou plusieurs gyroscopes dont un des axes pointe une étoile lointaine supposée fixe. L'effet va alors induire au gyroscope de tourner sur lui-même avec une vitesse angulaire de l'ordre de 10^{-14} rad.s^{-1}.

Cet effet devrait être mesuré dans un peu plus d'un an avec la sonde Gravity Probe B lancée en avril 2004. Le principe de la mesure dans ce satellite est de fixer quatre gyroscopes classiques (avec des sphères quasi-parfaites) sur une étoile lointaine dont les paramètres de déplacement dans le ciel sont connus à la plus grande précision accessible. Au bout de 16,5 mois, les gyroscopes auront subi une rotation mesurable permettant d'estimer l'effet Lense-Thirring avec une précision de l'ordre du pour cent. Cette mesure est donc une mesure intégrée, tandis qu'HYPER utiliserait des gyroscopes suffisamment sensibles pour faire une mesure instantanée. De surcroît, le défi technologique que ce dernier représente devrait suffire à justifier son lancement, même si ses performances le limitent à reproduire des mesures déjà effectuées par ailleurs.

En collaboration avec Philippe Tourrenc et Xavier Ovido (professeur du secondaire, qui, après son DEA, a décidé de faire de la recherche sur son temps libre sous ma direction), j'ai estimé l'influence des perturbations gravitationnelles sur la mesure de l'effet Lense-Thirring dans l'expérience HYPER (Angonin-Willaime, Ovido, Tourrenc, 2004). Pour ce calcul, j'ai défini une tétrade associée au satellite, en chute libre autour de la Terre, supposé contenir des interféromètres à ondes de matière liés à un télescope pointant une étoile lointaine. Ces interféromètres mesurent ainsi l'accélération et la rotation du repère inertiel local que l'on peut prédire en calculant l'évolution de la tétrade.

Pour obtenir cette évolution, il faut, d'une part, estimer les ordres de grandeurs intervenant dans l'expérience (nous avons définit l'ordre 1 comme le rapport de la vitesse du satellite à la vitesse de la lumière) et, d'autre part, expliciter la métrique locale du système. Nous avons choisi la méthode, surnommée dans l'article « LiZiNi », qui est une méthode de calcul par développement limité de la métrique locale d'un objet en déplacement dans une métrique au repos déjà déterminée. Nous avons alors calculé les termes de rotation dus à l'aberration de la lumière ainsi que sa déviation due au champ gravitationnel terrestre. Cela nous a conduit à déterminer que, pour avoir une précision meilleure que 20% sur la mesure de l'effet Lense-

[19] Pour une présentation plus complète de l'expérience :
http://sci.esa.int/science-e/www/area/index.cfm?fareaid=46

Thirring, il faut considérer, dans le calcul du déphasage décrivant l'état du système, tous les termes jusqu'à l'ordre 7. Concrètement, cela signifie, par exemple, que le moment quadrupolaire du champ de gravitation terrestre n'est pas négligeable.

La plupart des paramètres qui entrent en jeu à cet ordre peuvent être soit éliminés expérimentalement, soit déterminés avec suffisamment de précision pour ne pas perturber la mesure de l'effet Lense-Thirring. Cependant, en ajoutant des petites perturbations au système, nous avons déterminé les effets d'un gradient du champ gravitationnel sur le satellite et montré qu'ils ne sont ni négligeables et ni facilement modélisables. Nous proposons alors d'éviter cet écueil en provoquant un mouvement de rotation propre du satellite. Dans ce cadre, nous avons démontré que les différentes composantes du signal périodique obtenu permettent d'isoler l'effet Lense-Thirring, qui deviendrait alors mesurable. Il est évident que ce résultat ne pourra être confirmé que par une modélisation complète, plus réaliste, du système.

Avec les mêmes collaborateurs et en utilisant la même méthode, j'ai généralisé ensuite le calcul précédent pour une trajectoire circulaire de taille quelconque en effectuant les applications numériques dans le cas de missions autour de la Terre et de Jupiter. Les conclusions sont alors analogues : la rotation propre élevée de Jupiter induit un effet Lense-Thirring certes plus important ; mais cet effet est compensé par la taille élevée de la trajectoire, provoquant la nécessité de mener les calculs jusqu'au même ordre que dans le cas de la Terre. Il faut donc tenir compte des mêmes phénomènes pour la mesure de l'effet Lense-Thirring et, par exemple, provoquer un spin du satellite de la façon identique. En conséquence, il n'est pas plus intéressant de faire cette expérience autour de Jupiter qu'autour de la Terre. Cet article avait aussi pour but de montrer que la méthode proposée est une méthode applicable dans d'autres expériences où l'on doit tenir compte des effets relativistes (Tourrenc, Angonin, Ovido, 2004).

Le « processus oublié »

Dans toutes les expériences concernant les senseurs gravito-inertiels à ondes de matière, les ondes de matière sont en interaction avec des photons. Jusqu'à présent, la description de l'effet de la lumière sur ces ondes s'effectuait dans le cadre d'un formalisme de théorie quantique des champs, généralement assez lourd à manipuler. Avec Peter Wolf et Philippe Tourrenc, nous avons chercher à simplifier l'étude de ces phénomènes en développant une méthode plus intuitive, similaire à celle utilisée pour les laser optiques. Elle consiste en la généralisation des principes de calcul des coefficients d'Einstein en considérant que les particules des ondes de matière doivent suivre, au même titre que les photons, une distribution de Bose-Einstein (dont l'asymptote est la distribution de Boltzmann utilisée pour décrire les atomes « chauds » par Einstein dans son calcul[20]). Cette idée nous a amené à considérer , en plus des traditionnels coefficients A et B traduisant les transitions spontanées et induites par la présence de photons, le coefficient C (celui du « processus oublié ») correspondant à des transitions induites par la présence de l'onde atomique, elle-même. Les résultats obtenus par ce biais correspondent aux calculs effectués en théorie quantique des champs[21]. L'article correspondant à ces réflexions est plutôt à vocation pédagogique (Tourrenc, Angonin et Wolf, 2004).

[20] Einstein, Verhanal DPG, 1916, **18**, 318 ; Einstein, Phys Zs, 1917, **18**, 121

[21] Par exemple : Bordé, Phys Lett A, 1995, **204**, 217 ; et les autres références données dans l'article sur le « processus oublié ».

ARTICLES SUR LA GRAVITATION EXPERIMENTALE

- Angonin-Willaime M-C, Ovido X, Tourrenc Ph, 2004, General Relativity and Gravitation, vol. **36**, Issue 2, 411 : *Gravitational perturbations on local experiments in a satellite : The dragging of inertial frame in the HYPER project*
- Tourrenc Ph, Angonin M-C, Ovido X, 2004, General Relativity and Gravitation, vol. **36**, Issue 10, 2237: *Tidal gravitational effects in a satellite*
- Tourrenc Ph, Angonin M-C, Wolf P, version du 22/07/04 : *The forgotten process : the emission stimulated by matter waves.*

Gravitational perturbations on local experiments in a satellite : The dragging of inertial frame in the HYPER project

Angonin-Willaime M-C, Ovido X, Tourrenc Ph, 2004, General Relativity and Gravitation, vol. **36**, Issue 2, 411

Gravitational perturbations on local experiments in a satellite : The dragging of inertial frame in the HYPER project.

M-C. Angonin-Willaime,* X. Ovido, and Ph. Tourrenc
Université P. et M. Curie
ERGA, case 142
4, place Jussieu
F-75252 Paris CEDEX 05, France
(Dated: June 2, 2004)

We consider a nearly free falling Earth satellite where atomic wave interferometers are tied to a telescope pointing towards a faraway star. They measure the acceleration and the rotation relatively to the local inertial frame.

We calculate the rotation of the telescope due to the aberrations and the deflection of the light in the gravitational field of the Earth. We show that the deflection due to the quadrupolar momentum of the gravity is not negligible if one wants to observe the Lense-Thirring effect of the Earth.

We consider some perturbation to the ideal device and we discuss the orders of magnitude of the phase shifts due to the residual tidal gravitational field in the satellite and we exhibit the terms which must be taken into account to calculate and interpret the full signal.

Within the framework of a geometric model, we calculate the various periodic components of the signal which must be analyzed to detect the Lense-Tirring effect. We discuss the results which support a reasonable optimism.

As a conclusion we put forward the necessity of a more complete, realistic and powerful model in order to obtain a final conclusion on the theoretical feasibility of the experiment as far as the observation of the Lense-Thirring effect is involved.

I. INTRODUCTION

The quick development of atomic interferometry during the last ten years is impressive. The clocks, the accelerometers and the gyroscopes based on this principle are already among the best that have been constructed until now and further improvements are still expected. This situation favors a renewal in the conception of various experiments, such as the measurement of the fine structure constant or the tests of relativistic theories of gravitation currently developed by classical means (gravitational frequency shifts, equivalence principle[16], Lense-Thirring effect[17], etc...).

The performances of laser cooled atomic devices is limited on Earth by the gravity. Therefore further improvements demand that new experiments take place in free falling (or nearly free falling) satellites. A laser cooled

*Electronic address: m-c.angonin@obspm.fr

atomic clock, named PHARAO, will be a part of ACES (Atomic Clock Ensemble in Space), an ESA mission on the ISS planned for 2006. Various other experimental possibilities involving "Hyper-precision cold atom interferometry in space" are presently considered. They might result in a project (called "Hyper") in not too far a future. Most of the modern experiments display such a high sensitivity that their description must involve relativistic gravitation. This is not only true for the experiments which are designed to study the gravitation itself but also for any experiment such as Hyper where very small perturbations cannot be neglected any longer.

The present paper is a contribution to the current discussions on the feasibility of Hyper. We consider especially the effect of the inertial fields and the local gravitational fields in a satellite[18].

There are two kinds of gravitational perturbation.

1. The masses in the satellite produce a gravitational field which is not negligible. In some experiments, the mass distribution itself can play a role : This is, for instance, the case for GPB. However, some other experiments are only sensitive to the change of the mass distribution with the time. This is the case of Hyper where a signal is recorded as a function of the time and analyzed by Fourier methods at a given frequency. The modification of the mass distribution is due to mechanical and thermal effects. It depends on the construction of the satellite, the damping of the vibrations and the stabilization of the temperature. We will not study these effects which can be considered as technological perturbations. We do not claim that these perturbations are easy to cancel but only that it is possible in principle while it is impossible for tidal effects from the Earth.

2. The perturbations due to the gravity of far away bodies (the Earth, the Moon, the Sun and the surrounding planets) is the subject of the present paper. It is impossible to cancel their action.

The aim of this paper is to study the gravity in a nearly free falling satellite where the tidal effects remain.

The experimental set-up is tied to a telescope pointing towards a "fixed star". However, it experiences a rotation: the so called "Lense-Thirring" effect. It has been recently noticed that atomic interferometers display a sensitivity high enough to map the gravitomagnetic field of the Earth (included the Lense-Thirring effect). This could be one of the goals of the Hyper project [1]. The effect is so tiny that we will concentrate on this question.

We consider the case where the experimental set up is built out of several atomic interferometers similar to those which are currently developed in Hannover [2] and [3], Paris [4] and Orsay [5] and [6] (see section V).

In section 1 we introduce the metric, $g_{\alpha\beta}$, in the non rotating geocentric coordinates and we define a book-keeping of the orders of magnitude.

In order to study the local gravitational field in the satellite, we chose an origin, O, and a tetrad $u^{\alpha}_{(\sigma)}$ which defines the reference frame of the observer at point O. The time vector, $u^{\alpha}_{(0)}$, is the 4-velocity of O. The space vector $u^{\alpha}_{(1)}$ defines the axis of a telescope which points towards a "fixed" far away star. The tetrad is spinning around $u^{\alpha}_{(1)}$ with the angular velocity, ϖ.

In section 2, in order to define precisely the tetrad we study the apparent direction of the star.

Then, in section 3, following [7] and [8] we expand the metric in the neighborhood of O (the NiZiLi metric).

Finally we calculate the response of the experimental set-up and we emphasize the interest of spinning the satellite.

An ASU delivers a phase difference, $\delta\varphi$, between two matter waves. The phase difference is the amount of various terms. Some of them can be computed with the required accuracy; they produce a phase difference $\delta\varphi_k$. Then $\delta\varphi = \delta\varphi_k + \delta\varphi_u$ where $\delta\varphi$ is measured. Therefore one can consider that the ASU delivers $\delta\varphi_u$. This is this quantity that we want to calculate here.

In this paper, we point out the various contributions to $\delta\varphi_u$ with their order of magnitude. The method that we use to calculate $\delta\varphi_u$ is a first order perturbation method. A more precise method, valid for $\delta\varphi$ is now available [9]. It gives the possibility to model the ASU and therefore to study the signal due to the various perturbations which are expected.

II. GENERALITIES

A. Conventions and notations

In the non rotating geocentric frame we introduce the coordinates x^{α} with $\alpha = 0, 1, 2, 3$. We define the time coordinate $x^0 = ct$ where c is the celerity of the light in the vacuum. The space coordinates are x^k (in this paper the Latin indices run from 1 to 3). We use the notations $\vec{r} = \left\{x^k\right\} = \{x, y, z\}$ and we define the spherical coordinates $\{r, \theta, \varphi\}$, *i.e.* $x = r\sin\theta\cos\varphi$, $y = r\sin\theta\sin\varphi$, $z = r\cos\theta$. Therefore $r = \|\overrightarrow{r}\| = \sqrt{x^2 + y^2 + z^2}$.

We consider an Earth satellite and a point O which is chosen as the origin of the local coordinates in the satellite. We assume that the position of O is given by its three space coordinates, $\vec{r} = \{x, y, z\} = \left\{x^k\right\}$, as three known functions of the coordinate time, t. Then we define the velocity of point O as $\overrightarrow{v} = \dfrac{d\vec{r}}{dt}$.

The proper time at point O is s. The motion of O can be described as well by the four functions $x^\alpha = x^\alpha(s)$. The four-velocity is defined as $u^\alpha = \dfrac{dx^\alpha}{ds}$.

The Newtonian constant of gravitation is G.

We use geometrical units where the numerical value of G and c is equal to 1.

The metric tensor is $g_{\alpha\beta}$; it inverse is $g^{\alpha\beta}$. The Minkowski tensor is $\eta_{\alpha\beta} = diag\,[1,-1,-1,-1]$; its inverse is $\eta^{\alpha\beta}$.

We use the summation rule on repeated indices (one up and one down).

The partial derivative of $(\,)$ will be noted $(\,)_{,\alpha} = \partial_\alpha (\,) = \dfrac{\partial (\,)}{\partial x^\alpha}$.

In the sequel we introduce different tetrads, *i.e.* a set of four vectors $e^\alpha_{\hat\sigma}$ labeled by the means of an index called $\hat\sigma$ or (σ), such as $e^\alpha_{\hat\sigma} g_{\alpha\beta} e^\beta_{\hat\rho} = \eta_{\hat\sigma\hat\rho}$. The "Einstein" indices, α, β, σ, etc., and the "Minkowski" indices $\hat\alpha$, $\hat\beta$, etc., can be changed one into the other by the means of the tetrad : $(\,)_{\hat\alpha} = e^\mu_{\hat\alpha}\,(\,)_\mu$. The metric tensor is used to raise (or lower) the Einstein indices while the Minkowski tensor is used for Minkowski indices.

B. The fundamental element

In the sequel we consider the Parametrized Post Newtonian theories [10]. The relevant PPN parameters which appear below are γ and α_1. The parameter γ is the usual parameter connected to the deflection of a light ray by a central mass. The parameter α_1 couples the metric to the speed, $-\vec{w}$, of the preferred frame (if any) relatively to the geocentric frame. In general relativity, $\alpha_1 = 0$ and $\gamma = 1$.

The preferred frame is generally considered to be the rest frame of the Universe where the background radiation is isotropic ($\|\vec{w}\| \sim 10^{-3}$ in geometrical units).

Let us define now several quantities which will be used in the sequel :

- $2M_\oplus$ is the Schwarzschild's radius of the Earth ($M_\oplus \simeq 4.4\,\mathrm{mm}$). As we use geometrical units (G = c = 1), $M_\oplus$ is also called the "mass" of the Earth.
- $\vec{J}_\oplus$ is the angular momentum of the Earth in geometrical units. The relevant quantity which appears below, is $\vec{J} = \dfrac{1+\gamma+\alpha_1/4}{2}\vec{J}_\oplus$. We define $J = \left\|\vec{J}\right\| \simeq \left\|\vec{J}_\oplus\right\| = J_\oplus \simeq 145\,\mathrm{cm}^2$.
- $\vec{g} = -2\,\dfrac{\vec{J}\wedge\vec{r}}{r^3} + \dfrac{1}{2}\alpha_1 U\,\vec{w}$ is the definition of $\vec{g}$.

- U is the Newtonian potential

$$U = \frac{M_\oplus}{r}\left(1 - J_2\left(\frac{R_\oplus}{r}\right)^2 P_2 + \Delta\right) + U_* \tag{1}$$

where $R_\oplus$ is the radius of the Earth and U_* the potential due to the Moon, the Sun and the planets[19]. In spherical coordinates the Legendre polynomial P_2 reads $P_2 = \frac{1}{2}\left(3\cos^2\theta - 1\right)$. The quadrupole coefficient J_2 is of order of 10^{-3} and Δ represents the higher harmonics; it is of order of 10^{-6} [11]. It depends on the angle φ and on the time t because of the rotation of the Earth.

In the non rotating geocentric coordinates the significant fundamental element is

$$ds^2 = (1-2U)\,dt^2 + 2g_{0k}\,dx^k dt - (1+2\gamma U)\,\delta_{jk}\,dx^j dx^k \tag{2}$$

where $(\vec{g})_k = -(\vec{g})^k = g_{0k}$. In the expression (2), we have dropped post Newtonian corrections which are too small to be considered here.

C. Orders of magnitude

We consider a nearly free falling, Earth satellite on a nearly circular orbit of radius r (with $r \simeq 7000\,\mathrm{km}$).

1. *Orbital data.*

The velocity of the satellite is of order $O_1 \sim \sqrt{\frac{M_\oplus}{r}}$ (*i.e.* $O_1 \simeq 2.5\,10^{-5}$ for $r \simeq 7000\,\mathrm{km}$).

In the neighborhood of the satellite the potential U is of the order of the potential of the Earth $U \sim \frac{M_\oplus}{r} \sim O_2$; the coefficients g_{0k} fulfills the relation $|g_{0k}| \gtrsim \frac{J_\oplus}{M_\oplus^2}\left(\frac{M_\oplus}{r}\right)^2 \sim 750\,O_4 >> O_4$([20]).

The post Newtonian terms that we have neglected in the metric (2) are of order O_4.

2. *The size of the set-up.*

Now we define $d \sim r\,O_1$ (*i.e.* $d \simeq 175\,\mathrm{m}$ for $r \simeq 7000\,\mathrm{km}$). We assume that the size of the experimental set-up in the satellite is $X \sim \varepsilon\,d$ where

$\varepsilon < 1$. In the sequel we will consider an atomic Sagnac unit the size of which does not exceed 0.9 m (then $\varepsilon \sim 5\,10^{-3}$).

3. The local acceleration.

The acceleration, $\|\overrightarrow{a}\|$, can be measured by accelerometers comoving with the satellite. It is called "the acceleration of the satellite relatively to a local inertial frame". The satellite is nearly free falling, therefore $\|\overrightarrow{a}\| << a \lesssim O_2 \times \frac{1}{r}$.

Our assumptions are summarized below. The numerical values are obtained for the Earth with $r \sim 7000\,\mathrm{km}$, $M_\oplus/r \sim O_2 \sim 6\,10^{-10}$ and $v/c \sim O_1 \sim 2.5\,10^{-5}$ (*i.e.* $v \simeq 7.5\,\mathrm{km\cdot s^{-1}}$) where v is the velocity of the satellite relatively to the geocentric frame:

$M_\oplus/r \sim O_2 \sim v^2$	$X \lesssim \varepsilon O_1 r = \varepsilon\, d$,with $\varepsilon < 1$	$\|\overrightarrow{a}\| \ll a \sim O_2 \times \frac{1}{r}$

$M_\oplus \simeq 4.4\,\mathrm{mm}$	$J \simeq J_\oplus \simeq 145\,\mathrm{cm}^2$	$r \simeq 7\,000\,\mathrm{km}$	$\frac{J}{M_\oplus^2} \simeq 750 >> 1$

$O_1 \sim d/r$	$O_2 \sim r\,a$	$\lvert g_{0k}\rvert \sim 750\,O_4$	O_4
$2.5\,10^{-5}$	$6\,10^{-10}$	$3\,10^{-16}$	$4\,10^{-19}$

$d \sim 175\,\mathrm{m}$	$a \sim 8\,\mathrm{m\cdot s^{-2}}$

Table 1

In the sequel we will assume the preceding relations.

D. The NiZiLi comoving metric

Before closing this section dedicated to generalities, we give the expression of the fundamental element associated to the NiZiLi metric.

First we choose an origin, O, in the satellite and we choose a tetrad, $e^\alpha_{\hat{\sigma}}$ whose vector $e^\alpha_{\hat{0}} = u^\alpha$ is the 4-velocity, u^α, of point O. Thus, the vectors $e^\alpha_{\hat{k}}$ define the basis of the space vectors for the observer O. The coordinates which are associated to the tetrad are the space coordinates $X^{\hat{k}}$ and the time $X^{\hat{0}} = T$.

Following the procedure defined in [7] and [8] we find the fundamental element and the local metric tensor

$$ds^2 = G_{\hat{\alpha}\hat{\beta}}\, dX^{\hat{\alpha}} dX^{\hat{\beta}} + \varepsilon^2 O_6 \quad \text{with} \tag{3}$$

$$\begin{aligned} G_{\hat{0}\hat{0}} &= 1 + 2\,\vec{a}\cdot\vec{X} + \left(\vec{a}\cdot\vec{X}\right)^2 - \left(\vec{\Omega}\wedge\vec{X}\right)^2 \\ &\quad -R_{\hat{0}\hat{k}\hat{0}\hat{\jmath}}\, X^{\hat{k}} X^{\hat{\jmath}} - \frac{1}{3} R_{\hat{0}\hat{k}\hat{0}\hat{\jmath},\hat{\ell}} X^{\hat{k}} X^{\hat{\jmath}} X^{\hat{\ell}} + ... \\ G_{\hat{0}\hat{m}} &= \Omega_{\hat{m}\hat{k}}\, X^{\hat{k}} - \frac{2}{3} R_{\hat{0}\hat{k}\hat{m}\hat{\jmath}}\, X^{\hat{k}} X^{\hat{\jmath}} - \frac{1}{4} R_{\hat{0}\hat{k}\hat{m}\hat{\jmath},\hat{\ell}} X^{\hat{k}} X^{\hat{\jmath}} X^{\hat{\ell}} + ... \\ G_{\hat{n}\hat{m}} &= \eta_{\hat{n}\hat{m}} - \frac{1}{3} R_{\hat{n}\hat{k}\hat{m}\hat{\jmath}} X^{\hat{k}} X^{\hat{\jmath}} - \frac{1}{6} R_{\hat{n}\hat{k}\hat{m}\hat{\jmath},\hat{\ell}} X^{\hat{k}} X^{\hat{\jmath}} X^{\hat{\ell}} + ... \end{aligned}$$

where we have used vector notations *i.e.* $\overrightarrow{V}$ for $\left\{V^{\hat{k}}\right\}$, $\overrightarrow{V}\cdot\overrightarrow{W}$ for $\sum V^{\hat{k}}\, W^{\hat{k}}$, etc. Every quantity, except the space coordinates $X^{\hat{k}}$, are calculated at point O. Thus they are functions of the time T.

$R_{\hat{\alpha}\hat{\beta}\hat{\sigma}\hat{\mu}}$ is the Riemann tensor obtained from $R_{\alpha\beta\sigma\mu}$ at point O :

$$R_{\alpha\beta\sigma\mu} = \Gamma_{\alpha-\beta\mu,\sigma} - \Gamma_{\alpha-\beta\sigma,\mu} + \Gamma^{\varepsilon}_{\beta\sigma}\Gamma_{\varepsilon-\alpha\mu} - \Gamma^{\varepsilon}_{\beta\mu}\Gamma_{\varepsilon-\alpha\sigma} \tag{4}$$

where $\Gamma_{\alpha-\beta\mu}$ is the Christoffel symbol.

$\Omega_{\hat{\jmath}\hat{k}}$ is the antisymmetric quantity

$$\Omega_{\hat{\jmath}\hat{k}} = \frac{1}{2}\left(g_{\hat{0}\hat{\jmath},\hat{k}} - g_{\hat{0}\hat{k},\hat{\jmath}}\right)_O + \frac{1}{2}\left(\left(e^{\beta}_{\hat{\jmath}}\,\frac{de^{\alpha}_{\hat{k}}}{ds} - \frac{de^{\beta}_{\hat{\jmath}}}{ds}\,e^{\alpha}_{\hat{k}}\right) g_{\alpha\beta}\right)_O \tag{5}$$

Due to the antisymmetry of $\Omega_{\hat{m}\hat{k}}$, the quantity $\Omega_{\hat{m}\hat{k}}\, X^{\hat{k}} dX^{\hat{m}}$ which is present in the expression of ds^2 can be written as $\Omega_{\hat{m}\hat{k}}\, X^{\hat{k}} dX^{\hat{m}} = \left(\overrightarrow{\Omega}_0\wedge\overrightarrow{X}\right)\cdot d\overrightarrow{X}$. The space vector $\overrightarrow{\Omega}_0$ is the physical angular velocity. It is measured by gyroscopes tied to the three space orthonormal vectors $e^{\alpha}_{\hat{k}}$:

The vector $\overrightarrow{a}$ is the physical acceleration which can be measured by an accelerometer comoving with O. It is the spatial projection at point O of the 4-acceleration of point O.

At point O (*i.e.* $\overrightarrow{X} = \overrightarrow{0}$) the time T is the proper time delivered by an ideal clock comoving with O.

The first tetrad that we consider is actually called $e^{\alpha}_{\hat{\sigma}}$:

$$
\begin{aligned}
e_{\hat{0}}^{0} &= u^{0} = 1 + \frac{\vec{v}^{2}}{2} + U \ + O_4, \ \ e_{\hat{0}}^{k} = u^{k} = \left(1 + \frac{\vec{v}^{2}}{2} + U\right) v^{k} + O_4 \\
e_{\hat{k}}^{0} &= \left(1 + \frac{\vec{v}^{2}}{2} + U\right) v^{k} + \gamma U\, v^{k} - g_{0k} + O_4 \qquad (6) \\
e_{\hat{k}}^{j} &= \delta_{k}^{j} + \frac{1}{2} v^{j} v^{k} + \frac{1}{2} \gamma U\, \delta_{k}^{j} + O_4
\end{aligned}
$$

Calculating $\vec{\Omega}_0$ one finds

$$
\vec{\Omega}_0 = \vec{\Omega}_{LT} + \vec{\Omega}_{dS} + \vec{\Omega}_{Th} \qquad (7)
$$

$$
\left(\vec{\Omega}_{LT}\right)^{\hat{k}} \simeq \left(\frac{\vec{J}}{r^3} - \frac{3}{r^3}\left(\vec{J}\cdot\vec{n}\right)\vec{n} - \frac{\alpha_1}{4}\vec{\nabla}U \wedge \vec{w}\right)^{k} \qquad (8)
$$

$$
\left(\vec{\Omega}_{dS}\right)^{\hat{k}} \simeq \left((1+\gamma)\,\vec{\nabla}U \wedge \vec{v}\right)^{k} \text{ and } \quad \left(\vec{\Omega}_{Th}\right)^{\hat{k}} \simeq \left(\frac{1}{2}\vec{v} \wedge \frac{d\vec{v}}{dt}\right)^{k} \qquad (9)
$$

$\vec{\Omega}_{LT}$ is the Lense-Thirring angular velocity, $\vec{\Omega}_{dS}$ and $\vec{\Omega}_{Th}$ are the de Sitter and the Thomas terms [21].

Now it is straightforward to calculate the order of magnitude of the Lense-Thirring angular velocity. One finds $\frac{J}{M_{\oplus}^{2}} O_4 \frac{c}{r} \sim 10^{-14}\,\mathrm{rad}\cdot\mathrm{s}^{-1}$.

We will see that it is relevant to limit the expansion of the metric at order $\varepsilon^2\, O_6$; therefore we consider only the linear expression of the Riemann tensor above and we neglect he term $\left(\vec{a}\cdot\vec{X}\right)^2$ in the metric 3.

In the sequel we consider an other tetrad $u^{\alpha}_{(\sigma)}$. Except for the notations, the general results above still hold with the associated coordinates.

III. ABERRATION AND DEFLECTION OF THE LIGHT

In the satellite, the experimental set-up is tied to a telescope which points towards a "fixed" star. We assume that the star is far enough for the parallax to be negligible. However it is necessary to account for the gravitational deflection of the light ray and for the aberrations in order to describe the rotational motion of the telescope during the orbital motion of the satellite.

In space time, the direction of the light from the star is given by the 4-vector $L_\alpha = \left\{1, \frac{\partial_k \varphi}{\partial_0 \varphi}\right\}$ where φ is the phase of the light. In order to

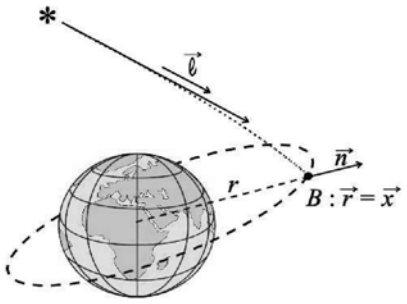

FIG. 1: The deflection of light.

calculate the phase $\varphi(t, x^k)$ at point $\{x^k\}$ and time t we use the method which is summarized in annex A [12].

The monopolar term of the Newtonian potential gives

$$L_\alpha = \left\{1,\ -\ell^k + (1+\gamma)\,\frac{M_\oplus}{r}\,\frac{n^k - \ell^k}{1 - \vec{n}\cdot\vec{\ell}}\right\} \tag{10}$$

where $\overrightarrow{\ell}$ is the unitary vector of figure 1 and $\overrightarrow{n} = \overrightarrow{r}/r$.

Several contributions must be added to the expression (10).

$$L_\alpha = \left\{1,\ -\ell^k + (1+\gamma)\,\frac{M}{r}\,\frac{n^k - \ell^k}{1 - \vec{n}\cdot\vec{\ell}} + \delta\ell^k + \delta L^k\right\}$$

- The term $\delta\ell^k$ is due to the quadrupolar term of the Earth. We give its value in appendix A. Its order of magnitude is $J_2 O_2 \sim 10^{-3} O_2$ when $\overrightarrow{\ell}$ is nearly orthogonal to the plane of the orbit.
- The term due to $\dfrac{1}{2}\alpha_1 U\, w^k$, a part of g_{0k} in the metric (2), results in the modification $M_\oplus \to M = M_\oplus\left(1 - \dfrac{\alpha_1\,\vec{w}\cdot\vec{\ell}}{2\,(1+\gamma)}\right)$. The demonstration is straight forward.
- The contribution due to the rotation of the Earth has already been considered in the literature ([13]). Since it is proportional to the ratio of the angular momentum and the square of r, it is negligible. The same conclusion holds for the term Δ in expression (1).
- The Sun, the Moon and the other planets, give a contribution due to U_* in (1); it varies slowly with the time and it is negligible, especially within the framework of a Fourier analysis at a much higher frequency.

For the observer O, the space direction of the light is the four vector $\lambda^\alpha = L^\alpha - L_\beta\, u^\beta\, u^\alpha$. The components of λ^α relatively to the tetrad $e^\beta_{\hat\alpha}$ are $\lambda_{\hat\alpha} = e^\beta_{\hat\alpha}\lambda_\beta$.

$$\lambda^{\hat k} = -\lambda_{\hat k} = -L_\alpha e^\alpha_{\hat k}\ ,\ \ \lambda^{\hat 0} = -\lambda_{\hat 0} = 0$$

In order to calculate $\lambda^{\hat k}$, we use the expression (6) for the tetrad. We normalize $\vec\lambda$, *i.e.* we define $\vec\Lambda = \Lambda\,\vec\lambda$ such as $-\Lambda_\alpha\Lambda^\alpha = \vec\Lambda\cdot\vec\Lambda = 1$. The tetrad (6) is especially useful to catch the orders of magnitude of the various terms involved. However it is not the comoving tetrad that we are looking for because the telescope that points towards the far away star rotates relatively to this tetrad. The angular velocity of the telescope relatively to $\left\{e^\alpha_{\hat k}\right\}$ is $\vec\Omega_* = \vec\Lambda\wedge\dfrac{d\vec\Lambda}{dt}$. Straightforward calculations give

$$\begin{aligned}\Lambda^{\hat k} \;=\; & \ell^k\left(1+\vec\ell\cdot\vec v-\frac{1}{2}\vec v^{\,2}+\left(\vec\ell\cdot\vec v\right)^2\right.\\ & \left.+(1+\gamma)\,\frac{M}{r}\,\frac{\vec n\cdot\vec\ell}{1-\vec n\cdot\vec\ell}-\vec\ell\cdot\left(\delta\vec\ell+\delta\vec L\right)\right)\\ & -v^k\left(1+\frac{1}{2}\left(\vec\ell\cdot\vec v\right)\right)-n^k\frac{M}{r}\,\frac{1+\gamma}{1-\vec n\cdot\vec\ell}+\delta\vec\ell+\delta\vec L+O_3\end{aligned}$$

and

$$\begin{aligned}\left(\vec\Omega_*\right)^{\hat k} \;=\; & -\left(\vec\ell\wedge\frac{d\vec v}{dt}\right)^k+\left(\vec v\wedge\frac{d\vec v}{dt}\right)^k \qquad (11)\\ & -\frac{3}{2}\left(\vec\ell\cdot\vec v\right)\left(\vec\ell\wedge\frac{d\vec v}{dt}\right)^k+\frac{1}{2}\left(\vec\ell\cdot\frac{d\vec v}{dt}\right)\left(\vec\ell\wedge\vec v\right)^k\\ & -\frac{M}{r^2}\,\frac{1+\gamma}{1-\vec n\cdot\vec\ell}\left(\left(\vec\ell\wedge\vec v\right)^k+\left(\vec\ell\wedge\vec n\right)^k\left[\frac{\vec\ell\cdot\vec v\ -\vec n\cdot\vec v}{1-\vec n\cdot\vec\ell}-\vec n\cdot\vec v\right]\right)\\ & +\left(\vec\ell\wedge\frac{d\delta\vec\ell}{dt}\right)^k+\frac{1}{r}\times O_4\end{aligned}$$

Let us notice that we neglect the terms of order $\dfrac{1}{r}\times O_4$, which are much smaller than the Lense-Thirring angular velocity ($\sim 750\,O_4\times\dfrac{1}{r}$).

Now we introduce the tetrad $u^\alpha_{(\sigma)}$ which is obtained from $e^\alpha_{\hat\rho}$ through a pure space rotation (*i.e.* $u^\alpha_{(0)} = e^\alpha_{\hat 0} = u^\alpha$) and whose vector $u^\alpha_{(1)}$ points

towards the far away star ($u^\alpha_{(1)} = -\Lambda^\alpha$). The rotation of the tetrad $\left\{u^\alpha_{(\sigma)}\right\}$ relatively to $\left\{e^\alpha_{\hat{\rho}}\right\}$ is characterized by the most general angular velocity $\vec{\Omega}_{u/e} = \vec{\Omega}_* - \varpi\vec{\Lambda}$ where $-\varpi\vec{\Lambda}$ is an arbitrary angular velocity around the apparent direction of the star.

IV. THE LOCAL METRIC IN THE SATELLITE

A. The relevant terms

Now we need to calculate the NiZiLi metric associated to the tetrad $u^\alpha_{(\sigma)}$. We limit the accuracy of our development to a few tens per cent in order to take advantage of important simplifications.

Let us assume that the fundamental element is known :

$$ds^2 = \left(1 + K_{(0)(0)}\right) dT^2 + 2K_{(0)(k)} dT dX^{(k)} + \left(\eta_{(k)(j)} + K_{(k)(j)}\right) dX^{(k)} dX^{(j)}$$

We want to calculate the effect of $K_{(\alpha)(\beta)}$ on the atom interferometer in the satellite. In order to use the method summarized in the appendix A we calculate the quantity Ψ which gives the physical quantities that one can measure :

$$\Psi = K_{(0)(0)} + 2K_{(0)(k)} v_g^{(k)} + K_{(k)(j)} v_g^{(k)} v_g^{(j)} \tag{12}$$

where $v_g^{(k)}$ is the velocity of the atoms (*i.e.* the unperturbed group velocity).

We are dealing with slow cold atoms, therefore $v_g \sim \eta O_1$ with $\eta << 1$ (we can take the value $\eta \sim O_1$ valid for current experiments). In Ψ, the Lense-Thirring term arises from $2K_{(0)(k)} v_g^{(k)}$; it is of order of $2\frac{J}{r^3} X v_g \sim 1500\,\eta\varepsilon O_6$. If the expansion of $K_{(0)(0)}$ is limited to order $\varepsilon^2 O_6$, the accuracy is of order $\dfrac{\varepsilon}{1500\eta} \sim 13\%$ with $v_g \simeq 20\,\mathrm{cm}\cdot\mathrm{s}^{-1}$.

In the case that we consider, the following orders of magnitude hold true : $\varepsilon \sim \sqrt{O_1} = O_{1/2}$ and $\eta \sim O_1$. Therefore, it is not necessary to consider terms smaller than $O_7 \sim \varepsilon^2 O_6$ in $K_{(0)(0)}$, smaller than O_5 in $K_{(0)(k)}$ and smaller than O_3 in $K_{(k)(j)}$. The same relations hold in the coordinate system associated to the tetrad $\left\{u^\alpha_{(\sigma)}\right\}$ as well as $\left\{e^\alpha_{\hat{\rho}}\right\}$ because both are next to each other.

It can be proved that in the expression 1 the time can be considered as a parameter and that, within the present approximations, it is not necessary

to consider time derivative in the expression 3. Therefore one obtains

$$G_{\hat{0}\hat{0}} = 1 + 2\,\vec{a}\cdot\vec{X} - \hat{U}_{,\hat{k}\hat{j}}\,X^{\hat{k}}X^{\hat{j}} - \frac{1}{3}\hat{U}_{,\hat{k}\hat{j}\hat{\ell}}\,X^{\hat{k}}X^{\hat{j}}X^{\hat{\ell}} + \varepsilon^2\,O_6$$
$$G_{\hat{0}\hat{m}} = -\left\{\vec{\Omega}_0\wedge\vec{X}\right\}^{\hat{m}} + \varepsilon^2\,O_5 \text{and } G_{\hat{n}\hat{m}} = \eta_{\hat{n}\hat{m}} + \varepsilon^2 O_4$$

where $\vec{\Omega}_0$ is given above (see expression 7) while the expressions such as $\hat{U}_{,\hat{k}\hat{j}}$ are nothing but $\left(U_{,mn}\,e^m_{\hat{k}}e^n_{\hat{j}}\right)_O$. The position of the observer changes with time, therefore this quantity is a function of T.

In $G_{\hat{0}\hat{0}}$, such an expansion is limited to the terms of order of $\varepsilon^2\,O_6$, thus the approximation $e^m_{\hat{k}} = \delta^m_{\hat{k}}$ is valid and $\hat{U}_{,\hat{k}\hat{j}} \simeq (U_{,kj})_O$. For $\vec{\Omega}_0$ the same holds true : $\left(\vec{\Omega}_0\right)^{\hat{k}} \simeq \left(\vec{\Omega}_0\right)^{k}$ (see expression 7). Therefore, one can identify the space vectors $\overrightarrow{e}_{\hat{k}}$ of the tetrad and the space vectors $\overrightarrow{\partial}_k$ of the natural basis associated to the geocentric coordinates. This would not be valid with an higher accuracy where terms smaller than $\varepsilon^2\,O_6$ are considered.

The change of the tetrad $u^\alpha_{(\sigma)} \longleftrightarrow e^\alpha_{\hat{\rho}}$ is just an ordinary change of basis in the space of the observer O. In this transformation, $d\hat{T}$, $G_{\hat{0}\hat{0}} = G_{(0)(0)}$, $G_{\hat{0}\hat{m}}dX^{\hat{m}} = G_{(0)(k)}dX^{(k)}$ and $G_{\hat{n}\hat{m}}dX^{\hat{m}}dX^{\hat{n}} = G_{(j)(k)}dX^{(j)}X^{(k)}$ behave as scalars.

As a consequence, we put forward that within the required accuracy, it is possible to give a simple description of the Hyper project with the Newtonian concept of space. It is now straightforward to calculate Ψ :

$$\Psi = 2\,\vec{a}\cdot\vec{X} - \hat{U}_{,(k)(j)}\,X^{(k)}X^{(j)} - \frac{1}{3}\hat{U}_{,(k)(j)(\ell)}\,X^{(k)}X^{(j)}X^{(\ell)}$$
$$-2\sum_{(k)}\left\{\left(\vec{\Omega}_0 + \vec{\Omega}_*\right)\wedge\vec{X}\right\}^{(k)} v_g^{(k)} + \varepsilon^2 O_6$$

Now we assume that any quantity can be known with an accuracy μ of order of $10^{-5} \lesssim O_1$. It means that the geometry of the experimental device is known with an accuracy of order of 10μm. The position of the point O on the trajectory of the satellite is known with an accuracy better than 70 m, the eccentricity can be controlled to be smaller than O_1, etc.

We consider that Ψ is the amount of two terms, Ψ_k and Ψ_u : the term Ψ_k can be modelled with the required accuracy while Ψ_u is unknown. The terms Ψ_k fulfills the condition $\mu\times\Psi_k \lesssim \varepsilon^2\,O_6$. With the previous orders of magnitude ($\varepsilon \sim O_{1/2} \sim 5\,10^{-3}$ and $\mu \sim O_1 \sim 2.5\,10^{-5}$) one finds

$$\Psi_u = 2\,\vec{a}\cdot\vec{X} - \hat{U}_{,(k)(j)}\,X^{(k)}X^{(j)} - 2\left\{\vec{\Omega}\wedge\vec{X}\right\}\cdot\overrightarrow{v}_g + \varepsilon^2 O_6/\mu$$

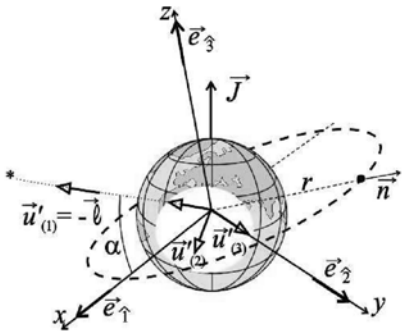

FIG. 2: The satellite and the fixed star.

$\hat{U}_{,(k)(j)}$ is obtained from the expression 1 of U limited to the monopolar and the quadrupolar terms and

$$\left(\vec{\Omega}\right)^{(k)} = \left(\vec{\Omega}_{LT} - \varpi\overrightarrow{\Lambda} - \overrightarrow{\Lambda} \wedge \frac{d\overrightarrow{v}}{dt}\right)^{(k)} + \frac{O_3}{r}$$

where $\vec{\Omega}_{LT}$ is obtained from 8 and $\frac{d\overrightarrow{v}}{dt} \simeq \overrightarrow{a} - \overrightarrow{\nabla}U \simeq \overrightarrow{a} + \frac{M_\oplus}{r^2}\overrightarrow{n}$.

B. Calculation of Ψ_u

We consider that the motion of the satellite is a Newtonian motion which takes place in the (x, y)-plane while the vector $\overrightarrow{\ell}$ lies in the (x, z)-plane. We assume that the eccentricity, e, does not exceed O_1.

We define

$$\begin{aligned} \vec{J} &= J_x\,\vec{e}_{\hat{1}} + J_y\,\vec{e}_{\hat{2}} + J_z\,\vec{e}_{\hat{3}}\,, \quad \vec{n} = \cos\theta\,\vec{e}_{\hat{1}} + \sin\theta\,\vec{e}_{\hat{2}} \\ -\vec{\ell} &= \cos\alpha\,\vec{e}_{\hat{1}} + \sin\alpha\,\vec{e}_{\hat{3}}\,, \quad \vec{w} = w_x\,\vec{e}_{\hat{1}} + w_y\,\vec{e}_{\hat{2}} + w_z\,\vec{e}_{\hat{3}} \end{aligned}$$

$\vec{J}$, $\vec{\ell}$ and $\vec{w}$ are constant vectors. The angle θ and the distance r depend on the time T.

First we define the special triad $\vec{u}'_{(n)}$:

$$\vec{u}'_{(1)} = \cos\alpha\,\overrightarrow{e}_{\hat{1}} + \sin\alpha\,\overrightarrow{e}_{\hat{3}}, \quad \vec{u}'_{(2)} = \sin\alpha\,\overrightarrow{e}_{\hat{1}} - \cos\alpha\,\overrightarrow{e}_{\hat{3}}, \quad \vec{u}'_{(3)} = \overrightarrow{e}_{\hat{2}}$$

Let us outline that we have defined $\left(\vec{u}'_{(1)}\right)^{\hat{k}} = -\left(\vec{\Lambda}\right)^{\hat{k}} + O_1$. Then, in order to obtain the final tetrad $u^{\alpha}_{(\sigma)}$, we perform an arbitrary rotation around $\vec{\Lambda}$:

$$\begin{array}{l} \vec{u}_{(1)} = -\vec{\Lambda} = \vec{u}'_{(1)} + O_1 \\ \vec{u}_{(2)} = \vec{u}'_{(2)}\cos\sigma + \vec{u}'_{(3)}\sin\sigma + O_1 \\ \vec{u}_{(3)} = -\vec{u}'_{(2)}\sin\sigma + \vec{u}'_{(3)}\cos\sigma + O_1 \end{array} \tag{13}$$

where $-\dfrac{d\sigma}{dT} = -\varpi$ is the angular velocity of the triad $\left\{\vec{u}_{(k)}\right\}$ relatively to $\left\{\vec{u}'_{(k)}\right\}$.

We can now assume that the experimental set-up is comoving with the triad $\vec{u}_{(n)}$ whose vector $\vec{u}_{(1)}$ points towards the fixed star.

In order to calculate the quadrupolar term in U, we define the unitary vector, $\overrightarrow{k}$ along the axi-symmetry axis. One obtains

$$U = \frac{M_{\oplus}}{r} - \frac{1}{2}J_2\frac{M_{\oplus}}{r}\left(\frac{R_{\oplus}}{r}\right)^2\left(3\left(\overrightarrow{k}\cdot\overrightarrow{n}\right)^2 - 1\right)$$

Therefore Ψ_u reads

$$\begin{array}{rll} \Psi_u = & -2\left(\left(\dfrac{\vec{J}}{r^3} - \dfrac{3\left(\vec{J}\cdot\vec{n}\right)}{r^3}\vec{n} + \dfrac{\alpha_1\, M_{\oplus}}{4\,r^2}\,\vec{n}\wedge\vec{w}\right)\wedge\vec{x}\right)\cdot\vec{v}_g & \left|\begin{array}{l} A \\ B \\ C \\ D \\ E \end{array}\right. \\ & -2\varpi\left(\vec{u}_{(1)}\wedge\vec{x}\right)\cdot\vec{v}_g & \\ & -2\dfrac{M_{\oplus}}{r^2}\left(\left(\vec{u}_{(1)}\wedge\vec{n}\right)\wedge\vec{x}\right)\cdot\vec{v}_g + 2\left(\left(\vec{u}_{(1)}\wedge\vec{a}\right)\wedge\vec{x}\right)\cdot\vec{v}_g & \\ & +\dfrac{M_{\oplus}}{r^3}\left(\vec{x}^2 - 3\left(\vec{n}\cdot\vec{x}\right)^2\right) + \dfrac{3}{2}J_2\dfrac{M_{\oplus}}{r^3}\left(\dfrac{R_{\oplus}}{r}\right)^2 Q & \\ & +2\,\vec{a}\cdot\vec{x} & \end{array} \tag{14}$$

with

$$\begin{array}{rcl} Q & = & \left(1 - 5\left(\overrightarrow{k}\cdot\overrightarrow{n}\right)^2\right)\overrightarrow{X}^{\,2} - 20\left(\overrightarrow{k}\cdot\overrightarrow{n}\right)\left(\overrightarrow{n}\cdot\overrightarrow{X}\right)\left(\overrightarrow{k}\cdot\overrightarrow{X}\right) \\ & & +5\left(7\left(\overrightarrow{k}\cdot\overrightarrow{n}\right)^2 - 3\right)\left(\overrightarrow{n}\cdot\overrightarrow{X}\right)^2 + 2\left(\overrightarrow{k}\cdot\overrightarrow{X}\right)^2 \end{array}$$

and

$$\overrightarrow{J} = J\,\overrightarrow{k}$$

In Ψ_u, the two terms $2\,\vec{a}\cdot\vec{X}$ and $-2\varpi\left(\vec{u}_{(1)}\wedge\overrightarrow{X}\right)\cdot\vec{v}_g$ are directly calculated in the local coordinates associated to the tetrad $u^{\alpha}_{(\sigma)}$ moreover, to

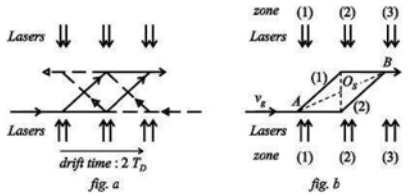

FIG. 3: An atomic Sagnac unit (ASU).

calculate the other quantities where $\vec{n}$ is involved, one can drop the terms of order O_1 in the expression of $\vec{u}_{(1)}$. The reason is that the quantities that we drop are either negligible or included in Ψ_k. Therefore, it is clear that we can consider the space as the ordinary space of Newtonian physics and that the usual formulae to change the basis $\overrightarrow{\partial}_k$ into $\overrightarrow{e}_{\hat{k}}$ or $\overrightarrow{u}_{(k)}$are valid.

In (14), the terms of lines A, B and C are due to various rotations : respectively the Lense-Thirring rotation, the spin around the view line of the star and the aberration. The term of line D gives the gravitational tidal effects (which are mainly due to the Earth) and the last term (line E) corresponds to some residual acceleration due to the fact that point O is not exactly in free fall.

It is now possible to calculate explicitly Ψ_u with the coordinates $X^{(k)}$, comoving with the experimental set-up [22].

V. THE EXPERIMENTAL SET-UP

A. The atomic Sagnac unit

An atomic Sagnac unit (ASU) is made of two counter-propagating atom interferometers which discriminate between rotation and acceleration (see figure 3-*a*).

Each interferometer is a so-called Ramsey-Bordé interferometer with a Mach-Zehnder geometry (figure 3-*b*). The atomic beam from a magneto-optical trap interacts three times with a laser field. In the first interaction zone the atomic beam is split coherently, by a Raman effect, into two beams which are redirected and recombined in the second and the third interaction zone.

The mass of the atom depends on its internal state, therefore it is not a constant along the different paths. However, the change of the mass is very small; it leads to negligible corrections on the main effects which is already very small. Considering cesium, we assume that the mass of the atom is a

constant $m = 133 \times 1.66 \times 10^{-27} = 2.2 \times 10^{-25}\,\mathrm{kg}$.

In this case the wave length of the lasers is $\lambda = 850\,\mathrm{nm}$. The momentum transferred to the atom during the interaction is $\frac{4\pi\hbar}{\lambda}$. The recoil of the atom results in a Sagnac loop which permits to measure the angular velocity of the set-up relatively to a local inertial frame. The device is also sensitive to the accelerations.

One can easily imagine that there are many difficulties to overcome if the Lense-Thirring effect is to be observed. In particular, the geometrical constraints appear to be crucial. In an ideal set-up the two interferometers are identical coplanar parallelograms with their center O_S and O'_S at the same point. One can consider several perturbation to this geometrical scheme.

1. A shift : O_S and O'_S are no longer at the same point;
2. A tilt : The plane of the two interferometers are now different;
3. A deformations : the interferometers are no longer identical lozenges, they are no longer parallelogram, even not plane interferometers.

The geometry of the device is fully determine by the interaction between the initial atomic beam and the lasers ; moreover the geometrical description is already an idealized model ; Therefore a full treatment of the atom-laser interaction in a gravitational field is obviously necessary to study the response of the ASU (see [9]). However the geometrical model is useful to give a physical intuition of the phenomena. In this context we study here the effect of a shift on the signal.

In the sequel we consider an ideal set-up where the beams are perfectly coherent and perfectly parallel, point O_S being a perfect center of symmetry for the atomic paths. We assume also that the two counter-propagating atom interferometers are identical and located in the same plane but that the separation of their center of symmetry, O_S and O'_S, is the vector $\vec{\delta} = \overrightarrow{O_S O'_S}$.

We will assume that the velocity, v_g, of the atoms is of the order of $20\,\mathrm{cm}\cdot\mathrm{s}^{-1}$ and that the size of the ASU is of order of 60 cm, therefore the drift time is $2T_D \sim 3\,\mathrm{s}$.

B. The phase differences

The configuration which is presently considered in the Hyper project is on figure 4.

We consider one among the four interferometers of the device above. Using the results of appendix A, we obtain the phase difference that we

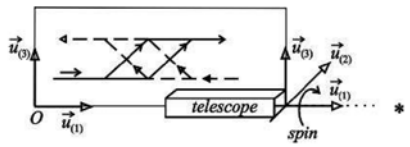

FIG. 4: The experimental set-up.

want to measure:

$$\delta\varphi = \frac{\omega}{2}\int_{t-2T_D/(2)}^{t} \psi\left(t'\right) dt' - \frac{\omega}{2}\int_{t-2T_D/(1)}^{t} \psi\left(t'\right) dt' \qquad (15)$$

The integrals are performed along path (2) and (1) of figure 3-*b*. The "angular frequency" ω is defined as $\dfrac{m\,c^2}{\hbar}$.

We consider that the origin is the center of symmetry O_S. The coordinates are $\overrightarrow{X} = \left\{X^{(k)}\right\}$. We define $\vec{v}_g = \dfrac{d\overrightarrow{X}}{dt}$ as the unperturbed group velocity of the atoms

We make use of the properties of the Newtonian trajectory :

$$r = \frac{r_0}{1+e\cos\theta},\ \vec{n} = \cos\theta\,\vec{e}_{\hat{1}} + \sin\theta\,\vec{e}_{\hat{2}},\ \frac{d\theta}{dT} = \Omega_S\left(1+e\cos\theta\right)^2$$

with $\Omega_S = \dfrac{M_\oplus}{r_0^2}$. We consider the case where the ellipticity, e, is much smaller than unity. Therefore, up to first order relatively to e, one obtains

$$\frac{1}{r} = \frac{1}{r_0}\left(1+e\cos\theta\right)\ ,\quad \theta \simeq \Omega_S\,t + \theta_0 + e\sin\left(\Omega_S\,t+\theta_0\right)$$

We assume $e \lesssim O_1$, therefore in the expression (14) of Ψ_u one can assume that $r = r_0$ is a constant because the corrections due to the eccentricity are included in Ψ_k.

During the flight time of an atom, one cannot consider that $\overrightarrow{n}$ remains a constant in expression (14). One can consider that the coordinate, $X = X^{(1)}$ of the atom is a function of the time: $X = v_g\left(T - T_0\right)$. Then $\overrightarrow{n} = \overrightarrow{n}_0 + \delta\overrightarrow{n}$ where $\overrightarrow{n}_0$ depends on T_0 only and $\delta\overrightarrow{n}$ on T_0 and X/v_g. Therefore, in expression (15), we expand the different terms relatively to X/v_g. Any of the correction can be included in Ψ_k except the first order correction, $\delta\psi_D$, of the first term in line D.

$$\delta\psi_D = -\frac{6M_\oplus}{r^4}\left(\overrightarrow{x}\cdot\frac{\overrightarrow{v}}{v_g}\right)\left(\overrightarrow{x}\cdot\overrightarrow{n}_0\right)x$$

The result of the integration is now straightforward. We change the notation : $\overrightarrow{n}_0 \to \overrightarrow{n}$ and $T_0 \to T$. In usual units one finds :

$$\left.\begin{array}{ll}
\delta\varphi = & -2\frac{mc}{\hbar\, r} S \left(\frac{\vec{J}}{r^2} - \frac{3\left(\vec{J}\cdot\vec{n}\right)}{r^2}\vec{n} + \frac{\alpha_1\, M_\oplus}{4\, r}\, \vec{n}\wedge\vec{w} \right)\cdot\vec{u}_{(2)} & A \\
& -2\frac{mc}{\hbar r} S \frac{M_\oplus}{r}\, \left(\vec{u}_{(1)}\wedge\vec{n}\right)\cdot\vec{u}_{(2)} - 2\frac{mc}{\hbar} S \left(\vec{u}_{(1)}\wedge\frac{\overrightarrow{a}}{c^2}\right)\cdot\vec{u}_{(2)} & C \\
& -\frac{4\pi\left(cT_D\right)^2}{\lambda}\left(\vec{u}_{(3)}\cdot\frac{\vec{a}_{O_S}}{c^2}\right) & E \\
& -\frac{mc}{2\,\hbar r} S \frac{\left(cT_D\right)^2}{r^2}\frac{M_\oplus}{r}\, \left(\left(\vec{u}_{(1)}\cdot\vec{n}\right)\left(\vec{u}_{(3)}\cdot\frac{\overrightarrow{v}}{c}\right) + \left(\vec{u}_{(3)}\cdot\vec{n}\right)\left(\vec{u}_{(1)}\cdot\frac{\overrightarrow{v}}{c}\right)\right) & F
\end{array}\right|$$

where $S = \dfrac{4\pi\hbar}{\lambda\, m} v_g T_D^2$ is the area of the Sagnac loop.

Line B in (14) gives no contribution because $\overrightarrow{X}$, $\vec{u}_{(1)}$ and $\overrightarrow{v}_g$ are in the same plane. The quadratic terms have disappeared because O_S is a center of symmetry.

The two interferometers of the same ASU are assumed to lie in the same plane but not necessarily with their center of symmetry O_S and O'_S at the same point. Therefore adding and subtracting the phase differences delivered by the two interferometers one finds the two basic quantities which are measured by the set-up *i.e.* :

$$\begin{aligned}
\mu_1 \;=\; & \frac{1}{2}\left(\delta\varphi' - \delta\varphi\right) = \frac{8\pi}{\lambda}\left(cT_D\right)^2 \left\{ \frac{M_\oplus}{r^2}\,\vec{u}_{(3)}\cdot\vec{n} + \vec{u}_{(3)}\cdot\overrightarrow{a} + \vec{\Omega}_{LT}\cdot\vec{u}_{(2)} \right\}\frac{v_g}{c} \\
& + \frac{2\pi\left(cT_D\right)^2}{\lambda}\left\{ \left(\frac{\vec{a}_{O_S}}{c^2} - \frac{\vec{a}_{O'_S}}{c^2}\right)\cdot\vec{u}_{(3)} \right\} \\
& - \frac{mc}{2\hbar}\frac{\left(cT_D\right)^2}{r^3} S \frac{M_\oplus}{r}\left(\left(\vec{u}_{(1)}\cdot\vec{n}\right)\left(\vec{u}_{(3)}\cdot\frac{\overrightarrow{v}}{c}\right) + \left(\vec{u}_{(3)}\cdot\vec{n}\right)\left(\vec{u}_{(1)}\cdot\frac{\overrightarrow{v}}{c}\right)\right) \\
\mu_2 \;=\; & \frac{1}{2}\left(\delta\varphi' + \delta\varphi\right) = -\frac{4\pi\left(cT_D\right)^2}{\lambda}\left\{ \frac{\overrightarrow{a}}{c^2}\cdot\vec{u}_{(3)} \right\}
\end{aligned}$$

where now $\overrightarrow{a} = \vec{a}_{O_S} + \vec{a}_{O'_S}$. In the expression above, we have dropped the term $-\dfrac{mc}{2\,\hbar r} S \dfrac{\left(cT_D\right)^2}{r^2}\dfrac{M_\oplus}{r}\dfrac{4\pi\hbar}{\lambda m v_g}\left(\vec{u}_{(3)}\cdot\vec{n}\right)\left(\vec{u}_{(3)}\cdot\overrightarrow{v}\right)$ because it can be included in Ψ_k.

$a^{(k)}_{O_S} u^\alpha_{(k)}$ is the 4-acceleration of point O_S. Therefore, one calculates $\left(\vec{a}_{O_S} - \vec{a}_{O'_S}\right)\cdot\vec{u}_{(3)} = -\hat{U}_{,(k)(3)} x^{(k)}_{O_S}$ where we have dropped the non significant terms which can be included in Ψ_k.

The quantities which can be measured are

$$\begin{aligned}
\mu_1 + 2v_g\mu_2 &= \frac{8\pi}{\lambda}\left(cT_D\right)^2\left\{\frac{M_\oplus}{r^2}\vec{u}_{(3)}\cdot\vec{n}+\vec{\Omega}_{LT}\cdot\vec{u}_{(2)}\right\}\frac{v_g}{c}\\
&-\frac{2\pi\left(cT_D\right)^2}{\lambda r}\frac{M_\oplus}{r}\left(\vec{u}_{(3)}\cdot\frac{\overrightarrow{\delta}}{r}-3\left(\vec{n}\cdot\vec{u}_{(3)}\right)\left(\vec{n}\cdot\frac{\overrightarrow{\delta}}{r}\right)\right)\\
&-\frac{2\pi}{\lambda}\left(cT_D\right)^2\left(\frac{v_gT_D}{r}\right)^2\frac{M_\oplus}{r^2}\left\{\left(\vec{u}_{(1)}\cdot\vec{n}\right)\left(\vec{u}_{(3)}\cdot\frac{\overrightarrow{v}}{c}\right)+\left(\vec{u}_{(3)}\cdot\vec{n}\right)\left(\vec{u}_{(1)}\cdot\frac{\overrightarrow{v}}{c}\right)\right\}\\
\mu_2 &= \frac{1}{2}\left(\delta\varphi'+\delta\varphi\right)=-\frac{4\pi\left(cT_D\right)^2}{\lambda}\left\{\frac{\overrightarrow{a}}{c^2}\cdot\vec{u}_{(3)}\right\}
\end{aligned}$$

where $\overrightarrow{\delta}=\overrightarrow{x}_{O'_S}-\overrightarrow{x}_{O_S}$.

C. Discussion

We define the projection, $\overrightarrow{J}_{//}$ of $\overrightarrow{J}$ on the plane of the orbit : $\overrightarrow{J}_{//}=J_{//}\left(\cos\theta_J\ \overrightarrow{e}_{\hat{1}}+\sin\theta_J\ \overrightarrow{e}_{\hat{2}}\right)$ and $\overrightarrow{w}_{//}=w_{//}\left(\cos\theta_w\ \overrightarrow{e}_{\hat{1}}+\sin\theta_w\ \overrightarrow{e}_{\hat{2}}\right)$. Going back to usual units (with $M_\oplus\simeq 4.4\,\mathrm{mm}$ and $J\simeq 145\,\mathrm{cm}^2$) we obtain

$$\begin{aligned}
\mu_1+2\frac{v_g}{c}\mu_2 &= \frac{2\pi\left(cT_D\right)^2}{\lambda r_0}\times\{K_0+K_\sigma+K_{2\sigma}+K_{2\theta}\\
&+K_{\theta-\sigma}+K_{\theta+\sigma}+K_{2\theta-\sigma}+K_{2\theta+\sigma}+K_{2\theta-2\sigma}+K_{2\theta+2\sigma}\}
\end{aligned}$$

with

$$\begin{aligned}
K_0 &= \frac{M_\oplus}{4\,r_0}\left(3\sin^2\alpha-1\right)\times\frac{\delta^{(3)}}{r_0}\\
K_\sigma &= \frac{v_g}{c}\left\{\left[(1-\sin\alpha)\cos\left(\sigma+\theta_J\right)-(1+\sin\alpha)\cos\left(\sigma-\theta_J\right)\right]\times\frac{J_{//}}{r_0^2}\right.\\
&\left.-4\cos\alpha\,\cos\sigma\times\frac{J^{\hat{3}}}{r_0^2}\right\}-\frac{3M_\oplus}{2r_0}\cos\alpha\sin\alpha\sin\sigma\times\frac{\delta^{(1)}}{r_0}\\
K_{2\sigma} &= \frac{3M_\oplus}{4r_0}\left(1-\sin^2\alpha\right)\left[\sin\left(2\sigma\right)\times\frac{\delta^{(2)}}{r_0}+\cos\left(2\sigma\right)\times\frac{\delta^{(3)}}{r_0}\right]\\
K_{2\theta} &= -\frac{3M_\oplus}{4r_0}\left(1-\sin^2\alpha\right)\cos\left(2\theta\right)\times\frac{\delta^{(3)}}{r_0}
\end{aligned}$$

$$
\begin{aligned}
K_{\theta-\sigma} &= \frac{M_\oplus}{r_0}\frac{v_g}{c}\times\{-2\,(1+\sin\alpha)\,\sin(\theta-\sigma)\\
&\quad+\frac{\alpha_1}{2}\cos\alpha\,\sin(\theta-\sigma-\theta_w)\times\frac{w_{\shortparallel}}{c}\\
&\quad+\frac{\alpha_1}{2}\,(1+\sin\alpha)\sin(\theta-\sigma)\times\frac{w^3}{c}\Big\}\\
K_{\theta+\sigma} &= \frac{M_\oplus}{r_0}\frac{v_g}{c}\times\{-2\,(1-\sin\alpha)\,\sin(\theta+\sigma)\\
&\quad+\frac{\alpha_1}{2}\cos\alpha\,\sin(\theta+\sigma-\theta_w)\times\frac{w_{\shortparallel}}{c}\\
&\quad-\frac{\alpha_1}{2}\,(1-\sin\alpha)\sin(\theta+\sigma)\times\frac{w^3}{c}\Big\}
\end{aligned}
$$

$$
\begin{aligned}
K_{2\theta-\sigma} &= -3\frac{v_g}{c}\,(1+\sin\alpha)\cos(2\theta-\sigma-\theta_J)\times\frac{J_{\shortparallel}}{r_0^2}\\
&\quad+\frac{3M_\oplus}{4r_0}\cos\alpha\,(1+\sin\alpha)\sin(2\theta-\sigma)\times\frac{\delta^{(1)}}{r_0}\\
&\quad-\left(\frac{M_\oplus}{r_0}\right)^{3/2}\frac{cv_gT_D^2}{2\,r_0^2}\,(1+\sin\alpha)\cos(2\theta-\sigma)\\
K_{2\theta+\sigma} &= 3\frac{v_g}{c}\,(1-\sin\alpha)\cos(2\theta+\sigma-\theta_J)\times\frac{J_{\shortparallel}}{r_0^2}\\
&\quad+\frac{3M_\oplus}{4r_0}\cos\alpha\,(1-\sin\alpha)\sin(2\theta+\sigma)\times\frac{\delta^{(1)}}{r_0}\\
&\quad-\left(\frac{M_\oplus}{r_0}\right)^{3/2}\frac{cv_gT_D^2}{2\,r_0^2}\,(1-\sin\alpha)\cos(2\theta+\sigma)
\end{aligned}
$$

$$
\begin{aligned}
K_{2\theta-2\sigma} &= \frac{3M_\oplus}{8\,r_0}\,(1+\sin\alpha)^2\left\{\sin(2\theta-2\sigma)\times\frac{\delta^{(2)}}{r_0}-\cos(2\theta-2\sigma)\times\frac{\delta^{(3)}}{r_0}\right\}\\
K_{2\theta+2\sigma} &= -\frac{3M_\oplus}{8\,r_0}\,(1-\sin\alpha)^2\left\{\sin(2\theta+2\sigma)\times\frac{\delta^{(2)}}{r_0}+\cos(2\theta+2\sigma)\times\frac{\delta^{(3)}}{r_0}\right\}
\end{aligned}
$$

Each of these terms, except K_0, has a specific frequency. These terms can be measured and distinguished from each other.

The Lense-Thirring effect due to the angular momentum of the Earth appears in the terms K_σ and $K_{2\theta\pm\sigma}$ while the possible existence of a preferred frame appears in $K_{\theta\pm\sigma}$ which depends on the components of $\alpha_1\overrightarrow{w}$.

The signal due to the Lense-Thirring effect is associated with the signal due to $\delta^{(1)}$. The two signals display the same order of magnitude when $\delta^{(1)}\sim 1\,\mathrm{nm}$. Today, it seems impossible to achieve such a precision, this is

the reason why $\delta^{(1)}$ should be calculated from the Fourier analysis of the signal itself, altogether with the angular momentum of the Earth, $\overrightarrow{J}$ and the velocity $\alpha_1 \overrightarrow{w}$.

If the sensitivity to measure the Lense-Thirring effect with an accuracy of 20% is achieved, it should be possible to know $\alpha_1 \overrightarrow{w}$ with an accuracy better than 10^{-7}. Considering that $\overrightarrow{w}$ is the velocity of the rest frame of the Universe ($\|\overrightarrow{w}\| \sim 10^{-3}$) it would give precision on α_1 of order of 10^{-4}.

The interest of the spin is obvious. If $\sigma = cte$ (no spin) the signal is the sum of two periodic signals with frequency ν_O and $2\nu_O$ where ν_O is the orbital frequency of the satellite ; therefore one ASU gives two informations (two functions of the time). When the satellite spins, we get 9 functions of the time t. The information is much more important in this case.

VI. CONCLUSION

In this paper we have sketched a method to take into account the residual gravitation in a nearly free falling satellite, namely the tidal and higher order effects. We have shown that these effects are not negligible in highly accurate experiments.

We have shown that many perturbations must be considered if one wants to observe the Lense-Thirring effect and we have exhibited the various terms that one needs to calculate in order to obtain the full signal.

Compared with GPB, the principle of the measure is not the same, the difficulties are quite different but the job is not easier. For instance, considering the quantities K_σ or $K_{2\theta\pm\sigma}$ above, one can check that $\delta^{(1)}$ must remain smaller than 2 nm for the corresponding signal to remain smaller than the Lense-Thirring one. It does not seem that such a precision can be controlled in the construction of the experimental device itself. It is therefore necessary to measure $\delta^{(1)}$ with such an accuracy.

In the problem that we have considered, there are 9 unknown parameters : i) the three component of $\overrightarrow{J}$, ii) the three components of $\alpha_1 \overrightarrow{w}$ and iii) the three components of $\overrightarrow{\delta}$. On the other hand, the experimental set-up displays 9 periodic functions but the distribution of the unknown parameters among the 9 functions happen in such way that the four parameters $\overrightarrow{J}$ and $\delta^{(1)}$ are present in the 3 functions K_σ or $K_{2\theta\pm\sigma}$ and the three parameters $\alpha_1 \overrightarrow{w}$ in the two functions $K_{\theta\pm\sigma}$. Only the two parameters $\delta^{(2)}$ and $\delta^{(3)}$ are over determined by the four functions $K_{2\theta}$, $K_{2\sigma}$ and $K_{2\theta\pm2\sigma}$.

Let us assume that θ and σ are known function of the time (frequency and phase). This implies that in the geometric scheme that we have explored, one can determine 18 unknown parameters. Therefore $\overrightarrow{J}$, $\overrightarrow{\delta}$ and $\alpha_1 \overrightarrow{w}$ can be known and the Lense-Thirring effect can be observed with an accuracy

of a few tens percent. The same sensitivity on the phase difference of matter waves in the interferometers yields an accuracy of 10^{-7} on $\alpha_1 \overrightarrow{w}$ which would increase our knowledge on α_1 by one order of magnitude. This optimistic conclusion must be tempered with the remark that only the shift has been considered here while several other geometrical perturbations play their role. Moreover a crucial point is the knowledge of the phase of the various periodic functions K. The geometric scheme fails to describe the change of the phase of the atomic wave when it goes through the laser beam and we believe that the preceding conclusion holds only in the case where the change of the phase along the two paths differs by a constant.

As a conclusion, we put forward that only a more powerful model can answer the question of the theoretical feasibility. This model should take into account all the gravitational perturbations that we have outlined here and it should consider the interaction between laser fields and matter waves in more a realistic manner.

APPENDIX A: THE GRAVITATIONAL PHASE SHIFTS

Let us assume that space time is quasi Minkowskian. Therefore, the metric is: $ds^2 = (\eta_{\alpha\beta} + h_{\alpha\beta})\, dx^\alpha dx^\beta$ with $|h_{\alpha\beta}| << 1$.

Let us consider, at the eikonal approximation, a wave which propagates from the point A to a point B. The phase at point A is known. It is $\varphi_A(t) = \omega t$ where ω is a constant and $t = x^0/c$ the time. The phase, $\varphi_B(t)$, at point B is the amount of the unperturbed phase, $\overset{\circ}{\varphi}_B(t)$, and the perturbation $\delta\varphi_B$ due to the term $h_{\alpha\beta}$ in the metric.

Two different cases are relevant for the problem that we study

1. Point A is a far away, fixed, star. It is the source of a light wave. From the knowledge of $\varphi_B(t)$ at every point B one can deduce the apparent direction of the star. Then it becomes possible to determine the vector $-L^\alpha$ which points towards A.

2. Point A is the source of an atomic wave which enters a matter wave interferometer. At point B interferences are observed on a detector (figure 3-*b*). The phases $\varphi_{B1}(t)$ and $\varphi_{B2}(t)$, of the waves which interfere at point B depend on the path, (1) or (2), that each wave has followed. The response of the detector at point B depends on the difference $\varphi_{B1}(t) - \varphi_{B2}(t)$. Therefore one can obtain the response of the interferometer once the phases $\varphi_{B1}(t)$ and $\varphi_{B2}(t)$ are known.

In order to calculate the phase $\varphi_B(t)$ at point B and time t we use the method developed in [12]. We summarize briefly the method for particles of mass m (for the light $m = 0$).

First we neglect the perturbation and we consider a point M which moves at the group velocity, v_g^k, and arrives at point B at time t. The worldline of M is $x^k = x^k(t')$ with $v_g^k = dx^k/dt'$ and $x^k(t) = x_B^k$. The point M has left A at time t_A such as $x^k(t_A) = x_A^k$. The time t_A is a function of t.

Now we define $\Psi = h_{00} + 2h_{0k}v_g^k + h_{kj}v_g^k v_g^j$ where Ψ is calculated at point M. Therefore Ψ is a function of t'.

One can prove that the perturbation $\delta\varphi_B$ is

$$\delta\varphi_B = \frac{\omega}{2}\int_{t_A}^{t} \Psi(t')\,dt'$$

where $\hbar\,\omega$ is the energy of the particle.

APPENDIX B: DEFLECTION OF THE LIGHT DUE TO THE QUADRUPOLAR TERMS OF THE EARTH

The Newtonian potential to be considered is

$$U = \frac{M_\oplus}{r}\left(1 - J_2\left(\frac{R_0}{r}\right)^2 P_2\right)$$

where $P_2 = \frac{1}{2}\left(3\cos^2\theta - 1\right)$. The unitary vector $\overrightarrow{k}$ defines the axi-symetry axis and $\cos\theta = \dfrac{\vec{k}\cdot\vec{r}}{r}$. The quadrupole contribution is due to the term $-J_2\dfrac{M_\oplus}{r}\left(\dfrac{R_0}{r}\right)^2 P_2$.

$$\delta\varphi = -\frac{\omega M_\oplus}{4}J_2 R_0^2\int_{-\infty}^{0}\left(3\frac{\left(\overrightarrow{r}'\cdot\overrightarrow{k}\right)^2}{r'^5} - \frac{1}{r'^3}\right)ds$$

where $\vec{x}_M(t') = \overrightarrow{r}' = \vec{x}_B + s\vec{\ell}$. Here s is $t' - t$, it varies from $s_A = -\infty$ (when A is far away) to $s_B = 0$ at point B.

We calculate the gradient of $\delta\varphi$ at point B the coordinates of which are $\overrightarrow{r} = \left\{x_B^k\right\}$:

$$\begin{aligned}
\overrightarrow{\nabla}\delta\varphi &= -\frac{\omega M_\oplus}{4}J_2 R_0^2\,\vec{Q} \text{ with} \\
\vec{Q} &= 6\vec{k}\int_{-\infty}^{0}\frac{\left(\overrightarrow{r}'\cdot\overrightarrow{k}\right)}{r'^5}ds - 15\,\overrightarrow{r}\int_{-\infty}^{0}\frac{\left(\overrightarrow{r}'\cdot\overrightarrow{k}\right)^2 ds}{r'^7} + 3\overrightarrow{r}\int_{-\infty}^{0}\frac{ds}{r'^5}
\end{aligned}$$

Each of these integral can be exactly computed. The deviation of the light ray is $\Delta\vec{\ell} = \frac{1}{\omega}\vec{\nabla}\delta\varphi$. We can eliminate some components parallel to $\vec{\ell}$ which would in any case disappear in the normalization procedure. One finds

$$\begin{aligned}
\delta\vec{\ell} &= -\frac{M_\oplus}{4r} J_2 \left(\frac{R_0}{r}\right)^2 \frac{a\,\vec{k} + b\,\vec{n}}{\left(1 - \vec{n}\cdot\vec{\ell}\right)^3} \text{ with} \\
a &= 2\left(\vec{n}\cdot\vec{k}\right)\left(\vec{n}\cdot\vec{\ell}\right)^2 \\
&\quad -6\left(\vec{n}\cdot\vec{k}\right)\left(\vec{n}\cdot\vec{\ell}\right) + 2\left(\vec{\ell}\cdot\vec{k}\right)\left(\vec{n}\cdot\vec{\ell}\right) \\
&\quad +4\left(\vec{n}\cdot\vec{k}\right) - 2\left(\vec{\ell}\cdot\vec{k}\right) \\
b &= -3\left(\vec{n}\cdot\vec{k}\right)^2\left(\vec{n}\cdot\vec{\ell}\right)^2 + 9\left(\vec{n}\cdot\vec{k}\right)^2\left(\vec{n}\cdot\vec{\ell}\right) \\
&\quad -2\left(\vec{n}\cdot\vec{k}\right)\left(\vec{\ell}\cdot\vec{k}\right)\left(\vec{n}\cdot\vec{\ell}\right) + \left(\vec{n}\cdot\vec{\ell}\right)^2 - 8\left(\vec{n}\cdot\vec{k}\right)^2 \\
&\quad -2\left(\vec{\ell}\cdot\vec{k}\right)^2 + 6\left(\vec{n}\cdot\vec{k}\right)\left(\vec{\ell}\cdot\vec{k}\right) - 3\left(\vec{n}\cdot\vec{\ell}\right) + 2
\end{aligned}$$

where $r = \sqrt{\vec{r}^2}$ and $\vec{n} = \vec{r}/r$.

When $\vec{\ell}$ is orthogonal to the orbit, the maximum of $\left\|\delta\vec{\ell}\right\|$ is $\frac{M_\oplus}{r} J_2 \left(\frac{R_0}{r}\right)^2 \sim 2\,10^{-3} O_2$ on a polar orbit of radius $r \sim 7000\,\text{km}$.

---

[1] E. Rasel *et al.*, *ESA Assessment Study Report* (ESA-SCI, 2000).
[2] C. Jentsch, T. Muellerand, S. Chelkowski, E. Rasel, and W. Ertmer, Verhanal DPG (VI) **38**, 167 (2003).
[3] M. Oberthaler, S. Bernet, E. Rasel, J. Schmiedmayer, and A. Zeilinger, Phys. Rev. A **54**, 3165 (1996).
[4] T. Gustavson, A. Landragin, and M. Kasevich, Class. Quantum Grav. **17**, 2385 (2000).
[5] Y. Le Coq, J. Thywissen, S. Rangwala, F. Gerbier, R. Richard, G. Delannoy, P. Bouyer, and A. Aspect, Phys. Rev. Lett. **87**, 170403 (2001).
[6] M. Snadden, J. McGuirk, P. Bouyer, K. Haritos, and M. Kasevich, Phys. Rev. Lett. **81**, 971 (1998).
[7] W.-T. Ni and M. Zimmermann, Phys. Rev. D **17**, 1473 (1978).
[8] W.-Q. Li and W.-T. Ni, J. Math. Phys. **20**, 1473 (1979).
[9] C. Antoine and C. Bordé, J. Opt. B **5**, S199 (2003).
[10] C. Will, *Theory and experiment in gravitational physics* (Cambridge University Press, 1981).

[11] C. Marchal, Bulletin du Muséum National d'Histoire Naturelle 4ème série section C **18**, 517 (1996).
[12] B. Linet and P. Tourrenc, Can. J. Phys. **54**, 1129 (1976).
[13] J. Ibáñez, Astron. Astrophys. **124**, 175 (1983).
[14] P. Touboul and M. Rodrigues, Class. Quantum Grav. **18**, 2487 (2001).
[15] A. Nobili, D. Bramanti, and G. Comandi *et al.*, New Astron. **8**, 371 (2003).
[16] MICROSCOPE [14] is a CNES mission designed to compare the motion of two free falling macroscopic masses in order to check the equivalence principle. It has been decided and should be launched in not too far a future (except for any possible delay!). Several other "classical" and more ambitious projects are also considered *i.e.* STEP (for more details, see e.g. : einstein.stanford.edu/STEP/index.html) and Galileo Galilei [15]
[17] Lense-Thirring effect originates in the diurnal rotation of the Earth. It results in an angular velocity that a gyroscope, pointing towards a far away star, can measure. Lense-Thirring angular velocity depends on the position of the satellite. GPB (Gravity Probe B; for more details, see e.g. : einstein.stanford.edu) is a NASA project designed to measure the secular precession of a mechanical gyroscope due to Lense-Thirring effect. It has been carefully studied for many years at Stanford University, it is now expected to be launched in a near future.
[18] Both fields are called "gravitational fields" in the sequel.
[19] An arbitrary constant can always be added to U_*. It is chosen in such a way that zero is the mean value of U_* at point O in the satellite.
[20] It does not mean that each g_{0k} fulfills the relation but that the terms g_{0k} are not all negligible compared to $750\, O_4$.
[21] The Thomas term reads $\vec{\Omega}_{Th} = \frac{1}{2}\vec{v} \wedge \vec{A}$ where $\vec{A}$ is the "acceleration". From the relativistic point of view, it would be better to define the Thomas term with the local physical acceleration, $\vec{A} \simeq \frac{d\vec{v}}{dt} - \vec{\nabla}U$, rather than the acceleration, $\frac{d\vec{v}}{dt}$, relatively to the geocentric frame.
[22] Let us emphasize that the de Sitter and the Thomas angular velocities are not involved in Ψ_u but in Ψ_K.

Tidal gravitational effects in a satellite

Tourrenc Ph, Angonin M-C, Ovido X, 2004, General Relativity and Gravitation, vol. **36**, Issue 10, 2237

Tidal gravitational effects in a satellite.

Ph. Tourrenc, M-C. Angonin, and X. Ovido
Université P. et M. Curie
ERGA, case 142
4, place Jussieu
F-75252 Paris CEDEX 05, France
(Dated: July 26, 2004)

Atomic wave interferometers are tied to a telescope pointing towards a faraway star in a nearly free falling satellite. Such a device is sensitive to the acceleration and the rotation relatively to the local inertial frame and to the tidal gravitational effects too.

We calculate the rotation of the telescope due to the aberration and the deflection of the light in the gravitational field of a central mass (the Earth and Jupiter). Within the framework of a general parametrized description of the problem, we discuss the contributions which must be taken into account in order to observe the Lense-Thirring effect.

Using a geometrical model, we consider some perturbations to the idealized device and we calculate the corresponding effect on the periodic components of the signal.

Some improvements in the knowledge of the gravitational field are still necessary as well as an increase of the experimental capabilities ; however our conclusions support a reasonable optimism for the future.

Finally we put forward the necessity of a more complete, realistic and powerful model in order to obtain a definitive conclusion on the feasibility of the experiment as far as the observation of the Lense-Thirring effect is involved.

I. INTRODUCTION

Clocks, accelerometers and gyroscopes based on cold atom interferometry are already among the best which have been constructed until now and further improvements are still expected. With the increase of the experimental capabilities it becomes necessary to consider more and more small effects in order to account for the signal, therefore (relativistic) gravitation has to be considered in any highly sensitive experiments, no matter what they are designed for.

The performances of laser cooled atomic devices is limited on Earth by gravity. Further improvements demand now that new experiments take place in free falling (or nearly free falling) satellites. A laser cooled atomic clock, named PHARAO, will be a part of ACES (Atomic Clock Ensemble in Space), an ESA mission on the ISS. Various other experimental possibilities involving "Hyper-precision cold atom interferometry in space" are presently considered. They might result in a project (called "Hyper") in the future [1].

The aim of the present paper is to hold the bookkeeping of the various gravito-inertial effects in a nearly free falling satellite. For this purpose we consider the most ambitious goal which has been considered for Hyper *i.e.* the measurement of the Lense-Thirring effect.

The Lense-Thirring effect is a local rotation of a gyroscope relatively to a telescope pointing towards a far away star. It is a relativistic consequence of the diurnal rotation of the Earth which "drags the inertial frames" in its neighborhood.

The angular velocity of the telescope relative to the gyroscopes depends on the position. Therefore, in a satellite, it is a function of the time. In Hyper, the angular velocity is measured by atomic-wave-gyroscopes and its time dependence is analyzed [9]. The consequence is that the device is sensitive to the variation of the gravitation in the satellite and no to the gravitation itself. We do not believe that it is easy to achieve the required stabilization of the gravitational field due to the local masses but it is not impossible in principle. For this reason we will study only the tidal field of far away masses whose effect cannot be removed at all.

The parameter which plays a role in the calculation of the Lense-Thirring effect is the angular momentum of the central mass. It is much bigger for Jupiter than the Earth. Therefore we will discuss both cases, without any consideration on the cost of the corresponding missions.

In the sequel the greek indices run from 0 to 3 and the Latin indices from 1 to 3. We use the summation rule of repeated indices (one up and one down).

The Minkowski tensor is $\eta_{\alpha\beta} = diag\,[1, -1, -1, -1]$; its inverse is $\eta^{\alpha\beta}$.

We use geometrical units where $c = G = 1$.

II. THE LOCAL EXPERIMENT IN A SATELLITE

In the satellite, the experimental set-up consists in a telescope pointing towards a far away star in the $\overrightarrow{u}_{(1)}$ direction and two orthogonal atomic Sagnac units in the planes $\left[\overrightarrow{u}_{(3)}, \overrightarrow{u}_{(1)}\right]$ and $\left[\overrightarrow{u}_{(2)}, \overrightarrow{u}_{(1)}\right]$ of fig. 1.

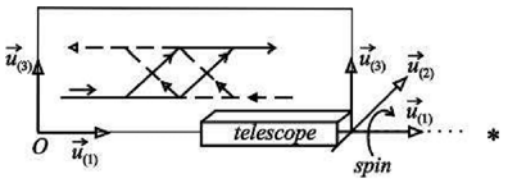

FIG. 1: The experimental setup.

A. The atomic Sagnac unit

An atomic Sagnac unit (ASU) is made of two counter-propagating atom interferometers which discriminate between rotation and acceleration (see figure 2-a).

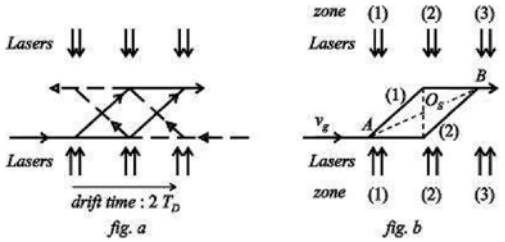

FIG. 2: An atomic Sagnac unit (ASU).

Each interferometer is a so-called Ramsey-Bordé interferometer with a Mach-Zehnder geometry (figure 2-b). The atomic beam from a magneto-optical trap interacts three times with a laser field. In the first interaction zone the atomic beam is split coherently, by a Raman effect, into two beams which are redirected and recombined in the second and the third interaction zone.

The mass of the atom depends on its internal state, therefore it is not a constant along the different paths. However, the change of the mass is very small; it leads to negligible corrections on the main effects which is already very small. In the case of the cesium, the mass is $m = 133 \times 1.66 \times 10^{-27} = 2.2 \times 10^{-25}$kg and the wave length of the lasers is $\lambda = 850$nm. The momentum transferred to the atom during the interaction is $\frac{4\pi\hbar}{\lambda}$. The recoil of the atom results in a Sagnac loop which permits to measure the angular velocity of the set-up relatively to a local inertial frame. The device is also sensitive to the accelerations.

In an ideal set-up the two interferometers are identical coplanar parallelograms with their center O_S and O'_S at the same point but many perturbations have to be considered. The geometry of the device is actually determined by the interaction between the initial atomic beam and the lasers ; Therefore a full treatment of the atom-laser interaction in a gravitational field is obviously necessary to study the response of the Atomic Sagnac Unit (ASU). However the geometrical model is useful to give a

physical intuition of the phenomena. In this context we assume that the two interferometers remain idealized identical parallelograms but that O_S and O'_S are no longer at the same point : This is the only perturbation that we consider here. It is sufficient to take the flavor of the gravitational perturbations which have to be taken into account and, more generally, of the difficulty inherent to such an experiment.

B. The phase difference

Let us assume that the fundamental element is known in some coordinates comoving with the experimental set-up :

$$\begin{aligned} ds^2 &= \left(1 + K_{(0)(0)}\right) dT^2 + 2K_{(0)(k)} dT dX^{(k)} \\ &\quad + \left(\eta_{(k)(j)} + K_{(k)(j)}\right) dX^{(k)} dX^{(j)} \end{aligned} \tag{1}$$

In order to calculate up to first order the gravitational perturbation of the phase due to $K_{(\alpha)(\beta)}$, we use a method which we summarize now [2].

First we calculate the quantity Ψ :

$$\Psi = K_{(0)(0)} + 2K_{(0)(k)} v_g^{(k)} + K_{(k)(j)} v_g^{(k)} v_g^{(j)} \tag{2}$$

where $v_g^{(k)}$ is the velocity of the atoms (*i.e.* the unperturbed group velocity).

The quantity Ψ is a function of the time and the position of the atom.

Then we consider an atom which arrives at time t at point B of figure 2-b . Now the position is a function of the time t' only because t is considered as a given quantity. The function Ψ is a function of the time, t', only. The phase difference is

$$\delta\varphi = \frac{\omega}{2} \int_{t-2T_D/(2)}^{t} \Psi\left(t'\right) dt' - \frac{\omega}{2} \int_{t-2T_D/(1)}^{t} \Psi\left(t'\right) dt' \tag{3}$$

The integrals are performed along path (2) and (1) of the interferometer (figure 2-b). The "angular frequency" ω is defined as $\dfrac{m\,c^2}{\hbar}$.

C. The local metric

In order to calculate $\delta\varphi$, we must know the local metric $G_{(\alpha)(\beta)} = \eta_{(\alpha)(\beta)} + K_{(\alpha)(\beta)}$.

We choose an origin, O, in the satellite and at point O a tetrad $\left\{u^\alpha_{(0)}, u^\alpha_{(1)}, u^\alpha_{(2)}, u^\alpha_{(3)}\right\}$ where $u^\alpha_{(0)}$ is the 4-velocity of point O and where

the three vectors $\left\{u^{\alpha}_{(k)}\right\} = \left\{0, \overrightarrow{u}_{(k)}\right\}$ are represented on the figure 1. The vectors of the tetrad are orthogonal : $u^{\alpha}_{(\mu)} u_{\alpha(\sigma)} = \eta_{(\mu)(\sigma)}$. The coordinate indices, α, β, σ, etc, are lowered or raised by the means of the metric tensor, $g_{\alpha\beta}$ or $g^{\alpha\beta}$; the Minkowski indices are raised or lowered with the Minkowski metric or its inverse, $\eta_{\alpha\beta}$ or $\eta^{\alpha\beta}$. An Einstein indice, α, can be changed into a Minkowski indice (ρ), by the means of the tetrad and vice versa : $u^{\alpha}_{(\rho)} \left(\ \right)_{\alpha} = \left(\ \right)_{(\rho)}$ and $u^{\alpha}_{(\rho)} \left(\ \right)^{(\rho)} = \left(\ \right)^{\alpha}$.

The tetrad is the natural basis at point O of comoving coordinates $X^{(\alpha)}$. The proper time at the origin is $X^{(0)}$. The space coordinates are the $X^{(k)}$.

Once the origin and the tetrad are chosen, the metric at point M and time t is expanded relatively to the space coordinates of M [3].

$$ds^2 = G_{(\alpha)(\beta)}\, dX^{(\alpha)} dX^{(\beta)} \quad \text{with} \tag{4}$$

$$\begin{aligned} G_{(0)(0)} &= 1 + 2\,\vec{a}\cdot\vec{X} + \left(\vec{a}\cdot\vec{X}\right)^2 - \left(\vec{\Omega}\times\vec{X}\right)^2 - R_{(0)(k)(0)(j)}\, X^{(k)} X^{(j)} \\ &\quad -\frac{1}{3} R_{(0)(k)(0)(j),(\ell)} X^{(k)} X^{(j)} X^{(\ell)} + ... \qquad (5) \\ G_{(0)(m)} &= \Omega_{(m)(k)}\, X^{(k)} - \frac{2}{3} R_{(0)(k)(m)(j)}\, X^{(k)} X^{(j)} \\ &\quad -\frac{1}{4} R_{(0)(k)(m)(j),(\ell)} X^{(k)} X^{(j)} X^{(\ell)} + .. \\ G_{(n)(m)} &= \eta_{(n)(m)} - \frac{1}{3} R_{(n)(k)(m)(j)} X^{(k)} X^{(j)} \\ &\quad -\frac{1}{6} R_{(n)(k)(m)(j),(\ell)} X^{(k)} X^{(j)} X^{(\ell)} + ... \end{aligned}$$

where we have used vector notations *i.e.* $\overrightarrow{a}$ for $\left\{a^{(\ell)}\right\}$, $\overrightarrow{a}\cdot\overrightarrow{X}$ for $\sum a^{(\ell)} X^{(\ell)}$, etc. Every quantity, except the space coordinates $X^{(\ell)}$, are calculated at point O. Thus they are functions of the time $T = X^{(0)}$.

$R_{(\alpha)(\beta)(\sigma)(\mu)}$ is the Riemann tensor obtained from $R_{\alpha\beta\sigma\mu}$ at point O :

$$R_{\alpha\beta\sigma\mu} = \Gamma_{\alpha-\beta\mu,\sigma} - \Gamma_{\alpha-\beta\sigma,\mu} + \Gamma^{\varepsilon}_{\beta\sigma}\Gamma_{\varepsilon-\alpha\mu} - \Gamma^{\varepsilon}_{\beta\mu}\Gamma_{\varepsilon-\alpha\sigma} \tag{6}$$

where $\Gamma_{\alpha-\beta\mu,\sigma}$ is the Christoffel symbol.

$\Omega_{(j)(k)}$ is the antisymmetric quantity

$$\begin{aligned} \Omega_{(j)(k)} &= \frac{1}{2}\left(g_{(0)(j),(k)} - g_{(0)(k),(j)}\right)_O \qquad (7) \\ &\quad + \frac{1}{2}\left(\left(u^{\beta}_{(j)}\,\frac{du^{\alpha}_{(k)}}{ds} - \frac{du^{\beta}_{(j)}}{ds}\,u^{\alpha}_{(k)}\right) g_{\alpha\beta}\right)_O \end{aligned}$$

Due to the antisymmetry of $\Omega_{(m)(k)}$, the quantity $\Omega_{(m)(k)}\, X^{(k)} dX^{(m)}$ which is present in the expression of ds^2 can be written as $\Omega_{(m)(k)}\, X^{(k)} dX^{(m)} = \left(\overrightarrow{\Omega}_0 \wedge \overrightarrow{X}\right) \cdot d\overrightarrow{X}$. The space vector $\overrightarrow{\Omega}_0$ is the physical angular velocity. It is measured by gyroscopes tied to the three space orthonormal vectors $u^{\alpha}_{(k)}$:

The vector $\overrightarrow{a}$ is the physical acceleration which can be measured by an accelerometer comoving with O. It is the spatial projection at point O of the 4-acceleration of point O.

At point O ($i.e.$ $\overrightarrow{X} = \overrightarrow{0}$) the time T is the proper time delivered by an ideal clock comoving with O.

III. FROM THE GEOCENTRIC COORDINATES TO THE COMOVING COORDINATES

A. The geocentric coordinates

We define the time coordinate $x^0 = ct$ and the space coordinates x^k. We use the notations $\vec{r} = \left\{x^k\right\} = \{x, y, z\}$ and we define the spherical coordinates $\{r, \theta, \varphi\}$, $i.e.$ $x = r\sin\theta\,\cos\varphi\,,\ \ y = r\sin\theta\,\sin\varphi\,,\ \ z = r\cos\theta$.

We consider a satellite and a point O which is the origin of the local coordinates in the satellite. We assume that the position of O is given by its three space coordinates, $\vec{r} = \{x, y, z\} = \left\{x^k\right\}$, considered as three known functions of the coordinate time, t. Then we define the velocity of point O as $\overrightarrow{v} = \dfrac{d\vec{r}}{dt}$.

The proper time at point O is $s = T = X^{(0)}$. The motion of O can be described as well by the four functions $x^{\alpha} = x^{\alpha}(s)$. The four-velocity is defined as $u^{\alpha} = \dfrac{dx^{\alpha}}{ds}$.

In the sequel we consider the Parametrized Post Newtonian theories [4]. The relevant PPN parameters which appear below are γ and α_1. The parameter γ is the usual parameter connected to the deflection of a light ray by a central mass. The parameter α_1 couples the metric to the speed, $-\vec{w}$, of the preferred frame (if any) relatively to the geocentric frame. In general relativity, $\alpha_1 = 0$ and $\gamma = 1$.

Let us define now several quantities which will be used in the sequel :

- $2M_{\circledS}$ is the Schwarzschild's radius of the central body ($i.e.$ the Earth or Jupiter). As we use geometrical units, $M_{\circledS}$ is also its "mass".
- $\vec{J}_{\circledS}$ is the angular momentum of the central body in geometrical units. The relevant quantity which appears below, is $\vec{J} = \dfrac{1 + \gamma + \alpha_1/4}{2}\vec{J}_{\circledS}$. We define $J = \left\|\vec{J}\right\| \simeq \left\|\vec{J}_{\circledS}\right\| = J_{\circledS}$

- $\vec{g} = -2\ \dfrac{\vec{J}\wedge\vec{r}}{r^3} + \dfrac{1}{2}\alpha_1 U\ \vec{w}$ is the definition of $\vec{g}$, where $\vec{w}$ is the velocity of the observer, relative to the preferred frame (if any).
- U is the Newtonian potential

$$U = \frac{M_{\circledS}}{r}\left(1 - J_2\left(\frac{R_{\circledS}}{r}\right)^2 P_2 + \Delta\right) + U_* \tag{8}$$

where $R_{\circledS}$ is the radius of the central body and U_* the potential due to its satellites, the Sun and the planets[10]. In spherical coordinates the Legendre polynomial P_2 reads $P_2 = \dfrac{1}{2}\left(3\cos^2\theta - 1\right)$. The quadrupole coefficient is J_2 and Δ represents the higher harmonics. It depends on the angle φ and on the time t because of the rotation of the central body.

In the non rotating geocentric coordinates the significant fundamental element is

$$ds^2 = (1-2U)\,dt^2 + 2g_{0k}\,dx^k dt - (1+2\gamma U)\,\delta_{jk}\,dx^j dx^k \tag{9}$$

where $(\vec{g})_k = -(\vec{g})^k = g_{0k}$. In eq. (9), we have dropped post Newtonian corrections which are too small to be considered here.

B. Orders of magnitude

Table 1 below gives the order of magnitude of the various parameters which have been introduced previously.

	$M_{\circledS}$	$J_{\circledS}$	$R_{\circledS}$	J_2	Δ
Earth	4.4mm	145cm^2	6400km	$\sim 10^{-3}$	$\sim 10^{-5}$
Jupiter	1.4m	1700m^2	71300km	$\sim 10^{-2}$	$\lesssim 10^{-3}$

Table 1.

In order to describe the physical situation we introduce four parameters : ξ, ε, η and μ.

First we define the order of magnitude $O_1 = \sqrt{\dfrac{M_{\circledS}}{R_{\circledS}}}$. The quantity $(O_1)^n$ is denoted by O_n.

Then we consider a nearly free falling satellite on a nearly circular orbit of radius $r \sim R_{\circledS}/\xi$. This expression gives the definition of ξ. The velocity of the satellite is of order $v = \xi^{1/2}O_1$ [11].

Now we define $d = R_{\circledS}O_1$ and ε such as $X = \varepsilon d$ where X is the size of the laboratory.

We define η. The velocity of the atoms is $v_g = \eta O_1$.

Finally we assume that the various quantities such as the position of O or the geometry of the experimental set-up is known with a relative accuracy of order of μ.

$O_1 = \sqrt{\frac{M_{\odot}}{R_{\odot}}}$	relative accuracy : μ
Orbital parameters	set-up parameters
radius $r = \frac{R_{\odot}}{\xi}$ velocity $v = O_1 \xi^{1/2}$ period $T = \frac{2\pi}{\xi^{1/2} O_1} \frac{R_{\odot}}{c\,\xi}$	size $X = R_{\odot} O_1\ \varepsilon \sim 60\text{cm}$ atom velocity $v_g = \eta O_1 \sim 20\text{cms}^{-1}/c$ Drift time $2T_D = X/v_g = R_{\odot}\ \frac{\varepsilon}{\eta} \sim 3\text{s}$

Table 2. : definition of O_1, ξ, ε and η

With $\xi \simeq 0.9$ one finds

	O_1	ε	η	r	v	T
Earth	$2.6\ 10^{-5}$	$3.6\ 10^{-3}$	$2.7\ 10^{-5}$	7000km	$2.9\ 10^{-5}$	5900s
Jupiter	$1.4\ 10^{-4}$	$6.0\ 10^{-5}$	$4.8\ 10^{-6}$	78400km	$1.5\ 10^{-5}$	12300s

Table 3.

C. Comoving non rotating coordinates

We consider the following tetrad, $e^{\alpha}_{\hat{\sigma}}$, comoving with O :

$$
\begin{aligned}
e^0_{\hat{0}} &= u^0 = 1 + \frac{\vec{v}^2}{2} + U\ + O_4,\ \ e^k_{\hat{0}} = u^k = \left(1 + \frac{\vec{v}^2}{2} + U\right) v^k + \xi^2 O_4 \\
e^0_{\hat{k}} &= \left(1 + \frac{\vec{v}^2}{2} + U\right) v^k + \gamma U\, v^k - g_{0k} + \xi^2 O_4 \qquad (10) \\
e^j_{\hat{k}} &= \delta^j_k + \frac{1}{2} v^j v^k + \frac{1}{2} \gamma U\, \delta^j_k + \xi^2 O_4
\end{aligned}
$$

The local metric is derived from 4 with the change in the notations $(\alpha) \to \hat{\alpha}$ and $u^{\alpha}_{(\sigma)} \to e^{\alpha}_{\hat{\sigma}}$.

We limit the expansion of the metric at order $\varepsilon^2\, \xi^{3/2} O_6$; therefore we consider only the linear expression of the Riemann tensor (eq. (6)) and we assume that the free fall is under control : $\|\vec{a}\| << \varepsilon O_3 \xi^{3/2} \times \frac{c^2}{X}$ (*i.e.* $\|\vec{a}\| << 8\text{ms}^{-2}$ for the Earth, $\|\vec{a}\| << 21\text{ms}^{-2}$ for Jupiter which is not very restrictive) therefore we neglect the term $\left(\vec{a} \cdot \vec{X}\right)^2$ in the metric (4). One finds

$$G_{\hat{0}\hat{0}} = 1 + 2\,\vec{a}\cdot\vec{X} - \hat{U}_{,\hat{k}\hat{j}}\,X^{\hat{k}}X^{\hat{j}} - \frac{1}{3}\hat{U}_{,\hat{k}\hat{j}\hat{\ell}}\,X^{\hat{k}}X^{\hat{j}}X^{\hat{\ell}} + \varepsilon^2\,\xi^3 O_6 \quad (11)$$

$$G_{\hat{0}\hat{m}} = -\left\{\vec{\Omega}_0 \wedge \vec{X}\right\}^{\hat{m}} + \varepsilon^2\xi^{5/2}O_5 \text{ and } G_{\hat{n}\hat{m}} = \eta_{\hat{n}\hat{m}} + \varepsilon^2\xi^2 O_4 \quad (12)$$

where $\vec{\Omega}_0$ is given below (see eq. (13)) while the expressions such as $\hat{U}_{,\hat{k}\hat{j}}$ are nothing but $\left(U_{,mn}\,e^m_{\hat{k}}e^n_{\hat{j}}\right)_O$. The position of the observer changes with time, therefore this quantity is a function of T.

We did not consider the time dependence of the potential U. One can prove that it is correct when $\dfrac{\Delta U}{U} \times \dfrac{r}{cT_c} << \xi O_2$ where $\dfrac{\Delta U}{U}$ is the relative change of the potential during the time T_c, at the distance r of the origin. This is generally the case.

In $G_{\hat{0}\hat{0}}$, the accuracy is limited to the terms of order of $\varepsilon^2\,\xi^3 O_6$. One can check that in such a case, the approximation $e^m_{\hat{k}} = \delta^m_{\hat{k}}$ is valid therefore $\hat{U}_{,\hat{k}\hat{j}} \simeq \left(U_{,kj}\right)_O$ and $\hat{U}_{,\hat{k}\hat{j}\hat{\ell}} = \left(U_{,kj\ell}\right)_O$. The same holds true for $\vec{\Omega}_0$ *i.e.* $\left(\vec{\Omega}_0\right)^{\hat{k}} \simeq \left(\vec{\Omega}_0\right)^k$ (see eq. (13)). Therefore, one can identify the space vectors $\overrightarrow{e}_{\hat{k}}$ of the tetrad and the space vectors $\overrightarrow{\partial}_k$ of the natural basis associated to the geocentric coordinates. This would not be valid with an higher accuracy where terms smaller than $\varepsilon^2\,\xi^3 O_6$ are considered.

Calculating $\vec{\Omega}_0$ one finds the usual following expression [5]

$$\vec{\Omega}_0 = \vec{\Omega}_{LT} + \vec{\Omega}_{dS} + \vec{\Omega}_{Th} \quad (13)$$

$$\left(\vec{\Omega}_{LT}\right)^{\hat{k}} \simeq \left(\frac{\vec{J}}{r^3} - \frac{3}{r^3}\left(\vec{J}\cdot\vec{n}\right)\vec{n} - \frac{\alpha_1}{4}\vec{\nabla}U \wedge \vec{w}\right)^k \quad (14)$$

$$\left(\vec{\Omega}_{dS}\right)^{\hat{k}} \simeq \left((1+\gamma)\,\vec{\nabla}U \wedge \vec{v}\right)^k \text{ and } \left(\vec{\Omega}_{Th}\right)^{\hat{k}} \simeq \left(\frac{1}{2}\vec{v} \wedge \frac{d\vec{v}}{dt}\right)^k \quad (15)$$

$\vec{n}$ is the direction of the satellite (fig. 3), $\vec{\Omega}_{LT}$ is the Lense-Thirring angular velocity, $\vec{\Omega}_{dS}$ and $\vec{\Omega}_{Th}$ are the de Sitter and the Thomas terms[12] :

Ω_{LT}	$\sim \dfrac{J_{\circledS}}{M^2_{\circledS}}\,\xi^2 O_4 \times \dfrac{c\xi}{R_{\circledS}}$
$\Omega_{dS} \sim \Omega_{Th}$	$\sim \xi^{3/2} O_3 \times \dfrac{c\xi}{R_{\circledS}}$

Table 4.

With $\xi \sim 0.9$, one finds

	$J_{\oplus}/M_{\oplus}^2$	Ω_{LT}	$\Omega_{dS} \sim \Omega_{Th}$
Earth	750	$\sim 10^{-14}\text{rads}^{-1}$	$\sim 10^{-12}\text{rads}^{-1}$
Jupiter	855	$\sim 10^{-12}\text{rads}^{-1}$	$\sim 10^{-11}\text{rads}^{-1}$

Table 5.

D. Aberration and deflection of the light

In the satellite, the experimental set-up is tied to a telescope which points towards a "fixed" star (see figure 1). We assume that the star is far enough for the parallax to be negligible. However the light rays suffer a gravitational deflection from the central body and an aberration which depends on the position and the velocity of the satellite. These effects result in an angular apparent velocity which must be compared to the Lense-Thirring effect.

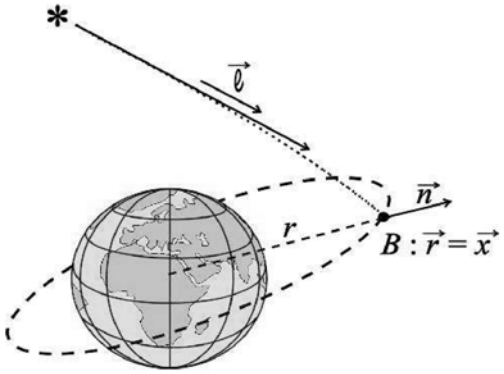

FIG. 3: The deflection of the light.

In space time, the direction of the light from the star is given by the 4-vector $L_\alpha = \left\{1, \dfrac{\partial_k \varphi}{\partial_0 \varphi}\right\}$ where φ is the phase of the light. In order to calculate the phase $\varphi(t, x^k)$ at point $\{x^k\}$ and time t we use the method which is summarized in paragraph II B. Now the line element is given by eq. (9), and ω is the angular frequency of the light at infinity. These

calculations are developed in another publication [6]. Here, we just give the useful results.

The main gravitational contribution is due to the monopolar term of the Newtonian potential :

$$L_\alpha = \left\{1,\ -\ell^k + (1+\gamma)\,\frac{M}{r}\,\frac{n^k - \ell^k}{1-\vec{n}\cdot\vec{\ell}} + \delta\ell^k + \delta L^k\right\} \tag{16}$$

where $\overrightarrow{\ell}$ is the unitary vector of figure 3 and $\overrightarrow{n} = \overrightarrow{r}/r$.

- The term $\delta\ell^k$ is due to the quadrupolar term of the central mass. This term is of order $J_2 O_2$ when $\overrightarrow{\ell}$ is nearly orthogonal to the plane of the orbit.
- The term due to $\dfrac{1}{2}\alpha_1 U\, w^k$, a part of g_{0k} in the metric (9), results in the modification $M_{\odot} \to M = M_{\odot}\left(1 - \dfrac{\alpha_1\, \vec{w}\cdot\vec{\ell}}{2\,(1+\gamma)}\right)$.
- The contribution due to the rotation of the central body is of order of $J_{\odot}/r^2$. The corresponding angular velocity is of order of $J_{\odot}/r^2/T \sim \dfrac{J_{\odot}}{M_{\odot}^2}\dfrac{\xi^{7/2}O_5}{2\pi}\dfrac{c}{R_{\odot}} \sim \dfrac{\xi^{1/2}O_1}{2\pi}\Omega_{LT} << \Omega_{LT}$. It is negligible. The same conclusion holds for the term Δ in eq. (8).
- The Sun, the satellites and the other planets, give a contribution due to U_* in (8); it varies slowly with the time and it is negligible, especially within the framework of a Fourier analysis at a much higher frequency. An exception concerns the two satellites of Jupiter, Andrastea and Metis whose period is approximately 25 10^3s which is the order of the period of a satellite on a low orbit. However their mass do not exceed 10^{17}kg and the gravitational deflections remain completely negligible.

For the observer O, the space direction of the light is the four vector $\lambda^\alpha = L^\alpha - L_\beta\, u^\beta\, u^\alpha$. The components of λ^α relatively to the tetrad are $\left\{\lambda^{\hat{\alpha}}\right\} = \left(0,\ \overrightarrow{\lambda}\right)$. We define $\vec{\Lambda} = \Lambda\,\vec{\lambda}$ such as $-\Lambda_\alpha\Lambda^\alpha = \vec{\Lambda}\cdot\vec{\Lambda} = 1$.

The tetrad (10) is especially useful to catch the orders of magnitude of the various terms involved. However it is not the comoving tetrad that we are looking for because the telescope that points towards the far away star rotates relatively to this tetrad. The angular velocity of the telescope

relatively to $\left\{e^\alpha_{\hat{k}}\right\}$ is $\vec{\Omega}_* = \vec{\Lambda} \wedge \dfrac{d\vec{\Lambda}}{dt}$. Straightforward calculations give

$$\begin{aligned}\left(\vec{\Omega}_*\right)^{\hat{k}} &= -\left(\vec{\ell}\wedge\frac{d\vec{v}}{dt}\right)^k + \left(\vec{v}\wedge\frac{d\vec{v}}{dt}\right)^k \\ &-\frac{3}{2}\left(\vec{\ell}\cdot\vec{v}\right)\left(\vec{\ell}\wedge\frac{d\vec{v}}{dt}\right)^k + \frac{1}{2}\left(\vec{\ell}\cdot\frac{d\vec{v}}{dt}\right)\left(\vec{\ell}\wedge\vec{v}\right)^k \\ &-\frac{M}{r^2}\frac{1+\gamma}{1-\vec{n}\cdot\vec{\ell}}\left(\left(\vec{\ell}\wedge\vec{v}\right)^k + \left(\vec{\ell}\wedge\vec{n}\right)^k\left[\frac{\vec{\ell}\cdot\vec{v}\ -\vec{n}\cdot\vec{v}}{1-\vec{n}\cdot\vec{\ell}} - \vec{n}\cdot\vec{v}\right]\right) \\ &+\left(\vec{\ell}\wedge\frac{d\delta\vec{\ell}}{dt}\right)^k + \frac{1}{r}\times\xi^2 O_4\end{aligned} \tag{17}$$

Let us notice that we neglect the terms of order $\dfrac{1}{r}\times\xi^2 O_4$, which are much smaller than the Lense-Thirring angular velocity because $\dfrac{J_{\textcircled{S}}}{M^2_{\textcircled{S}}} >> 1$ and $\xi \sim 1$.

E. Local coordinates tied to the telescope

Now we introduce the tetrad tied to the telescope and the interferometer $u^\alpha_{(\sigma)}$. It is obtained from $e^\alpha_{\hat{\rho}}$ through a pure space rotation (*i.e.* $u^\alpha_{(0)} = e^\alpha_{\hat{0}} = u^\alpha$) and whose vector $u^\alpha_{(1)}$ points towards the far away star ($u^\alpha_{(1)} = -\Lambda^\alpha$).

At the required accuracy, it is possible to give a description of the Hyper project with the Newtonian concept of space.

The rotation of the tetrad $\left\{u^\alpha_{(\sigma)}\right\}$ relatively to $\left\{e^\alpha_{\hat{\rho}}\right\}$ is characterized by the most general angular velocity $\vec{\Omega}_{u/e} = \vec{\Omega}_* - \varpi\vec{\Lambda}$ where $-\varpi\vec{\Lambda}$ is an arbitrary angular velocity around the apparent direction of the star. The change of the tetrad $u^\alpha_{(\sigma)} \longleftrightarrow e^\alpha_{\hat{\rho}}$ is just an ordinary change of basis in the space of the observer O. In this transformation, dT, $G_{\hat{0}\hat{0}} = G_{(0)(0)}$, $G_{\hat{0}\hat{m}}dX^{\hat{m}} = G_{(0)(k)}dX^{(k)}$ and $G_{\hat{n}\hat{m}}dX^{\hat{m}}dX^{\hat{n}} = G_{(j)(k)}dX^{(j)}X^{(k)}$ behave as scalars. We obtain the local metric from eqs. (11) and (12). Then, using the expression 2 of Ψ, a straight forward calculation gives :

$$\begin{aligned}\Psi &= 2\,\vec{a}\cdot\vec{X} - \hat{U}_{,(k)(j)}\ X^{(k)}X^{(j)} - \frac{1}{3}\hat{U}_{,(k)(j)(\ell)}\ X^{(k)}X^{(j)}X^{(\ell)} \\ &-2\sum_{(k)}\left\{\left(\vec{\Omega}_0 + \vec{\Omega}_*\right)\wedge\vec{X}\right\}^{(k)} v_g^{(k)} + \varepsilon^2\xi^3 O_6\end{aligned} \tag{18}$$

with $\left\{\left(\vec{\Omega}_0+\vec{\Omega}_*\right)\wedge\vec{X}\right\}\cdot\overrightarrow{v}_g = \left\{\left(\vec{\Omega}_{LT}-\left(\vec{\ell}\wedge\frac{d\vec{v}}{dt}\right)\right)\wedge\vec{X}\right\}\cdot\overrightarrow{v}_g + \eta\varepsilon\xi^{5/2}O_5$.

The Lense-Thirring contribution to Ψ is $\Psi_{LT}\sim\frac{J_{\circledS}}{M_{\circledS}^2}\xi^3\varepsilon\eta O_6$. Therefore, within the present framework, the expected accuracy is of order of

	Earth	Jupiter
$\frac{\varepsilon^2\xi^3O_6}{\left(J_{\circledS}/M_{\circledS}^2\right)\xi^3\varepsilon\eta O_6}\sim\frac{\varepsilon}{\left(J_{\circledS}/M_{\circledS}^2\right)\eta}$	18%	1.5%

Table 6.

IV. THE PHASE SHIFT

Let us assume that any quantity can be known with an accuracy $\mu\sim 10^{-4}$. This condition is not restrictive for the orbital parameters and does not seem out of the present possibilities as far as the geometry of the experimental device.

We consider that Ψ is the amount of two terms, Ψ_k and Ψ_u : the term Ψ_k is known; it can be modelled with the required accuracy while Ψ_u is unknown. The terms Ψ_k fulfills the condition $\mu\times\Psi_k\lesssim\varepsilon^2\,\xi^3O_6$. With the previous orders of magnitude one finds

		Earth	Jupiter
$\frac{\mu\hat{U}_{,(k)(j)}\,X^{(k)}X^{(j)}}{\varepsilon^2\xi^3O_6}\sim$	$\frac{\mu}{\xi O_2}\sim$	$1.6\ 10^5\in\Psi_u$	$5.7\ 10^3\in\Psi_u$
$\frac{\mu\hat{U}_{,(k)(j)(\ell)}\,X^{(k)}X^{(j)}X^{(\ell)}}{\varepsilon^2\xi^3O_6}\sim$	$\frac{\mu\varepsilon}{\xi^{1/2}O_1}\sim$	$1.5\ 10^{-2}\in\Psi_k$	$4.5\ 10^{-5}\in\Psi_k$
$\frac{\mu\left\{\left(\vec{\ell}\wedge\frac{d\vec{v}}{dt}\right)\wedge\vec{X}\right\}\cdot\overrightarrow{v}_g}{\varepsilon^2\xi^3O_6}\sim$	$\frac{\mu\eta}{\varepsilon\xi O_2}\sim$	$1.2\ 10^3\in\Psi_u$	$4.5\ 10^2\in\Psi_u$
$\frac{\mu\eta\varepsilon\xi^{5/2}O_5}{\varepsilon^2\xi^3O_6}\sim$	$\frac{\mu\eta}{\varepsilon\xi^{1/2}O_1}\sim$	$3\ 10^{-2}\in\Psi_k$	$6\ 10^{-2}\in\Psi_k$

Table 7.

Ψ_u reads

$$\Psi_u=2\,\vec{a}\cdot\vec{X}-\hat{U}_{,(k)(j)}\,X^{(k)}X^{(j)}-2\left\{\vec{\Omega}\wedge\vec{X}\right\}\cdot\overrightarrow{v}_g+\varepsilon^2\,\xi^3O_6/\mu \qquad (19)$$

where the contribution $\hat{U}_{,(k)(j)}\,X^{(k)}X^{(j)}$ needs to be defined with an accuracy better than $\varepsilon^2\,\xi^3O_6/\mu$. This implies that any known perturbation δU

can be included in Ψ_k when $\frac{\delta U}{U}$ does not exceed the value given in table 8 below :

	Earth	Jupiter
$\frac{\delta U}{U} \lesssim \frac{\varepsilon \xi O_2}{\mu}$	$2\ 10^{-8}$	10^{-8}

Table 8.

The quadrupolar contribution is bigger than 10^{-3}, it cannot be considered in known term, however higher multipole can be included in Ψ_k if the accuracy μ is smaller than 10^{-6} for the Earth instead of 10^{-4} and 10^{-9} for Jupiter. The accuracy $\mu \sim 10^{-6}$ remains a very difficult challenge as far as the geometry of the set-up is concerned (A. Landragin, private communication).

With the same order of magnitude for μ, we obtain

$$\left(\vec{\Omega}\right)^{(k)} = \left(\vec{\Omega}_{LT} - \varpi \overrightarrow{\Lambda} - \overrightarrow{\Lambda} \wedge \frac{d\overrightarrow{v}}{dt}\right)^{(k)} \tag{20}$$

where $\vec{\Omega}_{LT}$ is deduced from (14) and $\frac{d\overrightarrow{v}}{dt} \simeq \overrightarrow{a} - \overrightarrow{\nabla} U \simeq \overrightarrow{a} + \frac{M_{\textcircled{S}}}{r^2}\overrightarrow{n}$.

The satellites, such as the Moon for the Earth, can bring a contribution to $\hat{U}_{,(k)(j)}\ X^{(k)}X^{(j)}$ at the required level of accuracy but with such a value of μ, it could be included in Ψ_k.

Of course when modelling Ψ_k, one must be sure that every quantity is known at the required accuracy. This must hold for any value of μ, this is a necessary condition. Therfore the following relation must hold true : $\frac{\Delta U}{U} \lesssim \varepsilon \xi O_2$

	Earth	Jupiter
$\frac{\Delta U}{U} \lesssim \varepsilon \xi O_2$	$2\ 10^{-12}$	10^{-12}

Table 9.

Such an accuracy is not achieved for Jupiter. For the Earth, considering the difference between the various models (Godard Earth model 9 and 10) it appears that the values of the high order multipoles are neither known nor consistent at the required level (10^{-12}). One can hope that the lack of precision on the J_{kn} coefficients [13] is not important for $n \neq 0$ because the diurnal rotation modulates the frequency of the corresponding contribution in $\hat{U}_{,(k)(j)}\ X^{(k)}X^{(j)}$. However it is necessary to increase our knowledge of the axisymmetrical potential of the central body in order that $\xi^k\ \Delta J_{k0} \lesssim \varepsilon \xi O_2$ where ΔJ_{k0} is the uncertainty on $J_{k0} = J_k$. Such a relation holds true for $k = 2$. It could be presently achieved with low values of ξ (on

high orbits) but the Lense-Thirring effect is proportional to ξ^3 (see table 4 above) and it seems impossible to measure the Lense-Thirring effect for $\xi << 1$ in not to far a future.

This question is crucial but Hyper might, itself, bring an answer to this question by the means of the time analysis. Now we forget these problems because in the simple case that we consider the quadratic quantities do not bring any contribution to the signal.

A. Significant terms in Ψ_u

We consider that the motion of the satellite takes place in the (x, y)-plane while the vector $\overrightarrow{\ell}$ lies in the (x, z)-plane. We assume that the eccentricity, e, does not exceed $\xi^{1/2} O_1$.

We define

$$\vec{J} = J_x \vec{e}_{\hat{1}} + J_y \vec{e}_{\hat{2}} + J_z \vec{e}_{\hat{3}} , \quad \vec{n} = \cos\theta \vec{e}_{\hat{1}} + \sin\theta \vec{e}_{\hat{2}} \tag{21}$$

$$-\vec{\ell} = \cos\alpha \vec{e}_{\hat{1}} + \sin\alpha \vec{e}_{\hat{3}} , \quad \vec{w} = w_x \vec{e}_{\hat{1}} + w_y \vec{e}_{\hat{2}} + w_z \vec{e}_{\hat{3}} \tag{22}$$

$\vec{J}$, $\vec{\ell}$ and $\vec{w}$ are constant vectors. The angle θ and the distance r depend on the time T.

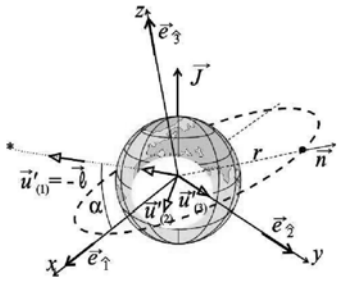

FIG. 4: The satellite and the fixed star

First we define the spatial triad $\vec{u}'_{(n)}$:

$$\vec{u}'_{(1)} = \cos\alpha \, \overrightarrow{e}_{\hat{1}} + \sin\alpha \, \overrightarrow{e}_{\hat{3}}, \quad \vec{u}'_{(2)} = \sin\alpha \, \overrightarrow{e}_{\hat{1}} - \cos\alpha \, \overrightarrow{e}_{\hat{3}}, \quad \vec{u}'_{(3)} = \overrightarrow{e}_{\hat{2}} \tag{23}$$

Let us outline that we have defined $\left(\vec{u}'_{(1)}\right)^{\hat{k}} = -\left(\vec{\Lambda}\right)^{\hat{k}} + \xi^{1/2}O_1$. Then, in order to obtain the final tetrad $u^{\alpha}_{(\sigma)}$, we perform an arbitrary rotation around $\vec{\Lambda}$:

$$\begin{array}{l} \vec{u}_{(1)} = -\vec{\Lambda} = \vec{u}'_{(1)} + \xi^{1/2}O_1 \\ \vec{u}_{(2)} = \vec{u}'_{(2)}\cos\sigma + \vec{u}'_{(3)}\sin\sigma + \xi^{1/2}O_1 \\ \vec{u}_{(3)} = -\vec{u}'_{(2)}\sin\sigma + \vec{u}'_{(3)}\cos\sigma + \xi^{1/2}O_1 \end{array} \tag{24}$$

where $-\dfrac{d\sigma}{dT} = -\varpi$ is the angular velocity of the triad $\left\{\vec{u}_{(k)}\right\}$ relatively to $\left\{\vec{u}'_{(k)}\right\}$.

We can now assume that the experimental set-up is comoving with the triad $\vec{u}_{(n)}$ whose vector $\vec{u}_{(1)}$ points towards the fixed star.

During the flight of the atom, the quantity $\hat{U}_{,(k)(j)}$ in equation 19 does not remain constant because the position of the satellite changes. One can consider that the coordinate, $X = X^{(1)}$ of the atom is a function of the time: $X = v_g\left(T - T_0\right)$.

Therefore we expand $\hat{U}_{,(k)(j)} = \hat{U}_{,(k)(j)}\left(T_0\right) + \hat{U}_{,(k)(j)(\ell)}\left(T_0\right)\ v^{(\ell)} \times \dfrac{X}{v_g}$ where $v^{(\ell)}\overrightarrow{u}_{(\ell)}$ is the orbital velocity.

Before performing explicit calculation we notice that $\hat{U}_{,(k)(j)}\left(T_0\right) X^{(k)}X^{(j)}$ will not bring any contribution to the phase difference 3 because O_S and O'_S are two centers of symmetry. For $\mu < 10^{-6}$ the term $\hat{U}_{,(k)(j)(\ell)}\left(T_0\right)\ \dfrac{v^{(\ell)}}{v_g} \times X\ X^{(k)}X^{(j)} \sim \varepsilon^3\xi^{5/2}O_5/\eta$ can be included in Ψ_k for Jupiter ($\dfrac{\mu\varepsilon^3\xi^{5/2}O_5/\eta}{\varepsilon^2\xi^3O_6} < 1$), but it must considered for the Earth $\left(\dfrac{\mu\varepsilon^3\xi^{5/2}O_5/\eta}{\varepsilon^2\xi^3O_6} \sim 5 > 1\right)$. However the quadrupole does not bring any contribution to the phase difference that we calculate from Ψ_u.

In equation 19, the spin $\varpi\vec{u}_{(1)}$ does not bring any contribution in the term $\left\{\vec{\Omega} \wedge \vec{X}\right\} \cdot \overrightarrow{v}_g$ because $\vec{u}_{(1)}$, $\overrightarrow{X}$ and $\vec{v}_g$ are in the same plane.

Then, one obtains

$$\begin{aligned}\Psi_u = -2\Bigg(&\left(\frac{\vec{J}}{r^3}-\frac{3\left(\vec{J}\cdot\vec{n}\right)}{r^3}\vec{n}+\frac{\alpha_1\,M_{\textcircled{S}}}{4\,r^2}\,\vec{n}\wedge\vec{w}\right)\wedge\overrightarrow{X}\Bigg)\cdot\vec{v}_g \quad \Big|A\\ &-2\frac{M_{\textcircled{S}}}{r^2}\left(\left(\vec{u}_{(1)}\wedge\vec{n}\right)\wedge\overrightarrow{X}\right)\cdot\vec{v}_g+2\left(\left(\vec{u}_{(1)}\wedge\vec{a}\right)\wedge\overrightarrow{X}\right)\cdot\vec{v}_g \Big|B\\ &-\frac{6M_{\textcircled{S}}}{r^4}\left(\overrightarrow{X}\cdot\frac{\overrightarrow{v}}{v_g}\right)\left(\overrightarrow{X}\cdot\overrightarrow{n}\right)X \Big|C\\ &+2\,\vec{a}\cdot\overrightarrow{X} \Big|D\end{aligned} \tag{25}$$

where $\overrightarrow{n}=\overrightarrow{n}\left(T_0\right)$.

In expression (eq. (25)) of Ψ_u one can assume that $r=r_0$ is a constant because we assume that the excentricity is small $e\lesssim O_1$, therefore the corrections are included in Ψ_k.

Moreover, for the same reason, one can drop the terms of order O_1 in the expression of the tetrads. Therefore, it is clear that we can consider the space as the ordinary space of Newtonian physics and that the usual formulae to change the basis $\overrightarrow{\partial}_k$ into $\overrightarrow{e}_{\hat{k}}$ or $\overrightarrow{u}_{(k)}$are valid.

In (25), the terms of lines A and B are due to various rotations : respectively the Lense-Thirring rotation and the aberration. The term of line C is due to the displacement of the satellite during the flight time of the atom and the term of line D corresponds to some residual acceleration due to the fact that point O is not exactly in free fall.

B. The phase differences

We use the expression (25) of Ψ_u in order to calculate $\delta\varphi$ given by 3. We find

$$\begin{aligned}\delta\varphi \;=\; &-2\frac{mc}{\hbar\,r}S\left(\frac{\vec{J}}{r_0^2}-\frac{3\left(\vec{J}\cdot\vec{n}\right)}{r_0^2}\vec{n}+\frac{\alpha_1\,M_{\textcircled{S}}}{4\,r_0}\,\vec{n}\wedge\vec{w}\right)\cdot\vec{u}_{(2)}\\ &-2\frac{mc}{\hbar r}S\,\frac{M_{\textcircled{S}}}{r_0}\,\left(\vec{u}_{(1)}\wedge\vec{n}\right)\cdot\vec{u}_{(2)}-2\frac{mc}{\hbar}S\left(\vec{u}_{(1)}\wedge\frac{\overrightarrow{a}}{c^2}\right)\cdot\vec{u}_{(2)}\\ &-\frac{4\pi\left(cT_D\right)^2}{\lambda}\,\left(\vec{u}_{(3)}\cdot\frac{\vec{a}_{O_S}}{c^2}\right)\\ &-\frac{mc}{2\,\hbar r}S\,\frac{\left(cT_D\right)^2}{r_0^2}\frac{M_{\textcircled{S}}}{r}\,\left(\left(\vec{u}_{(1)}\cdot\vec{n}\right)\left(\vec{u}_{(3)}\cdot\frac{\overrightarrow{v}}{c}\right)+\left(\vec{u}_{(3)}\cdot\vec{n}\right)\left(\vec{u}_{(1)}\cdot\frac{\overrightarrow{v}}{c}\right)\right)\end{aligned} \tag{26}$$

where $S = \frac{4\pi\hbar}{\lambda m} v_g T_D^2$ is the area of the Sagnac loop. As we mentionned before, $\vec{J}$ and $M_{\circledS}$ are expressed in geometrical units.

The two interferometers of the same ASU are assumed to lie in the same plane but not necessarily with their center of symmetry O_S and O'_S at the same point. Therefore adding and subtracting the phase differences delivered by the two interferometers one finds the two basic quantities which are measured by the set-up *i.e.* : $\mu_1 = \frac{1}{2}(\delta\varphi' - \delta\varphi)$ and $\mu_2 = \frac{1}{2}(\delta\varphi' + \delta\varphi)$.

We define the shift $\overrightarrow{\delta} = \overrightarrow{X}_{O'_S} - \overrightarrow{X}_{O_S}$ and the acceleration $\overrightarrow{a} = \frac{1}{2}\left(\vec{a}_{O_S} + \vec{a}_{O'_S}\right)$ where $\vec{a}_{O_S}$ and $\vec{a}_{O'_S}$ are the accelerations at point O_S and O'_S. We drop several terms which can be included into Ψ_k. Then we obtain the quantities which can be measured :

$$\begin{aligned}
\mu_1 + \frac{2v_g}{c}\mu_2 \;=\; & \frac{8\pi}{\lambda}(cT_D)^2 \left\{ \frac{M_{\circledS}}{r_0^2}\vec{u}_{(3)}\cdot\vec{n} + \vec{\Omega}_{LT}\cdot\vec{u}_{(2)} \right\}\frac{v_g}{c} \qquad (27)\\
& -\frac{2\pi(cT_D)^2}{\lambda r_0}\frac{M_{\circledS}}{r_0}\left(\vec{u}_{(3)}\cdot\frac{\overrightarrow{\delta}}{r} - 3\left(\vec{n}\cdot\vec{u}_{(3)}\right)\left(\vec{n}\cdot\frac{\overrightarrow{\delta}}{r}\right)\right)\\
& -\frac{2\pi}{\lambda}(cT_D)^2\left(\frac{v_g T_D}{r_0}\right)^2\frac{M_{\circledS}}{r_0^2}\left\{\left(\vec{u}_{(1)}\cdot\vec{n}\right)\left(\vec{u}_{(3)}\cdot\frac{\overrightarrow{v}}{c}\right)\right.\\
& \left. + \left(\vec{u}_{(3)}\cdot\vec{n}\right)\left(\vec{u}_{(1)}\cdot\frac{\overrightarrow{v}}{c}\right)\right\}\\
\mu_2 \;=\; & \frac{1}{2}(\delta\varphi' + \delta\varphi) = -\frac{4\pi(cT_D)^2}{\lambda}\left\{\frac{\overrightarrow{a}}{c^2}\cdot\vec{u}_{(3)}\right\} \qquad (28)
\end{aligned}$$

C. Discussion

We define α as the direction of the fixed star (fig. (4)), and the projection, $\overrightarrow{J}_{\shortparallel}$ of $\overrightarrow{J}$ on the plane of the orbit :
$\overrightarrow{J}_{\shortparallel} = J_{\shortparallel}(\cos\theta_J\ \overrightarrow{e}_{\hat{1}} + \sin\theta_J\ \overrightarrow{e}_{\hat{2}})$ and $\overrightarrow{w}_{\shortparallel} = w_{\shortparallel}(\cos\theta_w\ \overrightarrow{e}_{\hat{1}} + \sin\theta_w\ \overrightarrow{e}_{\hat{2}})$.
Then

$$\begin{aligned}
\mu_1 + 2\frac{v_g}{c}\mu_2 \;=\; & \frac{2\pi(cT_D)^2}{\lambda r_0}\times\{K_0 + K_\sigma + K_{2\sigma} + K_{2\theta} \qquad (29)\\
& + K_{\theta-\sigma} + K_{\theta+\sigma} + K_{2\theta-\sigma} + K_{2\theta+\sigma} + K_{2\theta-2\sigma} + K_{2\theta+2\sigma}\}
\end{aligned}$$

with

$$K_0 = \frac{M_{\odot}}{4\,r_0}\left(3\sin^2\alpha - 1\right) \times \frac{\delta^{(3)}}{r_0} \tag{30}$$

$$K_\sigma = \frac{v_g}{c}\left\{\left[(1-\sin\alpha)\cos\left(\sigma+\theta_J\right) - (1+\sin\alpha)\cos\left(\sigma-\theta_J\right)\right] \times \frac{J_{\shortparallel}}{r_0^2} - 4\cos\alpha\,\cos\sigma \times \frac{J^{\hat{3}}}{r_0^2}\right\} - \frac{3M_{\odot}}{2r_0}\cos\alpha\sin\alpha\sin\sigma \times \frac{\delta^{(1)}}{r_0} \tag{31}$$

$$K_{2\sigma} = \frac{3M_{\odot}}{4r_0}\left(1-\sin^2\alpha\right)\left[\sin\left(2\sigma\right) \times \frac{\delta^{(2)}}{r_0} + \cos\left(2\sigma\right) \times \frac{\delta^{(3)}}{r_0}\right] \tag{32}$$

$$K_{2\theta} = -\frac{3M_{\odot}}{4r_0}\left(1-\sin^2\alpha\right)\cos\left(2\theta\right) \times \frac{\delta^{(3)}}{r_0} \tag{33}$$

$$K_{\theta-\sigma} = \frac{M_{\odot}}{r_0}\frac{v_g}{c} \times \{-2\left(1+\sin\alpha\right)\,\sin\left(\theta-\sigma\right) + \frac{\alpha_1}{2}\cos\alpha\,\sin\left(\theta-\sigma-\theta_w\right) \times \frac{w_{\shortparallel}}{c} + \frac{\alpha_1}{2}\left(1+\sin\alpha\right)\sin\left(\theta-\sigma\right) \times \frac{w^{\hat{3}}}{c}\Big\} \tag{34}$$

$$K_{\theta+\sigma} = \frac{M_{\odot}}{r_0}\frac{v_g}{c} \times \{-2\left(1-\sin\alpha\right)\,\sin\left(\theta+\sigma\right) + \frac{\alpha_1}{2}\cos\alpha\,\sin\left(\theta+\sigma-\theta_w\right) \times \frac{w_{\shortparallel}}{c} - \frac{\alpha_1}{2}\left(1-\sin\alpha\right)\sin\left(\theta+\sigma\right) \times \frac{w^{\hat{3}}}{c}\Big\} \tag{35}$$

$$K_{2\theta-\sigma} = -3\frac{v_g}{c}\left(1+\sin\alpha\right)\cos\left(2\theta-\sigma-\theta_J\right) \times \frac{J_{\shortparallel}}{r_0^2} + \frac{3M_{\odot}}{4r_0}\cos\alpha\,\left(1+\sin\alpha\right)\sin\left(2\theta-\sigma\right) \times \frac{\delta^{(1)}}{r_0} - \left(\frac{M_{\odot}}{r_0}\right)^{3/2}\frac{cv_gT_D^2}{2\,r_0^2}\left(1+\sin\alpha\right)\cos\left(2\theta-\sigma\right) \tag{36}$$

$$K_{2\theta+\sigma} = 3\frac{v_g}{c}\left(1-\sin\alpha\right)\cos\left(2\theta+\sigma-\theta_J\right) \times \frac{J_{\shortparallel}}{r_0^2} + \frac{3M_{\odot}}{4r_0}\cos\alpha\,\left(1-\sin\alpha\right)\sin\left(2\theta+\sigma\right) \times \frac{\delta^{(1)}}{r_0} - \left(\frac{M_{\odot}}{r_0}\right)^{3/2}\frac{cv_gT_D^2}{2\,r_0^2}\left(1-\sin\alpha\right)\cos\left(2\theta+\sigma\right) \tag{37}$$

with

$$K_0 = \frac{M_{\odot}}{4\,r_0}\left(3\sin^2\alpha - 1\right) \times \frac{\delta^{(3)}}{r_0} \tag{30}$$

$$K_\sigma = \frac{v_g}{c}\left\{\left[(1-\sin\alpha)\cos\left(\sigma+\theta_J\right) - (1+\sin\alpha)\cos\left(\sigma-\theta_J\right)\right] \times \frac{J_{\shortparallel}}{r_0^2} - 4\cos\alpha\,\cos\sigma \times \frac{J^{\hat{3}}}{r_0^2}\right\} - \frac{3M_{\odot}}{2r_0}\cos\alpha\sin\alpha\sin\sigma \times \frac{\delta^{(1)}}{r_0} \tag{31}$$

$$K_{2\sigma} = \frac{3M_{\odot}}{4r_0}\left(1-\sin^2\alpha\right)\left[\sin\left(2\sigma\right) \times \frac{\delta^{(2)}}{r_0} + \cos\left(2\sigma\right) \times \frac{\delta^{(3)}}{r_0}\right] \tag{32}$$

$$K_{2\theta} = -\frac{3M_{\odot}}{4r_0}\left(1-\sin^2\alpha\right)\cos\left(2\theta\right) \times \frac{\delta^{(3)}}{r_0} \tag{33}$$

$$K_{\theta-\sigma} = \frac{M_{\odot}}{r_0}\frac{v_g}{c} \times \{-2\left(1+\sin\alpha\right)\,\sin\left(\theta-\sigma\right) + \frac{\alpha_1}{2}\cos\alpha\,\sin\left(\theta-\sigma-\theta_w\right) \times \frac{w_{\shortparallel}}{c} + \frac{\alpha_1}{2}\left(1+\sin\alpha\right)\sin\left(\theta-\sigma\right) \times \frac{w^{\hat{3}}}{c}\Big\} \tag{34}$$

$$K_{\theta+\sigma} = \frac{M_{\odot}}{r_0}\frac{v_g}{c} \times \{-2\left(1-\sin\alpha\right)\,\sin\left(\theta+\sigma\right) + \frac{\alpha_1}{2}\cos\alpha\,\sin\left(\theta+\sigma-\theta_w\right) \times \frac{w_{\shortparallel}}{c} - \frac{\alpha_1}{2}\left(1-\sin\alpha\right)\sin\left(\theta+\sigma\right) \times \frac{w^{\hat{3}}}{c}\Big\} \tag{35}$$

$$K_{2\theta-\sigma} = -3\frac{v_g}{c}\left(1+\sin\alpha\right)\cos\left(2\theta-\sigma-\theta_J\right) \times \frac{J_{\shortparallel}}{r_0^2} + \frac{3M_{\odot}}{4r_0}\cos\alpha\,\left(1+\sin\alpha\right)\sin\left(2\theta-\sigma\right) \times \frac{\delta^{(1)}}{r_0} - \left(\frac{M_{\odot}}{r_0}\right)^{3/2}\frac{cv_gT_D^2}{2\,r_0^2}\left(1+\sin\alpha\right)\cos\left(2\theta-\sigma\right) \tag{36}$$

$$K_{2\theta+\sigma} = 3\frac{v_g}{c}\left(1-\sin\alpha\right)\cos\left(2\theta+\sigma-\theta_J\right) \times \frac{J_{\shortparallel}}{r_0^2} + \frac{3M_{\odot}}{4r_0}\cos\alpha\,\left(1-\sin\alpha\right)\sin\left(2\theta+\sigma\right) \times \frac{\delta^{(1)}}{r_0} - \left(\frac{M_{\odot}}{r_0}\right)^{3/2}\frac{cv_gT_D^2}{2\,r_0^2}\left(1-\sin\alpha\right)\cos\left(2\theta+\sigma\right) \tag{37}$$

$$K_{2\theta-2\sigma} = \frac{3M_{\circledcirc}}{8\,r_0}\,(1+\sin\alpha)^2 \times \left\{\sin(2\theta-2\sigma)\times\frac{\delta^{(2)}}{r_0} - \cos(2\theta-2\sigma)\times\frac{\delta^{(3)}}{r_0}\right\} \quad (38)$$

$$K_{2\theta+2\sigma} = -\frac{3M_{\circledcirc}}{8\,r_0}\,(1-\sin\alpha)^2 \times \left\{\sin(2\theta+2\sigma)\times\frac{\delta^{(2)}}{r_0} + \cos(2\theta+2\sigma)\times\frac{\delta^{(3)}}{r_0}\right\} \quad (39)$$

Each of these terms, except K_0, has a specific frequency. They can be measured and distinguished from each other.

The Lense-Thirring effect due to the angular momentum of the central body appears in the terms K_σ and $K_{2\theta\pm\sigma}$ while the possible existence of a preferred frame appears in $K_{\theta\pm\sigma}$ which depends on the components of $\alpha_1\overrightarrow{w}$.

The signal due to the Lense-Thirring effect is associated with the signal due to $\delta^{(1)}$. Today, it seems impossible to reduce $\delta^{(1)}$ significantly, this is the reason why it should be calculated from the Fourier analysis of the signal itself altogether with the velocity $\alpha_1\overrightarrow{w}$.

The interest of the spin is obvious. If σ is constant (no spin) the signal is the sum of two periodic signals with frequency ν_O and $2\nu_O$ where ν_O is the orbital frequency of the satellite ; therefore one ASU gives two informations (two functions of the time). When the satellite spins, we get 9 functions of the time t. The information is much more important in this case.

V. CONCLUSION

In Hyper, the Lense-Thirring effect is associated with many perturbations which cannot be cancelled. We have exhibited the various terms that one needs to calculate in order to obtain the full signal and we have emphasized the necessity to increase our knowledge of the Newtonian gravitational potential. This is still more crucial for Jupiter despite the fact that the Lense-Thirring effect is much bigger.

Using four parameters, ξ, ε, η and μ defined in table 2, we have also sketched a method to take into account the residual gravitational field in a nearly free falling satellite, namely the tidal and higher order effects.

Compared with GPB, the principle of the measure is not the same, the difficulties are quite different but the job is not easier. For instance, considering the quantities K_σ or $K_{2\theta\pm\sigma}$ above, one can check that, for an Earth satellite, $\delta^{(1)}$ must remain smaller than 2nm for the corresponding signal to remain smaller than the Lense-Thirring one. It does not seem that such a precision can be controlled in the construction of the experimental device itself. It is therefore necessary to measure $\delta^{(1)}$ with such an accuracy.

What can be deduced from the time analysis depends on the accuracy of the various parameters. From $K_{2\theta\pm2\sigma}$ we deduce α. Then from $K_{\theta\pm\sigma}$ we obtain $\alpha_1 w_{\shortparallel}/c$ and $\alpha_1 w^{\hat{3}}/c$ as two functions of θ_w. Therefore one can check if $\alpha_1 w = 0$ or not.

From $K_{2\theta\pm\sigma}$ one can calculate $\dfrac{M_{\textcircled{s}}c}{r_0^2 v_g}\delta^{(1)}$ as a function $G_{(+)}$ of $J_{\shortparallel}/r_0^2$, θ_J and $\left(\dfrac{M_{\textcircled{s}}}{r_0}\right)^{3/2}\dfrac{c^2 T_D^2}{r_0^2}$ and as a different function, $G_{(-)}$ of the same arguments. One could check the equality $G_{(+)} = G_{(-)}$. If we assume that $\overrightarrow{J}_{\textcircled{s}}$ is known, then θ_J is known and from the equality $G_{(+)} = G_{(-)}$ we deduce the value of $J_{\shortparallel}$. Using the relation $J_{\shortparallel} = \dfrac{1+\gamma+\alpha_1/4}{2}\left(\overrightarrow{J}_{\textcircled{s}}\right)_{\shortparallel}$ one could check whether $\gamma + \alpha_1/4 = 1$.

K_σ would give $\dfrac{M_{\textcircled{s}}c}{r_0^2 v_g}\delta^{(1)}$ as a function of $J_{\shortparallel}/r_0^2$, θ_J and $J^{\hat{3}}/r_0^2$. Using the previous results, we obtain $J^{\hat{3}}$. The relation $J^{\hat{3}} = \dfrac{1+\gamma+\alpha_1/4}{2}\left(\overrightarrow{J}_{\textcircled{s}}\right)^{\hat{3}}$ gives an other test of the value of $\gamma + \alpha_1/4$.

But over all, the best test would be that the signal (as a function of the time) fits the theoretical prediction.

As a final conclusion let us put forwards that the geometric scheme which has been used is just a preliminary contribution to the discussion on the feasibility of Hyper. Only a more powerful model can answer the question. This model should take into account all the gravitational perturbations that we have outlined here and it should consider the interaction between laser fields and matter waves in more a realistic manner. Such an approach has been recently developed [7], [8] it could give definitive results in the future.

---

[1] R. Bingham *et al.*, *HYPER Hyper-Precision Cold Atom Interferometry in Space Assessment Study Report*, vol. 10 (ESA-SCI, 2000).

[2] B. Linet and P. Tourrenc, Can. J. Phys. **54**, 1129 (1976).

[3] W.-Q. Li and W.-T. Ni, J. Math. Phys. **20**, 1473 (1979).

[4] C. Will, *Theory and experiment in gravitational physics* (Cambridge University Press, 1981).

[5] C. W. Misner, K. S. Thorne, and J. A. Wheeler, *Gravitation* (San Francisco: W.H. Freeman and Co., 1973, 1973).

[6] M.-C. Angonin, X. Ovido, and P. Tourrenc, GRG **36**, 411 (2004).

[7] C. Antoine and C. Bordé, J. Opt. B **5**, S199 (2003).

[8] C. Bordé, accepted to GRG (2004).

[9] The Lense-Thirring effect results also in a secular precession which is not considered here but in Gravitational Probe B : a NASA experiment which

is planed to be launched on the 6th of December 2003.

[10] An arbitrary constant can always be added to U_*. It is chosen in such a way that zero is the mean value of U_* at point O in the satellite.

[11] Notice that the quantity $\xi^{1/2}O_1$ is what is called O_1 in Will's book quoted above

[12] The Thomas term reads $\vec{\Omega}_{Th} = \frac{1}{2}\vec{v} \wedge \vec{A}$ where $\vec{A}$ is the "acceleration". From the relativistic point of view, it would be better to define the Thomas term with the local physical acceleration, $\vec{A} \simeq \frac{d\vec{v}}{dt} - \vec{\nabla}U$, rather than the acceleration, $\frac{d\vec{v}}{dt}$, relatively to the geocentric frame.

[13] notations of the paper by Ch. Marchal in Bulletin du museum d'histoire naturelle, 4ème série, section C **18,** 517 (1996)

The forgotten process : the emission stimulated by matter waves.
Tourrenc Ph, Angonin M-C, Wolf P, version du 22/07/04

THE "FORGOTTEN" PROCESS : the emission stimulated by matter waves.

Philippe Tourrenc[1], Marie-Christine Angonin[1] and Peter Wolf [2,3]

[1] *Université Pierre et Marie Curie, ERGA, case 142, 4 Pl. Jussieu, 75252 Paris, CEDEX 05, France*
[2] *BNM-SYRTE, Observatoire de Paris, 61 Av. de l'Observatoire, 75014 Paris, France*
[3] *Bureau International des Poids et Mesures, Pavillon de Breteuil, 92312 Sèvres, CEDEX, France*

Abstract: In a famous paper where he introduces the A and B coefficients, Einstein considered that atomic decays of excited atoms can be stimulated by light waves. Here we consider that atomic decays can also be stimulated by atomic waves. It is however necessary to change the Maxwell-Boltzmann statistics of thermal equilibrium into Bose-Einstein statistics and to introduce a coefficient C which complements the list of the coefficients introduced by Einstein.

Stimulated emission of light can be considered as the first step towards the laser. Similarly, stimulated production of matter waves can be considered as the basic phenomenon for an atom-laser.

Most of the results that we obtain here are not new. However, the method that we use remains very close to elementary classical physics and emphasizes the symmetry between electromagnetic and matter waves from various points of view.

1 Introduction

In 1916 and 1917, Einstein introduced the well known A and B coefficients [1]. For the first time the stimulated emission of photons by electromagnetic radiation was suggested. In the present paper we generalize the argument of Einstein. We consider that an atom displays an internal structure and that a matter wave describes its space-time behavior. The decay of an atom towards its fundamental state can happen spontaneously. It can also be stimulated by the electromagnetic waves or the matter waves which bathe the atom. The latter (decay stimulated by matter waves) has been "forgotten" until the 1990s when it appeared in the context of Bose Einstein Condensation (BEC) and the atom laser [2, 3, 4, 5].

In his papers, Einstein put forward "a derivation of Planck's formula [...] closely related to Wien's original argument". Our goal is different: we want to emphasize the symmetry between electromagnetic and matter waves. However, we will follow Einstein in the sense that we will use arguments close to his

own within our specific framework, for our specific purpose. We thereby derive a simple description of the "forgotten" process via the introduction of a new coefficient C in addition to the Einstein coefficients A and B.

We first summarize the usual approach describing atom-photon interactions using Maxwell-Boltzmann statistics and the Einstein A and B coefficients. This is followed by a short summary of matter waves and their properties that are relevant to our purpose. In section 4 we restore the symmetry between electromagnetic and matter waves, which we then apply to the thermal equilibrium (section 5) leading to the derivation of transition probabilities for all processes. We obtain the usual Einstein coefficients and a "forgotten" coefficient from these probabilities in section 6 and conclude in section 7.

2 The usual approach

We consider two level atoms where E_1 and E_2 are the energy of the atom in each level (with $E_2 - E_1 = \hbar\omega_0 > 0$). The atoms are in an ideal electromagnetic cavity where they are interacting with the electromagnetic radiation. The thermal equilibrium, at temperature T, is achieved. The case of atoms in free space is obtained when the volume V of the cavity becomes infinite.

The electromagnetic energy is distributed among the different modes of the cavity. It is described by Planck's energy spectral density

$$\rho_\varphi(\omega, T) = d_\varphi \times \frac{4\pi\nu^2}{c^3} \times \hbar\omega \times \frac{1}{e^{\hbar\omega/k_B T} - 1} \tag{1}$$

where k_B is the Boltzmann constant.

Each term in $\rho_\varphi(\omega, T)$ has a precise meaning.

• The electromagnetic wave is characterized by a wave vector $\overrightarrow{k}$. We define $2\pi\,\nu = c\left\|\overrightarrow{k}\right\|$. The electromagnetic waves in an ideal cavity must satisfy boundary conditions. As a consequence, ν can take only resonant values: the number of possible values between ν and $\nu + d\nu$ is $d\mathcal{N}_\nu = \frac{4\pi\nu^2}{c^3} d\nu \times V$ where c is the speed of light in vacuum and V the volume of the cavity.

• The energy of a photon is $\hbar\omega$, where ω is the angular frequency. For an electomagnetic field the relation $\omega = 2\pi\nu$ holds true.

• Once $\overrightarrow{k}$ is given, ω is known. There remain however $d_\varphi = 2$ polarizations. The first factor, d_φ in relation (1), is precisely the number of polarizations (the degeneracy of photonic states) of the electromagnetic waves. Therefore the number of modes in the interval $[\nu,\, \nu + d\nu]$ is

$$d\mathcal{N}_m = d_\varphi \times \frac{4\pi\nu^2}{c^3} d\nu \times V \tag{2}$$

• Finally, following the Bose-Einstein statistics, the mean number of photons in a mode at thermal equilibrium is $\frac{1}{e^{\hbar\omega/k_B T} - 1}$.

The spectral energy density (1) represents the energy density per interval $d\nu$. It is sometimes useful to define a quantity $\tilde{\rho}_\varphi(\omega, T)$ that represents the energy density per corresponding interval $d\omega$, i.e.

$$\tilde{\rho}_\varphi(\omega, T) = \rho_\varphi(\omega, T)\frac{d\nu}{d\omega}. \tag{3}$$

For electromagnetic waves we have $\tilde{\rho}_\varphi(\omega, T) = \rho_\varphi(\omega, T)/2\pi$.

The thermal equilibrium in the cavity is secured by a connection to a thermal reservoir at temperature T. We assume the following properties:

A1 First we assume that the reservoir can exchange some energy with the atoms in order that the Maxwell-Boltzmann equilibrium law is fulfilled:

$$\frac{N_2}{N_1} = \frac{d_2}{d_1}e^{-\hbar\omega_0/k_BT} \tag{4}$$

where N_1 (or N_2) is the number of atoms with energy E_1 (or E_2) and d_1 (or d_2) the degeneracy of level E_1 (or E_2).

A2 Second we consider that photons can be either absorbed or emitted by the reservoir, in order to achieve the equilibrium spectral density, $\rho_\varphi(\omega, T)$, above.

A3 Finally we admit that once the thermal equilibrium is achieved, it remains without the help of the reservoir although it is a statistical equilibrium where absorption and emission of photons, excitation and decay of atoms, happen permanently.

Assuming conservation of energy, two kinds of effects are possible:

1. Spontaneous mechanisms happen even when no radiation is present in the cavity. This is the case of a spontaneous decay of an atom from energy E_2 to energy E_1 with the emission of a photon whose angular frequency is ω_0. The number of spontaneous decays per unit time is $A \times N_2$. In a large enough cavity two neighboring modes have very close properties and their frequencies can be considered to belong to a continuum. In such a case, A is a characteristic of the atom alone, independently of the cavity. We do not consider spontaneous excitation where energy would be created from nothing.

2. Stimulated mechanisms happen only because some radiation is already present. Two mechanisms are actually possible: i) the absorption of a photon with energy $\hbar\omega_0$ by an atom which is therefore excited from energy E_1 to energy E_2 and ii) the emission of a photon with energy $\hbar\omega_0$ by an atom which decays from energy E_2 to energy E_1. The number of events per unit time of each mechanism is $B_{(abs)} \times \rho_\varphi(\omega_0, T) N_1$ and $B_{(em)} \times \rho_\varphi(\omega_0, T) N_2$, where $\omega_0 = 2\pi\nu_0$.

The equilibrium condition is

$$AN_2 + B_{(em)}\rho_\varphi(\omega_0, T) N_2 = B_{(abs)}\rho_\varphi(\omega_0, T) N_1. \tag{5}$$

Within the preceding theoretical framework, one finds that the thermal equilibrium ((5) with (1) and (4)) is possible at any temperature T if and only if

$$B_{(abs)} = \frac{d_2}{d_1} B_{(em)} \quad \text{and} \quad A = \frac{8\pi\nu_0^2}{c^3}\hbar\omega_0 B_{(em)} \tag{6}$$

Therefore the existence of spontaneous emission (*i.e.* $A \neq 0$), implies that absorption and stimulated emission also exist (*i.e.* $A \neq 0 \Rightarrow B_{(em)} \neq 0$ and $B_{(abs)} \neq 0$).

These results are well known and can be found in many textbooks [6, 7, 8].

3 Matter waves

Matter waves were introduced in de Broglie's thesis in 1924. At this time the photoelectric effect had already been interpreted (Einstein 1905) and the Compton effect observed (Compton 1923). Thus, it was already known that light could behave as a flow of particles called photons[1]. The merit of Louis de Broglie was to reverse the proposition and to claim that particles, e.g. electrons, could behave like waves.

Since these early days, the similarity between light waves and matter waves never ceased to be emphasized, from the first observation of electronic interferences by Davisson and Germer in 1927 to atom interferometry, and recently Bose-Einstein condensation of atoms, first achieved in 1995.

Several examples can be given of matter waves and their applications: the electronic microscope and the Collela-Overhauser-Werner experiment with neutrons [9] are well known. More recently laser cooling of atoms has lead to the development of atom interferometry used, for example, for ultra precise inertial sensors such as gravimeters [10], gradiometers [11] and gyroscopes [12]. Ultimately the use of the forgotten process to produce Bose-Einstein condensates, i.e. coherent beams of matter waves with all atoms in the same mode, should result in atom lasers based on amplification of the matter fields via the forgotten process. These are expected to lead to significant improvements in matter wave interferometry and to new applications. Presently, what is often called an atom laser is a Bose-Einstein condensate which has been produced by other means.

Despite its complex structure, an atom can be considered as a particle with a mass M depending on its internal energy : $M = M_0 + E/c^2$ where E is the internal energy and M_0 the mass of the atom in its fundamental level. The total energy of the atom is then

$$\hbar\omega = \sqrt{(Mc^2)^2 + \left(c\hbar\overrightarrow{k}\right)^2} \approx Mc^2 + \frac{\hbar^2\overrightarrow{k}^2}{2M} \tag{7}$$

where ω is its angular frequency, $\hbar\overrightarrow{k}$ its momentum and the non-relativistic approximation holds for $\hbar\|\overrightarrow{k}\|/M \ll c$.

[1]The word "photon" was invented several years later but the concept of photon was already there.

An atom is generally characterized by its angular momentum, $\overrightarrow{J}$ which plays the role of some intrinsic spin. The value of $\overrightarrow{J}^2$ is $\hbar^2 j\,(j+1)$. General results in quantum mechanics lead to the conclusion that $2j$ is an integer which depends on the internal state of the atom, and that the atom is a boson when j itself is an integer. This is the only case that we consider in the sequel.[2]

The energy can be degenerate. Therefore, for a given mass, the internal state is a multi-component vector which belongs to a d_a dimensional space.

Keeping the definition $2\pi\,\nu = c\left\|\overrightarrow{k}\right\|$, the fundamental difference with respect to photons is that now the relation between ω and ν is the dispersion relation obtained from (7)

$$\hbar\omega = \sqrt{\left(Mc^2\right)^2 + \left(2\pi\hbar\nu\right)^2}. \tag{8}$$

Let us imagine that matter waves can be trapped in an ideal cavity where they appear as a superposition of the resonant modes of the cavity. The number of resonance values of ν in the interval $[\nu, \nu + d\nu]$ is

$$d\mathcal{N}_\nu = \frac{4\pi\nu^2}{c^3} d\nu \times V \tag{9}$$

and the number of modes $d\mathcal{N}_m = d_a \times d\mathcal{N}_\nu$.

As we consider bosons only, the mean number of particles per mode at thermal equilibrium is given by Bose-Einstein statistics

$$\overline{n} = \frac{1}{e^{(\hbar\omega)/(k_B T)} - 1}. \tag{10}$$

Therefore, the spectral energy density is

$$\rho_a\left(\omega, T\right) = d_a \times \frac{4\pi\nu^2}{c^3} \times \hbar\omega \times \frac{1}{e^{(\hbar\omega)/(k_B T)} - 1}. \tag{11}$$

Analogously to the electromagnetic case one can introduce a corresponding energy density per interval of angular frequency $\tilde{\rho}_a\left(\omega, T\right)$ defined by equation (3). But now $d\nu/d\omega$ is obtained from the dispersion relation (8) and therefore

$$\tilde{\rho}_a\left(\omega, T\right) = \frac{\rho_a\left(\omega, T\right)}{2\pi} \frac{\hbar\omega}{\sqrt{\left(\hbar\omega\right)^2 - \left(Mc^2\right)^2}} = \frac{\rho_a\left(\omega, T\right)}{2\pi} \frac{\omega}{2\pi\nu}. \tag{12}$$

One can check that the relations (8) to (12) are the same for matter waves and for light waves when setting $M = 0$ and $d_a = d_\varphi = 2$ for the photon.

[2]The sensitivity of atom interferometers is directly related to the number of atoms (presently of order of 10^5). Therefore, because of the Pauli exclusion principle, the use of fermions is of less interest and not considered here.

4 Restoring the symmetry between electromagnetic and matter waves

In section 2, the atoms and the photons have been considered from two very different points of view. For instance, the decay of an atom could be stimulated by the presence of the photons but the presence of the atoms did not produce any similar effect. Moreover, the atoms were not able to be created or annihilated, only their internal energy could change by emission or absorption of photons. However, considering what we know about the origin of the Universe, we have to admit that atoms can be created too. Of course, the corresponding mechanism can be complicated and slow but annihilation and creation of atoms are possible as well as annihilation and creation of photons; this is a matter of principle not of order of magnitude.

First, in order to restore the similarity between the atoms and the photons, let us modify the notations. Now, a is an atom in its fundamental state of energy E_a. This atom can absorb a photon φ, the corresponding excited state is $a\varphi$ whose internal energy is $E_{a\varphi}$. We consider that the thermal equilibrium is a statistical equilibrium driven by the chemical-like equation

$$a\varphi \rightleftharpoons a + \varphi \tag{13}$$

where φ, a and $a\varphi$ are bosons described by waves (i.e. electromagnetic waves and matter waves) which are trapped in an ideal cavity at temperature T.

An atom is considered as the quantum associated to a matter wave, therefore $N_{a\varphi}$ and N_a are now occupation numbers of matter-wave-modes, similar to the occupation number of the electromagnetic modes (i.e. the number of photons).

The mass of the atom depends on its internal energy. Thus we can interpret the change of the internal energy as the annihilation of an atom with the initial value of the mass and the creation of an atom with the final value of the mass.

The atoms and the photons are supposed to be trapped in an ideal cavity without losses. The cavity is coupled to a thermal reservoir at temperature T. We assume the following properties:

B1 The photons and the atoms occupy respectively electromagnetic-modes and matter-wave-modes. The equilibrium is achieved when the mean number of quanta per mode is given by the Bose-Einstein statistics $\overline{n} = \frac{1}{e^{\hbar\omega/k_BT}-1}$ i.e. we substitute equ. (10) to equ. (4).

B2 Second we consider that photons and atoms can be either absorbed or emitted by the reservoir, in order to achieve the equilibrium spectral densities (1) and (11).

B3 Finally we admit that once the thermal equilibrium is achieved, it remains without the help of the reservoir although it is a statistical equilibrium where annihilation and creation of photons and atoms, happen permanently.

From the old point of view the dissymmetry between matter and light lies in the difference between the assumptions **A1** and **A2** of section 2. Here, this

dissymmetry has disappeared but the Maxwell-Boltzmann statistics used in assumption **A1** has been changed into Bose-Einstein relativistic statistics.

The various modes of the excited atoms $a\varphi$ are labelled by a set of indexes called m; the modes of the atoms a are labelled by n and the modes of the photons φ by a set of indexes k. We use the notation $(a\varphi)_m$ for an excited atom $a\varphi$ in the mode m, and the similar notations $(a)_n$ and $(\varphi)_k$. With these notations equation (13) becomes

$$(a\varphi)_m \underset{(2)}{\overset{(1)}{\rightleftharpoons}} (a)_n + (\varphi)_k \,. \tag{14}$$

Following assumption **B3** above, we assume that the equilibrium is achieved when, during a given arbitrary time, the number of reactions to the right (reaction (1)) is the same as the number of reactions to the left (reaction (2)). Moreover we accept the usual assumption that the number of reactions per unit time is proportional to the number of quanta in the modes involved.

We introduce the concentrations $[a\varphi]_m$, $[a]_n$ and $[\varphi]_k$ i.e. the number of atoms or photons per unit volume respectively in mode m, n and k. The volume of the cavity is V. We define α, $\beta_{(abs)}$, $\beta_{(em)}$ and γ:
(i) The number of spontaneous reactions (1) per unit time is $\alpha \times [a\varphi]_m V$.
(ii) The number of reactions (2) per unit time is $\beta_{(abs)} \times [\varphi]_k V \times [a]_n V$.
(iii) Given an excited atom, $a\varphi$, in the mode m, we consider its decay (reaction (1)) stimulated by the presence of the photons in the mode k. The number of such reactions per unit time is $\beta_{(em)} \times [\varphi]_k V \times [a\varphi]_m V$.

With Maxwell-Boltzmann statistics where $M_0c^2 \gg \hbar\omega_0$ and $Mc^2 \gg k_BT$, and within the "broad band" approximation[3], these mechanisms result in equ. (5).
(iv) Finally, we assume that the reaction (1) can also be stimulated by the presence of the atoms a in the mode n, which restores the symmetry between electromagnetic waves and matter waves. We call this mechanism the "forgotten" process[4]. The number of such reactions per unit time is $\gamma \times [a]_n V \times [a\varphi]_m V$.

5 The thermal equilibrium and its consequences

Compared to the year 1917 the conception of matter has changed dramatically. We will now explain why this conceptual change leaves the description of the thermal equilibrium practically unchanged. However, we will emphasize the importance of the "forgotten" process.

[3]The "broad band" approximation is valid when the radiation in the cavity displays a line shape whose width is large compared to the width of the natural lineshape of the atomic decay.

[4]The short chronology that we gave shows that this process could not be considered before 1924. It was actually forgotten between 1924 and the 1990s when it first appeared in the context of Bose-Einstein condensation [2, 3, 4, 5].

Now we assume that the equilibrium is achieved when the mean number of quanta per mode is given by the Bose-Einstein statistics and when the number of reactions (1) per unit time is equal to the number of reactions (2). Therefore

$$\begin{aligned} [a]_n V &= \frac{1}{e^{(\hbar\omega_a)/(k_B T)} - 1}, \\ [\varphi]_k V &= \frac{1}{e^{(\hbar\omega_\varphi)/(k_B T)} - 1}, \\ [a\varphi]_m V &= \frac{1}{e^{(\hbar\omega_{a\varphi})/(k_B T)} - 1}, \end{aligned} \tag{15}$$

and

$$\begin{aligned} \beta_{(abs)} \times [\varphi]_k V \times [a]_n V &= \alpha \times [a\varphi]_m V + \beta_{(em)} \times [\varphi]_k V \times [a\varphi]_m V \\ &\quad + \gamma \times [a]_n V \times [a\varphi]_m V. \end{aligned} \tag{16}$$

The energy of the atom a in the mode n is $\hbar\omega_a$, similarly $\hbar\omega_\varphi$ is the energy of the photon in the mode k and $\hbar\omega_{a\varphi}$ is the energy of the excited atom $a\varphi$ in the mode m. We assume that the energy ($\hbar\omega_a$, $\hbar\omega_\varphi$ or $\hbar\omega_{a\varphi}$) defines the mode except for the polarization of the light and the degeneracy of the internal energy of the atoms[5].

One can check that the equality (16) holds true at any temperature if and only if

$$\omega_{a\varphi} = \omega_a + \omega_\varphi \quad \text{and} \quad \beta_{(abs)} = \alpha = \beta_{(em)} = \gamma \tag{17}$$

The first relation in (17) expresses the conservation of energy while the other relations imply that the "forgotten" process happens because spontaneous decay is an actual process ($\alpha \neq 0 \Rightarrow \gamma \neq 0$).

Let us now verify that at thermal equilibrium the results above are practically the usual ones when the "forgotten" process is neglected. We consider equ. (16) with $\beta_{(abs)} = \alpha = \beta_{(em)} = \gamma$. Then the sum of the last two terms is $\gamma \times [\varphi]_k V \times [a\varphi]_m V \left(1 + \frac{[a]_n}{[\varphi]_k}\right)$. Using (15) it is easy to check that $\frac{[a]_n}{[\varphi]_k} \ll 1$ even with extreme (impossible!) values of $\hbar\omega_\varphi$ and $k_B T$. Therefore the contribution $\gamma \times [a]_n V \times [a\varphi]_m V$ in (16) is completely negligible and the "forgotten" process does not play any significant role at thermal equilibrium.

Moreover one can easily calculate $N_{a\varphi}/N_a$ where $N_{a\varphi}$ (resp. N_a) is the mean number of atoms with energy $E_{a\varphi} = \hbar\omega_{a\varphi}$ (resp. $E_a = \hbar\omega_a$). It is the number of atoms in one mode with energy $\hbar\omega_{a\varphi}$ (resp. $\hbar\omega_a$) times the number of modes with such an energy. From the preceeding assumptions we obtain

$$N_{a\varphi} = \frac{d_{a\varphi}}{e^{(\hbar\omega_{a\varphi})/(k_B T)} - 1} \quad \text{and similarly} \quad N_a = \frac{d_a}{e^{(\hbar\omega_a)/(k_B T)} - 1}. \tag{18}$$

Finally, using the relation $\hbar\omega_{a\varphi} \sim \hbar\omega_a \sim M_0 c^2 \gg k_B T$ we obtain

[5] This is the case, for example, for an ideal rectangular cavity of suitable proportions.

$$\frac{N_{a\varphi}}{N_a} \simeq \frac{d_{a\varphi}}{d_a} \frac{e^{(\hbar\omega_a)/(k_B T)}}{e^{(\hbar\omega_{a\varphi})/(k_B T)}} = \frac{d_{a\varphi}}{d_a} e^{-(\hbar\omega_{a\varphi} - \hbar\omega_a)/(k_B T)} \tag{19}$$

which is identical to (4) under the simple change of notation ($a\varphi \to 2$, $a \to 1$ and $\hbar\omega_{a\varphi} - \hbar\omega_a = \hbar\omega_0$).

As a conclusion we can notice that at thermal equilibrium nothing is significantly modified if we use Maxwell-Boltzmann statistics instead of Bose-Einstein statistics and if we neglect the "forgotten" process. However, far from equilibrium this is not necessarily the case.

Now we can use standard methods to give an estimation of γ in the simplest case of a homogeneous line width.

α is the probability per unit time that an excited atom $a\varphi$, in a given mode m with given energy $\hbar\omega_{a\varphi}$, decays spontaneously into $a + \varphi$ where the photon φ is in the mode k with energy $\hbar\omega_\varphi$ and the atom a in the mode n with energy $\hbar\omega_a$. Let us define the probability per unit time, dp, that an excited atom decays spontaneously into a photon with angular frequency $\omega_\varphi \in [\omega_{\varphi k}, \omega_{\varphi k} + d\omega]$ and a ground state atom with angular frequency $\omega_a \in [\omega_{an} - d\omega, \omega_{an}]$ where $\omega_{a\varphi} = \omega_a + \omega_\varphi$. We then have

$$dp = \alpha \times d_\varphi d_a \times d\mathcal{N}_{a+\varphi} \tag{20}$$

where $d\mathcal{N}_{a+\varphi}$ is the number of pairs of resonance values (ν_a, ν_φ) that satisfy $\omega_\varphi \in [\omega_{\varphi k}, \omega_{\varphi k} + d\omega]$, $\omega_a \in [\omega_{an} - d\omega, \omega_{an}]$ and $\omega_{a\varphi} = \omega_a + \omega_\varphi$.

For the photons, the number of resonant values of ν_φ, $d\mathcal{N}_\varphi$, over the bandwidth $d\omega$ are given (c.f. equation (1)) by the number of possible values of ν, i.e. $\frac{4\pi\nu^2}{c^3} d\nu V$, and $2\pi\nu = \omega$ which holds true for photons, therefore

$$d\mathcal{N}_\varphi = \frac{\omega_\varphi \nu_\varphi d\omega}{\pi c^3} V. \tag{21}$$

Similarly for the ground state atom, the number of resonant values of ν_a over the bandwidth $d\omega$ are given by $\frac{4\pi\nu^2}{c^3} d\nu V$, but with the relation between ν and ω given in (8). This leads to

$$\begin{aligned} d\mathcal{N}_a &= \frac{\omega_a \nu_a d\omega}{\pi c^3} V = \frac{\omega_a \sqrt{(\hbar\omega_a)^2 - (M_0 c^2)^2}\, d\omega}{2\pi^2 c^3 \hbar} V \\ &\simeq \frac{(M_0 c^2)\sqrt{2 M_0 c^2 E_k}\, d\omega}{2\pi^2 c^3 \hbar^2} V \end{aligned} \tag{22}$$

where $E_k = \hbar\omega_a - M_0 c^2$ is the kinetic energy of a, and where we have used $\hbar\omega_a + M_0 c^2 \simeq 2 M_0 c^2$.

Comparing (21) to (22) we note that even in extreme conditions $d\mathcal{N}_a$ is much bigger than $d\mathcal{N}_\varphi$. For example, with $E_k \approx k_B T \approx 10^{-13}$ eV, $M_0 c^2 \approx 1$ GeV and $\hbar\omega_\varphi \approx 20$ eV we have $d\mathcal{N}_a \approx 10^4 d\mathcal{N}_\varphi$. As a result the number of possible energy pairs $d\mathcal{N}_{a+\varphi}$ is entirely determined by $d\mathcal{N}_\varphi$ as for each ω_φ there exists

a ω_a such that $\omega_{a\varphi} = \omega_a + \omega_\varphi$ (but not vice-versa), so we have $d\mathcal{N}_{a+\varphi} \simeq d\mathcal{N}_\varphi$. Under these conditions equation (20) becomes

$$dp = \alpha \times d_\varphi d_a \times \frac{\omega_\varphi \nu_\varphi d\omega}{\pi c^3} V. \tag{23}$$

On the other hand, under the assumption that the atom is at rest and the assumption of isotropy, the spontaneous emission of a photon is characterized by a function $f_\varphi(\omega_\varphi - \omega_{\varphi 0})$ which defines the line shape of the emitted light. The quantity $f_\varphi(\omega_\varphi - \omega_{\varphi 0})\, d\omega$ is interpreted as the probability that the emitted photon displays an angular frequency $\omega_\varphi \in [\omega_{\varphi k}, \omega_{\varphi k} + d\omega]$. Therefore

$$dp = \frac{1}{t_{sp}} f_\varphi(\omega_\varphi - \omega_{\varphi 0}) \tag{24}$$

where t_{sp} is the time constant which characterizes the spontaneous emission (i.e. $1/t_{sp} = A$, the Einstein coefficient).

It is then straightforward to obtain α by eliminating dp between (23) and (24)

$$\alpha = \beta_{abs} = \beta_{em} = \gamma = \frac{\pi c^3}{d_\varphi d_a \omega_\varphi \nu_\varphi} \frac{1}{t_{sp}} f_\varphi(\omega_\varphi - \omega_{\varphi 0}) \times \frac{1}{V}. \tag{25}$$

One can now calculate the probability per unit time, $W_{(em)}$, of stimulated decay of an excited atom $a\varphi$ in mode m into a photon φ in mode k and a ground state atom a in any mode. First we notice that the decay due to the photons in mode k, towards a special given mode of a, has a probability per unit time $\beta_{(em)} \times [\varphi]_k V$ (see the property (iii) of section 4 above). Therefore, the probability of a decay towards the various modes n of a which display the same energy is

$$W_{(em)} = d_a \times \beta_{(em)} \times [\varphi]_k V = \frac{\pi c^3}{d_\varphi \omega_\varphi \nu_\varphi} \frac{1}{t_{sp}} f_\varphi(\omega_\varphi - \omega_{\varphi 0}) \times \frac{u_k(\omega_\varphi)}{\hbar \omega_\varphi} \tag{26}$$

where we have introduced the electromagnetic energy density of the mode k defined as $u_k(\omega_\varphi) = [\varphi]_k \times \hbar \omega_\varphi$.

Similarly the probability per unit time, $W_{(abs)}$, of absorption of a photon φ in mode k by a ground state atom a in mode n to form an excited atom $a\varphi$ in any mode is

$$W_{(abs)} = d_{a\varphi} \times \beta_{(em)} \times [\varphi]_k V = \frac{d_{a\varphi}}{d_a} \frac{\pi c^3}{d_\varphi \omega_\varphi \nu_\varphi} \frac{1}{t_{sp}} f_\varphi(\omega_\varphi - \omega_{\varphi 0}) \times \frac{u_k(\omega_\varphi)}{\hbar \omega_\varphi}. \tag{27}$$

Expressions (26) and (27) are well known in the usual laser theory and can be found in many textbooks (e.g. [6]).

On the other hand, the "forgotten" process leads to new results. We calculate the probability per unit time, W_f, that an excited atom $a\varphi$ in mode m undertakes the forgotten process i.e. that it decays into a ground state atom a

in mode n and a photon φ in any mode. The decay due to the atoms a in mode n, towards a special given mode of φ, has a probability per unit time $\gamma \times [a]_n V$ (see the property (iv) of section 4 above). Therefore, the probability of a decay towards the various modes k of φ which display the same energy is

$$W_f = d_\varphi \times \gamma \times [a]_n V = \frac{\pi c^3}{d_a \omega_\varphi \nu_\varphi} \frac{1}{t_{sp}} f_\varphi(\omega_\varphi - \omega_{\varphi 0}) \times \frac{u_n(\omega_a)}{\hbar \omega_a} \tag{28}$$

where $u_n(\omega_a) = [a]_n \times \hbar\omega_a$ is the energy density of the ground state atoms in mode n.

At thermal equilibrium we have $[a]_n \ll [\varphi]_k$ (from (15)) which, using (26) and (28), implies $W_f \ll W_{(em)}$, i.e. the probability for an excited atom to decay via stimulation by a matter wave is much smaller than via stimulation by an electromagnetic wave, and the "forgotten" process is practically negligible. However, this may not be the case far from equilibrium. For example, one can imagine a situation where one particular mode $[a]_n$ is strongly populated. This would lead to decay preferentially towards that mode via the "forgotten" process, which in turn increases the population of that mode, and so on. That kind of mechanism is the basis of the experimental proposal for an atom laser in [4].

6 The Einstein and the "forgotten" coefficients

Now we consider a broad band electromagnetic radiation which is modelled by monochromatic radiations with angular frequencies $\omega_{\varphi\ell}$ where ℓ is an integer and $\omega_{\varphi\ell+1} - \omega_{\varphi\ell} = \delta\omega_\varphi$. The function $f_\varphi(\omega_{\varphi\ell} - \omega_{\varphi 0})$ has a maximum for $\omega_{\varphi\ell} \simeq \omega_0$; it is negligible for $|\omega_{\varphi\ell} - \omega_{\varphi 0}| > \Delta\omega$ with $\Delta\omega \ll \omega_{\varphi 0}$, and it fulfills the condition $\int_0^\infty f_\varphi(\omega_{\varphi\ell} - \omega_{\varphi 0}) d\omega = 1$. Assuming $\delta\omega_\varphi \ll \Delta\omega$ we can write :

$$\sum_\ell f_\varphi(\omega_{\varphi\ell} - \omega_{\varphi 0}) \delta\omega_\varphi \simeq 1 \qquad . \tag{29}$$

We consider a given initial state characterized by the number $N_{a\varphi}$ of atoms $a\varphi$ with angular frequency $\omega_{a\varphi}$, and the number N_a of atoms a with angular frequency ω_a. We use the preceding results in order to calculate the number dN of photons which are emitted or absorbed during dt, through the various processes.

Let us give the final results before we outline the derivation. One finds

(i) for the spontaneous emission : $dN_{sp} = A\ N_{a\varphi}\ dt = \frac{1}{t_{sp}} N_{a\varphi}\ dt$,

(ii) for the absorption : $dN_{abs} = B_{(abs)}\ \rho_\varphi\ (\omega_{\varphi 0})\ \ N_a dt$ with

$$B_{(abs)} = \frac{d_{a\varphi}}{d_a d_\varphi} \times \frac{c^3}{4\pi\hbar\omega_{\varphi 0}\nu_{\varphi 0}^2} \frac{1}{t_{sp}} \tag{30}$$

(iii) for the emission stimulated by the photons :

$dN_{em} = B_{(em)}\ \rho_\varphi(\omega_{\varphi 0})\ N_{a\varphi} dt$ with

$$B_{(em)} = \frac{1}{d_\varphi} \times \frac{c^3}{4\pi\hbar\omega_{\varphi 0}\nu_{\varphi 0}^2} \frac{1}{t_{sp}} \tag{31}$$

(iv) for the forgotten process (emission stimulated by the atoms) :
$dN_f = C\rho_a(\omega_{a0}) N_{a\varphi} dt$ with

$$C = \frac{1}{d_a} \times \frac{c^3}{4\pi\hbar\omega_{a0}\nu_{a0}^2} \frac{1}{t_{sp}} \tag{32}$$

where $\omega_{a0} = \omega_{a\varphi} - \omega_{\varphi 0}$.

$B_{(abs)}$ and $B_{(em)}$ are the well known Einstein coefficients but C is a new one (it is the "forgotten" coefficient which describes the "forgotten" process).

We now detail the derivation of the above expressions. Let us for instance calculate $B_{(em)}$. We consider that, at a given angular frequency ω_φ, the two electromagnetic polarizations display the same energy density $u_k(\omega_\varphi)$. Therefore the number of photons produced during dt by the stimulated emission due to the electromagnetic radiation at angular frequency ω_φ is $d_\varphi\ W_{(em)}\ N_{a\varphi}\ dt$ where $W_{(em)}$ is given by equ. (26). The stimulated emission due to the radiations at the various frequencies $\omega_{\varphi\ell}$ results in the number of emitted photons $dN_{(em)} = \sum_\ell d_\varphi\ W_{(em)}\ N_{a\varphi}\ dt$. The function $f_\varphi(\omega_\varphi - \omega_{\varphi 0})$ is a quickly varying function of ω_φ while $u_k(\omega_{\varphi\ell})$ is slowly varying within the framework of the broad band approximation. More precisely, we assume $u_k(\omega_{\varphi\ell}) \simeq u_k(\omega_{\varphi 0})$, $\omega_{\varphi\ell} \simeq \omega_{\varphi 0}$ and $\nu_{\varphi\ell} \simeq \nu_{\varphi 0}$, for $\omega_{\varphi 0} - \Delta\omega < \omega_{\varphi\ell} < \omega_{\varphi 0} + \Delta\omega$. Therefore we can take these expressions of $u_k(\omega_{\varphi\ell})$, $\omega_{\varphi\ell}$ and $\nu_{\varphi\ell}$ in order to calculate $dN_{(em)}$. We obtain

$$\begin{aligned} dN_{(em)} &= \sum_\ell d_\varphi \times W_{(em)}\ N_{a\varphi} dt \\ &= \sum_\ell d_\varphi \times \frac{1}{d_\varphi} \frac{\pi c^3}{\hbar\omega_{\varphi\ell}^2\nu_{\varphi\ell}} \frac{1}{t_{sp}} u_k(\omega_{\varphi\ell})\ f_\varphi(\omega_{\varphi\ell} - \omega_{\varphi 0})\ N_{a\varphi} dt \\ &\simeq \frac{1}{d_\varphi} \frac{\pi c^3}{\hbar\omega_{\varphi 0}^2\nu_{\varphi 0}} \frac{1}{t_{sp}} d_\varphi u_k(\omega_{\varphi 0}) \sum_\ell f_\varphi(\omega_{\varphi\ell} - \omega_{\varphi 0})\ N_{a\varphi} dt \end{aligned} \tag{33}$$

The spectral energy density is $\frac{d_\varphi\ u_k(\omega_{\varphi 0})}{\delta\omega_\varphi} = \tilde{\rho}_\varphi(\omega_{\varphi 0})$ where $\tilde{\rho}_\varphi$ is defined by relation (3) then

$$dN_{(em)} = \frac{1}{d_\varphi} \frac{\pi c^3}{\hbar\omega_{\varphi 0}^2\nu_{\varphi 0}} \frac{1}{t_{sp}} \tilde{\rho}_\varphi(\omega_{\varphi 0}) \sum_\ell f_\varphi(\omega_{\varphi\ell} - \omega_{\varphi 0})\, \delta\omega_\varphi\ N_{a\varphi} dt. \tag{34}$$

Finally, with (29) and (3) we find

$$dN_{(em)} = B_{(em)}\ \rho_\varphi(\omega_{\varphi 0})\ N_{a\varphi} dt \tag{35}$$

with

$$B_{(em)} = \frac{1}{d_\varphi} \times \frac{c^3}{4\pi\hbar\omega_{\varphi 0}\nu_{\varphi 0}^2} \frac{1}{t_{sp}}. \tag{36}$$

This expression of $B_{(em)}$ can be found in many textbooks such as [6] where it is calculated in a way very similar to the one presented above. It is also derived in [8].

Expression (30) for $B_{(abs)}$ is obtained by the same method and we will not detail it here.

In order to calculate C we express dN_f using expression (28) for W_f. In this expression, $\omega_a = \omega_{a\varphi} - \omega_{\varphi\ell}$ is a function of $\omega_{\varphi\ell}$ because the mode m, of the initial state is given.

We consider that the d_a atomic modes at the same frequency ω_a display the same energy density $u_n(\omega_a)$ so

$$\begin{aligned} dN_f &= \sum_\ell d_a \times W_f \; N_{a\varphi} \; dt \\ &= \sum_\ell \frac{1}{d_a} \frac{\pi c^3}{\omega_{\varphi\ell}\nu_{\varphi\ell}} \frac{1}{t_{sp}} f_\varphi(\omega_{\varphi\ell} - \omega_{\varphi 0}) \times \frac{d_a u_n(\omega_a)}{\hbar\omega_a} \; N_{a\varphi} \; dt. \end{aligned} \tag{37}$$

We assume that ω_a and $u_n(\omega_a)$ are two slowly varying functions of $\omega_{\varphi\ell}$, then, with the conditions that we have already assumed, we find

$$\begin{aligned} dN_f &= \frac{1}{d_a} \frac{\pi c^3}{\omega_{\varphi 0}\nu_{\varphi 0}} \frac{1}{t_{sp}} \times \frac{d_a u_n(\omega_{a0})}{\hbar\omega_{a0}} \sum_\ell f_\varphi(\omega_{\varphi\ell} - \omega_{\varphi 0}) \; N_{a\varphi} \; dt \\ &= \frac{1}{d_a} \frac{\pi c^3}{\omega_{\varphi 0}\nu_{\varphi 0}} \frac{1}{t_{sp}} \times \frac{1}{\hbar\omega_{a0}} \frac{d_a u_n(\omega_{a0})}{\delta\omega_\varphi} \; N_{a\varphi} \; dt. \end{aligned} \tag{38}$$

It is not obvious to introduce the spectral density $\rho_a(\omega_{a0})$ of the atoms because $\delta\omega_\varphi$ which appears in the expression above is not the angular frequency separation between two neighboring atomic rays.

In the bandwidth $\delta\omega_\varphi$, around ω_{a0}, the number of resonant atomic angular frequencies is given by expression (22): $\delta\mathcal{N}_a = \frac{\omega_{a0}\nu_{a0}}{\pi c^3}\delta\omega_\varphi \times V$. In the same bandwidth there is only one resonant frequency for the photons (the consequence of the definition of $\delta\omega_\varphi$) so $\delta\mathcal{N}_\varphi = \frac{\omega_{\varphi 0}\nu_{\varphi 0}}{\pi c^3}\delta\omega_\varphi \times V = 1$ (c.f. (21)). Therefore $\delta\mathcal{N}_a = \frac{\omega_{a0}\nu_{a0}}{\omega_{\varphi 0}\nu_{\varphi 0}}$. The spectral energy density is $\tilde{\rho}_a(\omega_{a0}, T) = \frac{d_a u_n(\omega_{a0})\delta\mathcal{N}_a}{\delta\omega_\varphi} = \frac{d_a u_n(\omega_{a0})}{\delta\omega_\varphi} \frac{\omega_{a0}\nu_{a0}}{\omega_{\varphi 0}\nu_{\varphi 0}}$. Substituting this into (38) and using the definition (12) of $\tilde{\rho}_a$ we finally obtain

$$dN_f = C \; \rho_a(\omega_{a0}) \; N_{a\varphi} \; dt \tag{39}$$

with

$$C = \frac{1}{d_a} \times \frac{c^3}{4\pi\hbar\omega_{a0}\nu_{a0}^2} \frac{1}{t_{sp}}. \tag{40}$$

One can notice the similarities between the expressions of C and $B_{(em)}$.

A permanent state is achieved when $dN_{sp} + dN_{em} + dN_f = dN_{abs}$. Therefore, at thermal equilibrium, equation (5) becomes

$$A\, N_{a\varphi} + B_{(em)}\rho_\varphi\left(\omega_{\varphi 0}, T\right)\, N_{a\varphi} + C\,\rho_a\left(\omega_{a0}, T\right)\, N_{a\varphi} = B_{(abs)}\rho_\varphi\left(\omega_{\varphi 0}, T\right)\, N_a. \tag{41}$$

One can easily check that the expressions obtained above guarantee the validity of equ. (41) at any temperature when $N_{a\varphi}$ and N_a satisfy Bose-Einstein statistics.

It is also possible to derive the conservation of energy and the coefficients $B_{(em)}$, $B_{(abs)}$ and C directly from equ. (41) where $N_{a\varphi}$ and N_a fulfill Bose-Einstein rather than the Maxwell-Boltzmann statistics. However, in this paper, we chose to emphasize the elementary underlying processes providing, for example, the transition probabilities $W_{(em)}$, $W_{(abs)}$ and W_f (equations (26), (27) and (28)) as functions of the observed electromagnetic line-shape $f_\varphi(\omega_\varphi - \omega_{\varphi 0})$.

7 Conclusion

We have derived a general description of atom-photon interactions of the form $a\varphi \rightleftharpoons a + \varphi$ that includes the "forgotten" process of decay stimulated by the matter waves a, additionally to the well known spontaneous decay and the decay stimulated by the electromagnetic waves φ. Our aim was to provide a description based on fundamental elementary principles, and to emphasize throughout this work the symmetry between atomic and matter waves. To do so, we have followed standard textbook descriptions of the involved known processes (in terms of transition probabilities, energy densities, observed line shapes, and Einstein coefficients) but applied them to also derive analogous expressions for the "forgotten" process that cannot be found in textbooks, yet.

Throughout this work the various mechanisms have been considered for the case of thermal equilibrium. But, similarly to the well known photonic processes, our results (in particular the transition probability W_f and coefficient C of the "forgotten" process) are quite general and remain valid far away from equilibrium. Non-equilibrium conditions (population inversions etc.) are the fundamental ingredients of lasers, and one expects the same to hold true for atom lasers i.e. sources of coherent matter waves. Atom lasers based on matter wave amplification have not been built yet, but several propositions for a practical realization based on the "forgotten" process can be found in the literature [2, 4, 5]. Indeed, any practical realization will necessarily involve conditions far from thermal equilibrium, as can easily be seen from equ. (15). For example, a single atom a inside a cavity corresponds to $[a]_n V = 1$ and therefore the thermal equilibrium condition (15) is only satisfied for temperatures $T \simeq 10^{13} K$ which are impossible to attain in practice.

It is easy to generalise the results that we have obtained to the general bosonic case $ab \rightleftharpoons a+b$ where ab, a and b are massive or massless bosons of any kind (photons, atoms, molecules, etc.). If we assume that the same concepts are valid for the decay of an atom and for the chemical reaction $ab \rightleftharpoons a+b$, i.e. the concept of line shape where $f_\varphi(\omega - \omega_{\varphi 0})$ becomes $f_b(\omega - \omega_{b0})$ and the concept of stimulated and spontaneous reactions, then all our considerations apply to the general bosonic case. Moreover if we assume that in the same elementary angular frequency interval $d\omega$, the number of resonance frequencies is much higher for b than for a, the developments of the preceeding sections (sections 3 to 6) remain unchanged, except for the substitution $\varphi \rightarrow b$ and $\nu_\varphi = \omega_\varphi/2\pi \rightarrow \nu_b = \sqrt{(\hbar\omega_b)^2 - (M_b c^2)^2}/2\pi\hbar$ where M_b is the mass of b in its fundamental state. Under these conditions, the formulae (26), (27), (28), (30), (31), and (32) hold true for the general bosonic case, and the photon case is simply recovered when setting $M_b = 0$ and $d_b = 2$. This simple generalisation further stresses the symmetry between electromagnetic and matter waves as now the atom-photon interaction is just a special case of a general bosonic interaction.

If a perfect symmetry exists between electromagnetic and matter waves, it may be relevant to raise the question of the physical nature of holography with atomic waves, a surely premature question for the time being.

References

[1] Einstein A., Verh. d. Deutschen physikal. Gesellschaft **18**, Nr. 13/14, 318, (1916); and Phys. Zs. **18**, 121, (1917).

[2] Olshanii M., Castin Y., Dalibard J., *Proc. XII Conf. on Laser Spectroscopy*, Inguscio M., Allegrini M., Sasso A., ed., World Scientific, (1995). Spreeuw R.J.C., et al., idem. Bordé. Ch.J., idem.

[3] Wiseman H.M., Collett M.J., Phys. Lett. **A202**, 246, (1995).

[4] Spreeuw R.J.C., et al., Europhys. Lett. **32**, 6, 469, (1995).

[5] Bordé, Ch.J., Phys. Lett. **A204**, 217, (1995).

[6] Yariv A., *Introduction to optical electronics*, Holt, Rinehart and Wilson, (1976).

[7] Sargent M. III, Scully M.O. and Lamb W.E. Jr, *Laser Physics*, Addison-Wesley, (1974).

[8] Hilborn R.C., Am. J. Phys. **50**, 11, 982, (1982) and references therein, (erratum in Am. J. Phys. **51**, 5, 471, (1983)).

[9] Colella R., Overhauser A.W., Werner S.A., Phys. Rev. Lett. **34**, 23, 1472, (1975).

[10] Peters A., Chung K.Y., Chu S., Nature **400**, 849, (1999).

[11] Snadden M.J., et al., Phys. Rev. Lett. **81**, 971, (1998).

[12] Gustavson T.L., Landragin A., Kasevich M.A., Class. Quant. Grav. **17**, 12, 2385 (2000).

CONCLUSION ET PERSPECTIVES

La gravitation expérimentale

La gravitation est une interaction universelle qui concerne toutes les formes de matière ou de rayonnement. Cependant, la gravitation relativiste a longtemps été considérée comme un domaine sans grande application concrète. Depuis un peu plus de vingt ans, la situation a évolué considérablement. Elle a commencé par des phénomènes « exotiques » et purement astrophysiques , tels que la mesure de la décroissance de la période des pulsars millisecondes ou la découverte des mirages gravitationnels, laboratoires naturels pour la gravitation puisque les échelles concernées sont suffisamment grandes pour que les phénomènes soient mesurables.
Mais, à présent, le développement des technologies de laboratoire font que la gravitation relativiste apparaît comme un effet perturbatif pour de nombreuses expériences. Et les perturbations correspondantes ne peuvent pas être négligées, non plus que les petites perturbations de toutes origines ; elles doivent être comprises et identifiées pour interpréter toute expérience de grande sensibilité et de haute précision. Dans ce cadre, on peut citer les détecteurs interférométriques d'ondes gravitationnelles (Virgo en France), où se développe une physique de pointe aux performances exceptionnelles dans les domaines de l'optique, de l'instrumentation, des laser, du développement de l'optomécanique, etc. De même, avec le système GNSS (constellation européenne de satellites destinées à la navigation et au positionnement dans l'espace) la navigation spatiale voit son importance s'affirmer à un niveau de précision tel que les corrections relativistes ne sont pas négligeables. Cela est aussi vrai pour des mission spatiale comme MICROSCOPE (test du principe d'équivalence) ou comme LISA (observation d'ondes gravitationnelles de basses fréquences) qui nécessitent de grandes capacités de contrôle des champs d'inertie locaux.

Nos connaissances sur la façon de modéliser l'effet des champs de gravitation et d'inertie sont limitées aujourd'hui. L'élaboration de méthodes générales reste encore du domaine de la recherche. Bien que cette recherche soit de nature théorique, il est nécessaire que celle-ci se développe en étroite collaboration avec l'expérimentation. Il est possible de décrire rapidement les domaines concernés :
- La gravitation est sans doute l'interaction physique la moins bien connue empiriquement (La précision de la constante newtonienne G n'excède pas 10^{-4} aujourd'hui). La mesure de G et l'interprétation des expériences (la prise en compte des petites forces de toutes nature comme la force de Casimir) est donc très importante, de même que l'interprétation des effets de relativité restreinte.
- Le problème de la matière noire reste aujourd'hui sans réponse. Les anomalies (écarts à la loi de Newton) constatées sur les sondes Pioneer et Ulysse restent inexpliquées. Ces questions importantes sont directement liées à l'observation d'accélérations inattendues et donc à la présence de champs d'inertie (ou de champs gravitationnels) dont l'origine est incomprise aujourd'hui.
- Indépendamment, les progrès rapides dans la mise en œuvre des ondes de matière laissent envisager à terme de nombreuses applications, permettant, par exemple, d'expérimenter sur les accélérations "anormales" mentionnées ci-dessus. L'échelle de temps nécessaire pour bâtir un projet spatial étant de l'ordre de 10 ans, de telles expérimentations ne doivent pas exclure l'observation astrophysique (courbes de rotation des galaxies ou mirages) qui pourrait conduire plus rapidement à une explication des phénomènes "anormaux".

- Le développement de ces nouveaux moyens d'investigation peut permettre aussi d'étudier toute accélération qui mettrait en défaut le principe d'équivalence (l'existence de telles accélérations est prévue par toutes les théories qui unifient la gravitation et les autres interactions fondamentales dans une même vision quantique) ou encore d'étudier, à terme, la constitution interne de la Terre (effet relativiste de précession des gyroscopes dus au moment cinétique terrestre).
- L'usage des ondes de matière pourrait bien, à terme, donner naissance à une nouvelle génération de détecteurs d'ondes gravitationnelles.
Tous ce sujets intéressent aujourd'hui la communauté des physiciens, principalement en Europe et aux Etats Unis et concernent des projets pour, au moins, les vingt années à venir. C'est dans ce cadre que je désire poursuivre mes recherches, à mi-chemin entre l'expérimentation et la théorie.

A plus court terme, les travaux vers lesquels je me tourne concernent l'utilisation de cavités à onde de matière. Ces cavités n'existent pas pour le moment, la notion de miroir pour des ondes de matières n'étant pas encore bien établie. Toutefois, rien n'exclut pour le moment le fait qu'un jour de telles configurations puissent exister. Les ondes atomiques peuvent être canalisées dans des guides de diverses formes[22], il est possible, dès à présent, de fabriquer des ions « froids » que l'on peut envisager de manipuler avec des champs électriques. A cela, on peut ajouter qu'il existe des expériences de condensation de molécules, ce qui permet d'imaginer une vaste variété dans les composants des systèmes à onde de matière[23].

Dans ce contexte, il paraît tout à fait utile de rechercher de nouvelles configurations d'expériences de physique fondamentale qui tireraient profit des propriétés des atomes froids.
L'idée est de configurer des détecteurs à ondes de matière avec la même philosophie que ceux existant avec des ondes électromagnétiques (Virgo/LIGO, LISA) en comparant les caractéristiques qu'imposent chacune de ces ondes. Il est possible alors d'étudier des systèmes de cavités de type Fabry-Perot à deux ou plusieurs miroirs, de géométrie uni-, bidimensionnelle ou plus si nécessaire.

Dans cet esprit, j'ai encadré le stage de DEA de Franck Genet sur une étude théorique des cavités à onde de matière. Je lui ai demandé de chercher des solutions de l'équation relativiste de Klein-Gordon dans diverses configurations de cavités. Tout d'abord, il a étudié le comportement d'une onde de matière dans un champ gravitationnel statique (typiquement la pesanteur). Il a alors vérifié que les solutions obtenues, si on les restreint au cas non-relativiste, correspondent aux solutions de l'équation de Schrödinger couramment utilisées pour ces configurations. Puis, il a commencé à étudier le cas de la détection d'ondes gravitationnelles dans un satellite, c'est-à-dire, le cas de perturbations gravitationnelles dépendantes du temps. Il a posé les bases du formalisme nécessaire pour étudier les solutions, mais n'a pas eu le temps de résoudre complètement les équations.

La suite de ce travail constitue le point de départ de la thèse de Pacôme Delva (débutée en octobre 2004). L'objectif de cette thèse est d'estimer la sensibilité au champ de gravitation des cavités à onde de matière. D'autres utilisations peuvent être envisagées pouvant en fonction des types d'onde pouvant aller jusqu'à la chimie des molécules.

---

[22] Voir, par exemple : K. Bongs et al., 2001, CRAS, **IV**-2, 671 ; R. Dall et al., 2001, CRAS, **IV**-2, 595 ; S. Al-Awli et M. Babiker, 2000, Phys. Rev. A, **61**, 033401 ; S. Al-Awli et M. Babiker, 1998, Phys. Rev. A, **58**-6, 4768 ; S. Al-Awli et M. Babiker, 1998, Phys. Rev. A, **58**-3, 2274.
[23] Les équipes travaillant sur ce sujet décrivent leurs avancées dans le « Cold Molecule Portal » : http://www.lac.u-psud/coldmolecules/network/

Le travail d'un enseignant-chercheur.

Les travaux de recherche présentés dans ce manuscrit vont de pair avec une vision globale de la place d'un enseignant-chercheur dans la communauté de la recherche. Un enseignant-chercheur se définit statutairement par une quantité d'enseignements à produire, la recherche étant définie comme un complément à ce travail. De fait, beaucoup considèrent que ces deux activités sont complètement indépendantes et les abordent avec plus ou moins d'enthousiasme et de volonté d'innovation. C'est regrettable, car j'ai la conviction qu'utiliser la complémentarité des deux facettes de ce métier enrichit à la fois l'enseignement et la recherche.

Je ne suis pas en train de dire qu'un enseignant-chercheur doive uniquement enseigner des thématiques en lien avec sa recherche[24]. Au contraire, les différentes parties de la physique abordées dans son enseignement (c'est-à-dire, pendant la moitié de son temps) et les différents interlocuteurs avec lesquels il interagit permettent à l'enseignant-chercheur de prendre du recul par rapport à son sujet de recherche et à l'aborder de façon plus globale. Ce recul est certainement un atout important qui peut, moyennant un choix judicieux de son sujet de recherche, combler un manque de compétitivité dû essentiellement à un manque de souplesse dans son emploi du temps. L'enseignant-chercheur peut ainsi servir de vecteur d'information et d'intérêt (de motivation) de la recherche vers les étudiants, mais aussi, à l'inverse, de modérateur et de rappel pour ses collaborateurs chercheurs emportés par le flot de la compétition internationale en revisitant le cadre de leurs recherches et en les rendant accessibles à un plus grand nombre. Ce travail est tout à fait essentiel pour permettre une vision à long terme des enjeux de cette recherche. Et c'est sans doute à ce prix que la partie recherche du travail de l'enseignant-chercheur pourra être pleinement reconnue par ses collègues chercheurs.

Il convient donc de soutenir les enseignants-chercheurs vers une telle orientation de leurs travaux au détriment d'une course illusoire à la compétitivité amenant à une confrontation directe avec les travaux des chercheurs « purs » lors de l'évaluation des carrières. Je vois deux points importants dans ce soutien.

D'une part, il faudrait un maintien fort des enseignants-chercheurs dans l'enseignement universitaire des trois premières années après le bac. L'orientation graduelle des enseignements de ces premières années vers un enseignement de type « super-lycée » où les enseignants ne feraient plus de recherche peut être très dommageable. Ce serait couper l'appel d'air pour les étudiants que représente un enseignement dynamique, au fait de l'actualité de la recherche, répondant rapidement aux besoins des employeurs qui n'interviennent généralement qu'au niveau des années ultérieures. Il ne faut pas oublier que l'enseignement universitaire en physique est en compétition directe avec celui des écoles d'ingénieurs, ce dernier constituant un enseignement plus classique, mais avec plus de moyens. Le manque de soutien en faveur d'une certaine originalité pour l'enseignement des premières années universitaires est, au moins en partie, à l'origine de la baisse des effectifs d'étudiants en physique. De plus, transformer les premières années universitaires en « super-lycée » serait limiter l'enseignement des enseignants-chercheurs à un enseignement au service de la recherche, ayant pour vocation de former des étudiants pour leurs laboratoires, ce qui dévalorise le rôle et les capacités des enseignants-chercheurs.

D'autre part, il serait utile que la part innovante de l'enseignement d'un enseignant-chercheur soit rétribuée largement en terme d'heures de service et en terme d'importance dans

[24] encore qu'il soit légitime qu'il puisse le revendiquer pour une petite partie de son enseignement : ce qui représente une manière élégante de joindre l'utile à l'agréable, mais qui est certainement un exercice très difficile car alors l'adaptation au niveau des étudiants est plus complexe.

l'évaluation de son dossier dans sa carrière. Pour un enseignant-chercheur, la rédaction d'un polycopié, la mise en place d'un enseignement nouveau (qu'il soit sous une forme traditionnelle ou qu'il utilise des aspects du multimédia), l'écriture d'un livre ou d'un article dans une revue pédagogique, l'organisation d'écoles sur des thématiques de recherche devraient être estimés et exigés au moins au même niveau que les articles de recherche par les commissions et par les tutelles.

Il est évident que je n'espère pas changer quoi que ce soit en écrivant ces quelques lignes. Je les ai cependant écrites pour justifier l'état d'esprit dans lequel j'ai participé à la publication des travaux de Nicolas Baumard sur Europe, ainsi que l'élaboration de l'article intitulé : The « forgotten » process. C'est aussi dans cet esprit que je projette de participer à la mise en place un système nouveau d'enseignement de la gravitation expérimentale.
La gravitation expérimentale, ainsi que j'espère l'avoir montré dans les pages précédentes, est un sujet vaste et concernant beaucoup d'expériences terrestres et spatiales de pointe à court et moyen terme. Par exemple, les applications liées aux réseaux de satellites de positionnement de type GNSS vont proposer un nombre de débouchés importants et croissants. Or, la formation à cette physique est très restreinte dans les cursus traditionnels. Pour éviter cette contradiction, plusieurs membres du GREX ont suggéré l'utilité de mettre en place une école pré-doctorale sur la gravitation expérimentale , école annuelle, de thématique variable, mais instituée dans un établissement fixe où les laboratoires de ce domaine sont bien représentés, tel que l'Université Pierre et Marie Curie. Cette école pourrait avoir lieu durant une ou deux semaines, pendant des vacances (Pâques ou juin-juillet), serait ouverte à toute personne dès la deuxième année de Master de physique. L'organisation d'une telle infrastructure pérenne nécessite non seulement l'obtention d'un budget suffisant, mais aussi la mobilisation d'un petit groupe de personnes motivées. L'idée et les objectifs d'une telle école ont été présentés dans la demande de Plan Pluri-Formations GRAVITE soumise à l'UPMC l'an passé et devraient mobiliser nos forces dès l'année prochaine.

Remerciements

Pour finir, je tiens à remercier tous ceux qui m'ont soutenue pendant la période que couvre ce dossier et, en particulier, trois hommes dont les personnalités m'ont profondément marquée : Christian Vanderriest, Pierre Encrenaz et Philippe Tourrenc.
Avec une pensée pour Kévin, Nathanaël, Maylis, Julien et Frédéric.